

The University of Sheffield



Investigation of Vibration in Switched Reluctance Machines

James Dexter

A thesis submitted in partial fulfilment of the requirements for the degree of
Doctor of Philosophy

The University of Sheffield
Faculty of Engineering
Department of Electrical and Electronic Engineering

January 2020

Abstract

The popularity of magnet-less electrical machines has increased due to the volatility of permanent magnet prices, prompting a rise in interest of switched reluctance machines (SRMs). SRMs are suitable for a wide range of applications, but limited by high torque ripple, acoustic noise and vibration. This thesis systematically investigates electromagnetically excited stator vibrations in a 6-stator-pole/4-rotor-pole (6s/4r) SRM.

With the aid of ANSYS Workbench finite element (FE) package, a series of electromagnetic and mechanical FE models are developed to investigate the vibration response. The 2D and 3D FE mechanical models are progressively built from a simple laminated annular ring to the final 6s/4r prototype with housing, and verified with experimental hammer impact tests at each stage of assembly. The mechanical connections of various SRM parts are investigated. It is found that the bolted connection of the endcaps to the housing frame has a significant influence on the natural modes and frequencies of the SRM, e.g. introducing new dual vibration modes of order 2. This phenomenon has not been previously covered, and in industrial applications this may cause unexpected and unwanted resonant frequencies, resulting in potential for worsened acoustic noise and vibration.

The influence of various control parameters is also investigated. The 6s/4r SRM is systematically simulated by FE models under different load conditions, turn-off and turn-on angles, in terms of electromagnetic forces and dominant vibration modes. It is shown that the load and turn-off angle have a significant impact on vibration response, while turn-on angle has minimal influence. The FE results are verified experimentally in single pulse voltage mode control. As the turn-off of current in each phase is the dominant source of acoustic noise and vibration in SRMs, the influence of current profile is investigated by two methods, in time domain and frequency domain, respectively.

In the time domain, the current profile is defined by a discrete series of points. With reference to the baseline unipolar square wave current profile, a continuous slope differential and a current step are introduced at turn-off. It is shown that significant reduction in vibration response can be achieved by increasing the duration of the continuous slope due to reduced severity of radial force change. It is also found that a current step reduces vibration response but the duration of the step has no influence.

In the frequency domain, the baseline unipolar square wave current profile is decomposed by the Fourier transform into a series of harmonic components. Through progressive reintroduction of harmonic contents it is found that with low order current harmonics only, the vibration response is significantly reduced, albeit with electromagnetic performance affected. The largest influence on vibration response is due to the amplitude of the first current harmonic amplitude. It is also found that the 2nd current harmonic amplitude can improve the electromagnetic torque but has minimal effect on vibration response. By operating the motor under current control with harmonic components, the vibration response can be reduced whilst simplifying the control strategy and hardware, lowering cost which is a critical factor for industrial applications.

Acknowledgements

I would like to express my sincere thanks and gratitude to Professor Zi-Qiang Zhu for his support and guidance throughout the duration of my PhD study.

I would also like to thank Dr Liren Huang for his help and support, particularly in technical discussions. Further thanks to Jaguar Land Rover for their partial financial support and helpful comments and discussions, particularly Mr Xavier Vinamata. I would also like to thank the staff and post graduate research students in the Electrical Machines and Drives Research Group at the University of Sheffield for their support and help.

Finally, I would especially like to thank my partner, family and friends for their support and encouragement throughout the research.

List of Symbols

CCM	continuous conduction mode
DITC	direct instantaneous torque control
FE	finite element
PM	permanent magnet
PWM	pulse width modulation
SRM	switched reluctance machine
UMF	unbalanced magnet forces
VFRM	variable flux reluctance machine
B_r	radial flux density, T
B_t	tangential flux density, T
D_b	active bolt diameter, mm
$E_{x, y, z}$	Young's modulus in x, y or z axis, Pa
F_{rad}	radial force, N
F_{tan}	tangential force, N
G_{XY}	shear modulus in xy-plane, Pa
G_{XZ}	shear modulus in xz-plane, Pa
G_{YZ}	shear modulus in yz-plane, Pa
i	time dependent current, A
I_k	k^{th} current harmonic amplitude
L	inductance, H
L_b	active bolt length, mm
L_{stack}	axial stack length, m
m	axial mode order
n	circumferential mode order
$R_{x, y, z}$	rotational freedom about x, y or z axis
T	torque, Nm
$T_{x, y, z}$	translational freedom in x, y or z direction
x	region of overlapping poles, m
α_k	k^{th} current harmonic phase
θ	rotor position, radians
τ_a	duration of full alignment, s
τ_u	duration of unalignment, s
Ψ_{ph}	phase winding flux linkage, Wb
μ	frictional coefficient
μ_0	permeability of free space, H/m

Contents

<u>Abstract</u>	<u>i</u>
<u>Acknowledgements</u>	<u>ii</u>
<u>List of Symbols</u>	<u>iii</u>
<u>Chapter 1 General Introduction</u>	<u>1</u>
1.1 Development and operation of switched reluctance machines	3
1.2 Fundamentals of acoustic noise and vibration	7
1.2.1 Introduction to noise and vibration in SRMs	8
1.2.2 Sources of noise and vibration	10
1.2.3 Influence of control on noise and vibration	13
1.2.4 Structural vibrations in SRMs.....	14
1.2.5 Noise reduction techniques	15
1.3 Scope of thesis and contributions.....	18
<u>Chapter 2 Finite Element Modal and Vibration Analysis</u>	<u>21</u>
2.1 Introduction	21
2.2 Validation of FEA with 2D annular ring.....	22
2.2.1 Identification of natural modes and frequencies	22
2.2.2 2D vs 3D model	28
2.2.3 Mesh sizing optimizations	30
2.2.4 Refinement of material properties.....	33
2.3 Influence of teeth and verification of stator mechanical properties	37
2.3.1 Stator parameters and introduction	37
2.3.2 Identification of modes	37
2.4 Influence of casing and endcaps.....	46
2.4.1 Addition of casing framework (No endcaps).....	46
2.4.2 Influence and modelling of endcaps	50
2.5 Final mounted modal analysis.....	58
2.6 Summary	59
<u>Chapter 3 Investigation of Vibration Under Voltage Control</u>	<u>61</u>
3.1 Introduction	61

3.2	Forces acting on stator poles	62
3.3	Influence of load/current	71
3.3.1	Electromagnetic results	72
3.3.2	Vibration response	78
3.4	Influence of conduction angle	82
3.4.1	Fixed turn-off	82
3.4.2	Fixed turn-on.....	92
3.5	Experimental verification of trends.....	103
3.5.1	Experimental setup and testing	103
3.5.2	Vibration response under varied load	107
3.5.3	Vibration response under fixed turn-off conditions	110
3.5.4	Vibration response under fixed turn-on conditions.....	112
3.6	Summary	114
<u>Chapter 4 Investigation of Influence of Current Profiling in Time Domain..</u>		115
4.1	Introduction	115
4.2	Influence of turn-on and turn-off	115
4.3	Continuous slope differential at turn-off.....	119
4.3.1	Electromagnetic results	121
4.3.2	Vibration response	126
4.4	Two step control.....	130
4.4.1	Electromagnetic results	131
4.4.2	Vibration response	135
4.5	Summary	139
<u>Chapter 5 Investigation of Influence of Current Profiling in Frequency Domain</u>		140
.....		140
5.1	Introduction	140
5.2	Decomposition by Fourier series.....	140
5.2.1	Electromagnetic results	141
5.2.2	Vibration response	146
5.3	Amplitude of DC + 1 st current harmonic	151

5.3.1	Electromagnetic results	152
5.3.2	Vibration response	157
5.4	Influence of 1 st current harmonic amplitude	161
5.4.1	Electromagnetic results	162
5.4.2	Vibration response	167
5.5	Influence of second harmonic amplitude	171
5.5.1	Electromagnetic results	172
5.5.2	Vibration response	176
5.6	Summary	180
<u>Chapter 6 General Conclusions</u>		<u>181</u>
6.1	Modelling of SR machine	182
6.2	Time domain investigation.....	183
6.3	Frequency domain investigation	184
6.4	Future work	184
<u>References</u>		<u>186</u>

Chapter 1 General Introduction

Electrical machines and drives can be found throughout daily life and have become an integral part of the world we live in. It is stated in [Bin01] that approximately 30% of energy consumption in domestic applications is as a result of electrical drives, a figure likely to have increased in recent years. Hence, the improvement of these electrical machines is critical in terms of efficiency, energy saving and improved performance. The application typically defines the optimal machine type, such that machines can be optimised for specific performance and roles. For example, a fan-drive generally operates at a fixed speed and torque, or fixed operating point, and therefore, it can be designed to operate consistently at this target point. Permanent magnet (PM) machines perform well for applications such as this since the permanent magnet field allows for high efficiency if designed carefully as well as producing sufficiently steady torque speed performance. All machine types come with inherent advantages and disadvantages, in terms of performance, manufacture, cost, losses and more factors. The use of rare-earth PMs may significantly increase costs. Furthermore, surface mount PM machines may be limited in high speed applications due to the centrifugal forces acting on the rotor, a second more viable option is interior PM machines. However, the manufacturing may incur additional costs, restricting use in applications with lower costings. For mass production, increases in cost and volatility of permanent magnet prices are a concern for many manufacturers.

Electric vehicles (EVs) have recently seen significant interest and progress, utilising both PM machines and induction machines in place of internal combustion engines. The high efficiency and power factor of PM machines provide an attractive solution to the growing issue of EV drives. EV applications require the machine to operate over a wide torque and speed range, and hence, a PM machine shall be designed for maximum efficiency over a typical driving cycle. A second machine type utilised for EV applications and in production is induction machines, which have also been widely used in a variety of other applications. At high speeds, PM machines suffer from the requirement of additional current in the flux weakening region, not an issue for induction machines due to the lack of permanent magnets. As with all machines, induction machines also exhibit disadvantages, such as the high losses caused by high rotor current at low speeds. A significant issue with many PM machines is the longevity and sustainability of producing them, since they are inherently unsustainable as the magnetic material is limited and 'rare'. Other machines in production for EV applications include axial machines for in-hub motors. A summary table of advantages and disadvantages for some popular motor types can be found in **Table 1.1**.

Table 1.1 Electric motor summary

Induction Motors (IM)	
Advantages <ul style="list-style-type: none"> • Simple robust design • Relatively low maintenance • High starting torque with good overload capability (3 phase) • High efficiency 	Disadvantages <ul style="list-style-type: none"> • No self-starting in a single phase induction motor • Low efficiency and power factor under light load
Permanent Magnet Synchronous Motors (PMSM)	
Advantages <ul style="list-style-type: none"> • High efficiency • High torque density, compact design • High torque even at low speeds 	Disadvantages <ul style="list-style-type: none"> • High material cost (e.g. NdFeB) • Unsustainable rare-earth magnets • Irreversible demagnetization • Potentially complex manufacturing
Synchronous Reluctance Motor (SynRM)	
Advantages <ul style="list-style-type: none"> • Low cost • Reliable • Robust structure • No permanent magnets • Higher torque density than IM 	Disadvantages <ul style="list-style-type: none"> • Complicated rotor construction • Non-linear torque vs current • Complex control algorithms • Lower torque density compared to PMSM
Switched Reluctance Motor (SRM)	
Advantages <ul style="list-style-type: none"> • Low maintenance • Low material cost • No permanent magnets • Simple, robust structure • Good fault tolerant capability 	Disadvantages <ul style="list-style-type: none"> • High acoustic noise and vibrations • High iron losses • High torque ripple

An alternative machine topology suitable for a number of applications is that of the switched reluctance machine (SRM). As seen in many writings and publications on SRMs, they exhibit inherent advantages including robust topology and simple structure, ease of manufacturing and lack of permanent magnets. Furthermore, SR machines offer high power density at a reasonable cost due to the lack of permanent magnets, as well as high speed operation. The nature of control in SR machines is

the sequential excitation of phases, producing independent operation of each phase. Hence, it is possible for a SR machine to operate with redundant phases, caused by a potential defect in a winding for example. Therefore, the SR machine is an attractive proposition for fault-tolerant applications and applications where safety is paramount. For example, in the aerospace industry there is evidence of these properties [Ham04]. However, these advantages are offset by the inherently high torque ripple, acoustic noise and vibration [Cam92], [Hus02], [Lon01] and [Pil99]. Approaching these issues and providing an insight into potential solutions will allow for consideration of these effects. This thesis aims to analyse the impact and influence of varying parameters from an electromagnetic perspective, alongside the vibration response caused by electromagnetic excitation.

1.1 Development and operation of switched reluctance machines

Historically, examples of SRMs can be found as far back as the late 1890s [Sch97]. In this case, an SRM is utilised as a variable speed traction machine for use in an electric vehicle (EV). In early variations of SRMs, the switching of stator windings was performed mechanically, and hence, the progression of the technology was relatively slow and limited. Advancements made in switching technologies and specifically switching speeds resulted in the improved viability of SRMs. More recently, SRMs can be found in fan and pump applications, namely vacuum cleaners produced by Dyson and LG [SRDrives]. Considering that advancements in SR technologies is relatively recent, the market competitions are machines optimised through decades of research. One of the earliest papers relating to the design and fundamentals of SRMs was P. Lawrenson's paper in 1980 [Law80]. This lays the general foundations for the practical design of a family of SRMs. It demonstrates that machines in this family are capable of extremely high levels of performance, can be controlled in exceptionally simple and flexible ways, and are simple and cheap to manufacture. Lawrenson compares the design and restrictions of other machines to that of SRMs to highlight the advantages of SRMs when it comes to a simple and robust nature. Compared to AC machines much more freedom can be found as follows:

- the number of phases to be employed is an open choice between one and many;
- the ratio of phase number to stator pole number is not fixed;
- the ratio of rotor pole number to stator pole number is open to a wide variety of choices.

However, there are some drawbacks and limitations when designing SRMs:

- the 'best' values of rotor pole arc and stator pole arc have to be considered;
- attention has to be paid to starting capability.

The primary issues facing development and introduction of SR machines to mass markets are the torque ripple and high acoustic noise and vibrations. Torque ripple has been widely covered and an example of successful reduction in torque ripple can be found in [Ind02]. These are often considered to

be separate problems, and therefore, the contribution of torque ripples to acoustic noise and vibration is widely neglected from calculations. The major source of acoustic noise and vibration is attributed to stator vibrations with major influence from radial force. As the radial force is perpendicular to tangential force it is considered that the influence of tangential force, and torque ripple, is minimal. However, the torque ripple contributes to rotor and shaft as well as stator vibrational oscillation leading to acoustic noise and vibration from mechanical interactions such as bearings and construction [Sri04].

Design optimisation of any electrical machine is determined by the specification and constraints of an application. Typically, this includes cost, weight, size and performance as the key defining factors. Some of these factors may be considered as hard targets such as limits on size, others require a multi-objective optimisation design process. To optimise the design of SR machines, firstly the fundamental operation and design must be introduced. Further details of the design may be found in [Mil93], [Mil01] and [Kri01]. As previously stated the work by Lawrenson [Law80] provides an in depth introduction into the design and operation of SR machines. A step by step design guide in the form of [Kri88] supplements the work by Lawrenson, beginning with output equations and targeting the final dimensions of the machine to match the application requirements. From this, it is possible to calculate the required machine length, number of winding turns and also take into account thermal considerations.

The torque produced in SRMs is referred to as reluctance torque. This is the torque produced as a result of the rotor being drawn to the position of minimum reluctance, and in the case of SR machines this is the position of full alignment between stator and rotor poles. **Fig 1.1** illustrates the single phase inductance profile and corresponding torque production for an idealised waveform, where L and T indicate the inductance level and torque produced, respectively. Furthermore, τ_a and τ_u represent the duration of full alignment and unalignment, respectively, and θ represents the electrical rotor position. Under unsaturated conditions, the torque production is defined by equation (1.1). By definition, the optimum torque per ampere ratio is obtained by maximising the aligned and unaligned inductance ratio.

$$T = \frac{1}{2} i^2 \frac{dL(\theta)}{d\theta} \quad (1.1)$$

This derivation can be found in [Boe13]. It is derived from the flux linkage and co-energy, assuming that the operation of the SR is a linear example such that the flux linkage is only a function of position, and therefore, proportional to the inductance. For an introduction to the derivation of work done in SR machines, it can be seen in [Don11]. By considering the flux linkage in the aligned and unaligned position and magnetic co-energy and treating phases individually [Pul98], the per-phase expression for SRMs is derived in terms of co-energy only. This is then converted into (1.1) through the assumption of a magnetically linear machine. The derivation method in [Boe13] is also utilised in [Sta95] for synchronous reluctance machines and in [Sta96] for PM surface mount and induction machines.

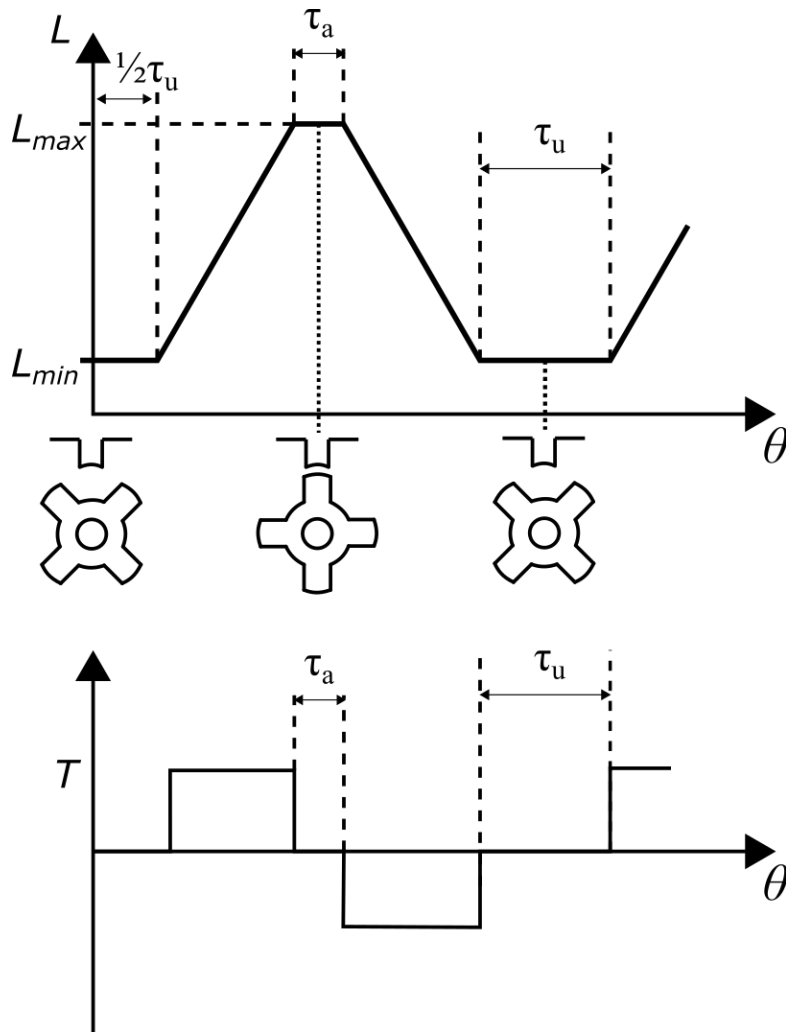


Fig. 1.1 Idealised inductance profile of 6s/4r SR machine with resultant torque considering a constant phase current.

Generic control of SRMs can be categorised as follows:

- Single-pulse mode;
- Current hysteresis control;
- PWM control;
- Direct instantaneous torque control (DITC);
- Continuous conduction mode (CCM).

This list is not exclusive since it only seeks to identify the major control strategies used in the operation of SRMs. Single-pulse mode control is operated by applying a single voltage pulse to each phase consecutively. This corresponds to an equivalent pulse in the current, with inherent rise and fall times determined by the inductance characteristics of the electrical machine. Current hysteresis control is both fast and simple to implement although for a non-linear inductance profile this shall not supply smooth torque. It works on the principle that given a range of position values, the phase shall be excited and the current in this period shall be kept approximately constant within predefined limits. A key

advantage of current hysteresis is the lack of requirement for high sampling rate, given the only parameters required are turn-on, turn-off, current limits and free wheeling angle. Therefore, it can still be well suited to high speed applications where, for example a PWM switching current, there is a high sampling rate required. It has also been used to approach the issue of acoustic noise and vibration reduction in [Kas10].

It may be decided that the SRM is operated under DITC or short PWM-DITC [Fue07], in which case current profiles may be determined to provide a specific torque dependent on requirements [Fie04], [Ind02] and [Ind03]. Whilst DITC operates as an analogue control strategy based on predetermined torque, PWM-DITC is a model-based strategy. Through the utilisation of a fixed frequency PWM, the switching frequency is fixed, and hence, no longer a function of speed. Finally, by extending the conduction angle, continuous conduction mode is achieved, with current not falling to zero. This produces an increased output, although it comes at the cost of significantly reduced efficiency. For the experimental verification in this thesis, single-pulse mode under voltage control is utilised. The 6-stator-pole 4-rotor-pole (6s/4r) machine used for investigations in this thesis can be seen in **Fig. 1.2**.

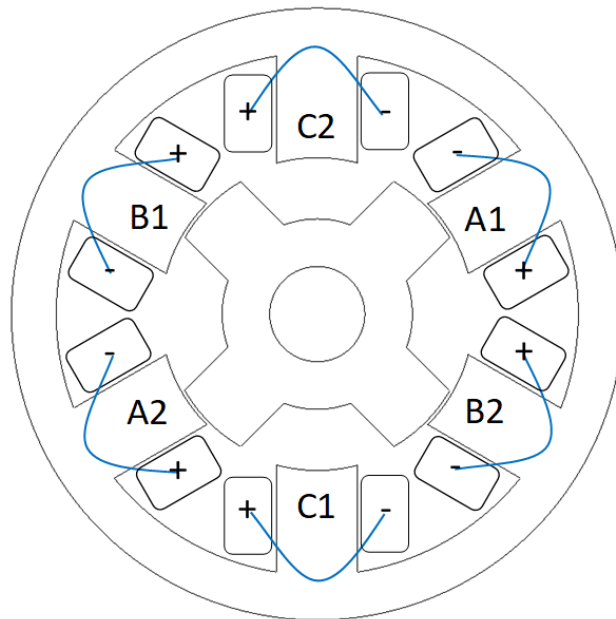


Fig. 1.2 Winding configuration of 6s/4r prototype SRM investigated in this study.

1.2 Fundamentals of acoustic noise and vibration

Acoustic noise is separated from the perceived noise of electrical machines, and hence, it can be difficult to quantify. It is noted that although ‘low-noise’ performance is deemed to be the desirable characteristic and target for SRMs, this is a relative term. That is to say, the level of acceptable acoustic noise produced by a vacuum cleaner will differ greatly when compared to the acoustic noise produced by a luxury EV. In order to quantify the acoustic noise and simulate the vibration response as a product of electrical excitation in a machine, the process of noise production must be understood. In order to simulate and understand causes of acoustic noise and vibration, firstly the causal path from electromagnetic excitation through to noise production must be developed, **Fig. 1.3**.

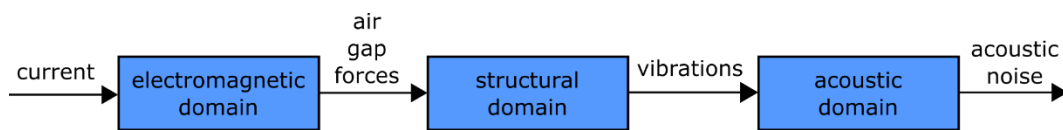


Fig. 1.3 Causal path of noise production in electrical machines.

Considering the entire system in this way gives an insight into the multiple disciplines required to fully understand and solve problems relating to acoustic noise. Acoustic modelling requires the integration of multiple models, specifically the electromagnetic modelling and a mechanical model. Furthermore, the modelling can be a time-consuming process, and as such it must be developed in order to create a reliable and repeatable system that achieves a time efficient solution. By creating a model based on this causal flow chart, general conclusions may be drawn for drive influences, and then, adapted and fine-tuned through measurement and experimental analysis.

The causal path from the perspective of electromagnetic stator excitation starts with the electromagnetic excitation of the windings. Through current excitation (and PMs if applicable) the stator is excited, generating a vibration response. This response is then transferred through multiple mediums, such as the frame work and cooling systems, onto the air thus becoming air-borne sound or sound pressure. This approach of separating excitations into 3 stages is firstly seen in [Jor50] by Jordan. A similar causal path can be found at the beginning of many works, see [Gie06], [Le08], [Kas10] and [Gie11]. Generally, and in the case of this study, the modelling procedure closely follows the causal path. Firstly, the electromagnetic response of the machine must be found and air gap forces calculated. These air gap forces are then applied onto a structural model, in which the natural frequencies are found through modal analysis. Finally, the response of the mechanical system may be obtained, and if required transferred into the acoustic domain such that the air-borne noise is found. Given this introduction into acoustic noise production, the application of this process with 3-phase SRMs is investigated. There is also work in the area of noise and vibration reduction in induction machines, along with studies on 4-phase switched reluctance (SR) machines [Pil99], [Hus00], [Nev97] and [Nev99].

1.2.1 Introduction to noise and vibration in SRMs

Considerable research and work have been performed to investigate the source and cause of the inherently high acoustic noise and vibration response in SR machines. A review of noise sources and detailed response of electrical machines can be found in [Mil93], [Mil01] and [Kri01]. Miller provides an extensive breakdown of SR machines from the perspective of torque production, design, and acoustic response. These papers and studies offer an insight into causes of extreme acoustic noise and vibration response, which may be then be approached from the perspective of current profiling in this thesis.

$$F_{rad} = \frac{B^2 x L_{stack}}{2\mu_0} \quad (1.2)$$

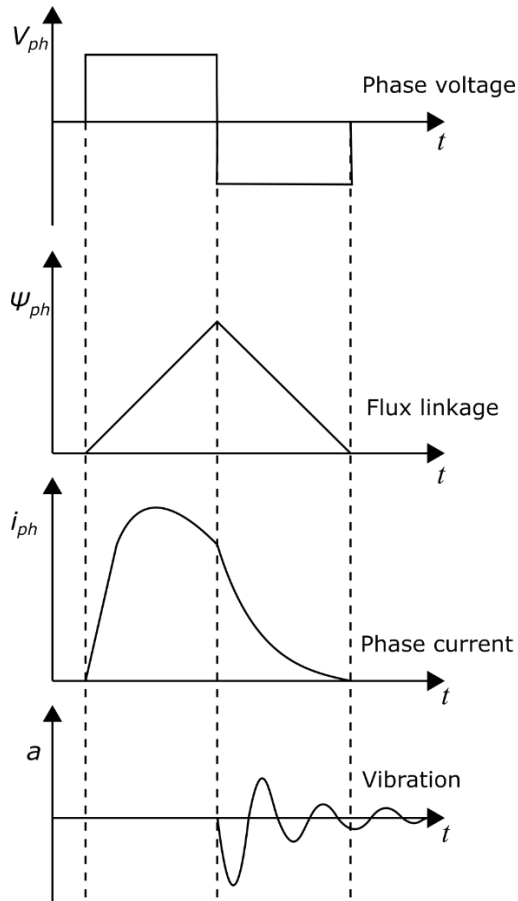


Fig. 1.4 Operating characteristics of SR machines.

The machine topology investigated throughout this study is introduced in **Fig. 1.2**, comprising of laminated stator and rotor cores, with salient teeth, and concentrated windings on the stator teeth. Having determined the phase current and torque produced as defined in **Fig. 1.4**, the air gap forces must be considered. The radial force in electric machines is shown in (1.2), where B is the flux density, x is

the region of overlapping teeth, L is the stack length, and μ_0 is the permeability of air. The tangential force is also defined, but this is often neglected in the modelling of stator vibrations and attributed solely to the production of torque on the rotor side [ANS12]. Peak radial force is experienced by the stator at the instance of greatest overlap between stator and rotor poles. Under conventional unipolar square wave control this is also the instance of phase turn-off, when the current rapidly decreases. The drop in current results in a significant reduction in flux density at the same moment, and hence a significant reduction in radial forces. The radial forces draw the stator inwards at the excited poles, compressing the overall shape and machine. At the moment of turn-off in each phase, the radial forces are released and hence, the compressed machine state is also released from a mechanical perspective. This then sends the stator into a period of free oscillation, exciting natural frequencies. The period of free oscillation and resultant behaviour is analogous with a mass-spring damper system. The stator is considered to be the spring, as the compression or spring is released, there is then the free oscillation period. Consequently, acceleration measured behind stator poles will exhibit dominant traits of the stator natural frequencies. The dominant frequencies in the oscillation waveform correlate to the dominant natural modes of the stator, which will be expanded upon in Chapter 2.

The alignment of stator exciting forces, such as radial forces, and the natural frequencies of the stator body is referred to as resonance. It is this resonance in electric machines that causes the most severe and significant vibrations and acoustic noise. As a whole, the electric machine shall also experience significant damping, both inherently and from mechanical limitations. Damping refers to the ability of the machine and material to absorb vibrational energy, and hence, reduce the amplitude of vibration response. It also refers to the ability of a material to transfer vibrational energy, the propagation of vibrations through a medium. It is also stated in [Lon01] that under significant damping, the natural frequencies shall be reduced, not only their amplitudes. The effect and estimation of damping effects is considered in the initial modal analysis, with a simple stator model. However, as the manufacturing of the machine advances and more components and boundaries are introduced, it becomes complex and time consuming to include damping effects reliably. Its importance to the amplitude of acoustic noise and perceived noise should not be ignored. However, it does not fall within the coverage of this thesis.

The measurement and simulation of acoustic noise is a difficult task, further complicated by the perception of noise not just the numerical values. The human ear has a frequency hearing range of 20Hz - 20kHz, but the perception of noise across the frequency range is not linear. A subjective 'loudness' perceived by the human ear may be assigned to any noise source. The industry standard defining a spectrum of perceived noise and sound pressure is the A-weighted sound pressure, taken from [Bru84].

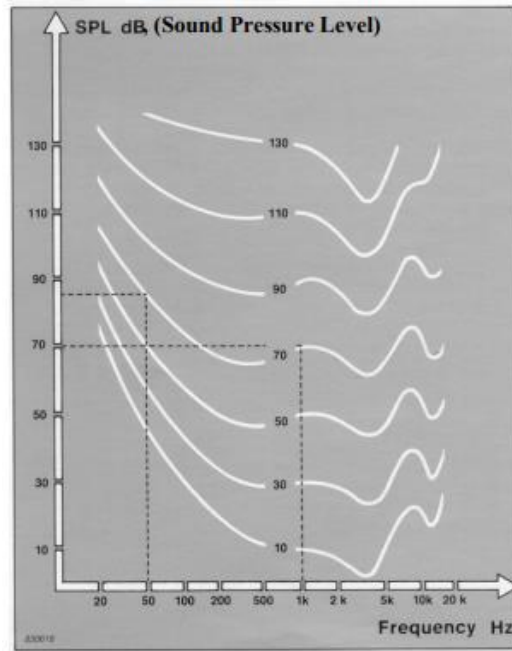


Fig. 1.5 Perceived ‘loudness’ contours equating frequencies taken from [Bru84].

1.2.2 Sources of noise and vibration

Sources of vibration in SRMs can be categorized broadly into the following sections:

- Electromagnetic
 - Unbalanced magnetic forces (UMF)
 - Torque ripples
 - Radial magnetic forces
- Mechanical
 - Mechanical resonance
 - Bearings
- Aerodynamic noise

Many of these sources are evident in all machine topologies and not limited to SR machines. For SRMs in particular, it is regarded that the electromagnetically induced noise is dominant. The mechanical noise is considered to have a lesser influence and is often neglected, this includes bearings and couplings, as well as boundary conditions between components. Finally, the aerodynamic noise which may be produced by the salient nature of rotor poles acting as ‘fan blades’. This becomes a more significant issue at higher speeds. Given these examples, the noise produced as a result of electromagnetic excitations is most apparent in SR machines.

In order to investigate the influence of electromagnetically induced noise, Cameron et al first ran an 8s/4r, 4 phase machine without excitation [Cam92]. Then, the machine is excited and operated at the same speed before being allowed to slow to zero. Experimental results show the insignificance of the

noise produced when unexcited, compared to operation under excitation. It is also considered that the electromagnetic forces acting on the stator are not limited to the radial forces during operation, although this is often the condition used in simulated studies. Other potential forces excited via the electromagnetic excitation include fluctuating air gap forces from rotor vibrations, and forces imposed on the windings. In [Cam92] it is shown, through the use of multiple accelerometers at a range of locations around the machine, that minimum emissions are observed during periods of misalignment. The forces acting on windings in the slots are at a maximum when the rotor is in misalignment, and hence, it is concluded that the significance of this source is negligible [Cam92].

The unbalanced magnetic forces acting in an SR machine are typically a result of eccentricities in the rotor, resulting in magnetic asymmetry. This causes higher air gap flux in the portion of the rotor with the reduced air gap length. This phenomenon is covered in many literature including [Mil95], [Hus00], [Aya99], [Wu96] and [Cam92]. Cameron et al perform measurements once again on an 8s/4r 4 phase machine, and it is deemed that in this situation unbalanced magnet forces are not a significant source of noise and vibration. However, from the perspective of additional mode introduction, [Wu96] and [Aya99] conclude that it is possible for eccentricity to cause issues. Although it may not directly increase the perceived noise, the introduction of additional modes into the vibration spectra is not desirable. In a 6s/4r SRM operated with sequential phase excitation, odd modes are eliminated due to equal forces acting on diametrically opposite poles. However, eccentricity in the rotor and the resulting asymmetric forces will negate this effect. Therefore, odd modes and specifically mode 3 are ‘reintroduced’ into the vibration spectra [Aya99]. It is also noted that in [Wu96] the unbalanced magnet force causes additional centrifugal forces on the rotor and thus, vibrations may be transmitted to the housing and bearings. In reviewing previous work, it is concluded that the influence of rotor eccentricity and UMF is less of a problem under heavy levels of saturation.

SRMs suffer from inherently high torque ripple, attributed to their doubly salient structure and non-sinusoidal excitation currents. In order to minimise the torque ripple, current shaping and current profiling have both been implemented [Lov94] and [Tur98]. However, these methodologies are often limited to specific machines or SR topologies. It is also possible to vary the rotor pole geometry in order to reduce torque ripple, with [Meh92] utilising this for marginal reduction. The staggering of poles in the constant torque production region of operation is also utilised in order to extend this region, such that the dip of torque is reduced [Bar99]. These studies apply a focus on torque ripple and torque production without application to acoustic noise and vibrations. An extensive study into the impact of torque ripple in SR machines can be found in [Hus05], [Hus02] and [Hus96]. Torque sharing functions have been used to control and implement torque ripple minimisation in [Xue09]. For further consideration of torque ripple in SRMs and influence on acoustic noise and vibration, the following works may be considered [Cha06], [Cho07], [Rus98], [Sah00], [Leo12], [Zhu06] and [Zhu11]. The torque ripple is a derivation of tangential air gap forces acting on the rotor poles. Therefore, it is considered that these forces impact the rotor side, and hence, will have a negligible effect on the stator

borne vibrations. Tangential force contributes to shaft and stator vibrational oscillation and influences the acoustic noise and vibration produced from bearings and mechanical construction [Zhu91], [Sri03]. Vibrations induced by torque ripples are negligible as the direction is perpendicular to the radiating surface. However, these vibrations may be transmitted through other components and coupled parts and then emitted as acoustic noise [Zhu91]. Torque ripple also influences the teeth bending modes, these are determined by the stiffness and material properties of teeth and windings. Due to the winding nature and potting of the machine, these are negligible in comparison to larger radial vibrations but may contribute to additional modes [Lon01].

Analysis of acoustic noise and vibrations highlights a number of issues and phenomena that may otherwise go unnoticed. Wu and Pollock [Wu93] and [Wu95] observe the significance of the turn-on and turn-off influence, the instances of major vibration response measured behind poles. The vibration response is as a result of the stator and rotor poles coming into alignment, followed by the turn-off of phase excitation. Hence, the radial force decays and the stator goes from a stage of compression into oscillation, a result only observable in time domain. The phenomena also align with finite element (FE) analysis, in which it is shown that the calculated radial forces are maximum at alignment of poles [Pul93]. It is suggested that in order to reduce the vibration response and acoustic noise produced at turn-off, the radial force shall also be required to be reduced at the instance of phase turn-off.

Furthermore, not only a reduction in radial force is required, a focus must also be applied to the rate of reduction in radial force [Wu93]. Reducing the radial force is advantageous as the deformation of the stator shall also be reduced, and hence, the acoustic noise and vibrations. However, if this reduction is extended over a longer time period, little to no oscillation shall occur. Therefore, as radial force and phase currents are closely linked, it can be said that a rapid reduction in current is also not desirable.

Radial force is considered to be the dominant source of acoustic noise and vibrations in SRMs, as covered extensively in [Mil93]. The most significant vibration occurs behind a tooth at the moment of full alignment between stator and rotor poles [Mil93], [Mil95], [Mil01], [Mil02], [Wu93] and [Wu95]. This phenomenon is the basis for a considerable percentage of research into reducing acoustic noise and vibrations in SRMs. It has also been shown experimentally that the response of end shields is negligible compared to radial stator vibrations [Zhu91]. The dominant mode shapes in terms of resonance in radial-flux machines are defined by the radial deformation of the stator, further supporting the evidence that radial components of electromagnetic forces are significant. Radial force is identified as the dominant source of vibrations in SR machines in [Cai01], [Cam92], [Anw00], [Li09], [Pol03], [Kur15a] and [Tak15].

1.2.3 Influence of control on noise and vibration

Given the origin and sources of acoustic noise and vibration, the influence of parameters of operation must be investigated, such that the machine shall be designed in a manner that minimises inherent disadvantages. The following parameters have already been seen in some studies:

- Operating speed;
- Chopping and PWM frequency;
- Switching angles.

Firstly, the impact of operating speed and PWM cycle shall be reviewed, such that the relationship between these and the acoustic noise production may be analysed. This is achieved in [Pul93] over a range of operating conditions. It is known that for any specific machine, the harmonic content of the acoustic noise and vibration is dominated by the natural vibration modes of the machine, and not the operation. However, the operating speed shall influence the amplitude of vibration response, as seen when the exciting forces resonate with natural frequencies. Qualitative results are found in [Cam92], in which it is observed that at specific speeds the acoustic noise is increased. The fundamental frequency, a function of rotational speed, and stator natural frequencies coincide causing resonance, this is also observed in [Col96]. Furthermore, [Cam92] determines that in the linear operating region the radial force produced is proportional to the square of the excitation current.

Research into PWM switching frequency and hysteresis control determines that the random switching nature of hysteresis control excites a wide range of resonant modes [Gab97]. In order to approach this issue, a constant PWM switching frequency is introduced and it is found that the emitted noise is lower. There is a lack of definable evidence for this, as generally speaking the same vibration modes are excited regardless of the switching control. It is considered that this a result of the constant switching frequency applying the majority of excitation at f_s (switching frequency), as opposed to the wide range of frequencies excited from hysteresis control. [Gab97] also compares the uses of soft and hard chopping under voltage control, for acceleration only with neglect of the sound pressure level. This idea is further developed in [Lon02], comparing results in the time and frequency domain as well the sound pressure level.

Finally, the switching angles of the SRM control are reviewed, these are critical in control of SR machines and allow for a multitude of performance characteristics including maximum efficiency, minimum torque ripple, maximum torque per ampere etc. Therefore, it could be hypothesised that for any given machine, there shall also exist a set of switching angles to produce minimum acoustic noise and vibration. It is noted that as stated earlier, the optimal performance of SR machines relies upon minimum noise level whilst producing the required torque and power for applications, and therefore, it is a multi-disciplinary problem. The influence of switching angles is acknowledged in [Bes94]. However, it is not acted on, with no experimental details or analysis. [Wu93] covers the topic in more detail, with a particular focus on the turn-off angle and influence on radial force components. A 6s/4r

SR machine is analysed for varied turn-on angle and fixed turn-off angle in [Bla94], where little to no variation in sound pressure level is observed. This is confirmed via simulated and experimental analysis in this thesis, with a more detailed explanation. A purely simulated study may be found in [Nev97] which considers the impact of switching angles on a 4 phase 8s/4r machine.

1.2.4 Structural vibrations in SRMs

As shown previously, the dominant source of vibrations in SR machines is accredited the stator borne vibrations, and a number of works investigated and acknowledged this [Col96], [Mah96] [Liu12b], [Lon01], [Nev97], [Nev01], [Pil99], [Sad96] and [Tan97]. The influence of stator modelling is also included and combined with electromagnetic analyses in [Sad96], [Tan97], [Nev97], [Bes98], [Gab99], [Tak15], [Bay16], [Lon01], [Liu12] and [Cai99]. The analyses in these studies are applied in both 2D FE analysis and more recently, 3D FE analysis. Influence of the following features have been investigated:

- Stator yoke;
- Stator frame and housing;
- Windings;
- Damping ratio.

The stator yoke thickness is known to have a significant impact on the natural frequencies of the machine, and thus, bear significant impact on the vibration response. The influence is majorly attributed to the stiffness the stator yoke adds to the machine. The influence of stator yoke thickness is analysed through FE in [Bes98] and [Cai99] and performed analytically in [Col96] and [Pil99]. These studies seek to find the influence of yoke thickness by increasing thickness whilst maintaining a constant outer diameter. Hence, this results in an increase in the natural frequencies. Analysis and investigation of the natural frequencies and vibration modes may be achieved analytically [Zhu91]. However, it is generally accepted that the fastest most efficient method is the use of evolving FE modelling technologies. Given the influence of stator yoke thickness, it follows that the housing of the stator results in a similar effect. Assuming a perfect contact between stator and stator housing significantly increases the modelled natural frequencies [Cai99] and [Pil99]. However, in practical applications the contact is often located at more specific points such as bolted connections, it is possible that these connections shall increase natural frequencies as well as the potential to introduce new vibration modes. The modelling of endcaps is a difficult process and often ignored [Nev99], in some cases it is modelled separately from the rest of the housing [Mah96]. In this thesis, the endcaps and their connections are modelled, it is found they have a significant impact on the final vibration response.

The stator windings provide difficulty and complications when modelling, dependent on the arrangement and connection. They are often neglected when considering stator vibration modes.

However, [Yon97] and [Lon01] both investigate the influence. The material is typically assumed to be homogenous or a composite material to account for potting and gaps between windings. In SR machines, the typical winding structure is that of concentrated windings allowing for simpler modelling and analysis. It is determined by Long [Lon02] that for a 6s/4r SR machine, the stator windings may be neglected in order to produce the most accurate simulated results for stator vibrations. It is shown that the mass of the windings on teeth reduce the natural frequencies, whilst at the same time through potting add additional stiffness to the model. The effects of each of these phenomena are considered to cancel each other out, and thus the windings may be neglected. In [Lon02] an extensive modelling process is performed so as to identify the most appropriate modelling technique to account for stator tooth windings.

Generally, it is regarded that the damping ratio for SRMs is relatively low and has little to no impact on the natural frequencies of the stator and machine. Rather, the damping ratio applies to the amplitude of vibrations and the decaying nature of the oscillations. The damping factor of specific machines are derived with use of FE modelling and experimental methods in [Gab99b] and [Nev99]. This is a simple procedure for simple structures such as unwound stators or laminated rings, as complexity of structure increases the modelling of damping ratio becomes more difficult. As such, the influence of damping ratio has not been heavily investigated for complicated structures. Furthermore, it is considered that in order to achieve accurate results, a combination of experimental and simulated analyses is required. That is to say, the machine must already be manufactured in order for it to be characterised, and thus, the damping ratio cannot be predetermined for any machine. The damping ratio can also be considered as part of a mass-spring-damper system, as found in [Tan97], [And97], [Mah96] and [Wu93].

1.2.5 Noise reduction techniques

The focus of this thesis and study is to investigate parameters influencing the acoustic noise and vibration characteristics of SR machines. Historically, there has been a focus on current control strategies as well as structural designs in order to minimise the acoustic noise and vibration whilst maintaining reasonable torque production. More recently, a second machine type has been derived from the SR machine, a variable flux reluctance machine (VFRM). The review of noise reduction strategies can be outlined as follows:

- Random turn-on and turn-off;
- Random PWM;
- Active vibration cancellation (AVC);
- Geometric design – windows, yoke bolstering;
- Variable flux reluctance machines;
- Radial force sum minimisation.

In terms of noise and vibration reduction in SR machines, one of the earliest found strategies is proposed by Cameron et al [Cam92]. The idea of ‘dither’ is introduced to the turn-on and turn-off times, randomly shifting the switching angles by 0° or $+1^\circ$ mechanically. In random varying of the turn-on and turn-off angles the level of excitation in natural frequencies is said to be reduced, and this is then confirmed in later studies [Bla94]. However, there is little information on this confirmation, and based on other works such as [Wu93], it is determined that the variance in turn-off is most effective and thus the random turn-on and turn-off would only provide a low level of reduction. [Bla94] also introduces the possibility of noise reduction via random PWM switching. The influence of this strategy applies to the switching frequencies only, by spreading the switching frequency across the spectrum and thus reducing excitation levels of natural frequencies. However, this is also shown to not reduce acoustic noise significantly. Furthermore, it is possible to utilise a switching frequency above 20kHz, and hence, not excite any natural frequencies in the audible range.

One of the most popular and notable methods of acoustic noise and vibration reduction in SRMs is the active vibration cancellation technique [Wu95]. Wu and Pollock developed a method that seeks to reduce the vibration response via the introduction of an antiphase oscillation that counter acts the natural oscillation at turn-off. With a prior understanding of the stator vibrations and natural frequencies of the stator, a controlled step may be applied to the voltage that shall induce an additional vibration response. The second oscillation induced by the step opposes the acceleration produced by turn-off, and thus, reduces the total vibration response. The anti-phase vibration is determined by the opening of the switch for a second step, the time step determined by half the frequency of dominant oscillation. This methodology is referred to as a ‘2-stage’ cancellation technique, most commonly implemented with the use of an asymmetric half bridge circuit [Pol97]. This technique is well regarded and simple to implement, but there are disadvantages associated. The technique is limited by its ability to only introduce an anti-phase oscillation at a single targeted frequency, typically the dominant frequency. Furthermore, the time delay is defined by the speed of the motor and hence, the technique is heavily dependent on accurate speed calculation and feedback. An illustration of the active vibration cancellation technique can be found in **Fig. 1.6**.

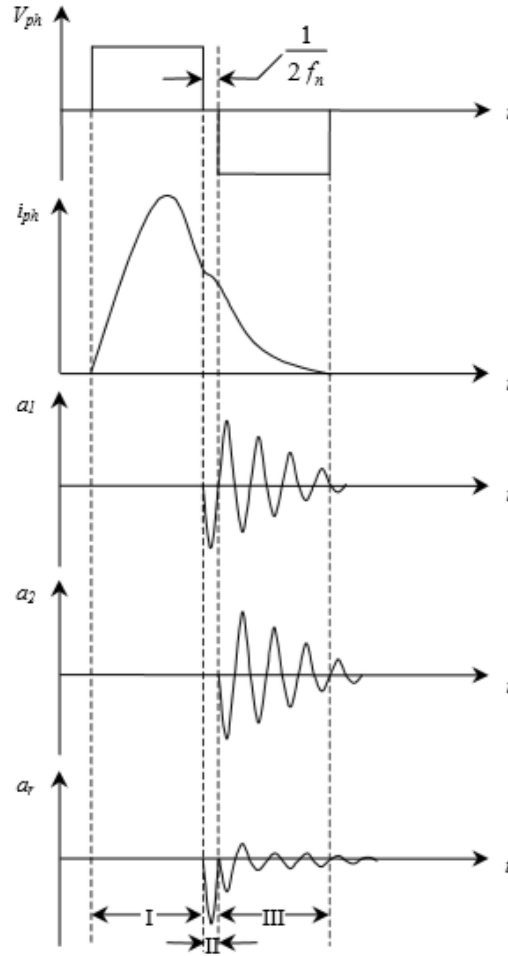


Fig. 1.6 Representation of active vibration cancellation, as illustrated in [Lon02].

Further to control strategies for reducing the acoustic noise and vibration in SR machines, there are also a number mechanical and geometric technologies that can be implemented. One such technique is the introduction of stator spacers between stator teeth [Ras01] and [Gie01]. These support the stator structure and the stator teeth, stiffening the structure and reducing the level of vibrations. The impact of skewing has also been investigated in [Gan15] with the target of torque ripple minimisation, as well in [Yan13] for a single phase SRM. Simplifying the study in [Yan13], it works on the principle of graduating the change in radial force, considering the severity of radial force change is considered to be a significant factor in acoustic noise and vibration production. [Cho07] utilises pole optimisation in order to reduce torque ripple also, via the introduction of eccentricity into the stator teeth. Although this may reduce torque ripple and may be considered advantageous for reduce noise, this neglects the introduction of additional vibration modes due to asymmetry. [Mil93] is considered to be a comprehensive and detailed guide to SRMs, and it is commented here that an increased pole arc may aid in reduction of acoustic noise and vibration response. The conception of utilising holes in the stator teeth, similar to flux paths in SR machines, is firstly seen in [Nak02]. More recently this has been developed and optimised for different windowing positions in the tooth, and verified with experimental

analysis [Ela18]. It is noted that in order for this to be a viable option, one must take into account the structural integrity of the stator teeth and the thermal capabilities also.

In recent years, the development of the variable flux reluctance machine (VFRM) derived from an SR machine also shows significantly reduced noise and vibration characteristics [Liu13]. The novel machine is firstly introduced in [Fuk12]. The inherent noise and vibration reduction is demonstrated in [Liu12b] and experimentally verified also. The VFRM shares its topology and doubly salient nature with an SRM, but differs in winding structure. The VFRM is formed with each tooth having a DC winding and 3-phase AC winding. It is operated with a constant DC excitation producing a constant field, and hence, through synchronisation of the DC field and AC field the machine generates a torque. The torque ripple is significantly lower than an equivalent SRM, although it also noted the SRM exhibits higher average torque [Liu12a]. Recently, the development of VFRMs, particularly within the Electrical Machines and Drives group at the University of Sheffield, has resulted in improved torque density, torque ripple reduction, and increased average torque [Hua19a], [Hua19b], [Lee17], [Dex18], [Hua18], [Hua17] and [Zhu17].

Finally, investigation into the optimisation of current profiles from the perspective of radial forces acting on stator teeth has been developed [Tak15], [Kur15a], [Kur15b] and [Bay16]. The study focuses on a high pole number SR machine, 36s/24r, in which the teeth of each phase are relatively close spatially. Typically, the radial force per tooth is investigated when considering the influence on acoustic noise and vibration. However, [Tak15] introduces the consideration of a sum of radial forces acting on each set of teeth, given the windings are concentrated and sequential. The profile of the sum of radial forces is derived, and the 3rd harmonic component eliminated. Therefore, given that the radial force and phase currents are proportional, the current profile may be optimised to eliminate the 3rd harmonic component, provided the current is comprised of the dc, 1st, 2nd and 3rd components only. The resultant current profile and control is shown to be effective in reduction of acoustic noise and vibration. However, it is noted that this method is most effective on electric machines and motors with a high pole number, such that the stator poles are suitably close together. Therefore, the influence of adjacent phases is increased, and thus, the radial force sum of adjacent teeth is not dominated by the central tooth when considering a 3-phase motor. In a 6s/4r SRM, the teeth are significantly separated, and therefore, the method is more difficult to implement and less effective.

1.3 Scope of thesis and contributions

The work and investigations into acoustic noise and vibration reduction has increased recently, given the volatility of PM prices and limited materials. It is accepted that simulation and modelling of acoustic noise and vibration response is a time consuming and difficult task, requiring the combination of many disciplines. The effect of many parts may be neglected in order to produce a time efficient solution whilst retaining an acceptable level of accuracy in results, this is particularly applicable to the modal analysis and modelling. Historically, much of the research into SRMs has focused on the time

domain perspective of current profiling, with focus at turn-on and turn-off instances, and control of steady current through hysteresis control or PWM control.

This thesis seeks to provide an extensive investigation into the modelling of switched reluctance machines from the perspective of both electromagnetic performance and vibration response. Without reasonable electromagnetic performance, the vibration response has no importance. In other words, a silent machine that produces no torque is useless in application. Through thorough modelling and verification, the influence of various current profiling strategies is examined. The contents of the thesis are as follows:

Chapter 2 introduces the finite element model used in all further investigations in this study. Through a systematic process of modelling, the machine is expanded from a simple annular ring through to a full prototype model. Verification of modal analysis is performed at each incremental stage of modelling, to ensure reliable and accurate final results. It also introduces a suitable finite element solution to the bonding of endcap to the stator housing, introducing dual modes into the frequency response of the machine. The introduction of dual modes is verified with experimental hammer and excitation tests.

Chapter 3 verifies the model produced in Chapter 2 under load conditions. Previously, the model has been verified under static testing conditions, the on load operation of the machine introduces multiple factors. In order to verify the suitability of the model, a series of simulations are performed with variations to the current profile. The trends in vibration response are then mapped and analysed experimentally also. The machine is operated under single pulse voltage control so as to avoid any PWM switching frequency which interferes with the natural modes of the stator. Showing good correlation between experimental and simulated trends, it is reasonable to consider future simulations as reliable.

Chapter 4 considers the influence of current control parameters from the perspective of the time domain. The baseline current profile used for verification is expanded, introducing new current components. By introducing variations one at a time, the influence of each parameter may be understood and quantified. Firstly, a slope of constant gradient is introduced to the falling edge of the current profile, similar to that of the inductance profile. Next, the influence of a current step is investigated, the time duration of the step is extended to variable instances before turn-off. The drop in current is kept constant to focus on solely the step in time.

Chapter 5 considers the influence of current harmonic components on the electromagnetic performance and vibration response. Through the decomposition of the baseline unipolar square wave, the current harmonic amplitudes and phases are derived as a Fourier series. For comparison to the baseline, the phase of each harmonic is fixed. Firstly, the baseline is gradually rebuilt with inclusion of an increasing

number of harmonics. Following this, the influences of amplitudes of the DC component, 1st harmonic and 2nd harmonic are investigated and compared.

Chapter 6 concludes the findings and investigations in the previous chapters and number of criteria in current profiling are suggested and their relative influence is examined. Suggestions for future investigations and work are also commented on, in terms of modelling and expansion of work.

The major contributions included within this thesis can be summarised as follows:

1. The modelling and simulation of electric machines for acoustic noise and vibration is a difficult and multidisciplinary task. Following a rigorous and extensive modelling process taking care at each stage of production, it is possible to produce a model which provides reliable results in a time efficient manner for both electromagnetic results and vibration response. Moreover, the influence of endcaps and their connection is investigated, showing the significant influence bolted connections can have in defining the dominant modes in small machines. The significance is such that dual modes may be introduced and the amplitude of response may increase (Chapter 2).
2. The current waveform of a conventional SRM heavily influences the electromagnetic sources of vibration in the stator. By defining a simple baseline (Chapter 3) with verification, the influence of more complex current parameters may be addressed. Considering two separate domains for building the current profile, the number of parameters influencing the profile increases. From the perspective of time domain, some known ideas are verified such as dominant influence of turn-off, as well focusing on the influence of individual characteristics such as slope at turn-off (Chapter 4). Manipulating the current in the frequency domain, the contribution of each current harmonic amplitude on electromagnetic performance and vibration response is investigated.

Publications

- [1]. James Dexter, Liren Huang, Z.Q. Zhu, and X. Vinamata, "Comparison of torque production and design of switched reluctance and variable flux reluctance machines," Int. Conf. on Electrical Machines and Systems, ICEMS2018, 7-10 Oct. 2018, Jeju Island, Korea, pp.1-6.
- [2]. James Dexter, Liren Huang, Z.Q. Zhu, and X. Vinamata, "Comparison of frequency and time domain based current profiling techniques for acoustic noise reduction in switched reluctance machines," Int. Conf. on Electrical Machines and Systems, ICEMS2018, 7-10 Oct. 2018, Jeju Island, Korea, pp.1-6.

Chapter 2 Finite Element Modal and Vibration Analysis

2.1 Introduction

This chapter aims to accurately model the vibration response of a prototype 6-stator-pole/4-rotor-pole (6s/4r) switched reluctance machine (SRM). The structure presented is that of many modern conventional SRMs, with concentrated windings wound on each tooth and an internal salient pole rotor. The SRM is housed with an aluminium casing and no specific cooling measures, such as cooling fins or a water jacket. Hence, the SRM investigated has a relatively simple structure, although the modelling process is still extensive. Specification of the 6s/4r SRM can be found in **Table 2.1**.

Table 2.1 Machine parameters

Machine Parameters	Value	Machine Parameters	Value
Number of phases	3	Stator outer diameter	90.0mm
Number of stator poles	6	Stator inner diameter	47.4mm
Number of rotor poles	4	Stator pole arc	30°
Number of turns per phase	366	Rotor pole arc	32°
Winding resistance	3Ω	Rotor & stator yoke thickness	8mm
Stack length	25mm	Air gap	0.5mm

Any object shall exhibit a number of natural frequencies, which cause a phenomenon referred to as resonance when excited. In the case of electrical machines, the machines are typically cylindrical in nature as seen for the 6s/4r SRM. The most popular and time efficient method of modal analysis, or natural frequency calculation, is the use of finite element (FE) analysis. FE models are based on the principle of breaking down a complex shape into discrete elements. The influence and behaviour of each element is calculated, and then summed and combined so as to produce a full simulated model of a more complex nature.



(a)



(b)

Fig. 2.1 (a) Cross section of SRM and casing, (b) 4-pole internal rotor.

2.2 Validation of FEA with 2D annular ring

2.2.1 Identification of natural modes and frequencies

In order to successfully design a switched reluctance machine (SRM) for low noise operation it is important to model some key components of noise contribution, particularly the natural modes contributing to mechanical resonances which lead to high acoustic noise and vibration. The FE software used is the ANSYS Workbench package which allows the combinations of the Electromagnetics Suite and the ANSYS Mechanical package, such that the radial forces can be mapped across. Initially a simple annular ring is tested experimentally, then modelled in 2D and 3D to find the natural modes and frequencies. It is excited via a strike from a force hammer, the measured force is then input into the FE software to identify a reasonable damping factor for the material and verify the simple model. These tests are then repeated for the following:

- Laminated unwound stator
- Wound stator in casing framework
- Unmounted machine with endplates attached
- Prototype mounted onto mounting bracket
- Full machine mounted onto test rig

Initially, the natural frequencies and mode shapes (eigenmodes) must be verified in the finite element simulation. In rotary electrical machines the major contributor of noise and vibration is the stator and stator housing, often of a cylindrical nature. It is widely considered that the most dominant forces for noise production are the radial forces in the air gap of the machine. The excitations in the stator produced by these forces are amplified by the natural mode vibrations of the system, referred to as eigenmodes. Eigenmodes are made up of characteristic shapes and frequencies, detailed below for a simple cylindrical structure, **Fig. 2.2**. Under excitation, the forces produced may align with the frequency of a specific eigenmode, causing resonance and increased vibration. The force hammer impact test is a method used to identify eigenmodes and identify dominant modes of the system.

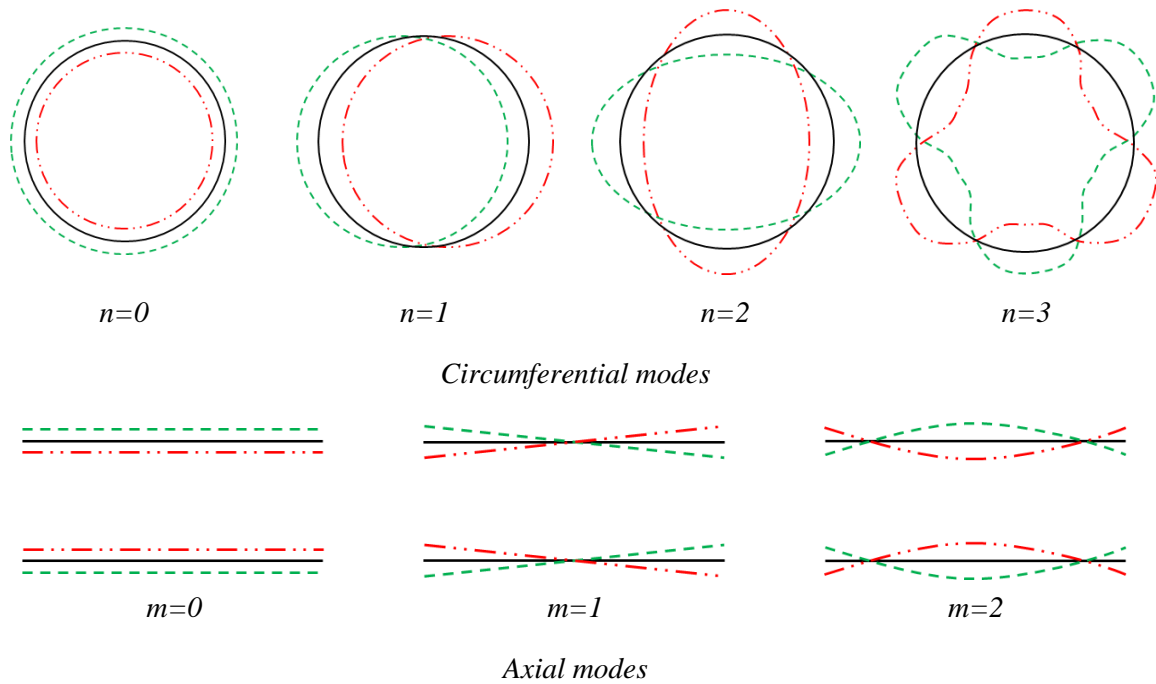


Fig. 2.2 Definition of circumferential and axial vibration modes based on a simple cylinder.

For noise reduction and vibration cancellation techniques, it is important to identify these modes and the frequencies associated with their shapes. Modal analysis is used both experimentally and with FE software, to correctly identify natural frequencies of the prototype machine at different stages of construction. It also verifies the finite element model as a viable method of simulating the potential vibration characteristics of the machine under various excitations, such as impact tests, current impulses, and full 3 phase operation. This can then be expanded, using the model to simulate potential new control strategies or mechanical designs to reduce noise and vibration output. Eigenmodes are categorized by their axial and circumferential mode shapes, defined by m and n respectively, **Fig. 2.2**. The axial and circumferential mode shapes are determined by the number of sine waves in the axial direction and about the circumference respectively, where $m = 0$ denotes a mode shape with no axial deformation but instead a “breathing mode” as an example. Using the example of a simple annular ring, these shapes are heavily dependent on the material, geometry and shape as identified by Rayleigh [Ray49]. The number of eigenmodes of a particular system is infinite. However, this study will focus on eigenmodes in the audible range of the human ear, 20Hz to 20kHz. In general, the circumferential mode $(0, n)$ increases with frequency however it is possible for a lower order mode to appear at a higher frequency.

Before calculating the eigenmodes and their influence with FE software, the experimental data must first be acquired for use as a reference. Due to the nature of simulating noise and vibration it is important to establish a strong baseline and verify the FE results. To do this, multiple hammer tests were carried out to find the natural frequencies and associated amplitudes of vibration. Through the use of a force hammer, the input force can be measured in the time domain then its harmonic spectra can be used in the FE simulation to excite the model as a harmonic response system. The experimental setup can be seen below, **Fig.1.2**, with specifications found in **Table 2.2**.

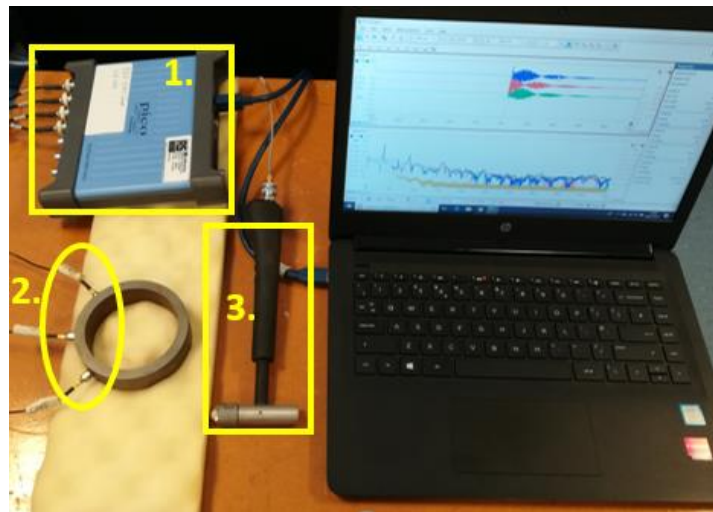


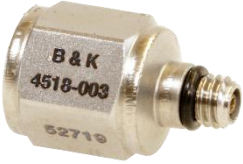
Fig. 2.3 Experimental setup for impact hammer test.

Table 2.2 Equipment and sensors (Fig. 2.3)


1. PicoScope

<i>Manufacturer</i>	Pico Technology	
<i>Model</i>	4824	
<i>Channels</i>	8-channel	
<i>Sample Rate</i>	80 MS/s	
<i>Memory</i>	256 MS	
<i>Bandwidth</i>	80 MHz	


2. Acceleration sensors

<i>Manufacturer</i>	Brüel and Kjær	
<i>Model</i>	4518-003	
<i>Technology</i>	Piezoelectric	
<i>Range</i>	+/- 50g	
<i>Sensitivity (@160Hz)</i>	100 mV/g +/-10%	
<i>Mounted resonance</i>	> 60kHz	
<i>Mounting</i>	Adhesive	

3. Force hammer

<i>Manufacturer</i>	Brüel and Kjær	
<i>Model</i>	8206	
<i>Maximum force</i>	4448 N	
<i>Sensitivity (@160Hz)</i>	22.5 mV/N	
<i>Tip attachment</i>	Hard tip	

4. Signal amplifier

<i>Manufacturer</i>	Brüel and Kjær	
<i>Model</i>	Type 2694-B	
<i>Channels</i>	16	
<i>Supported gains</i>	0 dB or 20 dB	
<i>Communication</i>	RS232	

A large number of impact tests were employed across the range of different structures, in order to clearly identify the location of the impact and the output at the accelerometer position the following visual depiction is used throughout:

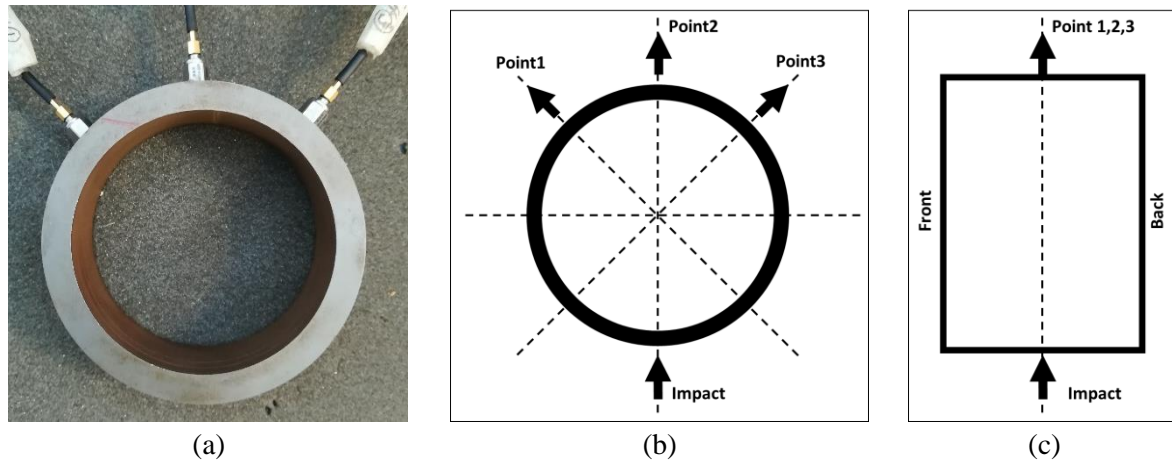


Fig. 2.4 Visual depiction of impact and sensor location.

This shows the circumferential location of the impact as a force acting inwards, and the accelerometers denoted by an arrow out of the system. The axial location is defined with reference to the length of the model shown in **Fig. 2.4**. For tested models, a range of accelerometer and impact locations were tested, focused on identifying the maximum number of circumferential modes. Due to the short stack length of the annular ring, axial modes are unlikely to be present.

The PicoScope allows a high sampling rate suitable for calculating the frequency domain results to a high range whilst retaining reasonable step size. However, this requires careful manipulation of the data to achieve the correct FFT result and produces a large amount of data. It is important to calculate the FFT of both the accelerometer results and hammer forces with a slight negative delay, such that the impulse force is fully captured. It is also vital to allow the acceleration and hammer force signals time to settle, if this time window for calculation is too small then the amplitudes of the vibration results will be misleading. Therefore, the signals are triggered off the hammer impulse with a slight delay and calculated across a duration that allows for reasonable decay of the sinusoidal vibration output. No signal-windowing techniques to improve the quality of FFT (i.e. Hanning) are employed or required at this stage of testing. To verify results and calculated FFT, a dynamic signal analyser (DSA), Agilent 35670A FFT DSA, is used to compare frequency domain results for both amplitude and frequency. This DSA is not suitable for further testing, in particular on load testing, due to the limited time window and frequency range combinations. For example, at maximum resolution of 800 samples, the Agilent DSA will measure up to 12.8kHz for a time range of ~60ms. As the prototype machine is operated at only ~800rpm max. this time range is still too low to see a full electrical cycle.

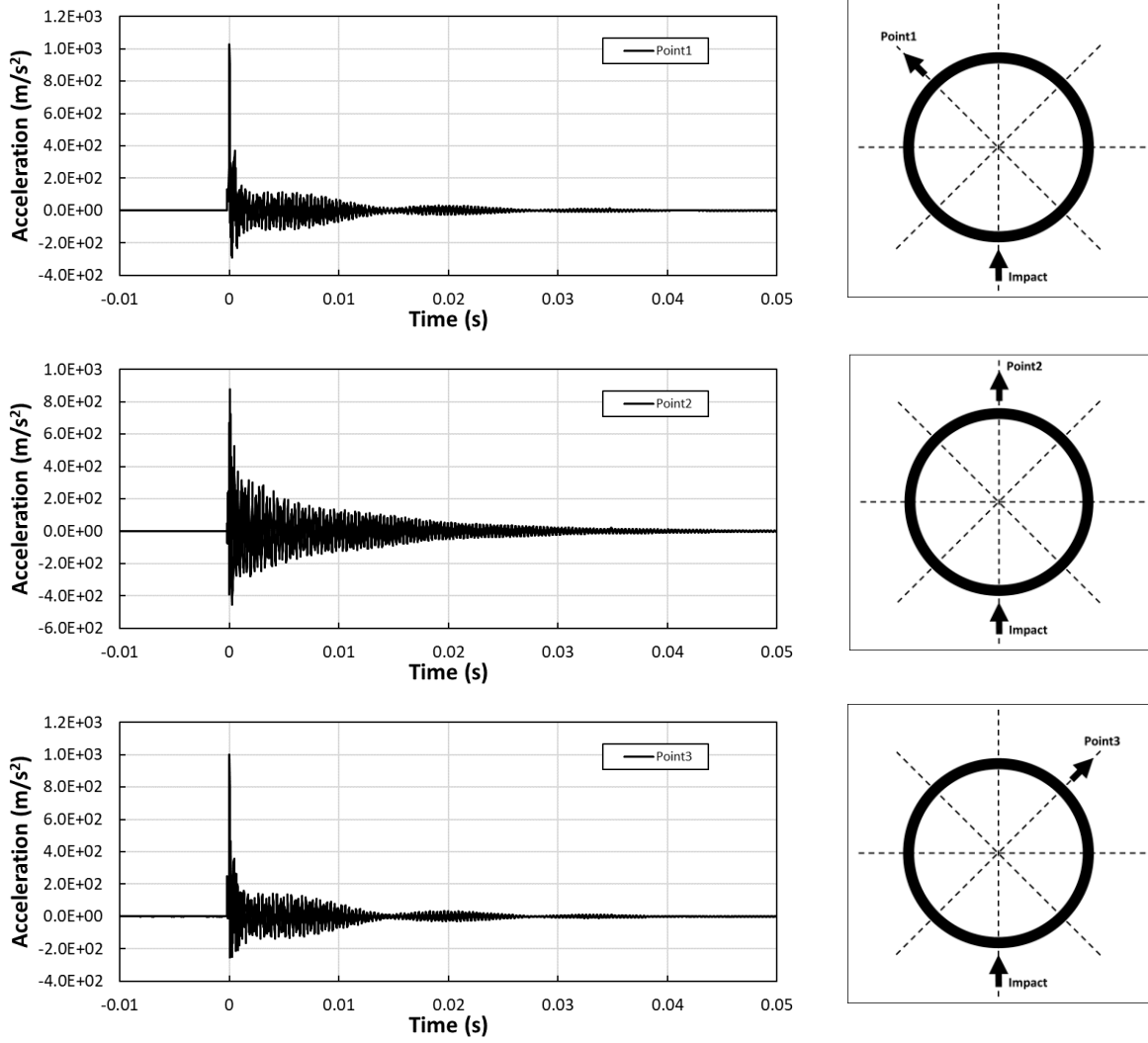


Fig. 2.5 Acceleration response in the time domain for 3 axially central points on the annular ring.

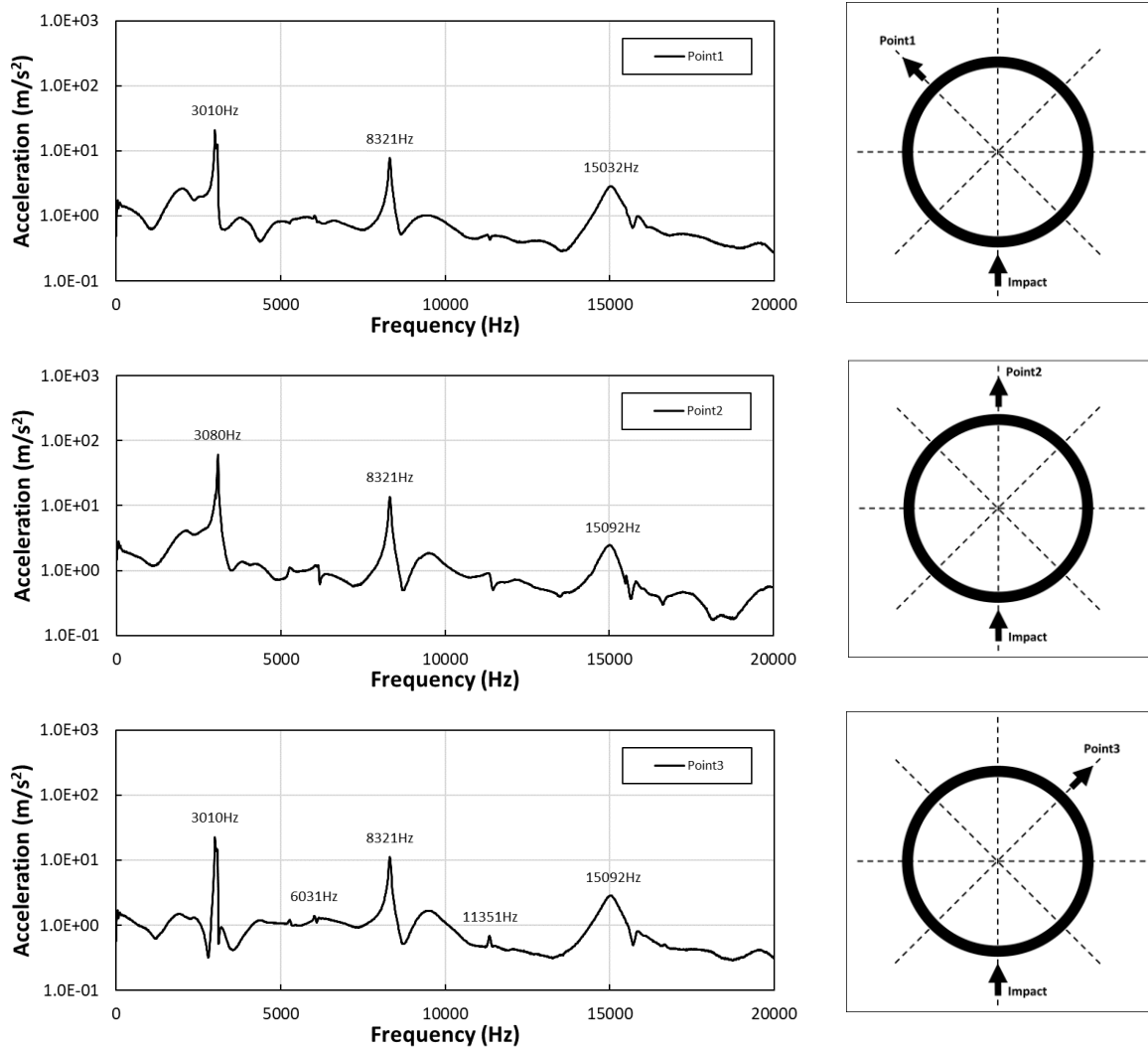


Fig. 2.6 Frequency response of acceleration, measured at 3 individual points on the annular ring, axially central.

2.2.2 2D vs 3D model

Firstly, a simple 2D model of the annular ring is simulated as a time efficient guideline for results. Due to the simplicity of the model this yields reasonable results in a time efficient manner. However, as complexity increases a 3D model is required. Utilising a 3D model allows for consideration of axial modes if required, along with the influence of connections between parts specifically in this study the bolted endcaps. Material properties for the ring are defined from the data sheet with isotropic properties for initial simulations. As can be seen in **Table 2.3** the 2D simulation yields reasonable results for a simple structure. Comparatively, the 3D model increases the simulation time by a minimal amount, and allows observation of axial modes from the modal analysis results. It is also possible to account for the lamination effect in the 3D model via the parametric analysis of material properties including mass density, Young's modulus and Poisson's ratio, to align the experimental natural frequencies with FE.

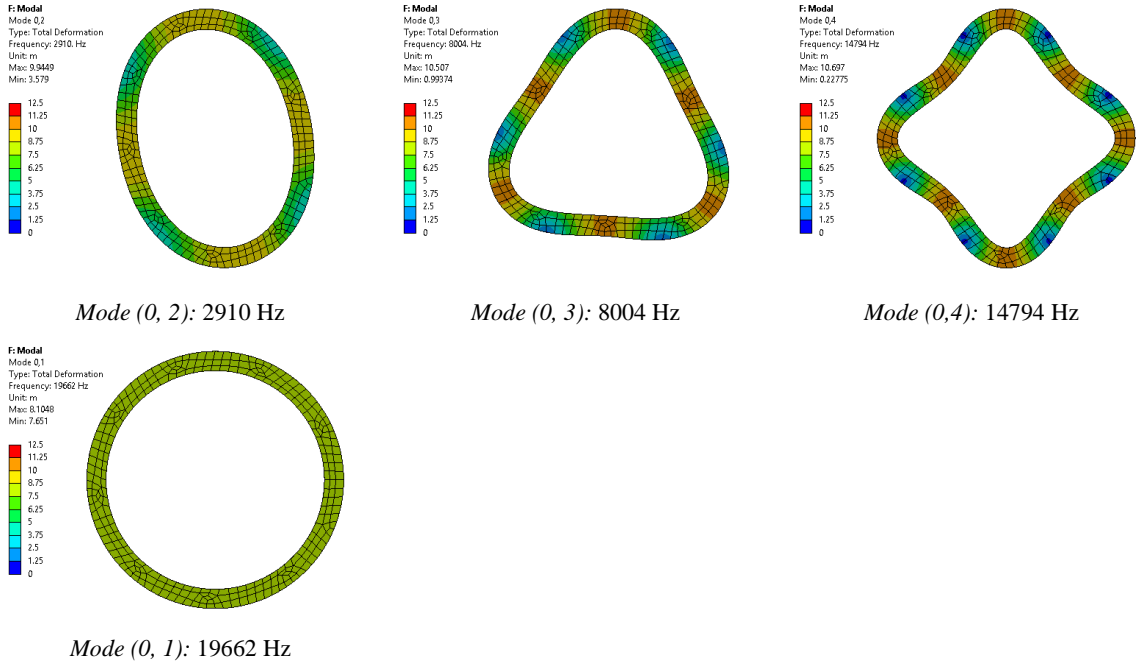


Fig. 2.7 Mode shapes simulated on 2D annular ring.

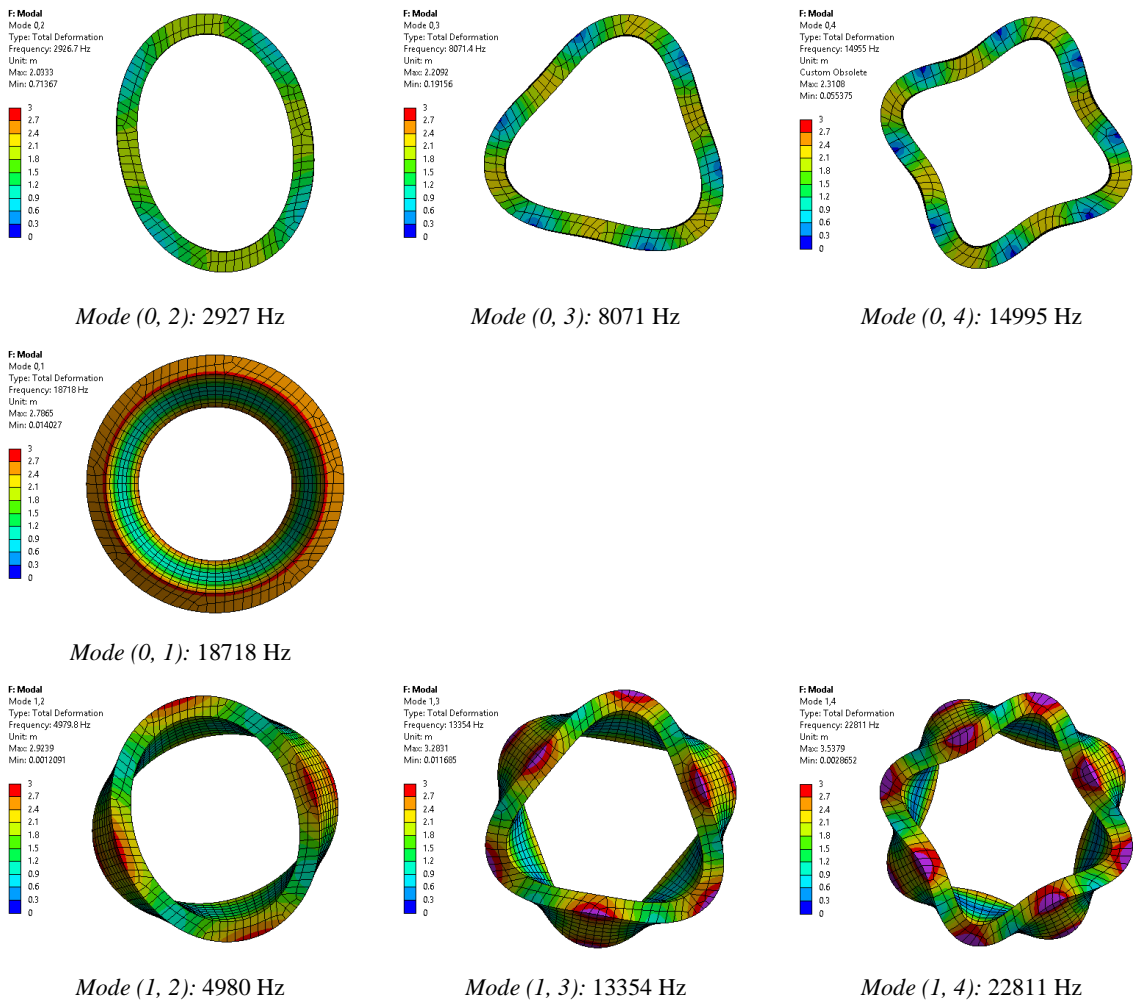


Fig. 2.8 Eigenmodes simulated in 3D, for axial mode $m=0$ and $m=1$.

Table 2.3 - Comparison of 2D and 3D simulated modal analysis on an annular ring

Mode Shape (m, n)	Natural Frequencies, Hz				
	Measured	2D FEA	Error, Hz	3D FEA (<i>Solid</i>)	Error, Hz
(0, 2)	3010	2910	100 (3.3%)	2927	83 (2.8%)
(0, 3)	8321	8004	317 (3.8%)	8071	250 (3.0%)
(0, 4)	15092	14794	298 (2.0%)	14995	97 (0.6%)
(0, 1)	-	19662	-	18718	-

2.2.3 Mesh sizing optimizations

A convergence study is used to ensure that the simulated results from the FE software are accurate for an optimal computation time. To achieve this, the software package offers multiple meshing variations suitable for a wide array of applications. The meshing method for analysis in this study is a mechanical mesh with quadrilateral (8-dot) node assignment, as shown in **Fig. 2.9**. It is common practice for mechanical and structural analysis to use a hexahedral mesh creating cuboid elements, as opposed to traditional meshing in electromagnetic applications where a prism mesh is beneficial. Implementing the 8-dot quadrilateral meshing allows for the element number to be kept low, whilst increasing the node number. As forces are applied to the nodes and the response is also measured from the nodes it is a useful technique to minimise the element number, thus saving computation time.

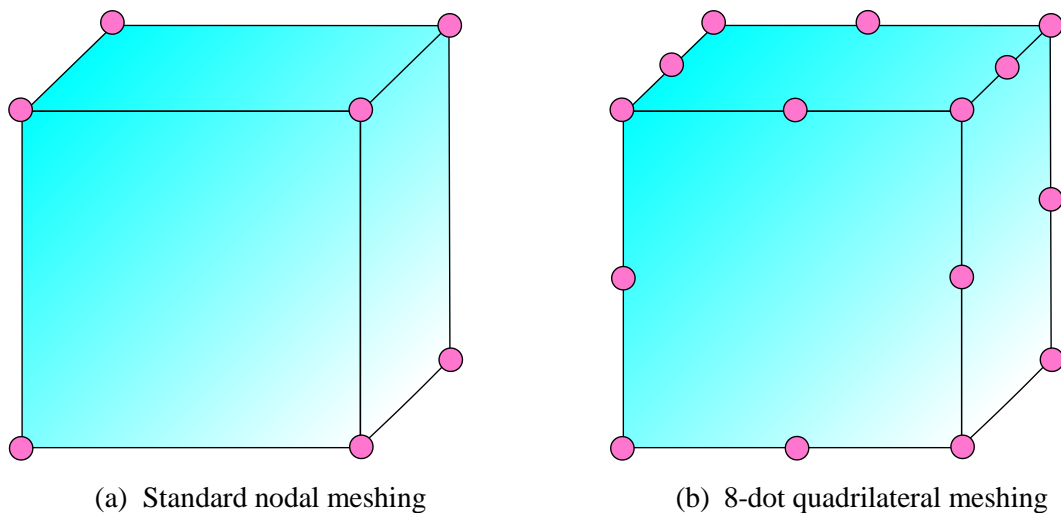


Fig. 2.9 Meshing standard utilised in modelling.

To optimize accuracy of results whilst retaining an acceptable simulation time, different meshing assignments are compared, specifically:

- Automatic meshing, defined by element size for each object.
- Edge sizing, defined by either the size of elements on each edge or the number of divisions per edge.

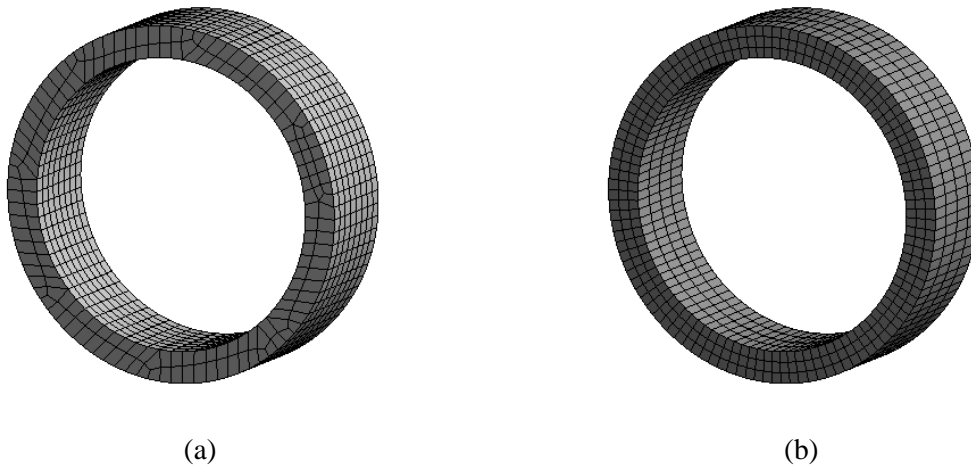
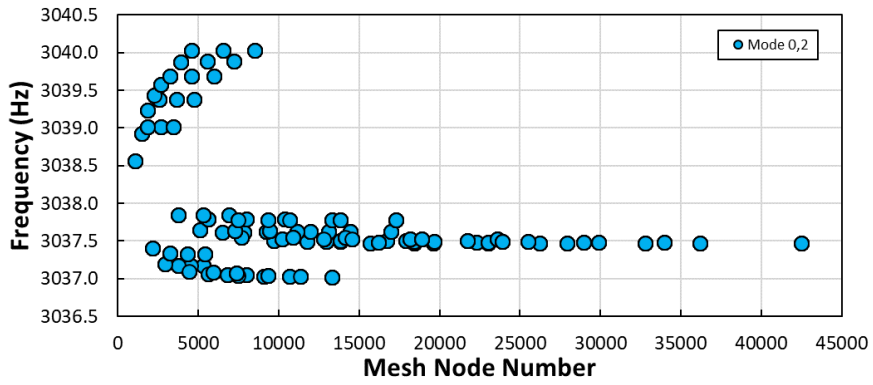
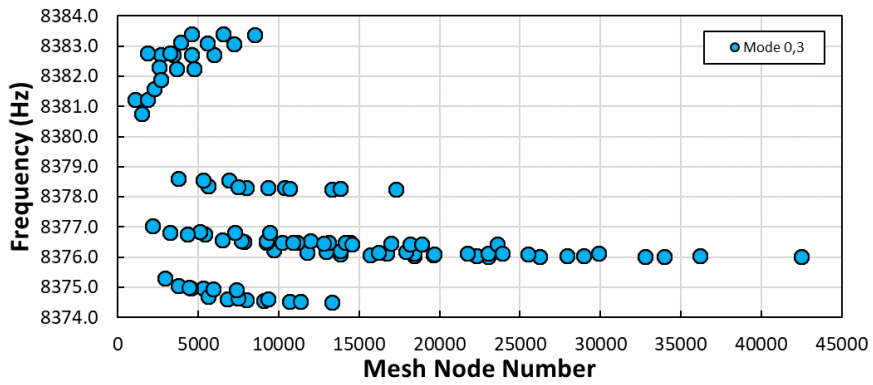


Fig. 2.10 (a) Automatic meshing with size limitation (b) Meshing defined by divisions per edge.

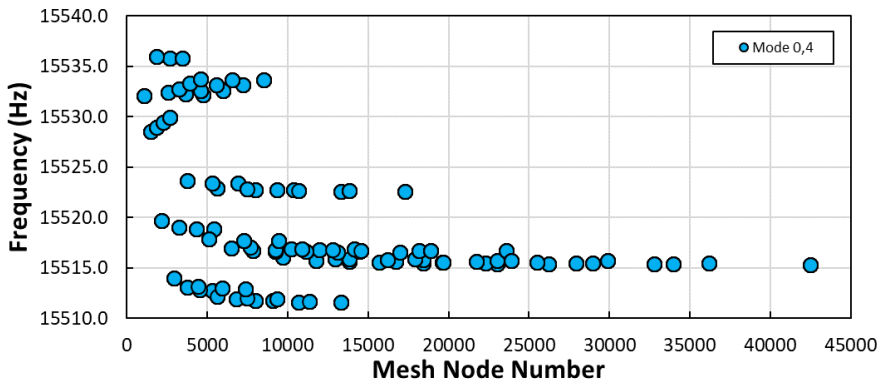
Utilizing the automatic meshing for an edge or part allows for fast assignment and meshing. However, the element shaping is less uniform leading to potential asymmetries in meshing. The size is specified as a targeted element size, with a tolerance, and it is also limited by the general mesh size settings. Due to the potential for various element sizes and asymmetries, this method will not be used to optimize the 3D mesh. Instead, a more rigorous uniform meshing method is selected. Edge sizing can define either the target element length, or the number of divisions across an edge. For the same reasons as mentioned previously, the number of divisions is the method used for optimizing the mesh. Therefore, by splitting the model into parts, the mesh divisions can be predetermined for each edge individually, resulting in a uniform symmetrical mesh. These divisions are then varied between two values specified in **Table 2.4**, and the minimum frequency result for each mode is calculated. As mesh density increases the frequency for each mode reduces, until the density is saturated such that the frequency is stable. Hence, results in the constant natural frequency range are optimized based on minimum element and node number, thus minimal computation time. The mesh node number directly correlates to the computational time required to solve the model for modal analysis. As this is the base model for harmonic response analysis, a time save through minimum number of mesh nodes is amplified into for future analysis. A typical modal analysis for this ring takes approximately 20 seconds. However, the final complete motor is approximately 4 minutes for modal analysis and a further 1 hour for harmonic analysis. The convergence results are shown in **Fig. 2.11**, with the bottom left quarter of each graph containing potential optimal mesh combinations for reliable results and minimal computational time.



(a)




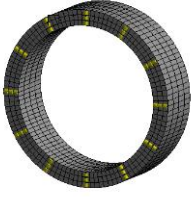

(b)



(c)

Fig. 2.11 Mesh convergence for annular ring, showing (a) Mode (0, 2), (b) Mode (0, 3), (c) Mode (0, 4).

Table 2.4 – Mesh parameters and results

	Radial Divisions	Min. Divisions = 18	Max. Divisions = 90	Optimal: 54
	Yoke Divisions	Min. Divisions = 2	Max. Divisions = 6	Optimal: 5
	Stack Divisions	Min. Divisions = 2	Max. Divisions = 8	Optimal: 4

2.2.4 Refinement of material properties

Finally, initial results indicate a reasonable alignment for natural frequencies particularly for the modes focused on where $m = 0$. However, the damping factor and amplitudes must also be considered, along with further fine tuning with material properties. Firstly, the Young's Moduli in each plane are defined as E_x , E_y , and E_z , Shear Moduli defined as G_{xy} , G_{xz} , G_{yz} and Poisson's Ratio ν_{xy} , ν_{xz} , and ν_{yz} .

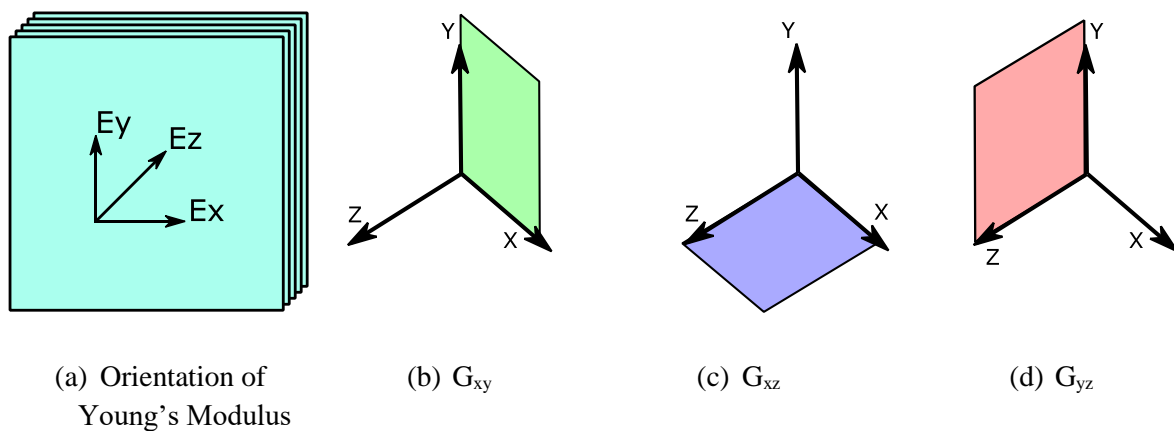


Fig. 2.12 Young's Modulus and Shear Modulus plane definitions.

Determining the effective properties of an anisotropic material can be a difficult task, further complicated by the welding of laminations under specific clamping pressure. To make the task achievable some assumptions must be made. Initially, the mass density of the material is measured by weighing the laminated ring and calculating experimentally. It is found to be slightly lower than the data sheet specified as 7650kg/m^3 , down to 7350 kg/m^3 . Beyond this, the first assumption considers the X-Y plane variables of the material properties to be unchanged given that the laminations are stacked in the Z-direction. As the Poisson's Ratio is a measure of elongation in a direction against reduction in cross sectional area, this is assumed not to change in any plane for this study. The influence of welds in the axial directions is beyond the scope of this study, but it can be noted that in the event of a stress in the Z-direction the stress will act not on the laminations but on the welds. For the Young's Moduli in the X and Y-direction, these are considered to be the same as specified for MH330-35A. However, E_z is assumed to be lower than the specified. This can be attributed to discontinuities between individual laminations. The Shear Modulus is more complex, with G_{xy} denoting any deformation seen in the X-Y plane but caused by the X-Z and Y-Z stress. As this is influenced by planes in the direction of the stack it can be concluded that G_{xy} will be reduced. By similar logic, G_{xz} and G_{yz} are deformations seen in the X-Z and Y-Z planes respectively, these are assumed to be equal to each other but lower than G_{xy} . Convergence for the material parameters is calculated via parametric simulations with a target of the experimental natural frequencies for modes $m=0$, $n=2$ through 4 with a material mass density of 7350kg/m^3 . It is found that there is a small variance in Young's Modulus in the Z-direction. However, a more significant change in the XZ and YZ-planes of Shear Moduli, caused by the effect of the lamination stack and welding not directly modelled in the FE simulation.

Table 2.5 Original material properties of M330-35A steel

Mass Density	7650 kg/m^3
Poisson's Ratio	0.3
Young Modulus, E	210 GPa
Shear Modulus, G	80 GPa

Table 2.6 Finalised stator material properties from parametric study and resultant modes

Material Properties				Natural Frequencies, Hz (% error)		
E_x & E_y	E_z	G_{xy}	G_{xz}/G_{yz}	Mode (0, 2)	Mode (0, 3)	Mode (0, 4)
210 GPa	200 GPa	74.0 GPa	10.3 GPa	3008 (0.07%)	8342 (0.25%)	15409 (2.10%)

The final verification of finite element analysis determines the damping factor for eigenmodes such that the measured acceleration correlates with the amplitude of predicted results. To achieve this, the simulation is modelled as a harmonic response system based on modal superposition. The modal results gathered thus far are used to simulate an input force obtained from the force hammer, applied in the frequency domain. There are many methods for calculating damping factors including the -3dB method. In this case, a parametric sweep of damping factor in FE is used to align amplitudes with experimental results. However, due to the nature of the annular ring and force hammer available, the frequency domain impulse of the force hammer is only reliable up to 5kHz as demonstrated from the harmonic response of the input force, shown in **Fig. 2.13**. Furthermore, it is considered that the damping factor will vary with frequency, such that each mode may have a different damping factor. For the purpose of these simulations and this system, the damping factor will be assumed to be a constant damping factor for the system, verified for mode (0, 2) which falls in the constant region of the impact hammer. It is noted that in reality this damping factor will not be constant across the frequency ranges measured in this study.

This modelling methodology verifies the accuracy and reliability of the FE software, a process repeated at each construction stage in order to obtain reasonable simulation results for a full system under operating conditions. Based on the evidence and study thus far, it is concluded that the material properties of the MH330-35A annular ring are specified in **Table 2.7**.

Table 2.7 Material properties for M330-35A steel laminated stator

Mass Density	7650 kg/m ³
Poisson's Ratio	0.3
Young Modulus, E _x	210 GPa
Young Modulus, E _y	210 GPa
Young Modulus, E _z	200 GPa
Shear Modulus, G _{xy}	74.0 GPa
Shear Modulus, G _{xz}	10.3 GPa
Shear Modulus, G _{yz}	10.3 GPa
Damping factor	0.0012

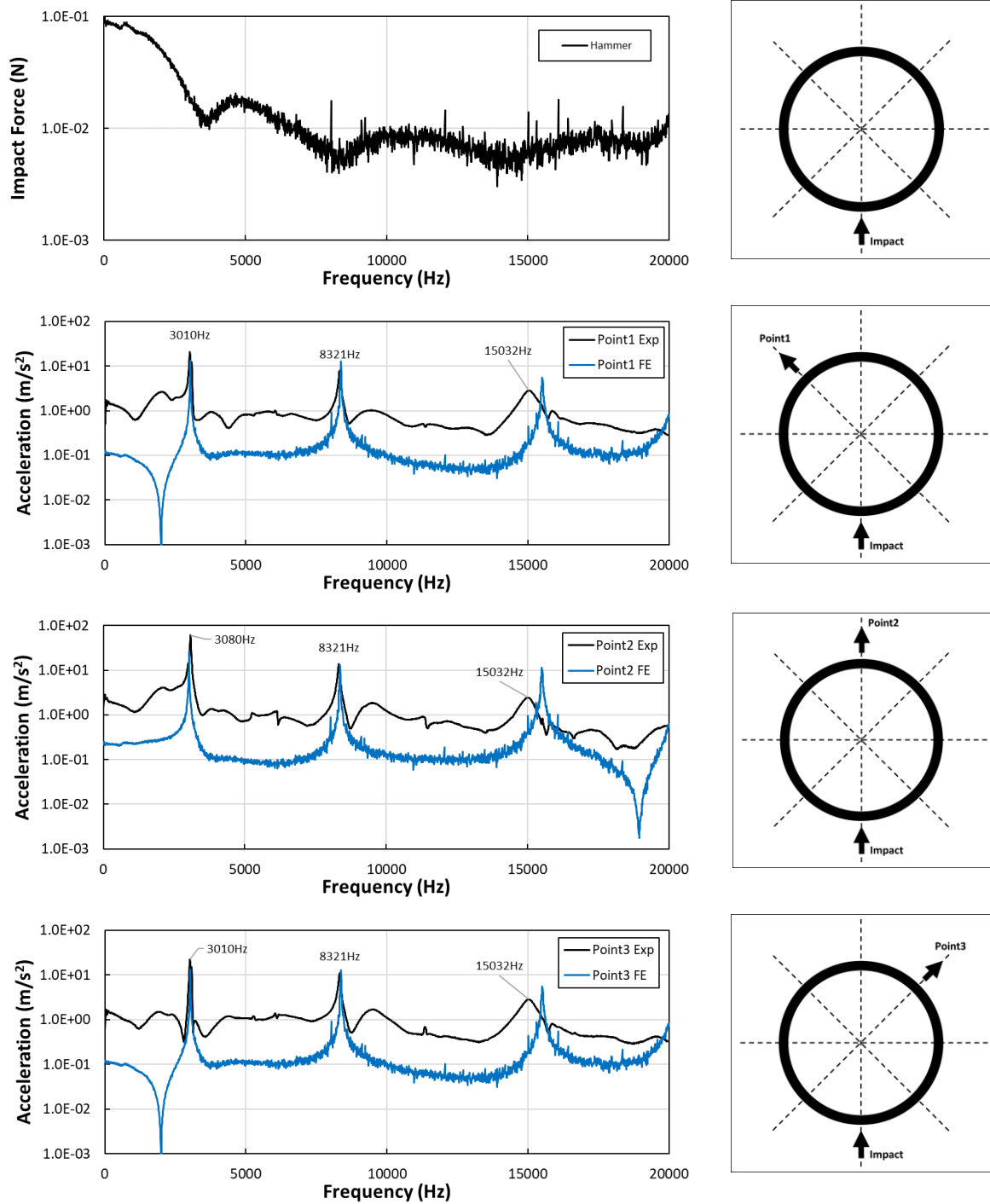


Fig. 2.13 Comparison of experimental impact test and FE simulation for damping factor of 0.12%.

2.3 Influence of teeth and verification of stator mechanical properties

2.3.1 Stator parameters and introduction

Further to the study of the laminated annular ring, the stator teeth are introduced to the design. This adds complexity and influences the eigenmode frequencies, due to the asymmetry of the new system. This study focuses on a 6-pole stator, assumed to have no eccentricities and a uniform air gap, but due to the addition of poles to the ring, dual modes are separated and identifiable individually. In general, when compared to the annular ring, the introduction of poles into the system will increase the acoustic noise and vibration. It is worth noting that this is not only caused by the additional modes from asymmetries, but also caused by the lowering of natural frequencies which have the potential to then introduce more modes into the audible spectrum. The stator has been modelled on the specification in **Table 2.1**. This unwound stator matches the prototype and shall be used for all subsequent testing.

2.3.2 Identification of modes

As with the laminated annular ring, it is pivotal to correctly identify and locate the eigenmodes of the stator. These will differ from the annular ring due to the asymmetries introduced with the teeth, and also the additional mass added to the system. Firstly, the hammer test is repeated to find the frequencies of new modes and find any potential new peaks introduced into the audible frequency range. Mode 5 is introduced into the frequency range (15889Hz), although minimal in amplitude, along with asymmetric modes identifiable for variations of mode 3, with zero axial attenuation ($m=0$). Furthermore, the symmetrical and asymmetric modes can be classified by **Fig. 2.14**, relating to the movement of poles in particular modes. [Lon01] demonstrates that as the number of poles introduced increases both symmetrical and asymmetric modes will be reduced significantly, with relation to the natural frequencies, where the symmetrical modes are less affected. This effect is shown in the table of comparison between the annular ring and 6-pole stator, **Table 2.8**.

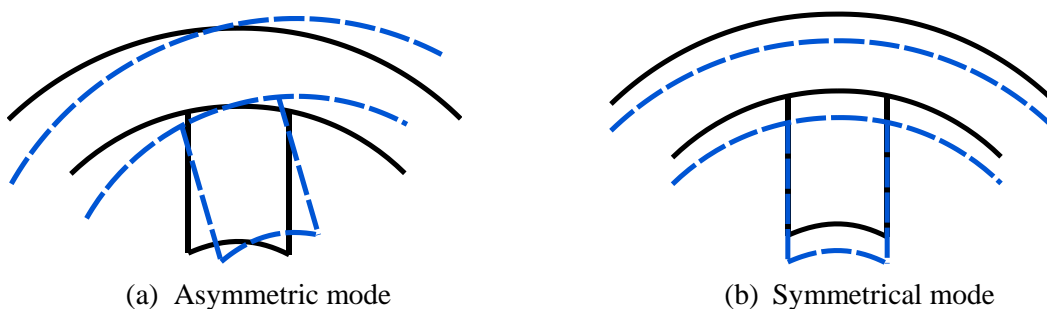


Fig. 2.14 Symmetrical and anti-symmetrical vibration modes denoted by m, na and m, nb respectively.

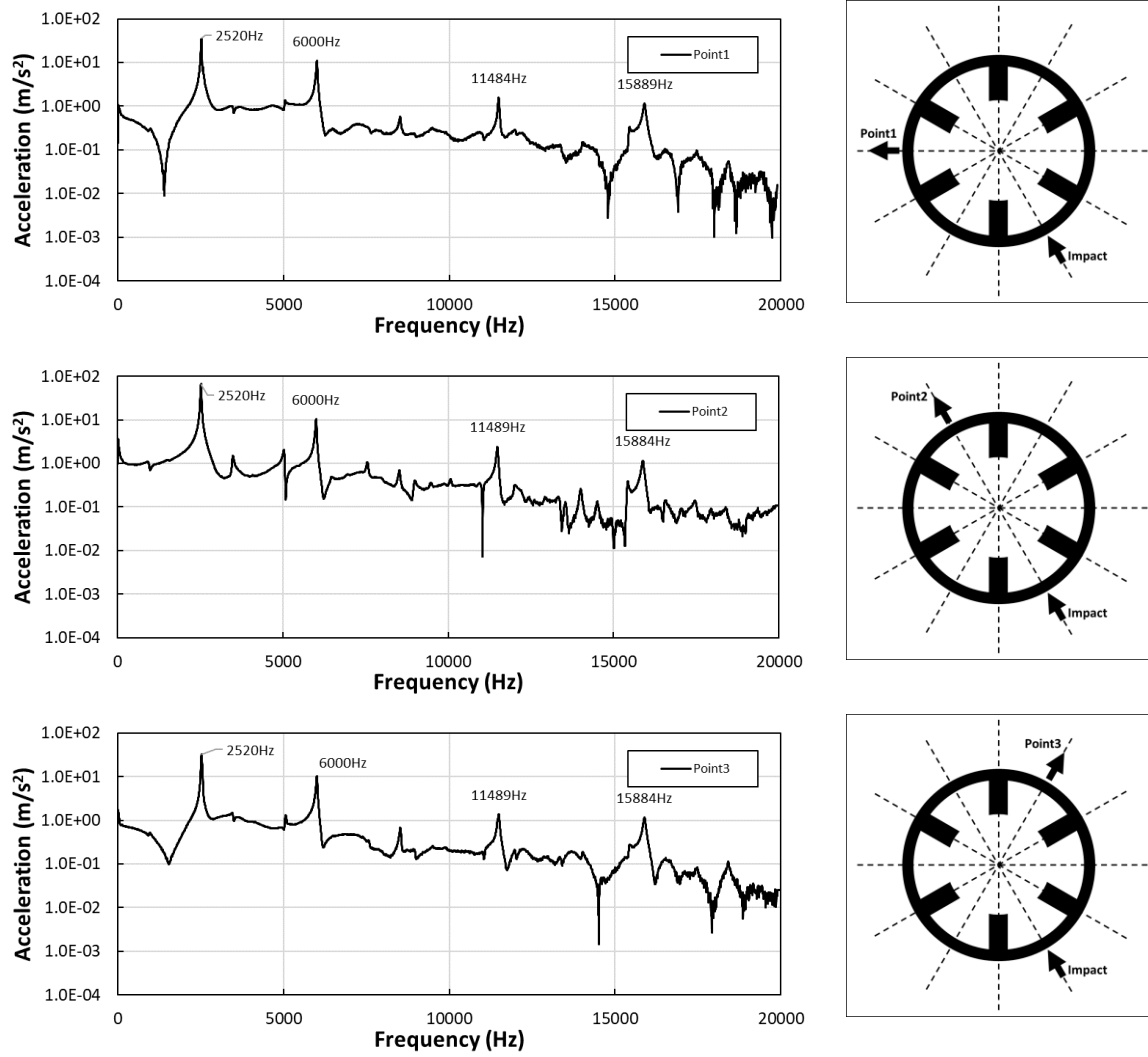


Fig. 2.15 Vibration response for accelerometers placed behind slots with an impact force applied behind a slot.

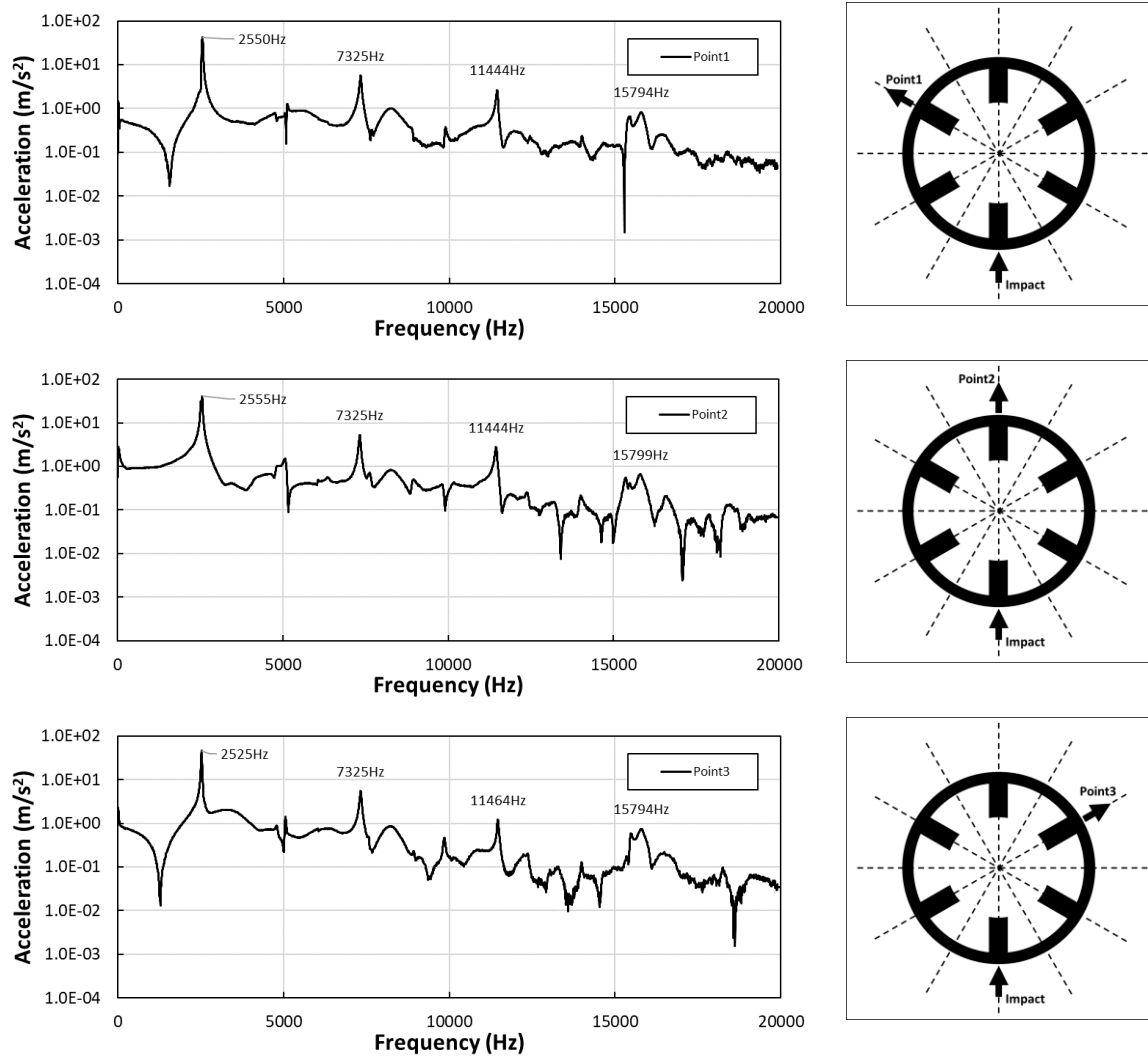


Fig. 2.16 Vibration response for accelerometers placed behind teeth with an impact force applied behind a tooth.

Mode (0, 3a) can be considered as a mode 3 shape with maximum deformation behind the slots, whilst mode (0, 3b) is of mode shape 3 with maximum deformation behind teeth. From the experimental hammer test, it is possible to excite mode 3a with a strike behind a slot and identify it with an accelerometer positioned behind a slot also. In this case, mode 3b will not be seen in the response as the deformation behind slots for mode 3b is zero because the slot falls between two maximums. The opposite can be said for measuring mode 3b, where the impact occurs behind a tooth and the response is measured behind other teeth. These teeth exhibit maximum deformation for mode 3b but minimum deformation for mode 3a. Hence, it is a simple test to separate these two mode shapes. The hammer test indicates a reduction in frequency for eigenmodes with axial order 0, caused by the increase of mass to the system.

Table 2.8 - Modal frequencies for annular ring and stator of equal dimensions

Mode Shape $0, n$	Natural Frequencies, Hz	
	Annular Ring	Laminated Stator
2	3010	2520
3a	8321	6000
3b	-	7325
4a/b	15032	11489
5	-	15884

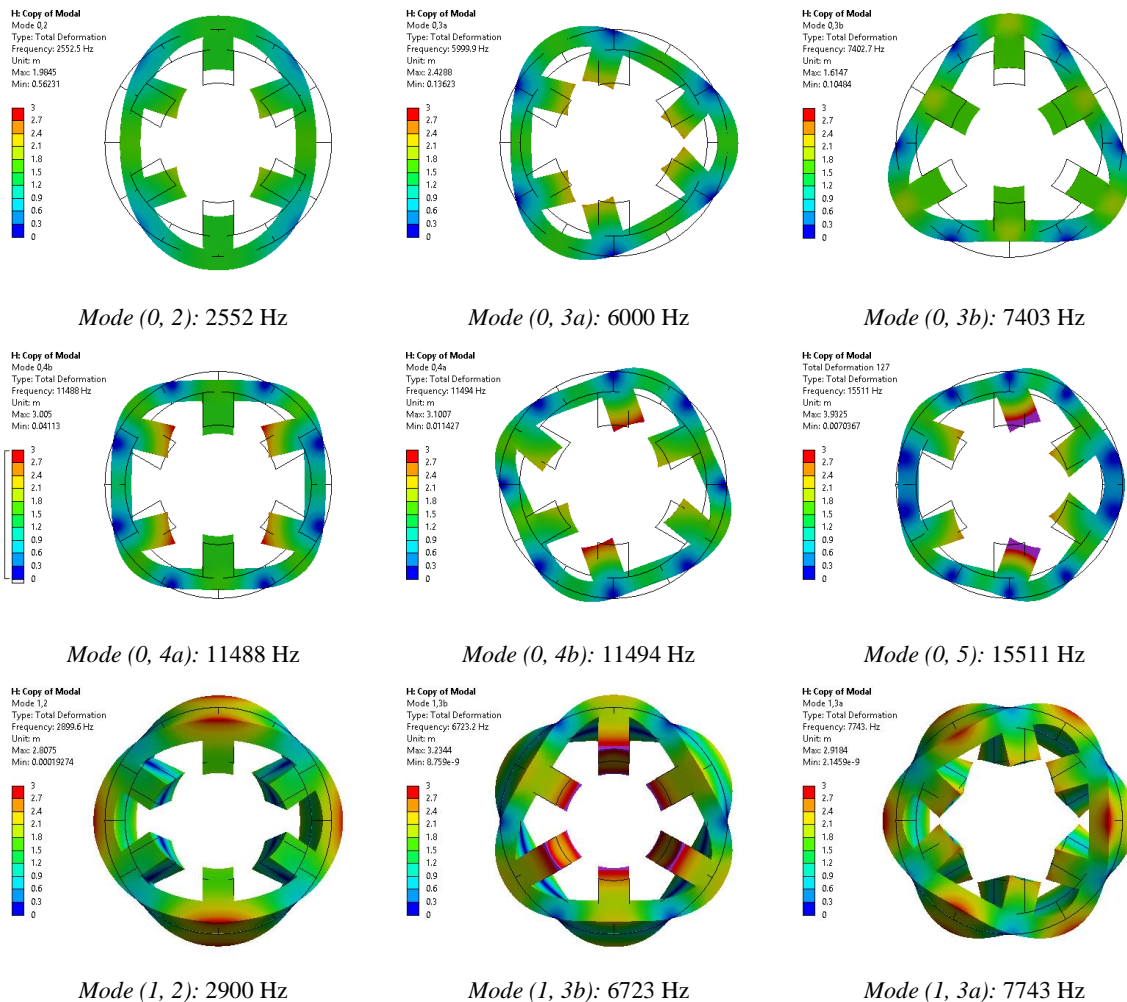
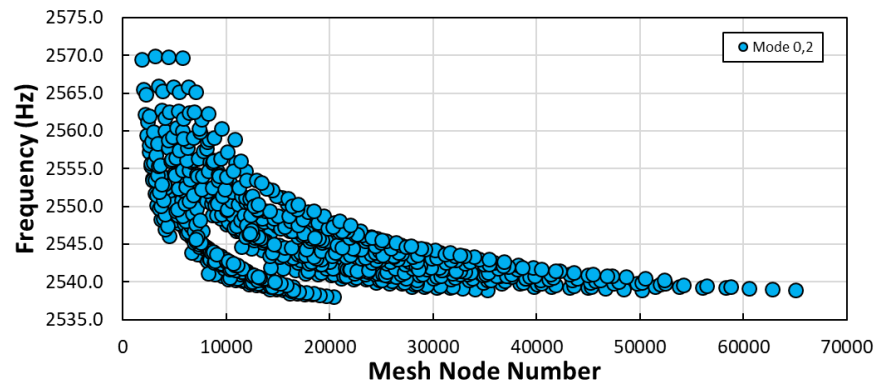


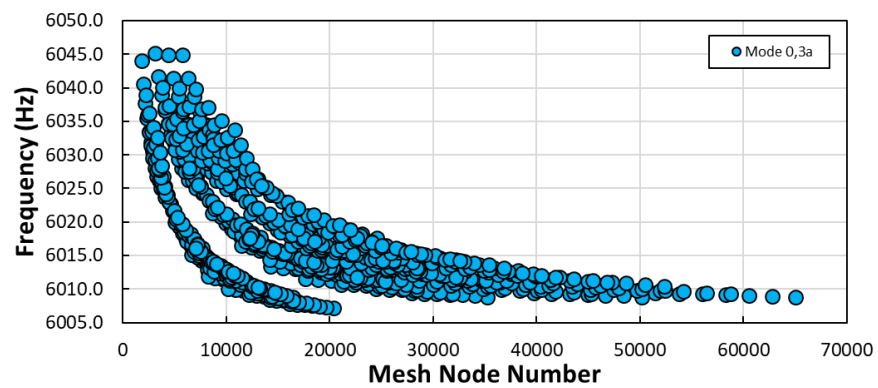
Fig. 2.17 Stator eigenmodes simulated in 3D, for axial mode $m=0$ and $m=1$.

The influence of the addition of poles to the annular ring is clear. Hence, a new FE study is derived where the mesh shall be recalculated and material properties reassessed for the laminated stator. Therefore, in similar fashion to the annular ring, a convergence study is performed for optimal mesh

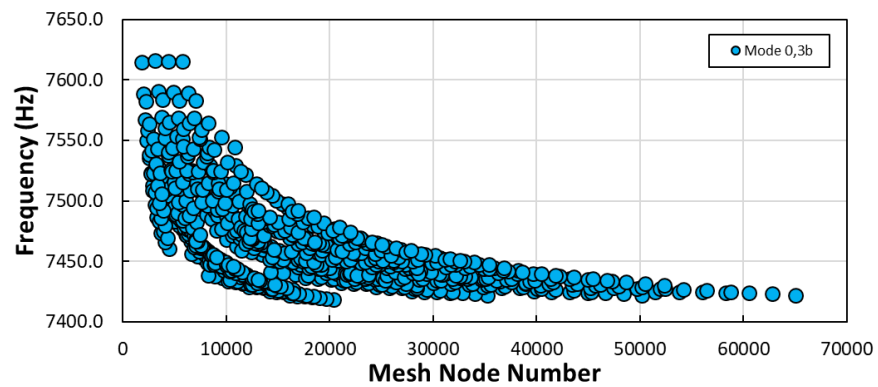
and material properties to match natural frequencies found in the hammer test study. As discussed previously, the optimal approach used in this convergence is defining the target edges of the model and perform a parametric optimization of the mesh. Therefore, the optimal mesh is derived from the number of divisions in the back-iron, stack length, stator yoke and pole height. A uniform mesh is advantageous to the structural analysis, and hence, the ratio of divisions in the pole tip to back iron, for one pole, is equivalent to the pole pitch, in this case 0.33. Finally, the convergence results and final mesh are shown in **Fig. 2.18**, these results are used to implement a study of material properties to confirm results found for the annular ring.



(a)



(b)



(c)

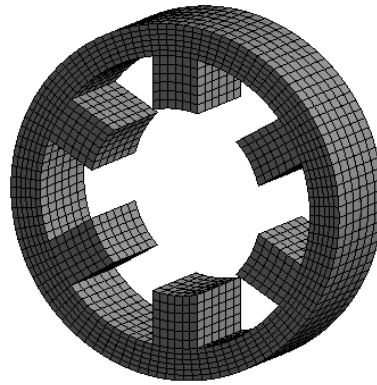
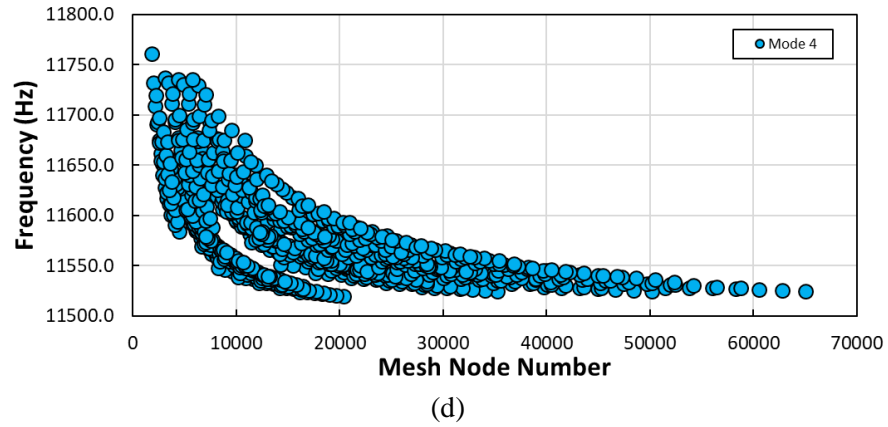


Fig. 2.18 Mesh convergence for stator, showing (a) Mode (0, 2), (b) Mode (0, 3a), (c) Mode (0, 3b), (d) Mode (0, 4), (e) Final meshed stator model.

Table 2.9 Final modal results for laminated stator with refined mesh

Mode Shape (m, n)	Natural Frequencies, Hz		
	Measured, Hz	3D FEA, Hz	Error, Hz (%)
(0, 2)	2520	2552	32 (1.3%)
(0, 3a)	6000	6000	0 (0.0%)
(0, 3b)	7325	7403	78 (1.1%)
(0, 4)	11489	11494	5 (0.04%)
(0, 5)	15884	15511	373 (2.3%)

It is established within this study that FE modelling for the stator is a reasonable prediction for the natural frequencies of key eigenmodes, with focus on modes with $m=0$. To verify the use of the predicted results for further analysis, the amplitudes of the natural modes must also be calibrated against the experimental results. The force hammer is limited for the maximum frequency range the impact

force can be applied to, and to maximize this range a metallic tip is used. From the hammer impact, **Fig. 2.19(a)**, it is concluded that only mode 2 falls into the reliable range of input force. Therefore, the damping factor for the system is optimized for mode (0, 2) only. A parametric sweep of damping factor with a target of matching mode (0, 2) amplitude yields a constant damping factor of 0.5%. The results, **Fig. 2.15** and **Fig. 2.16**, show a strong match for the simulated results on a relatively simple structure, both for amplitude and frequency. As the stator modes are the dominant influence on the vibration modes of the full prototype, this shows the suitability of simulations to analyse methods of reducing vibrations in this SR machine. It should be noted that as the complexity of the machine increases the match between experimental and FE results diverges. This is caused by more complex mechanical boundaries, environmental parameters such as temperature and assumptions that must be made in order to produce a time efficient method for estimating the vibration response. Simulating the response under on-load conditions is also heavily dependent on the calculation of forces in the electromagnetics, in the case of hammer tests the force applied may be directly taken from the test results leading to good correlation between FE and experimental results.

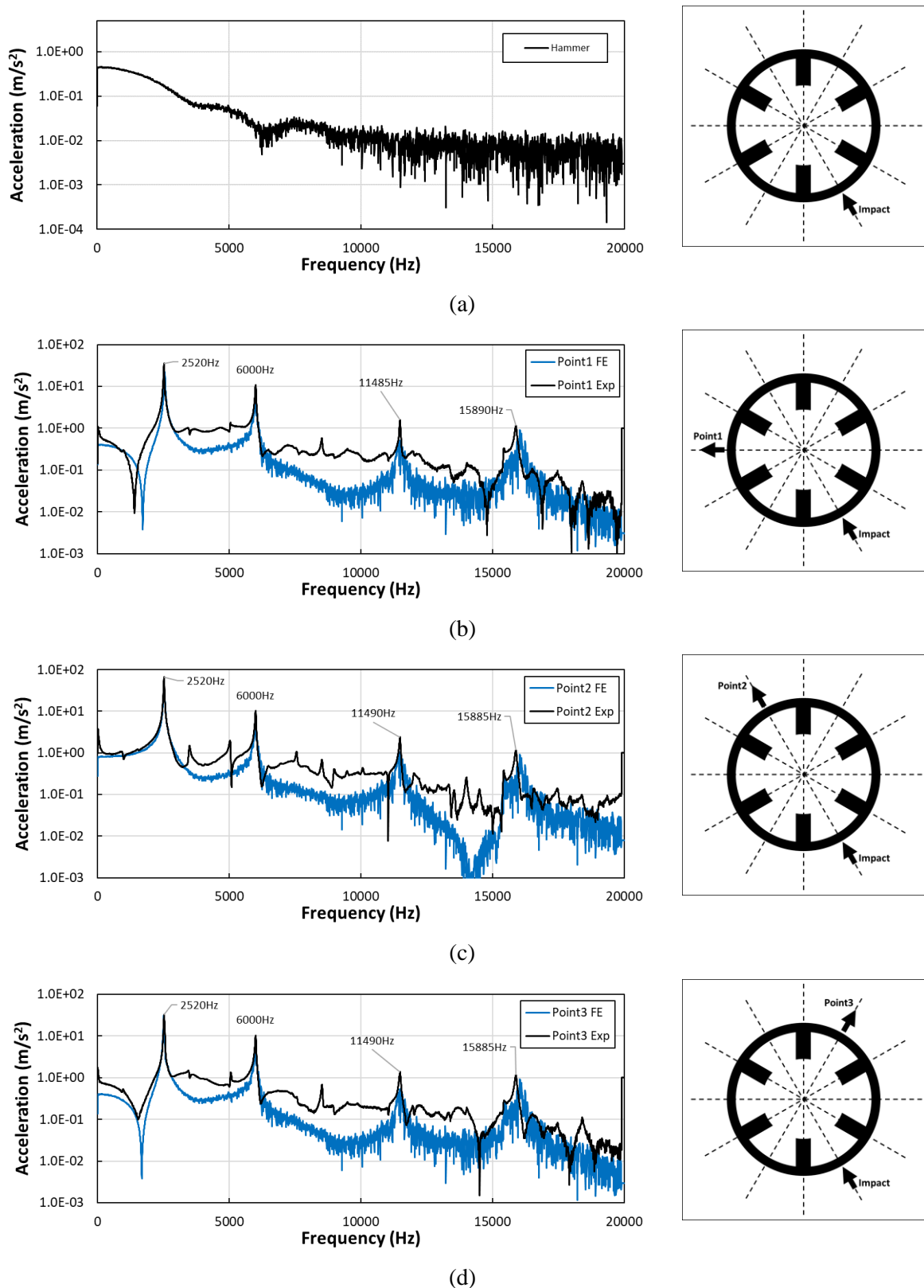


Fig. 2.19 Vibration response of impact behind a slot from experimental test and FE simulation for damping factor of 0.5%, measured behind 3 teeth. (a) Force hammer impact, (b) Point 1 response, (c) Point 2 response, (d) Point 3 response.

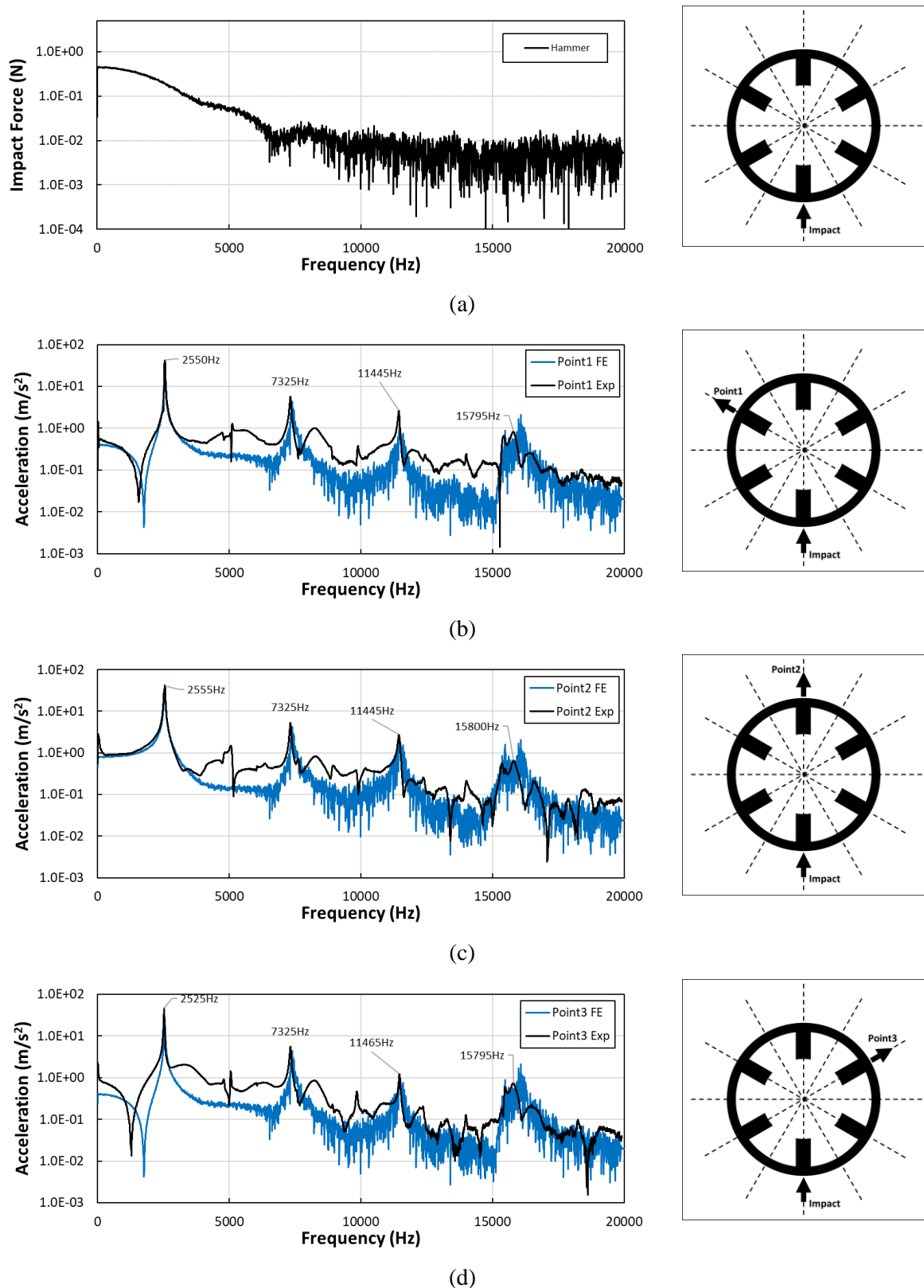


Fig. 2.20 Vibration response of impact behind a tooth from experimental test and FE simulation for damping factor of 0.5%, measured behind 3 teeth. (a) Force hammer impact, (b) Point 1 response, (c) Point 2 response, (d) Point 3 response.

This hammer test involves multiple single strike tests averaged across multiple samples, and hence, it is a force acting only at a single point. It cannot account for symmetrical or asymmetric forces acting on multiple poles at the same point in time. It is expected that due to the symmetry of the stator odd modes will be negated for symmetrical forces, but not for asymmetric forces. As shown in **Fig. 2.21** a constant symmetrical force is applied to opposite poles, resulting in the cancellation of mode 3 in the harmonic spectrum, for reference mode $(0, 3a) = 6000\text{Hz}$ and mode $(0, 3b) = 7325\text{Hz}$. However, if these forces become unbalanced mode 3 will be excited. This unbalanced force can be caused by multiple factors, including but not limited to, unequal air gap, unbalanced assembly, tolerance errors in rotor/stator manufacturing and misalignment of shaft. This phenomenon should be noted and considered particularly during on-load testing of the machine.

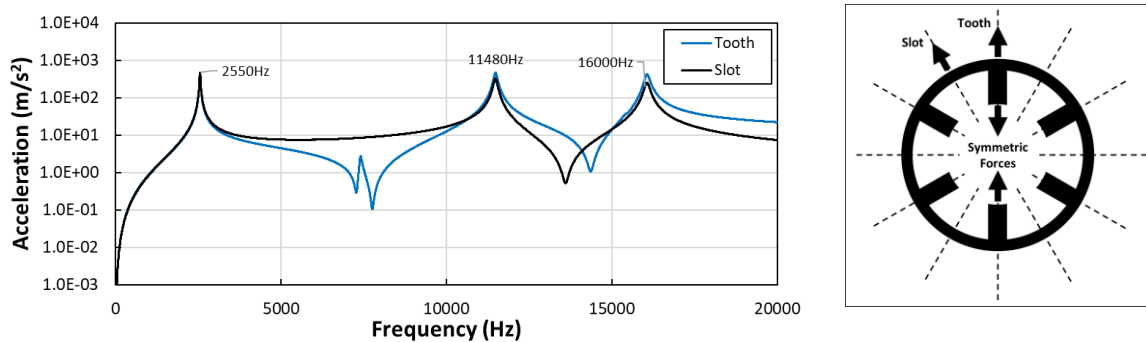


Fig. 2.21 Vibration responses under excitation of equal and opposite 1N forces acting on teeth.

2.4 Influence of casing and endcaps

2.4.1 Addition of casing framework (No endcaps)

The influence of windings on several machine types has been covered, notably for SRMs in [Lon01] and [Yon97]. The study shows that for a salient 6-pole machine with concentrated windings, the stiffness and mass of the windings may be neglected due to the nature of their cancellation effect. The conclusion drawn indicates that the stiffness effect compensates for the additional mass of the windings, whilst also reducing computation time significantly. The increase in computation time when modelling windings results from the multiple modes produced by the end windings, which for the case of a concentrated SR machine are short and therefore insignificant. It is noted that when comparing an unwound stator to a wound stator [Lon02] shows that there is a significant drop in amplitude for mode 2, whilst the frequencies are similar. The investigation into the damping effect of windings is a time consuming and arduous task, not considered in this study but should be of interest for future study in this body of work.

Therefore, as the windings may be neglected, the influence of the frame must be modelled and analysed. It is clear from previous studies on induction machines [Gir79], [Nod87] as well as SRMs [Pil01], [Lon01], [Zhu93], [Wu93] that the frame has a significant impact on the noise and vibration

characteristics of the machine, both for natural frequencies and amplitudes. The frame for the prototype is machined from aluminium with material properties indicated in **Table 2.10**. The casing is designed such that the stator is glued into the housing against a step, with the inner diameter of the casing matching that of the stator outer diameter in order to guarantee a close fit. Typically, in other machines, the bonding of stator into the frame housing can be achieved by heat shrink or glue depending on availability of processes and ease of manufacture. The final prototype machine features endcaps at each end of the casing, fixed with four equally spaced threaded bolt holes. Compared with the rest of the machine and stator, these holes are insignificant and feature only at the ends of the casing, the influence on natural frequencies and eigenmodes is negligible. **Table 2.12** shows a summary of measured natural frequencies. These results define the target for each natural frequency in the FE simulation.

Table 2.10 Material properties for aluminium casing and endcaps

Mass Density	2800 kg/m ³
Poisson's Ratio	0.35
Young Modulus	67 GPa



Fig. 2.22 Machine cross-section with wound stator inside aluminium stator housing.

Fig. 2.22 shows the close fit of the wound stator and housing, ideally a perfect bonding between the two faces. Although in reality this is not “perfect” the influence of the boundary connection can be significant and it is important to model this connection correctly. To do this, multiple models were generated with varying connections, as outlined below, with each variant compared to the experimental

results. Prior to modelling the phenomena of each connection variant, a mesh convergence study is performed with the casing included. Connection variants:

- Frictionless;
- Frictional;
- Rough;
- No separation;
- Bonded.

As the standard of fit is not quantifiable it is important to use the FE predicted model to verify if it is a strong bonded fit, or potentially better modelled with a frictional coefficient or less. Initially, a modal analysis is carried out on the casing without the stator, this will predict the natural modes of the frame. The stator is the dominant component of the system with relation to eigenmodes and natural frequencies. However, the natural mode shapes of the casing will affect the vibration spectra also.

A frictionless boundary connection allows free movement between two bodies in any direction, typically defined as sliding (tangential) and opening (losing contact). In this case, the frictional coefficient, μ , equals 0, regardless of the forces applied to the body such that the bodies are seen as separate bodies with no physical connection but a boundary between them. Similarly, a frictional boundary condition operates the same except a frictional coefficient determines the level of sliding or opening dependent on the force applied. In this case, if $F_{\text{sliding}} > F_{\text{friction}}$ for sliding to occur, where F_{sliding} and F_{friction} are the sliding and frictional forces, respectively. No separation allows sliding under any acting force, $\mu = 0$. However, once the contact is detected it shall not open. This connection boundary is useful for applications such as joints or bearings, where two connected parts shall slide across each other but not separate. The inverse of no separation is defined as rough, where a gap can occur but the frictional coefficient μ is infinite. Finally, a bonded boundary condition sees the two bodies as a single part where no gap and no sliding occur, and this is most appropriate for the modelling in this study. These definitions are summarized in **Table 2.11**.

Table 2.11 Definition of connection types in terms of opening and sliding interactions

Type	Opening	Sliding
Frictionless	Yes	Yes, $\mu = 0$
Frictional	Yes	Yes, if $F_{\text{sliding}} > F_{\text{friction}}$
Rough	Yes	No, infinite μ
No separation	No	Yes, $\mu = 0$
Bonded	No	No

A bonded fit in the FE software assumes that no sliding between elements and no free movement is allowed. Consequently, this is a perfect fit where the stator and casing become one part, with differing material properties, similar to a heat shrink fit. As the stator is pressed in against the step and glued, with matching diameters for stator and inner edge of casing, it is assumed to be bonded. The accuracy of the bonded connection is demonstrated and exhibits similar vibrational behaviour with reference to measured results in terms of natural frequencies. The boundary connection for the stator and casing is selected for minimum error in mode (0, 2), in this case a bonded connection type, **Table 2.13**.

Table 2.12 Natural mode frequencies for casing - stator boundary conditions

Mode (0, n)	Natural Frequencies, Hz						
	Measured	Frictionless	Frictional $\mu = 0.01$	Frictional $\mu = 0.2$	Rough	No separation	Bonded
2	4350	2623	4258	4299	4334	2623	4346
3a	10390	6686	9581	9690	9789	6686	9821
3b	10670	7397	10777	10886	10985	7398	11015
4	16400	12390	16107	16270	16412	12392	16480

Table 2.13 Natural mode frequency error % for casing - stator boundary conditions

Mode (0, n)	Natural Frequencies, % error						
	Measured, Hz	Frictionless	Frictional $\mu = 0.01$	Frictional $\mu = 0.2$	Rough	No separation	Bonded
2	4350	-39.70	-2.11	-1.17	-0.37	-39.70	-0.09
3a	10390	-35.65	-7.79	-6.74	-5.78	-35.65	-5.48
3b	10670	-30.67	1.00	2.02	2.95	-30.67	3.23
4	16400	-24.45	-1.79	-0.79	0.07	-24.44	0.49

2.4.2 Influence and modelling of endcaps

The final stage of mechanical modelling for the prototype stator involves the addition of the endcaps to the modelling process and their impact on natural frequencies. Endcaps at both ends are connected to the frame via four bolts, equally spaced around the frame with two of the bolt holes coinciding with stator poles, and two bolt holes aligning with centre of a slot. The location of the bolted connections is aligned with radial modes previously investigated, and hence, the influence of bolts must be investigated. The correlation between measured and predicted results is strong when the endcaps are not involved. As the endcaps are not uniformly connected to the frame for the prototype it is difficult to replicate the connection in the FE model. Initially, it is assumed that there is an intimate contact between the frame and the endcaps at all points, modelled as a bonded connection. It is seen that this stiffens the system too much, increasing natural frequencies to twice the measured result, and hence, a further systematic modelling analysis is performed. The connection between the frame and endcaps is iteratively modelled in the following variations:

- Bonded;
- No separation;
- Frictionless;
- Bolts modelled as cylindrical shafts.

Firstly, the natural modes of the prototype are investigated experimentally. It is found that due to the location of the bolts connecting the endcaps and frame housing the stator, a dual mode 2 is introduced, as a result of the additional stiffness introduced at the location of the bolts, causing geometric asymmetry in the machine. Considering this effect from the perspective of the stator teeth, with no bolts it can be seen there are 3 variations of radial order 2 mode shapes, aligned with each pair of opposite teeth at the same frequency. The additional mass and stiffness introduced behind the stator poles of a single phase, in this case, phase C, differentiate these poles from the other two pairs in a 6s/4r SRM. Hence, asymmetry is caused and dual modes (0, 2a) and (0, 2b) are created. The static testing is repeated with endcaps connected, and the influence of the dual modes can be observed from the hammer test. It is noted that at this point in the assembly process, the SR machine is complex with multiple mechanical boundaries and influences. Therefore, the damping factor is complex and difficult to analyse or calculate reliably, and hence, may be seen as arbitrary.

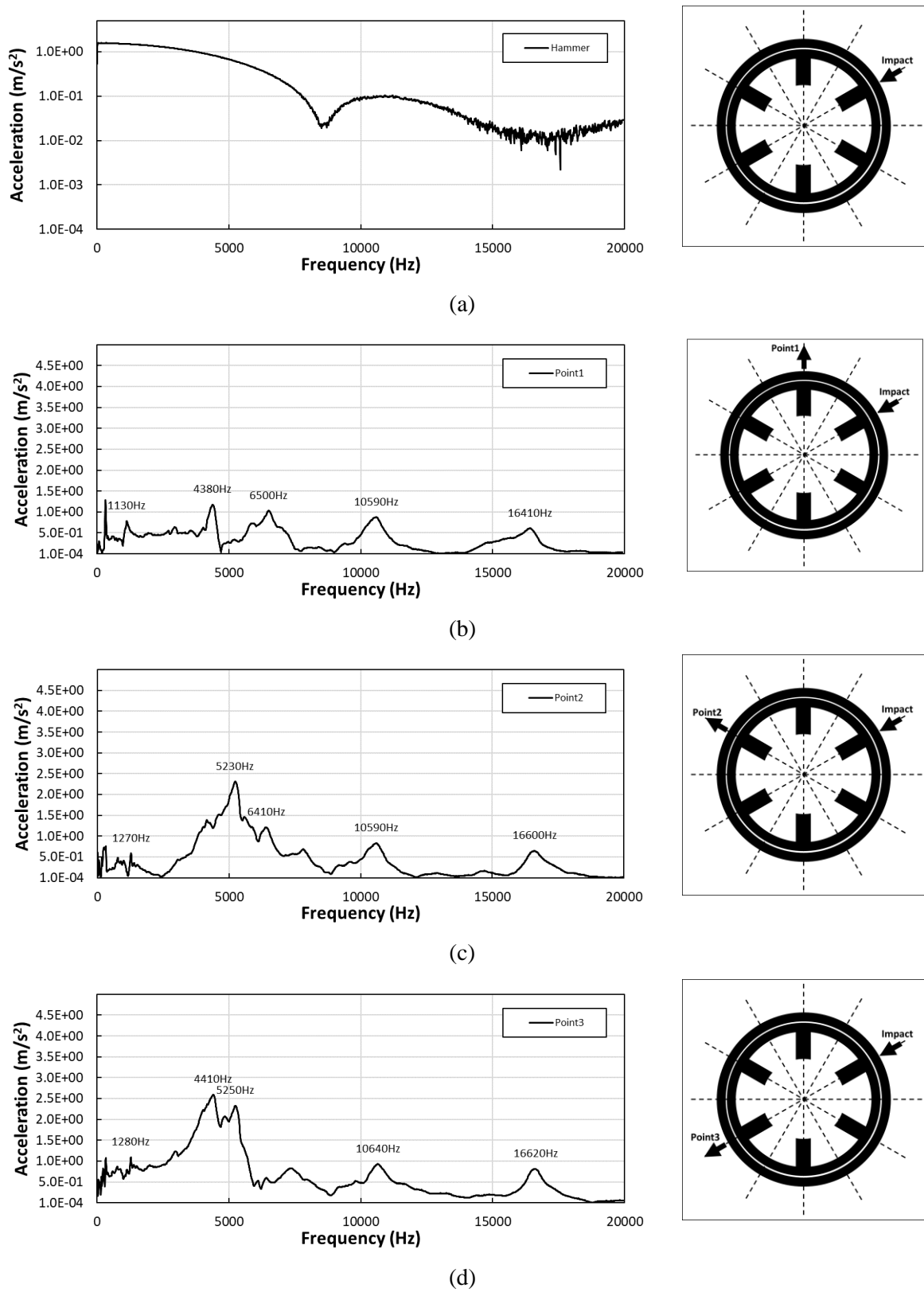


Fig. 2.23 Vibration response of impact behind tooth A1 from experimental test with accelerometers behind teeth. (a) Force hammer impact, (b) Point 1 response, (c) Point 2 response, (d) Point 3 response.

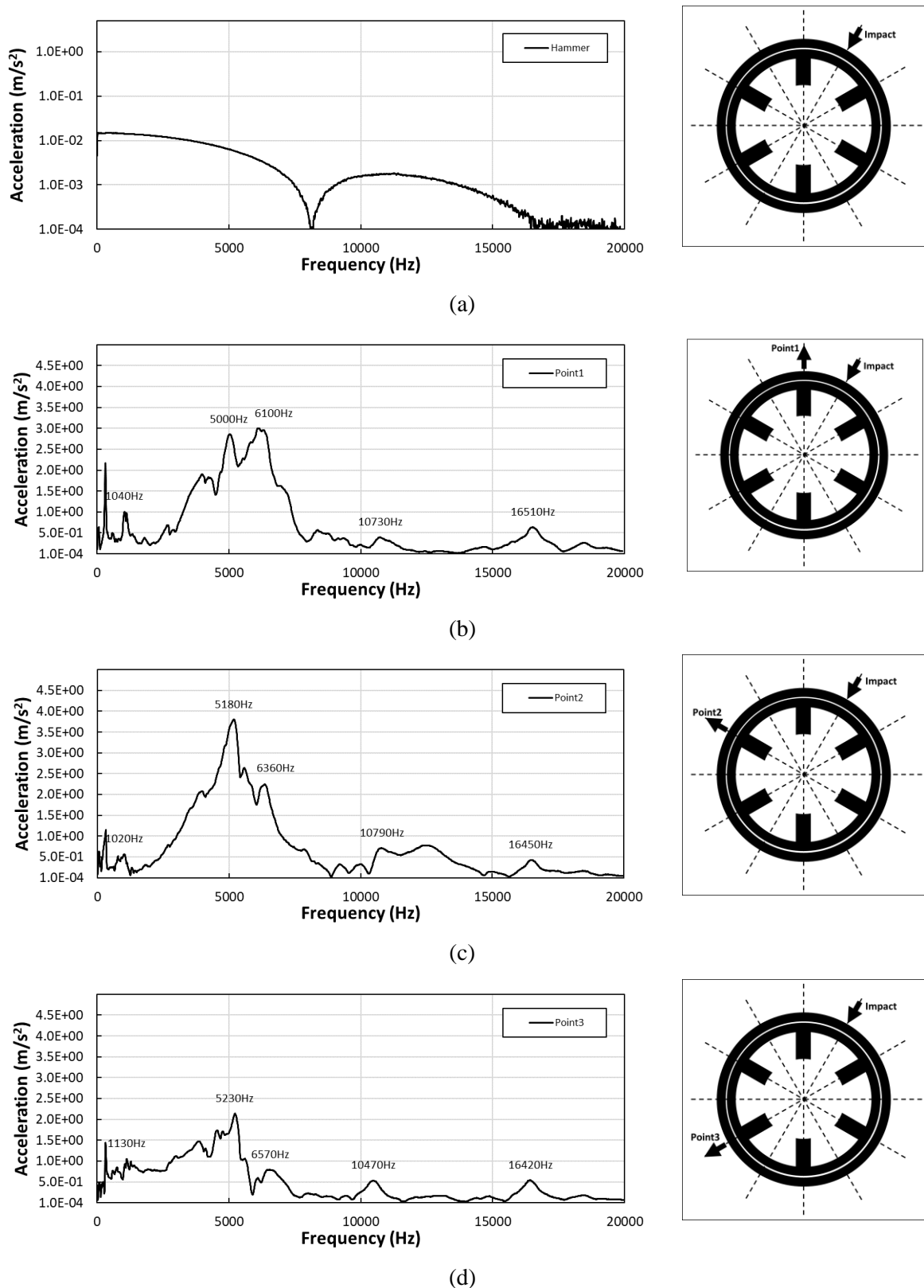


Fig. 2.24 Vibration response of impact behind slot A1C2 from experimental test with accelerometers behind teeth. (a) Force hammer impact, (b) Point 1 response, (c) Point 2 response, (d) Point 3 response.

The experimental results from hammer impact tests on the prototype SRM confirm the introduction of a new natural mode, and thus, the FE model must be correctly defined to represent this. **Table 2.14** indicates the simulated modal analysis and percentage error associated with each boundary condition established thus far. It is seen that for the bonding of bolt faces as depicted in **Table 2.14**, the natural frequencies are closest to the measured response, within 10% of the target frequency across all modes. Furthermore, the boundary condition of no connection between the two parts exhibits similar behaviour to that of the experimental prototype. This indicates that there is minimal to zero influence of modes (0, 2a), (0, 3a), (0, 3b) and (0, 4a). Moreover, this may be interpreted as the natural mode shapes not influenced by the addition of bolted endcaps.

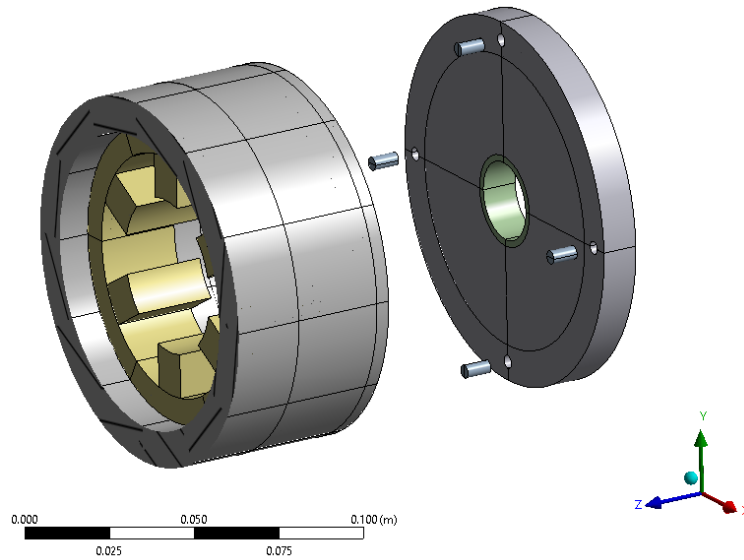
Table 2.14 Natural mode frequencies for endcap-casing boundary conditions

Mode $0,n$	Natural Frequencies, Hz			
	Measured	No Connection	Bonded	Bolt Face Bonded
2a	4410	4348	7476	4756
2b	5230	-	-	5878
2c	6300	-	-	5988
3a	10390	9767	12042	10478
3b	10670	10907	13738	11885
4a	14900	15599	18343	15941
4b	16400	16452	-	16806
4c	-	-	-	17304

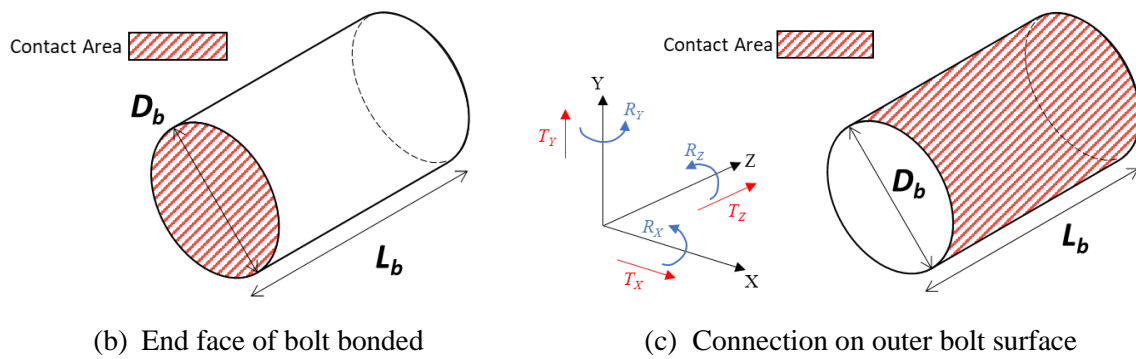
There is a lack of significant study and material on the influence and modelling of endcap connections or bolted connections in electrical machines. Hence the bolted connection boundary condition is investigated further to verify the optimal time efficient modelling method, so as to develop a reasonable FE mechanical model. Modelling the full bolt with thread and all forces is a time consuming process, both initial modelling and the analysis due to the mesh sizing and complexity of design. The clamping force joining the two parts together can be considered to act on an active area correlating to the size of the bolt head and pressure. Hence, two modelling methods are introduced to model the boundary connection of these bolts in a time efficient manner, defined as follows:

1. Face to face bonded condition from frame to bolt to endcap.
2. Outer bolt surface to frame/endcap inner surface, free in T_x , T_y and R_z , as defined in **Fig. 2.25** (c).

The bolt is modelled with an active length, L_b , and an active diameter, D_b , which are optimised for the experimental result.



(a) Endcaps connected by 4 equally spaced bolts, modelled with an active length and diameter.

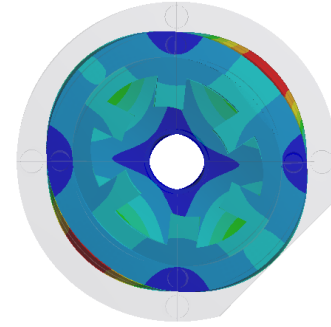
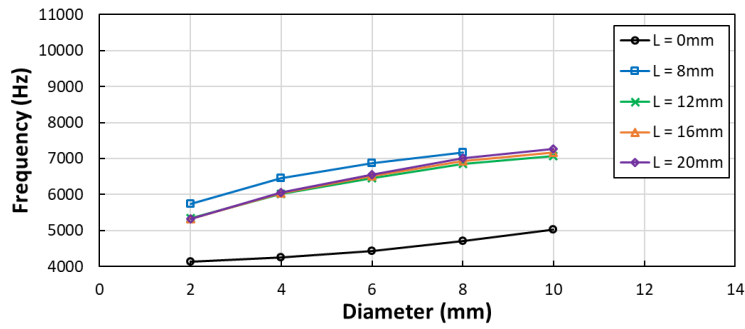


(b) End face of bolt bonded

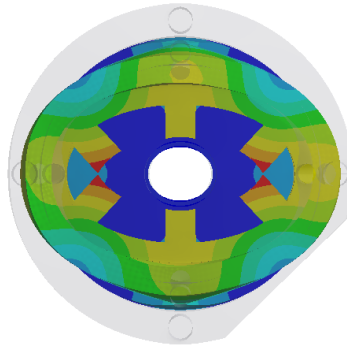
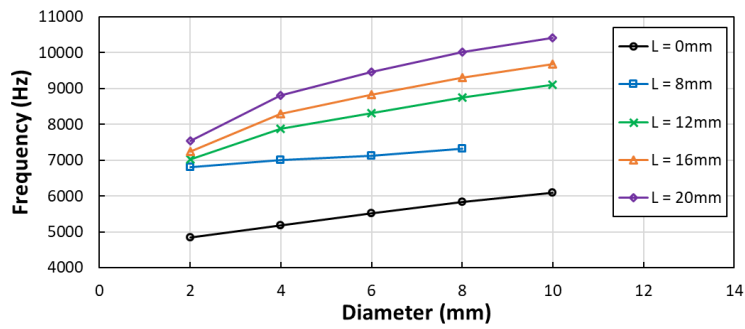
(c) Connection on outer bolt surface

Fig. 2.25 (a) Modelled bolt locations, (b) Face bonded joint conditions, (c) Surface support with boundary constraints, free in T_x , T_y , and R_z .

Under the conditions of face to face bonding, condition 1, it is possible to model the active axial length L_b from 0mm to 20mm. In these cases, a surface is defined on the endcap and the frame. From **Fig. 2.26**, the influence of diameter is apparent across all axial lengths, with increasing natural frequency as the active bolt diameter D_b is also increased. This is a result of increased stiffness in the FE model as more elements are fixed in all axes and planes, deformation may only occur around these locations. Mode (0, 2b) is the asymmetric mode of order 2, with mode 2a being considered the inherent mode. Based on this consideration, it is clear that mode 2a is affected far less by axial length variations, excluding the special case of 0 axial length, as the mode shape is dominated by the stator-frame boundary. However, mode 2b is caused by the endcap-frame boundary so the impact of active axial length and active diameter is evident.



(a) Mode (0, 2a)



(b) Mode (0, 2b)

Fig. 2.26 Natural frequencies of modes 2a and 2b for variance in active length L_b , and active diameter D_b , with parts bonded by end faces.

It is also reasonable to model the bolt with an active length, and thus, define the boundary condition based on the outer bolt surface and the inner surface of connecting parts. For this to be achieved, the degrees of freedom shown in **Fig. 2.27** must be defined as follows: T_x , T_y , T_z , R_x , R_y , R_z representing the translational freedom in direction of x, y and z axes, and rotational freedom about the x, y and z axes, respectively. An initial study into the various application and restrictions of this connection condition is investigated, in which T_z is fixed due to the clamping force and a combination of fixations in rotational freedom is analysed. T_x and T_y are free, but constrained by the diameter of the bolt hole, where T_z is fixed to reflect the clamping force applied. Furthermore, modal analysis is simulated under the following conditions:

- (a) All degrees of freedom fixed;
- (b) T_z fixed, $R_{x, y, z}$ fixed;
- (c) T_z fixed, $R_{x, y, z}$ free;
- (d) T_z fixed, R_z free.

It is shown from this investigation in **Table 2.15** that the modelling of the boundary condition in this way significantly changes the simulated natural frequencies. However, the variance between degrees of freedom applied to the bolts produces no variance in mode (0, 2a) or mode (0, 2b), for an equivalent active length. It is noted that small changes are seen in mode shapes of order 4, but these are

not regarded as significant. Following this, it is determined that the most reasonable condition of this method is the case of T_z fixed due to clamping force, and R_z is considered to be free. Hence, the influence of active bolt length L_b is investigated.

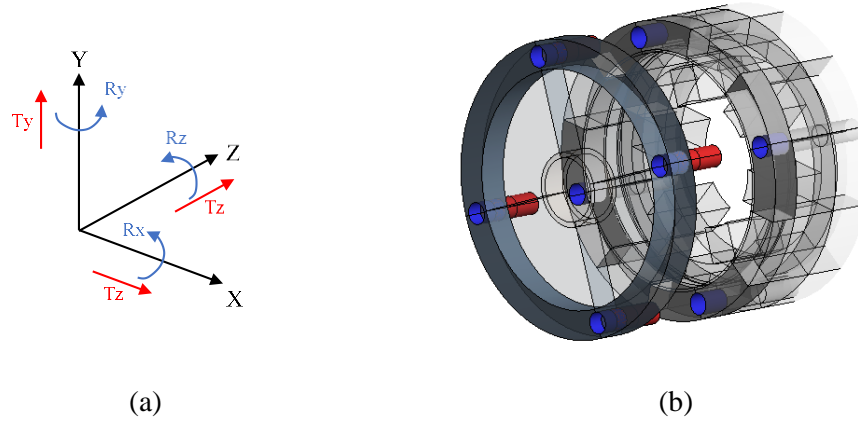


Fig. 2.27 Illustration of boundary condition 2, (a) Degrees of freedom manipulated, (b) regions of connection boundaries.

Table 2.15 Natural mode frequencies for various degrees of freedom in bolted connection

Mode $0,n$	Natural Frequencies, Hz				
	Measured	(a)	(b)	(c)	(d)
2a	4410	8087	8087	8087	8087
2b	6300	10643	10643	10643	10643
3a	10390	11956	11956	11956	11956
3b	10670	12705	12705	12663	12740
4a	14900	16207	16207	16207	16207
4b	16400	17640	17404	17404	17640

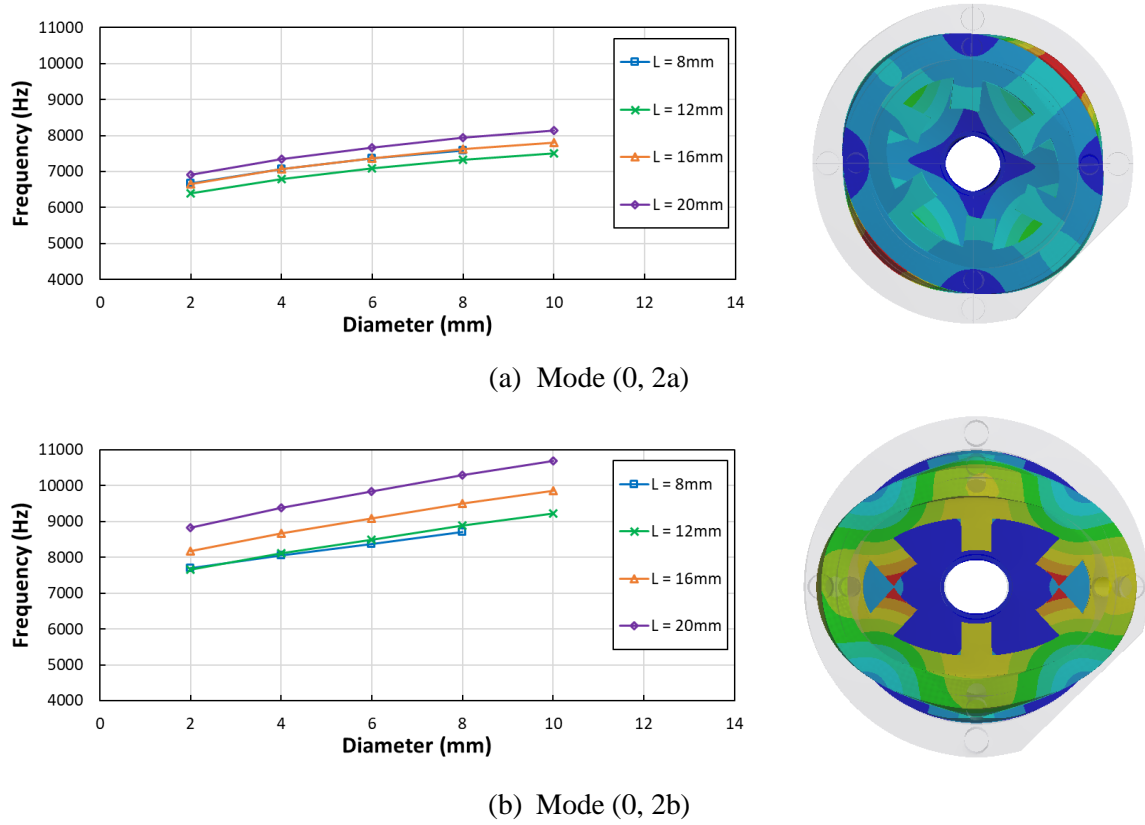


Fig. 2.28 Natural frequencies of modes 2a and 2b for variance in active length L_b , and active diameter D_b , with surface conditions with freedom in T_x , T_y , and R_z .

From the simulated results, it can be seen that the increase in active diameter D_b is proportional with the increase in natural frequencies for a focus on modes of radial shape 2. Furthermore, an increase in active length L_b also corresponds to an increase in the natural frequencies. However, with reference back to the measured results, the natural frequencies simulated are significantly higher as shown in **Fig. 2.29**. Consequently, the modelling method used in the final model for the connection between the endcaps and the stator housing is a face-face bonding method acting on an area equivalent to the clamping force.

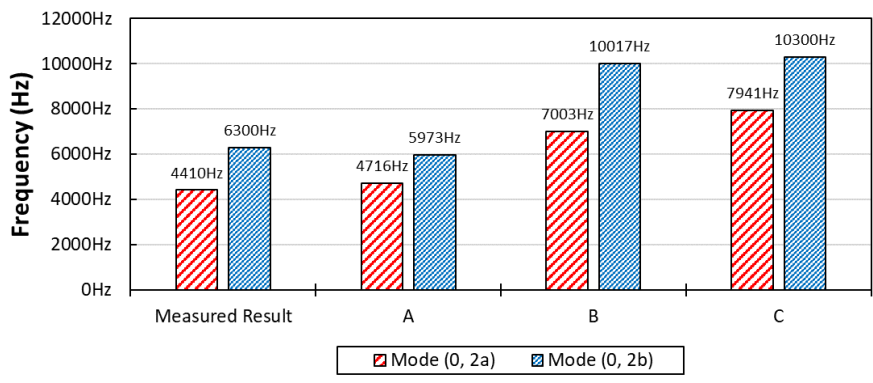


Fig. 2.29 Comparison of joint types for modes (0, 2a) and (0, 2b), for an active diameter $D_b = 8\text{mm}$, where A is face bonded with $L_b = 0\text{mm}$, B is face bonded with $L_b = 20\text{mm}$ and C is a surface joint where $L_b = 20\text{mm}$.

2.5 Final mounted modal analysis

The final FE model is developed to include the mounting bracket, such that all major mechanical influences are accounted for. It is found that the mounting bracket only has a minor impact on the natural frequencies. Furthermore, the bearings are modelled with a bonded connection to the endcaps. However, these are also found to have minimal impact, the major introduction is the slightly increased mass on the endcaps. The stator eigenmodes are shown to be dominant, combined with influence of the cylindrical stator housing, or casing, in which the stator is inserted. The final FE model natural frequencies and vibration behaviour is shown in **Fig. 2.30**.

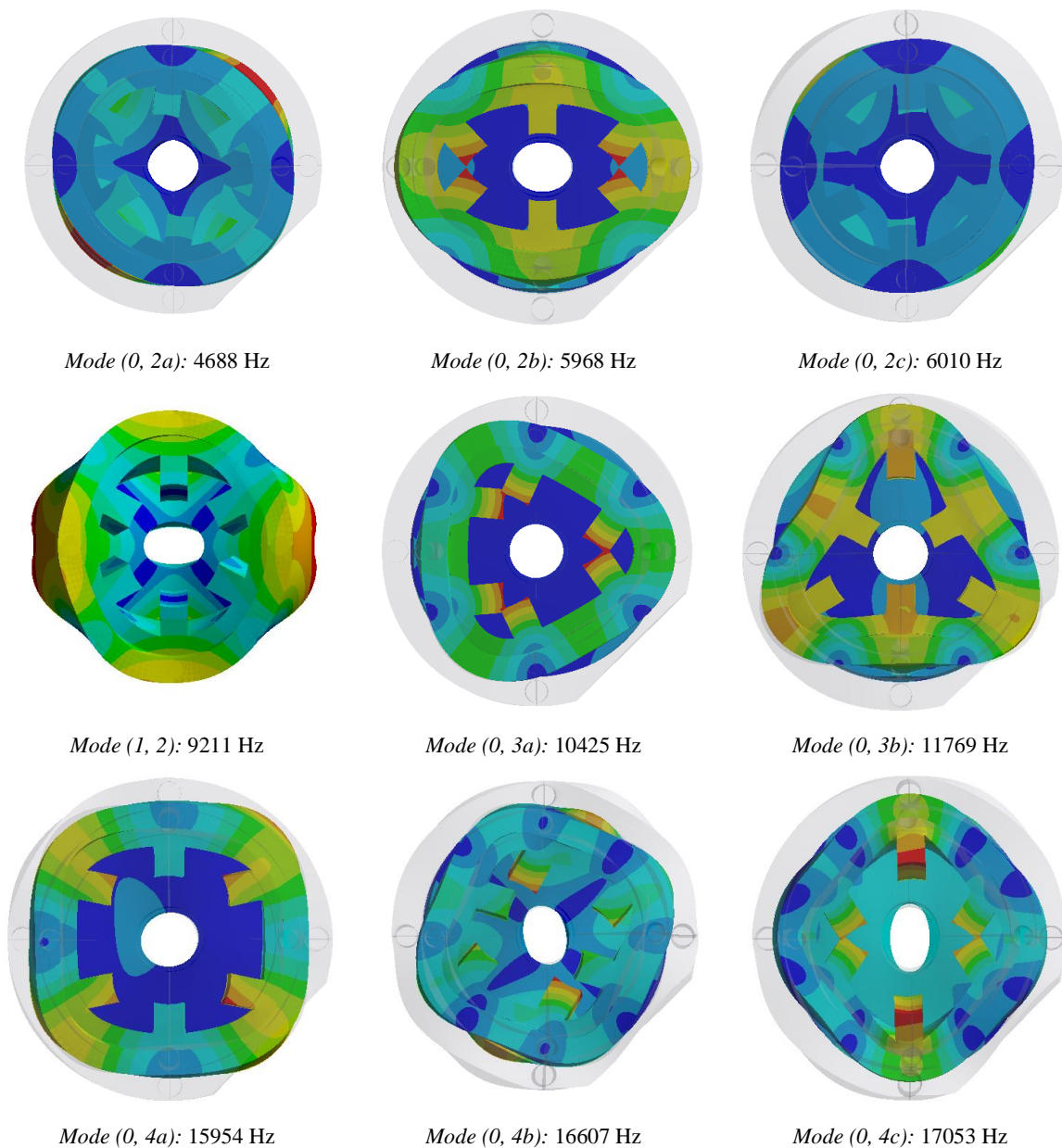


Fig. 2.30 Mounted prototype simulated eigenmodes in the audible frequency range.

2.6 Summary

The work in this chapter presents a systematic modelling process, in which the influence of multiple construction parameters on natural frequencies is investigated. The FE model is verified and optimised with the aid of experimental results at each stage of assembly. Consequently, it is found that the dominant natural modes in the prototype are produced from a combination of the stator and the casing in which the stator is housed. Furthermore, the influence of machine asymmetries is introduced, namely the influence of stator teeth and the connection of endcaps.

Firstly, a laminated annular ring is modelled and verified to introduce key ideas in the analysis of natural frequencies. The methodology of suitable meshing methods and comparison of 2D and 3D FE analysis verifies the accuracy of the simulations for a simple structure. Subsequently, the addition of stator teeth is simulated, with note of new dual modes introduced due to the asymmetry. It is shown that for a 6-pole stator dual modes of order 3 are present. However, due to the geometric and electrical symmetry in the 6s/4r SRM, natural frequencies of mode shape 3 are negated. This is a result of equal and opposite forces acting aligned with stator teeth. It is noted that this phenomenon is present under sequential phase excitation as seen in SRMs, but it is unlikely to be entirely eliminated. Minor eccentricities in current excitation or manufacturing eccentricities will also affect the vibration behaviour and natural frequencies of an electrical machine.

Having established and verified a suitable model for the laminated stator eigenmodes and natural frequencies, the conditions of boundary connections is investigated. The influence and modelling of concentrated windings in SRMs has previously been investigated in [Lon01], and hence, the windings are neglected from the modelling process. By neglecting the windings, significant processing time is saved during simulation studies, and it is shown in [Lon01] that the additional mass of the windings is offset by the increased stiffness for a 6s/4r SRM. The connections between parts of the mechanical model must be carefully and extensively studied so as to develop an accurate and reliable mechanical FE model. The various connection types afforded by the FE software are presented with definitions and examples. Through an iterative process comparing the connection types, it is determined that a bonded fit for the casing to stator connection is reasonable. Furthermore, the addition of the casing to house the stator is shown to significantly increase the natural frequencies of the electrical machine. The material of the aluminium is also investigated so as to avoid accuracy errors due to material variance, and it is found that a generic set of properties for aluminium is suitable.

Finally, the influence of addition of endcaps is examined. It is shown that for a small scale 6s/4r SRM, the bolted connection of endcaps to the stator housing contributes considerably to the final natural frequencies of the SRM. The bolts are located at 4 equally spaced points in the yoke of the aluminium casing, 2 of which are aligned with stator poles, 2 aligned with the middle of slots. Due to the symmetry of the machine, bolts aligned with stator poles both lie behind phase C windings. Multiple methods of modelling the bolted connection are investigated, taking into account the active diameter of the acting

clamping force, and the active length of the bolts. By modelling the bolt as a simple cylinder, the outer surface may be joined to an equivalent inner surface on each part to be connected. Subsequently, the degrees of freedom of the bolt may be defined, that is to say the allowable deformation and translation of the part may be defined. The influence of translational and rotational freedoms in each axis is examined, and it is found that for a bonded connection between the bolt and the parts the degrees of freedom have low influence. The most suitable connection method is determined to be bonding of an area equivalent to the active diameter of the clamping force on each part, for example the bolt head diameter. Under these conditions, it is shown that this introduces a further asymmetry to the electrical machine. Hence, dual modes of order 2 and 4 are found to be introduced due to the additional stiffness caused by the fixed bolted connection behind poles. This can be considered as an amplification of the pre-existing modes which are caused by stator teeth. The final model is analysed with addition of the mounting plate, although this is confirmed to be insignificant in the identification and FE modelling of axially central modes.

Chapter 3 Investigation of Vibration Under Voltage Control

3.1 Introduction

Without considering the acoustic radiation efficiency of an electrical machine [Zhu94], resultant acoustic noise response may be considered to bear similar trends to vibration response, provided the transfer is through a constant medium, in most cases, air. Therefore, this chapter seeks to compare trends found in properties of the radial force and vibration response as a result solely of electromagnetic excitation of the stator poles. Furthermore, the torque and tangential forces are analysed as the torque production of the machine is ultimately the crucial factor in assessing the performance, a current profile that provides zero noise but also zero torque is useless. The analysis is performed in ANSYS for both electromagnetic and mechanical simulations, and then, trends are verified such that further analysis may be considered reliable. The motor used for verification was first developed as a research prototype to compare SRMs and VFRMs, with sizing based upon the motor defined by T. Miller [Mil93].

Table 3.1 Machine parameters

Machine Parameters	Value	Machine Parameters	Value
Number of phases	3	Stator outer diameter	90.0mm
DC-bus voltage	48V	Rated speed	400rpm
Rated torque	1.7Nm	Rate power	70W
Number of stator poles	6	Stator inner diameter	47.4mm
Number of rotor poles	4	Stator pole arc	30°
Number of turns per phase	366	Rotor pole arc	32°
Winding resistance	3Ω	Rotor & stator yoke thickness	8mm
Stack length	25mm	Air gap	0.5mm

The analysis of spatial air gap forces in these studies provides a background for the analysis performed in this chapter. This chapter includes experimental verification for the 6s/4r SR machine under voltage control conditions. This is due to the frequencies of eigenmodes present during operation the potential interference with PWM switching frequencies during current control operation. Typically, the switching frequency of PWM is around 10kHz and the amplitude of the interference is large enough to impact heavily and potentially swamp results in the vibration spectra. Therefore, the experimental analysis may only be reliably performed under voltage control, providing verification of trends found in FEA analysis.

3.2 Forces acting on stator poles

In order to simulate the vibration response of an electrical machine under operating conditions, the forces must first be calculated from the electromagnetics. The interaction of magnetic fields produced and the currents applied results in the electromagnetic torque which in turn causes rotor rotation in the machine. The torque is produced as an application of the tangential forces created onto the rotor. However, radial forces are also created under operating conditions. By applying the harmonic content of these electromagnetic radial forces onto the stator teeth of the mechanical model, the frequency domain response can be directly simulated. The radial and tangential forces are calculated via the Maxwell Stress Tensor equations (3.1) and (3.2) from [Pil99], where F_{rad} and F_{tan} are the radial and tangential forces, respectively. Furthermore, L_{stack} , μ_0 , B_r and B_t represent the stack length, permeability of air, radial flux density and tangential flux density, respectively. [Cha89] demonstrates the use of Maxwell Stress Tensors for calculating torque in permanent magnet synchronous motors as well as other finite element and analytic methods. The calculation of radial air gap forces and tooth tip forces is further investigated in [Jor50], [Gie09], [Gie06], [Sei92] and [Gar97].

$$F_{rad} = \frac{L_{stack}}{2\mu_0} \oint (B_r^2 - B_t^2) \cdot dl \quad (3.1)$$

$$F_{tan} = \frac{L_{stack}}{\mu_0} \oint (B_r \cdot B_t) \cdot dl \quad (3.2)$$

These forces in turn contribute to a force and a moment acting on each tooth. The moment is a turning force and for the simplification of analyses this is considered to have no effect on the resultant vibration produced. It is assumed that the tangential force has minimal effect on the total vibration and acoustic noise produced, with the radial force identified as the dominant source of vibrations in SR machines in [Cai01], [Cam92], [Anw00], [Li09], [Pol03], [Kur15a] and [Tak15]. For full analysis, the radial force is measured as an integral across 1 slot pitch in the middle of the air gap, centred at the midpoint of the tooth (**Fig. 3.2**). When considering the influence of radial and tangential force harmonics on acoustic noise and vibration response, one must consider the effective harmonics of the system. In a 3 phase system harmonics of order 3 cancel out due to their phase, and hence, the summed component is 0. The effective harmonics can be determined as those which dominate particular modes and therefore resonate the system. It is the interaction of effective harmonics from the radial electromagnetic forces with natural harmonic frequencies of the stator that causes significant noise and vibration in SRMs.

Due to conventional control strategies of SRMs, consisting of a constant current in the period of excitation followed by a sharp turn-off, multiple issues arise in terms of resonance. A constant current in the period of excitation consists of current harmonics extending to the high order harmonic range.

Hence, it could be considered that a unipolar square wave has high current harmonic content. This results in a wide range of frequencies excited by current harmonics, and thus, more opportunities for resonance between current harmonics and natural frequencies of the stator and motor. This accounts for harmonics produced in the constant current excitation period, the turn-off of current introduces a second phenomenon. At turn-off, the current waveform can be considered to be a negative pulse assuming ideal conditions. This results in a significant current harmonic at a single frequency, determined by the control strategy and operation speed of the motor. For conventional control in a 3-phase SRM, this frequency shall be equal to 3 times the electrical frequency of the motor. In this study, the speed of the machine is relatively low, and hence, the resonance of that current harmonic is less significant. However, the mechanical implications of instantaneous turn-off and the natural oscillation of the stator at turn-off are investigated thoroughly, with particularly reference to the impact on radial force and rate of change in radial force.

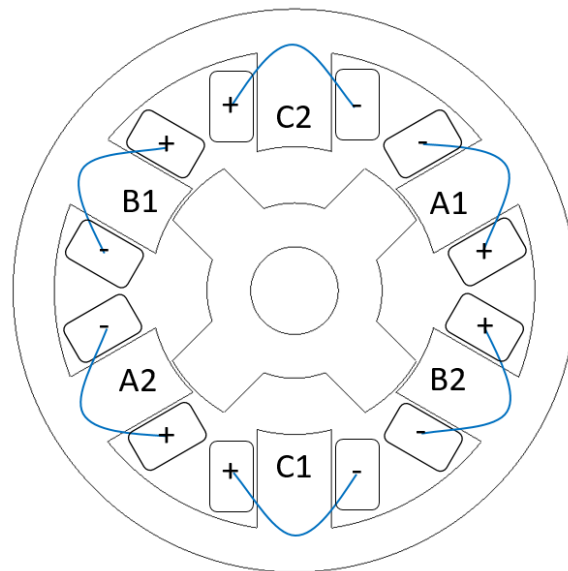


Fig. 3.1 Winding configuration for 6s/4r doubly salient SR machine.

Under 3-phase operation for the winding configuration depicted in **Fig. 3.1** the machine experiences equal and opposite forces from opposing teeth, at the same point in time. Hence, the radial forces produced in the air gap and acting on the stator teeth are symmetrical, which is the condition of simulation for all simulated results. In reality, it is likely that the forces will be asymmetric, with one force showing higher magnitude or varied phase. Multiple factors can cause asymmetric forces, including tolerance variation, unequal air gap and variance in windings on opposing teeth. Further study and an example of asymmetric forces can be found in [Zhu07]. For a switched reluctance machine, considering the forces in the time domain they can be considered as sequential forces acting on each phase tooth for one electrical cycle, and hence, resulting in poor acoustic noise and vibration performance of SRs.

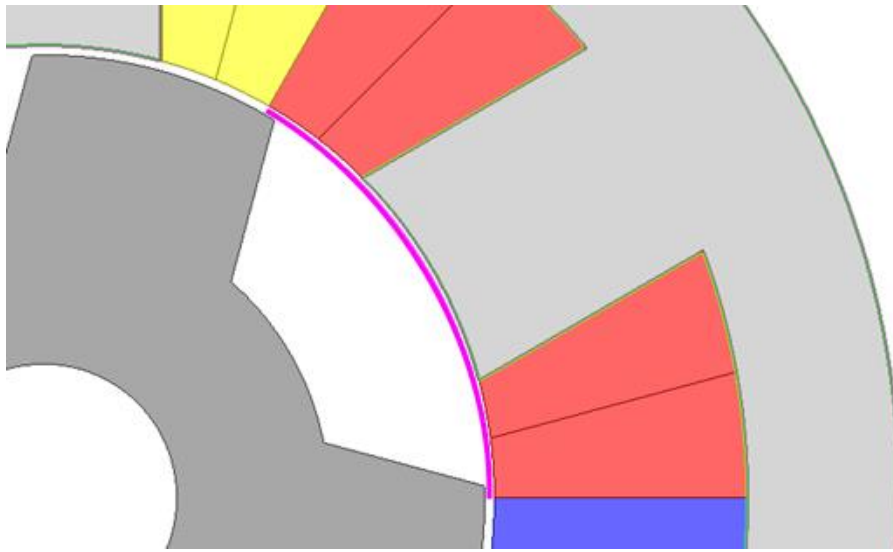


Fig. 3.2 Line in the air gap spanning one stator pole pitch for radial force calculation.

Firstly, a baseline for the SR machine under simple on/off voltage control must be created as a reference point for comparison against future current profiling. Hence, the baseline for these test conditions is an ideal rectangular current response operating from 0-120° electrical, where the turn-on and turn-off transients are neglected. To model effects of turn-on and turn-off transients within the FE software is possible. However, it adds considerable time and memory requirement to the simulation steps. Thus, for this study these effects are ignored in favour of a time efficient model. The simulated vibration response trends under these conditions are verified experimentally to validate the FE model and modelling conditions.

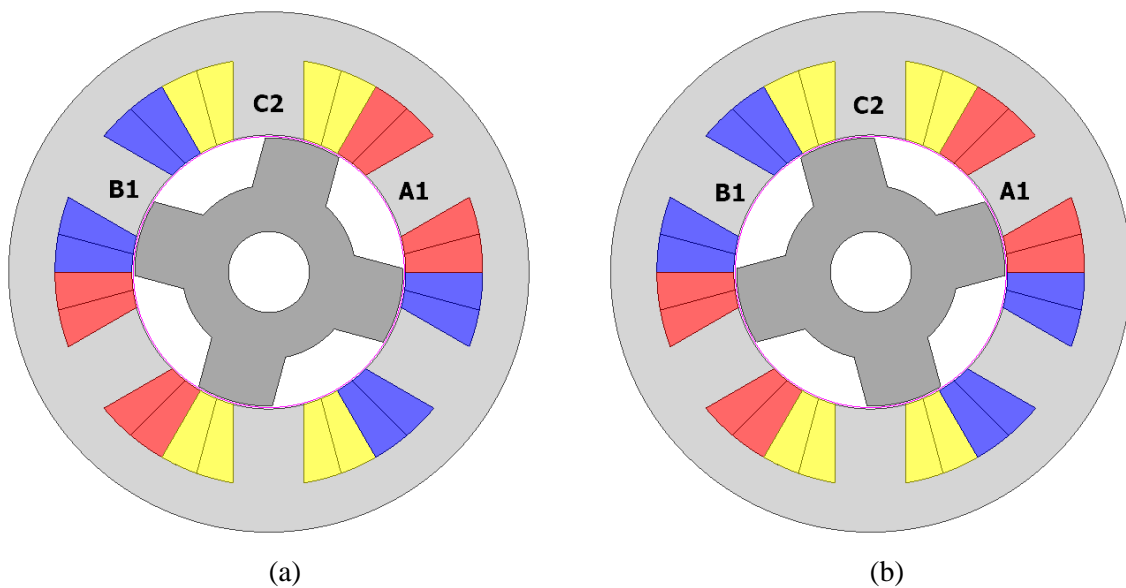


Fig. 3.3 Rotor position relating to phase A. (a) turn-on, (b) turn-off.

In order to obtain reasonable experimental verification, the speed of operation is set to constant 150rpm rotational speed. 1 electrical revolution at this speed provides a minimum frequency step for vibration response of 10Hz. This is considered to be a reasonable resolution given modal frequencies start at 4.5kHz. Furthermore, the initial position is set to the fully unaligned position as explained in [Mil01] and [Mil93] and simulated for conduction angle of 120° electrical. This defines the electromagnetic simulation setup, with radial forces extracted in post-processing. The radial force per tooth is assigned to the stator tooth face in 3D mechanical analysis to simulate the harmonic response at 10Hz intervals, up to the maximum audible range 20kHz [ANS12], [Ras99] and [Fie06]. It is known that the radial force is a key identifier in acoustic noise and vibration responses.

In literature it is often stated, and widely considered, that the radial air gap forces, F_{rad} , are the major contributor to stator-borne vibrations in radial flux machines compared to tangential air gap forces, F_{tan} . Therefore, to minimise computational time and simplify the application of air gap forces onto the stator teeth, the tangential forces are often neglected from the calculation and assumed to have minimal impact on the vibration response of the motor. Despite this assumption often being used and stated, there is little verification in literature in terms of FE analysis or experimental verification. The tangential forces are directly related to torque ripples, which are considered to have influence on final vibrations. It is important not to ignore this influence without further investigation to justify the exclusion of tangential air gap force components, and hence, a comparison between vibration response of load forces $F_{rad} + F_{tan}$ and solely F_{rad} is performed. This comparison seeks to fill a gap in current literature and verify the hypothesis and assumptions of many other works.

To perform the comparison, a baseline vibration response as outlined further in Section 3.3 is used as a reference point. The equations of F_{rad} and F_{tan} are shown in (3.1) and (3.2). The forces are calculated from the air gap flux density across an arc spanning one stator pole pitch in the centre of the air gap. In order to map the forces onto the stator tooth face of a 3D model, the forces must first be manipulated into the frequency domain. These forces are then applied to the relevant stator tooth face in terms of real and imaginary components of x, y and z-axis orientation. Given the motor is a conventional radial flux SRM, the z-axis component of both radial and tangential forces can be assumed to be zero. The process of calculating these forces and converting them into the frequency domain can be seen in **Fig. 3.4** and **Fig. 3.5**. The simulation method presented here is relatively simple yet the concept and problem can be extended further [Dev17]. The influence of tangential flux density on the radial flux can be further investigated, thus linking the torque ripples and radial forces, which in turn may provide a link between torque ripple and stator vibrations. This is a topic that shall be of much interest to industry applications, where both torque ripple minimisation and acoustic noise and vibration response are key parameters for optimisation.

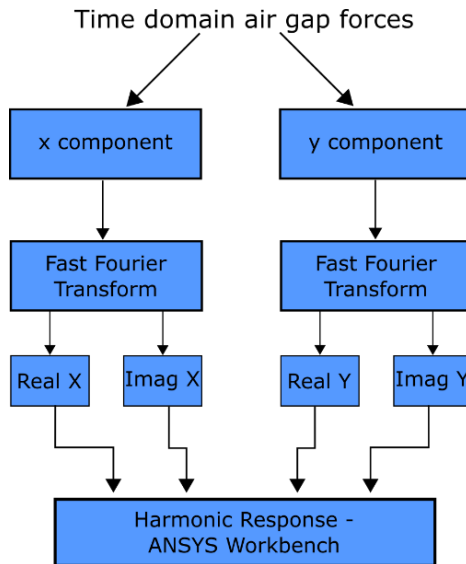
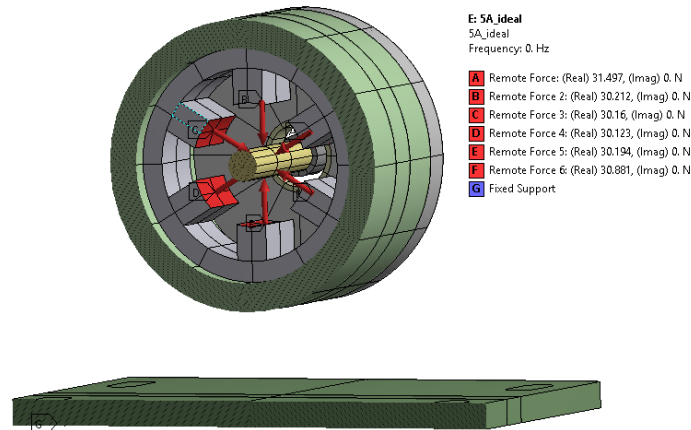
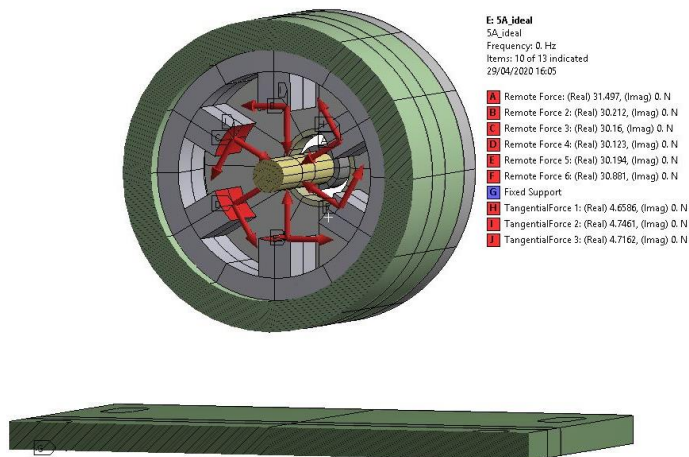


Fig. 3.4 Process of converting air gap forces for 3D mechanical mapping.



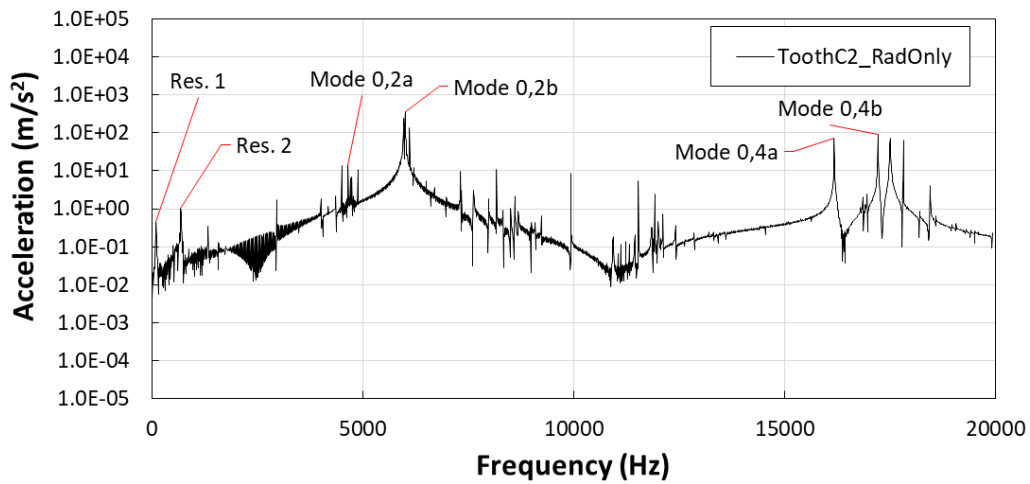
(a)



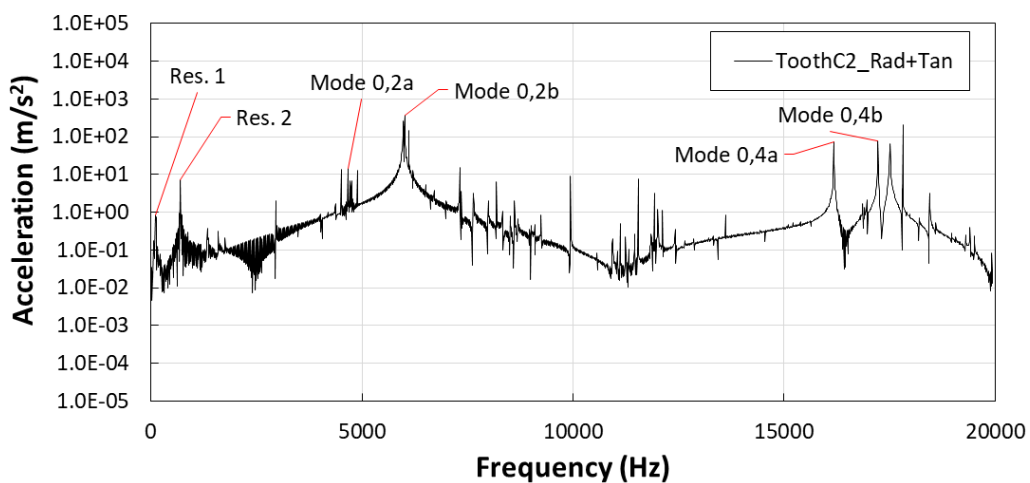
(b)

Fig. 3.5 Harmonic response setup with (a) radial forces and (b) radial + tangential forces applied to inner stator tooth faces.

The results comparing the inclusion of tangential forces in the vibration response calculation are identified in **Fig. 3.6**, focusing on the mechanical resonance relating to speed (identified as Res. 1 and Res. 2) and the natural eigenmodes of the motor assembly. The frequency of resonant frequencies and eigenmodes is unchanged, and therefore, the amplitude of acceleration is compared. The addition of tangential forces when simulating the vibration response of the motor at a constant speed results in an increase in acceleration amplitude across the majority of key frequencies. The influence on peak caused by mechanical resonance is most significant, as the tangential forces are composed of cyclic waveforms for constant speed. Therefore, the harmonic content of the tangential waveforms is dominated by the mechanical resonance and derivatives. Mode 0,2b is the most significant mode shape from the modal analysis, and thus, the dominant source of vibrations in the 6s/4r SRM. It can be seen that the inclusion of tangential forces increases the acceleration amplitude for this mode, behind both teeth and slots.

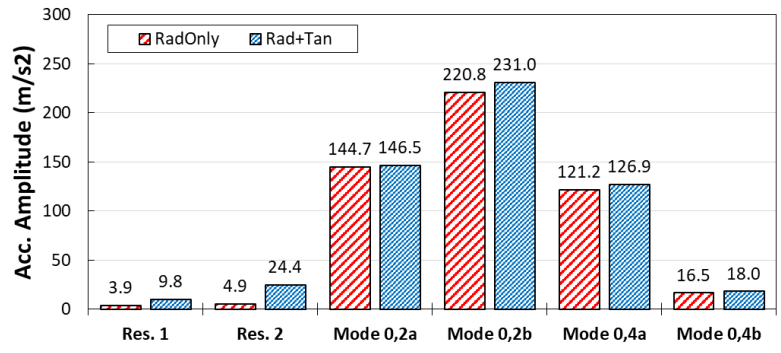


(a)

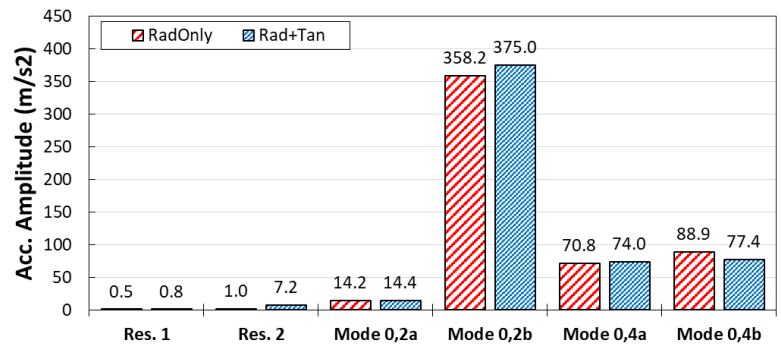


(b)

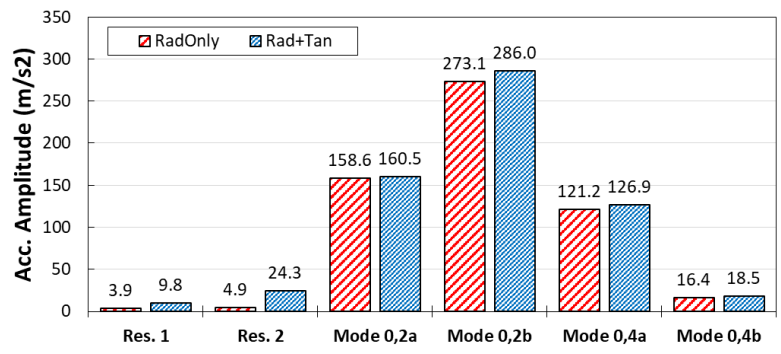
Fig. 3.6 Identification of compared frequencies in vibration response for (a) applied radial force only, (b) inclusion of radial and tangential forces.



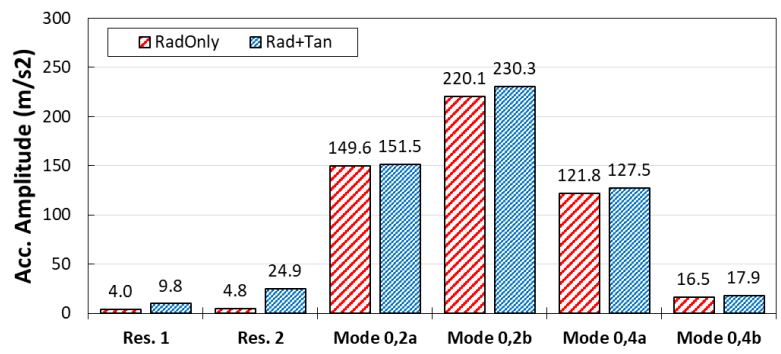
(a) Tooth A1



(b) Tooth C2

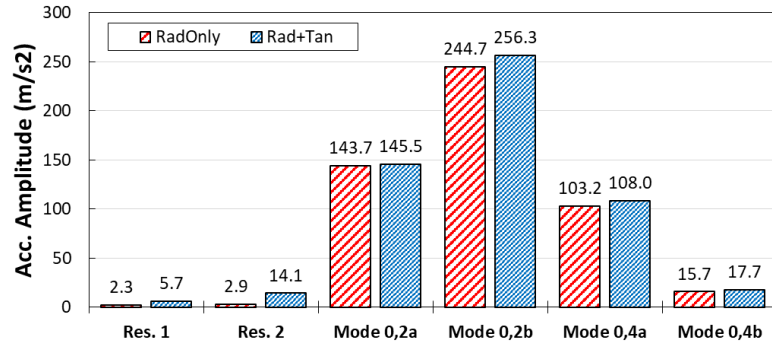


(c) Tooth B1

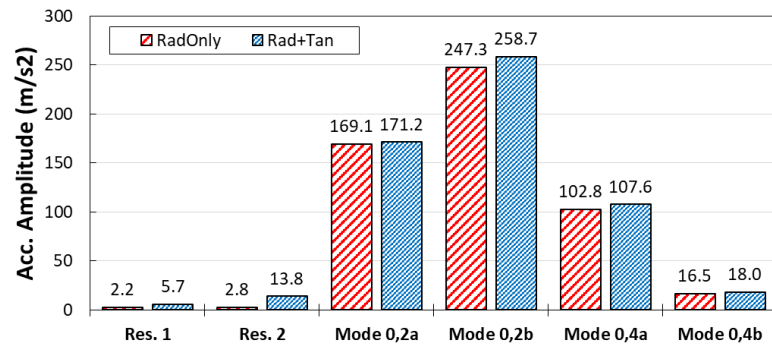


(d) Tooth A2

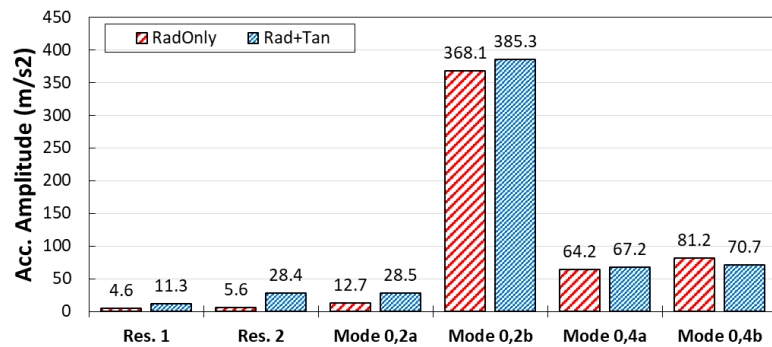
Fig. 3.7 Amplitude of acceleration behind teeth, compared for radial force only and radial + tangential force application.



(a) Slot A1C2



(b) Slot C2B1



(c) Slot B1A2

Fig. 3.8 Amplitude of acceleration behind slots, compared for radial force only and radial + tangential force application.

The study in this chapter and following chapters focuses on the influence of control strategies and current profile components on the final vibration response for low speed operation. The low speed operation is a limit of the experimental testing and allows for simulated analysis of the motor showing the impact of electromagnetic forces only, without influence of mechanical resonance. As the tangential forces impact the mechanical resonant frequencies most, it can be reasoned that the neglect of the tangential force application is reasonable in this case. However, it shall be noted that reduction in vibration response may be overestimated when neglecting tangential forces. Furthermore, if operating at higher speeds it is acknowledged that the influence of tangential forces, and potentially torque ripple,

will be more significant. The influence of these forces should not be neglected without consideration or verification of the impact first. In this case, it is clear that F_{rad} is the dominant component and mechanical resonance does not interfere with natural mode shapes of the motor, and hence, the tangential force components are neglected from the calculation.

Hence, F_{rad} is analysed with multiple methods. Firstly, the radial force per tooth is analysed. Then, a further focus is applied to the rate of change in radial force F_{rad} and the integration of the radial force profile. The peak rate of change in F_{rad} occurs at turn-off, in the cases examined in this chapter this is directly related to the peak radial force due to the ‘ideal’ current profile used as a baseline. The area under the force-time curve is equivalent to a quantity called impulse. This is equivalent to the change in momentum of the stator tooth, which provides an indication as to the overall deformation experienced. For example, the same radial force acting over a longer period of time may be more desirable than a short duration, high amplitude force, but the impulse of forces may be equally resulting in similar vibration response.

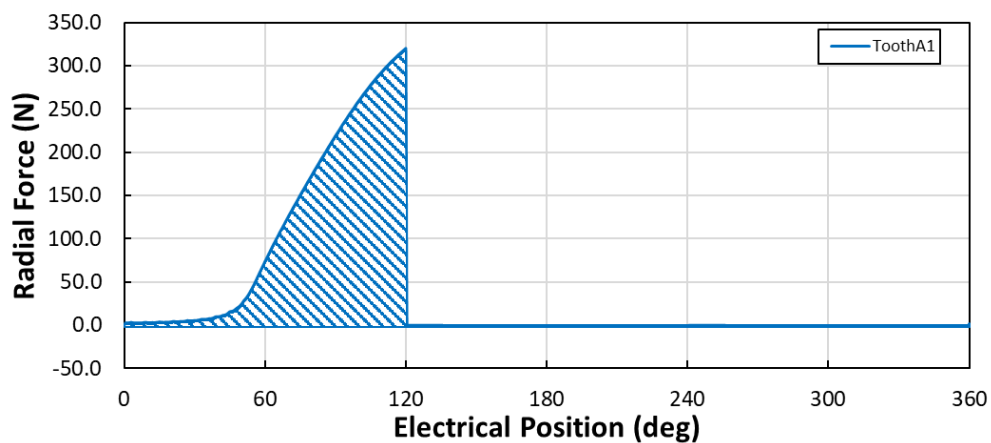
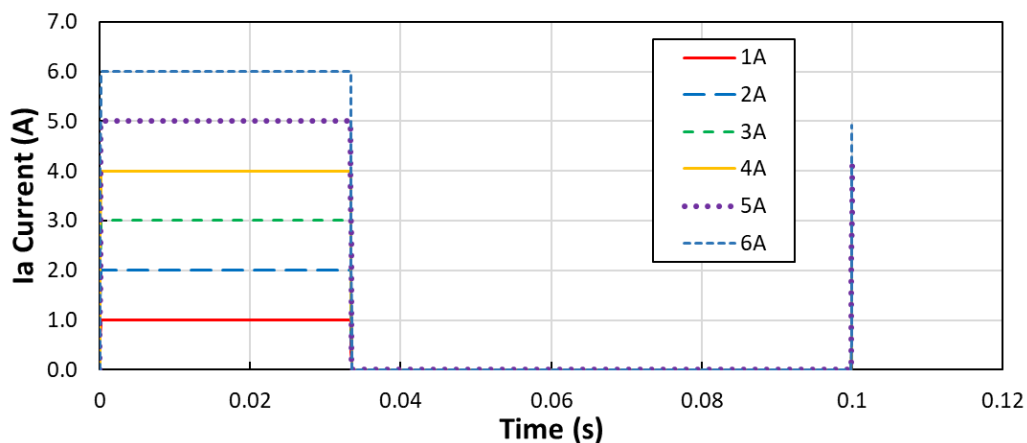


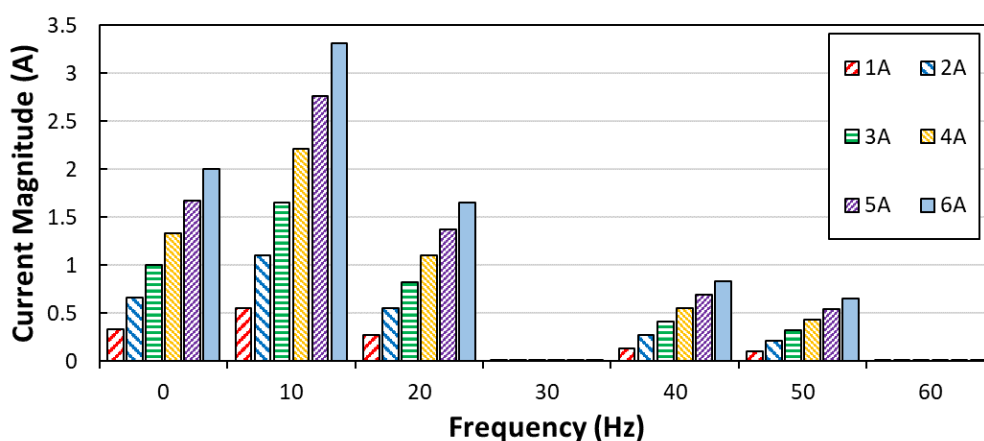
Fig. 3.9 Integral of radial force calculated as area under curve for force acting over one pole pitch.

3.3 Influence of load/current

Initially the influence of the phase current applied to the windings is analysed. The load is varied from 1A up to 6A, based on the achievable range of phase current in the experimental prototype, and the results can then be verified. Furthermore, the conduction angle is fixed at 120° electrical, with the turn-on position equal to the fully unaligned position as previously specified. The rectangular waveform applied assumes no influence of inductance or winding resistance, termed the ‘ideal’ current waveform in this instance. This allows clear trends to be identified between the current profiling and the simulated vibration results. Due to the multiple influence parameters involved in simulating the vibration response due to phase winding excitation, it is useful to simplify the model to clarify potential sources and variations. The harmonic content of the resultant varied load current waveforms shows a linear trend with equal contribution of each harmonic, i.e. the ratio of 1st to 2nd harmonic is constant as load current increases.



(a)

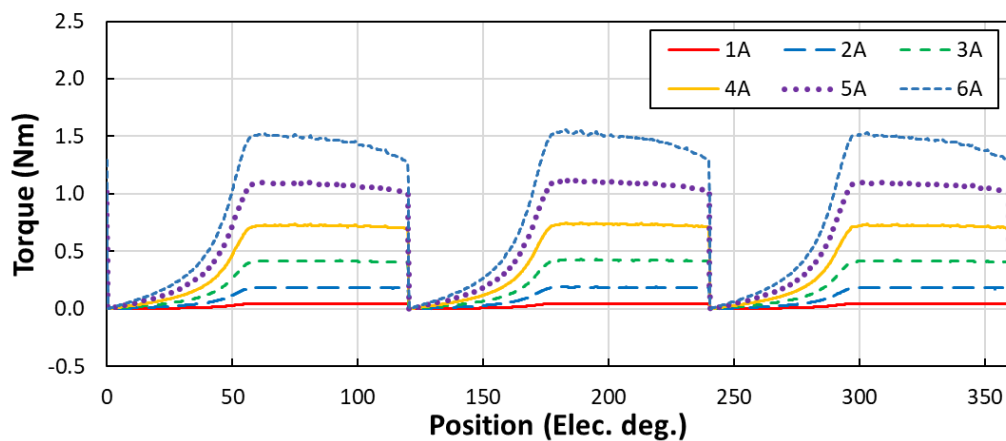


(b)

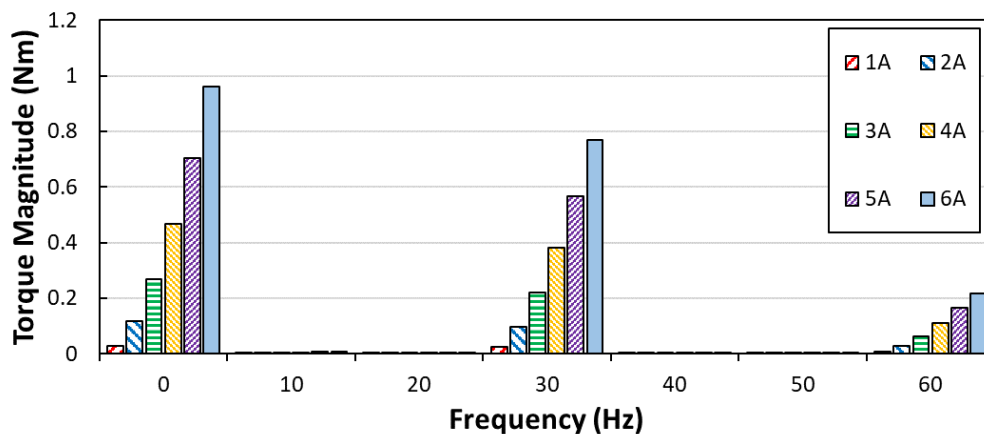
Fig. 3.10 (a) Variation in phase current illustrated for phase A only, (b) harmonic components up to 60Hz based on 150rpm operating speed.

3.3.1 Electromagnetic results

It could be said that the machine operating with minimum acoustic noise and vibration is a machine which produces zero torque. Hence, it is important to always consider the impact any current profiling will have on the torque of the machine. Torque production of the SR machine is directly linked to the input current. Hence, a linear trend in torque produced and increased load is observed. In the case of simulations performed in this chapter, it is seen that the torque will drop to 0Nm at the end of each phase excitation. This is due to the nature of the ‘ideal’ current profile used and the removal of transient inertial effects of the rotor. In real world applications, providing adequate coupling between the machine and load, and accounting for the effect of inductance and resistance, the torque shall not drop to zero. The purpose of these simulations is to demonstrate the suitability of the FE model against experimental results, and give an indication as to the impact and influence of varying parameters within the control of the machine.



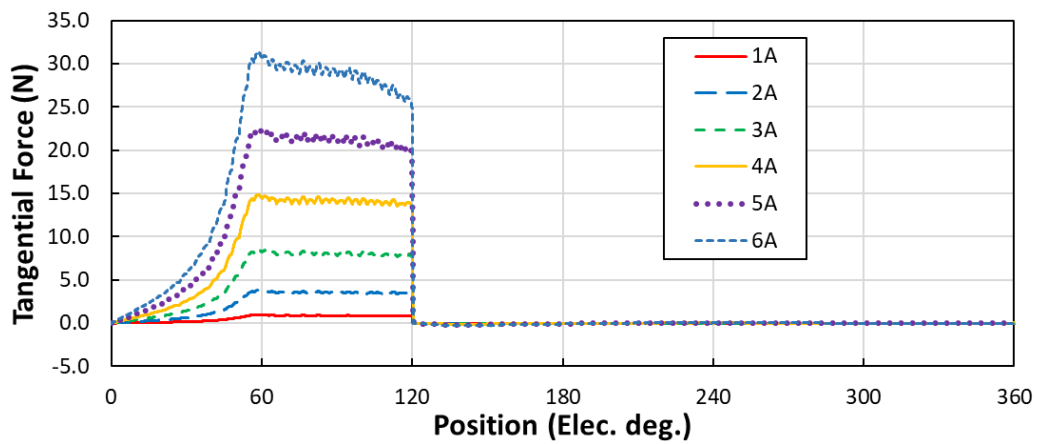
(a)



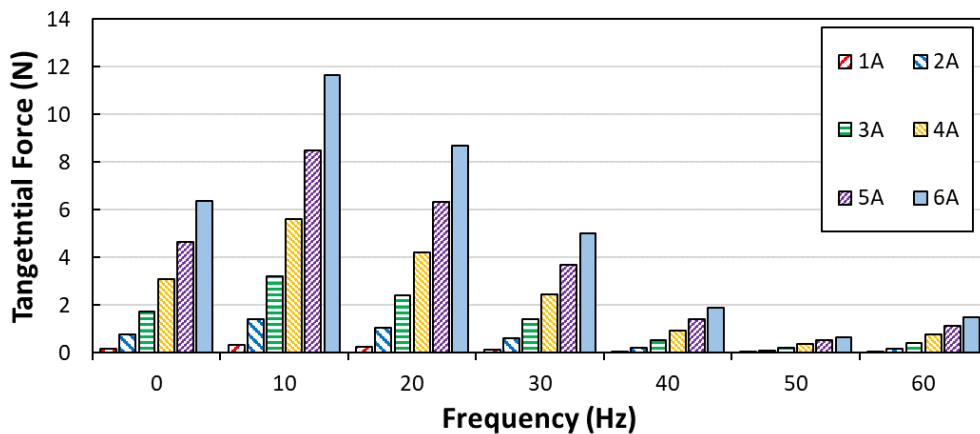
(b)

Fig. 3.11 (a) Influence of load current on torque, (b) harmonic content of torque produced up to 60Hz operating at 150rpm.

As the rotor rotates within the machine and flux passes across the air gap, both radial and tangential forces are generated. In general, it is considered that the tangential force is the major contributor to torque in the machine, whilst radial forces influence the acoustic noise and vibration. The tangential forces are integrated along a line in the middle of the air gap, across 1 stator pole pitch. Hence the results shown are relatable to the torque produced by each phase of the machine. The initial rise in tangential force is due to the limited flux path at the unaligned position, as the rotor and stator begin to align the tangential forces increase as the stator saturates. At this point in operation, $\sim 60^\circ$ electrical in this case, the maximum allowable flux is crossing the air gap with minimal overlapping of salient poles. This produces the maximum tangential forces as the contribution of flux to radial forces is minimal. At turn-off, forces fall to 0N as no flux crosses the air gap. For tangential forces, this will have significant influence on torque ripple and potentially the acoustic noise and vibration response also.



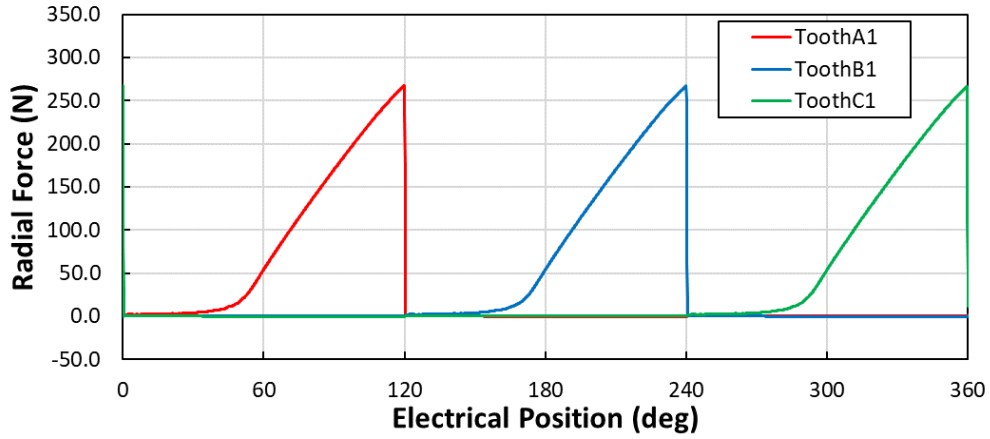
(a)



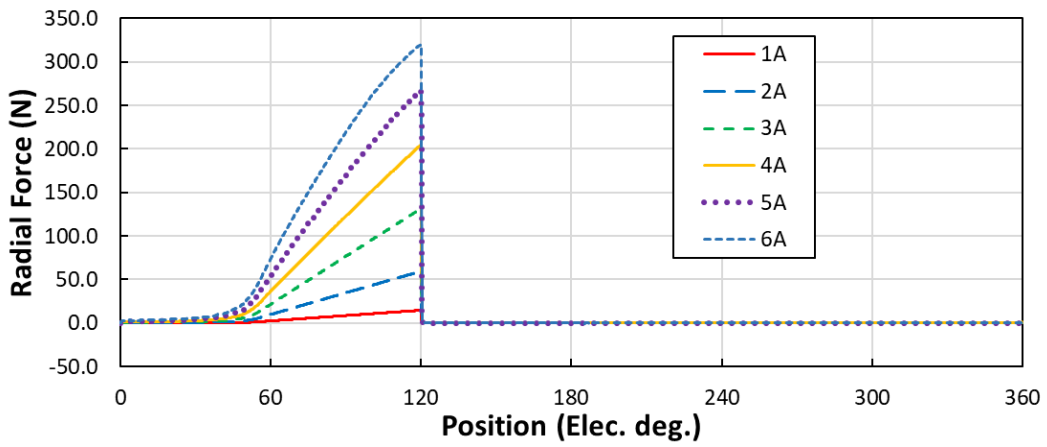
(b)

Fig. 3.12 (a) Air gap tangential forces measured across 1 pole pitch (tooth A1), (b) harmonic content of tangential forces produced up to 60Hz operating at 150rpm.

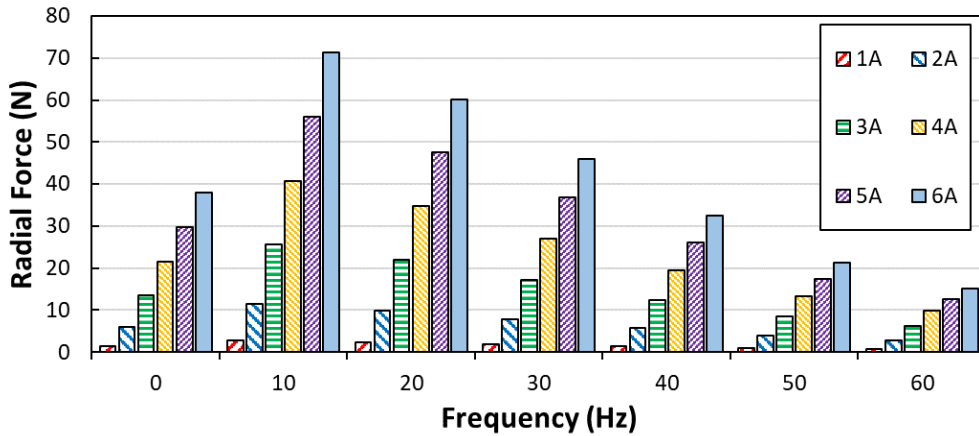
As previously mentioned, radial force is considered to have a significant impact and contribution to the acoustic noise and vibration characteristics of SR machines. The radial force is similar to a saw tooth waveform in profile, with the rising edge delayed by the transition of unaligned to aligned position. As can be seen in **Fig. 3.13** (a), the radial force is approximately equal for each tooth, allowing for minor variance in meshing in the air gap. In the cases simulated in this study, turn-off is considered to be ‘ideal’ with an instantaneous drop to zero. This results in an equivalent instantaneous drop in radial force. This may potentially increase the amplitude of the resultant vibration and acoustic noise due to the severity of change rate of radial force, dF_{rad}/dt . However, the inductance of the machine defines the rate of decay in current after turn-off, as this is an intrinsic property of the machine for bang-bang control it is reasonable to use the ‘ideal’ unipolar square wave current waveform as a reference point to compare trends. Considering the influence of a change in amplitude of load current, the peak radial force increases. As the machine nears heavy saturation the rise in radial force begins to saturate earlier in the electrical cycle. This will impact vibrations significantly. Considering the stator back-iron as a mass-spring damper system, if duration of maximum radial force increases the deformation of the stator also increases. At the point of turn-off this stored energy is then released, higher deformation leads to higher acceleration. This can also be shown by considering Newton’s law of motion, $F = ma$ where in this case the mass is constant so an increase in force results in a proportional increase in acceleration. This trend in increased amplitude can also be seen across all harmonic components of the radial force. The influence of turn-on is considered to be less compared to the influence of turn-off in current. At the instance of turn-on, the stator is in a neutral position relative to the pole being excited. Furthermore, based on the rotor position at turn-on the flux crossing the air gap is minimal, and hence, the radial forces are also minimal. Afterwards, the stator will be attracted by more or less “constant” force. As radial forces are low at turn-on and the stator is being deformed gradually from a neutral relative position, it follows that the influence on producing vibrations and resonance at turn-on is minimal. As the rotor transitions from the fully unaligned position to partially aligned, the position defined as turn-off, the flux crossing the air gap gradually increases. This results in a corresponding graduation of radial air gap forces. The radial force is reduced so quickly, the stator is almost in natural vibration with frequencies dominated by the resonant frequencies.



(a)



(b)



(c)

Fig. 3.13 (a) Air gap radial forces calculated for the case of 5A load condition, (b) Air gap radial forces measured across 1 pole pitch (tooth A1), (c) harmonic content of radial forces produced up to 60Hz operating at 150rpm.

The maximum change in radial force across one electrical period is also considered, also referred to as the rate of change of radial force. This factor will provide an indication as to the severity in the rise and fall of the radial force waveform per tooth. Under the circumstances presented for this baseline examination, the radial force decreases instantaneously to zero due to the current waveform hence, the trend in peak rate of change of radial force is equivalent to the maximum radial force. In later current shaping and profiling, the turn-off component of the current waveform is varied and as such dF_{rad}/dt no longer equates to a maximum radial force, but rather has a decaying trend or harmonic component. It may also be noted that along with the gradient at turn-off, the change in gradient is of interest. At the moment of instantaneous turn-off, the gradient of the profile changes phase from a positive slope to a negative slope, it is the extreme change like this which results in significant vibration.

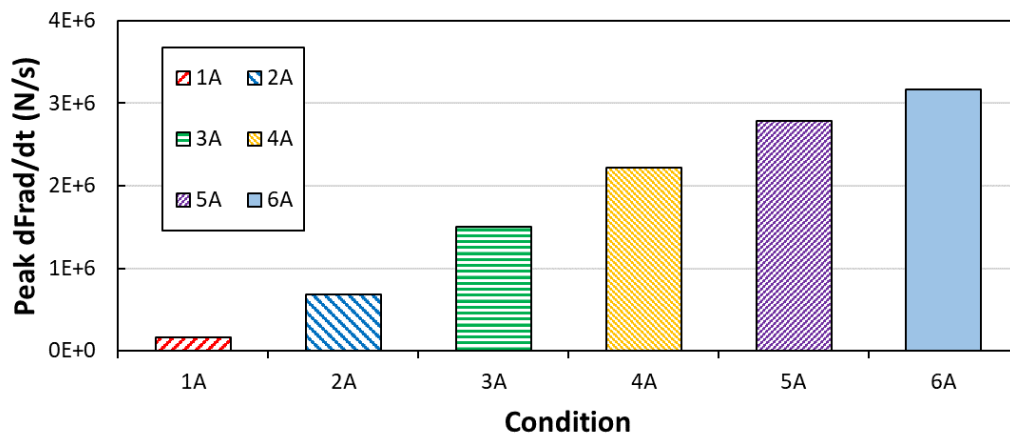


Fig. 3.14 Peak change in radial force with respect to time.

Considering the impact of the area under the force curve can be equated to the change in momentum experienced by the stator across one electrical period, due to the forces on that singular tooth. The integral of the waveform delivers change in momentum result, or force multiplied by time, which is referred to as the impulse acting on the tooth. This gives an indication to the impact of the force, for example a machine with exceptionally high current, hence high saturation, will experience a similar peak radial force per tooth. However, if this peak force is applied for a longer duration, the deformation is increased and also the resultant vibration. Calculating the impulse (or change in momentum) provides an indicator as to the duration of the applied force. In the cases of increasing load current investigated, it is clear the machine is not under heavy saturation with the trend of impulse closely related to the peak radial force trend.

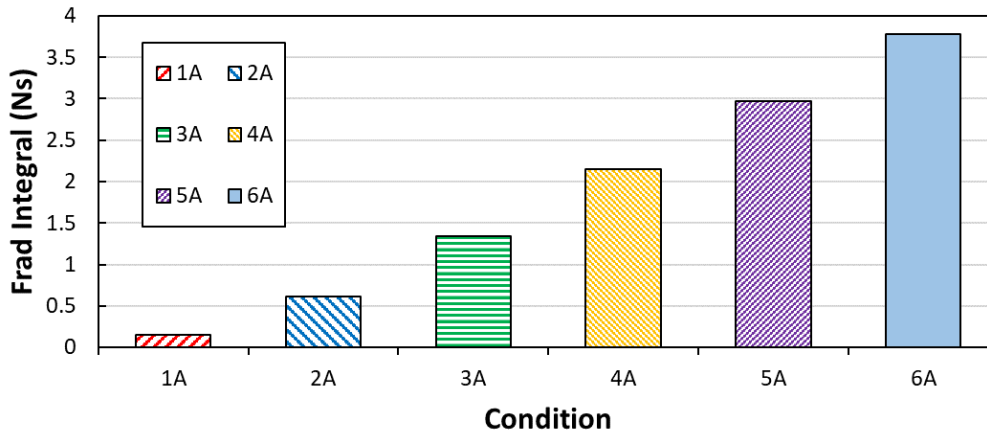


Fig. 3.15 Integral of radial force profile, equating to change in momentum.

The fundamental component of radial force acting across each stator pole is shown in **Fig. 3.16**, this demonstrates the total average force acting on a tooth due the electromagnetic excitation. It should be noted that mechanical sources of noise are due to the resonance between low order harmonic content in the electromagnetic spectrum and the cyclic rotational speed of the machine. This illustration does not account for these. However, as the speed of operation is low and focus is solely on the electromagnetic excitation this is a reasonable demonstration of the harmonic forces acting on the stator across one electrical period. It can also be considered that these are the independent forces acting on each pole with no interaction from other phases. The self-radial force is shown, neglecting the mutual radial forces. For a 6s/4r SR machine this is reasonable as there is no overlap of phases and the teeth are a considerable distance apart. However, for higher order stator/rotor pole combinations the mutual radial forces will have a larger impact on low frequency eigenmodes, as seen in [Tak15], [Kur15a], [Kur15b] and [Bay16]. It is clear that the fundamental component of radial force increases proportionally with the load current under the turn-off and conduction angle specified by the current waveform. Therefore, it is reasonable to suggest that the vibration response will produce similar conclusions.

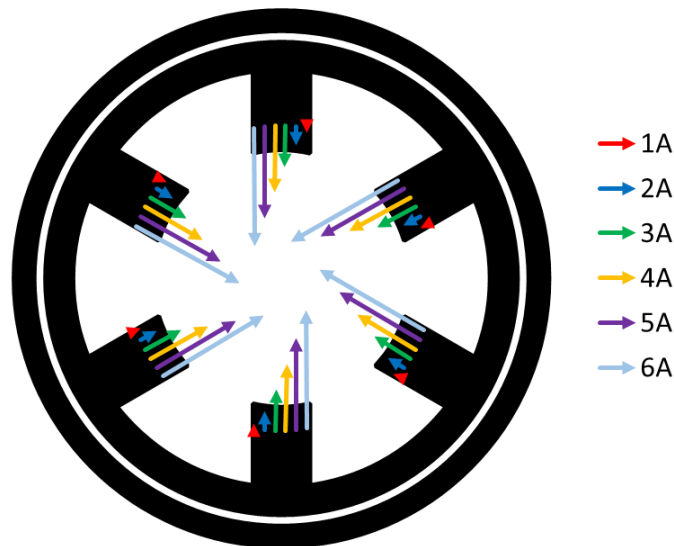


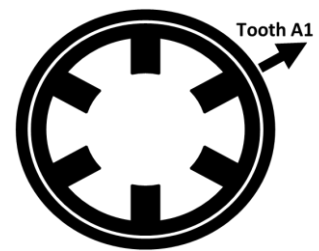
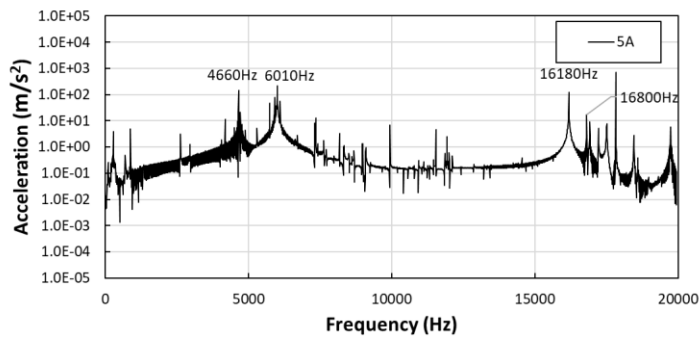
Fig. 3.16 Fundamental components of radial force on each pole shown acting on relative teeth, showing variance in magnitude of harmonic forces.

3.3.2 Vibration response

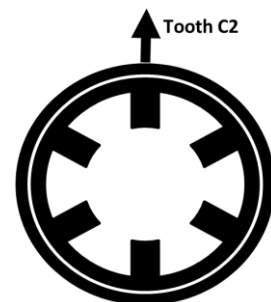
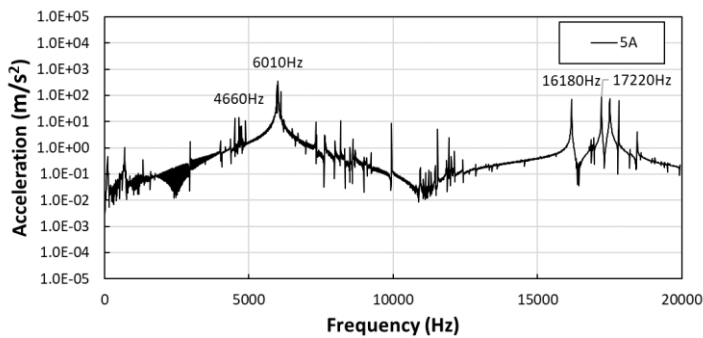
The vibration responses are measured at 7 points located on the stator casing at an axial central position relative to the stator. Furthermore, the locations of the vibration response simulations consist of 4 nodes behind teeth, and 3 nodes behind slots. The locations are selected to provide an overall picture of the total vibration response, with tooth C1 and slot B1A2 aligned with the bolt locations, hence experiencing significant vibration response due to mode (0, 2b) mode shape. Evidence from **Fig. 3.17** under 5A load current illustrates the dominance of mode (0, 2b) behind tooth C1, whilst behind other teeth the amplitude of the vibration response is approximately equal in magnitude. It can be concluded from the results shown that the vibration response across slots and teeth is approximately equal. However, behind bolted location specific modes are enhanced. This is caused by the additional stiffness introduced by the bolts and the additional mass comparative to the rest of the frame ends. Considering equal forces acting at high frequencies, due to the low speed and therefore lack of mechanical excitation, the amplitude of acceleration behind bolted locations is higher than respective locations without bolts. Equal force application behind a tooth and bolt compared to tooth and no bolt causes higher amplitude of response due to additional mass and a higher modal frequency caused by increased stiffness.

The influence of the bolted connection between modes is evident in the comparison of mode (0, 2a) and (0, 2b) results. For mode (0, 2b), the response behind tooth C1 and slot B1A2 indicates a dominant mode 2 maximum at approximately 6000Hz, with little to no excitation of mode (0, 2a). There is a minor peak caused by “flapping” of the endcaps, resulting in small deformation behind these locations for mode (0, 2a) at approximately 4600Hz. However, the dominant source of vibration in this case is mode (0, 2b). Conversely, in the case of non-bolt oriented locations (Teeth A1, B1, A2, slots

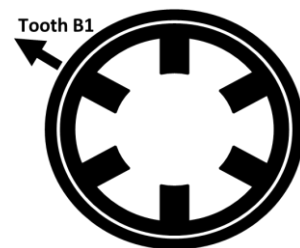
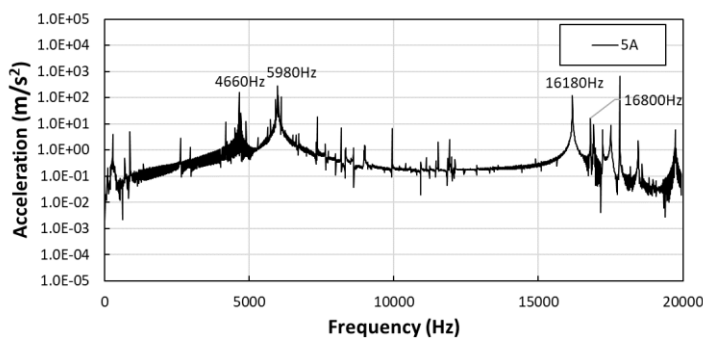
A1C2, C2B1) both identified eigenmodes of radial shaping 2 are clear. Across all mode shapes identified, the increase amplitude is clear and evident, with mode 2 variations dominant. As expected from trends seen in peak radial force, the increase in amplitude of vibration response is also close to linear proportionality. This study demonstrates the effect of current load on the vibration response, along with establishing a baseline expectation for results. Mode (0, 2b) is dominant, whilst mode (0, 2a) is also significantly higher than eigenmodes of mode (0, 4) variation. It is concluded from simulations that the vibration response is equal at slots and teeth not supported with bolts in the same plane of alignment, and the equivalent can be said for teeth and slots with bolts in the same plane.



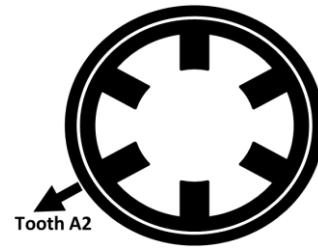
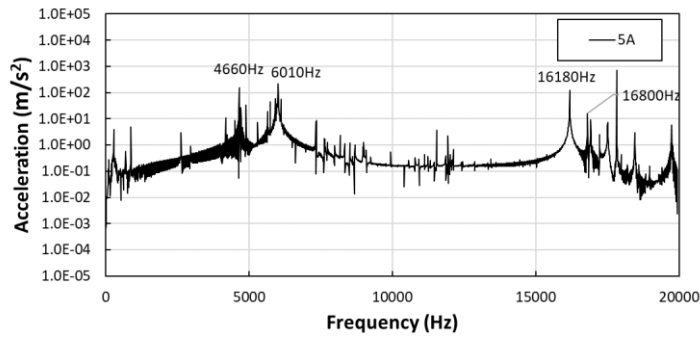
(a)



(b)

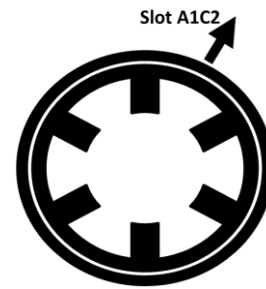
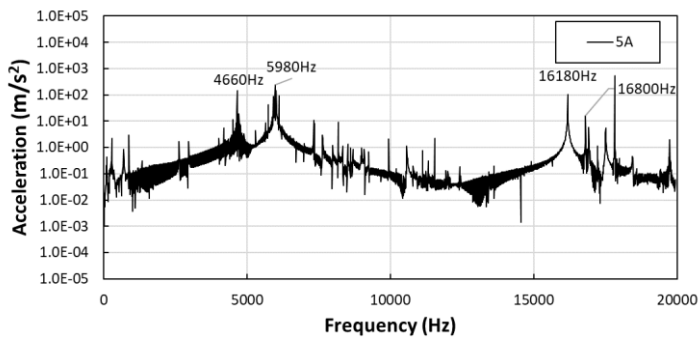


(c)

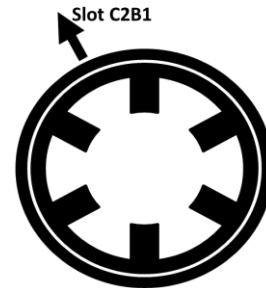
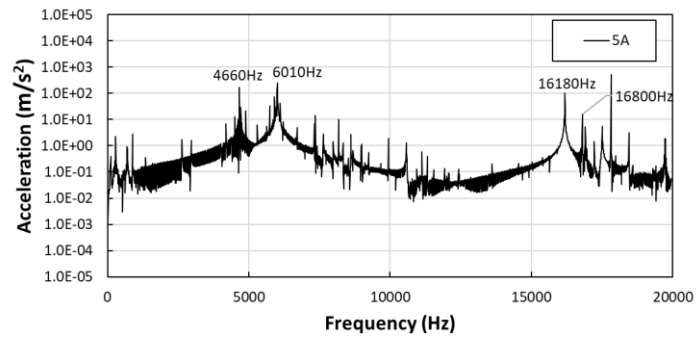


(d)

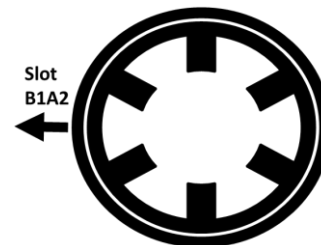
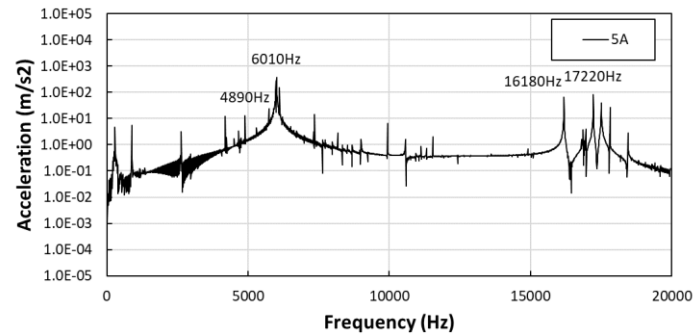
Fig. 3.17 Vibration response of 5A load current, simulated acceleration response on the casing behind teeth (a) A1, (b) C2, (c) B1, (d) A2.



(a)

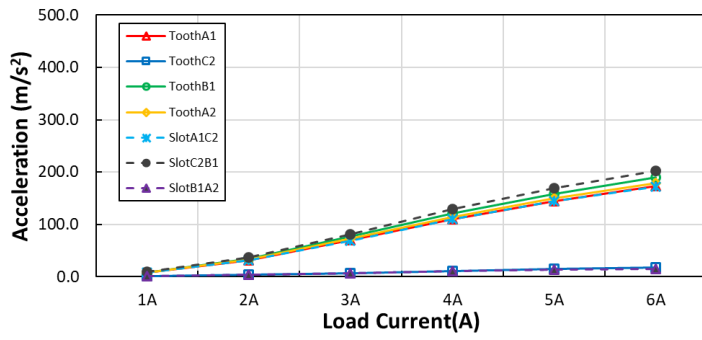


(b)

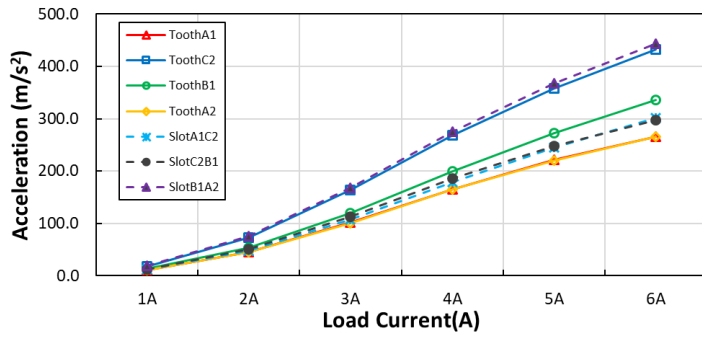
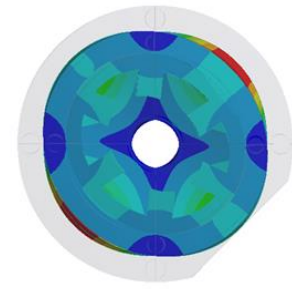


(c)

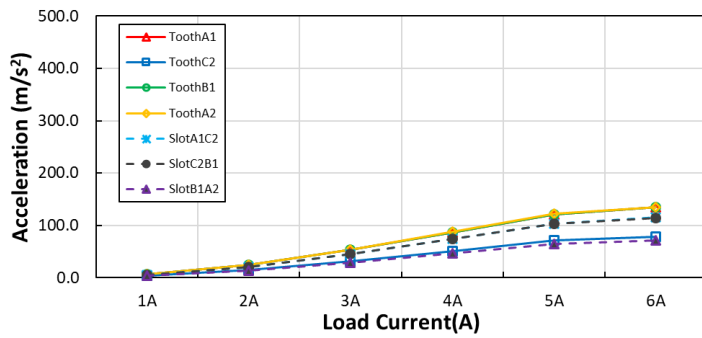
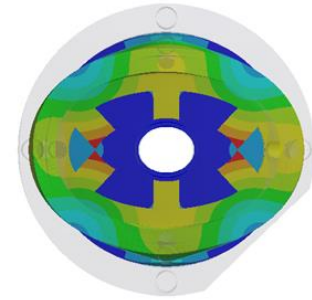
Fig. 3.18 Vibration response of 5A load current, simulated output on the casing behind slots (a) A1, (b) C2, (c) B1, (d) A2.



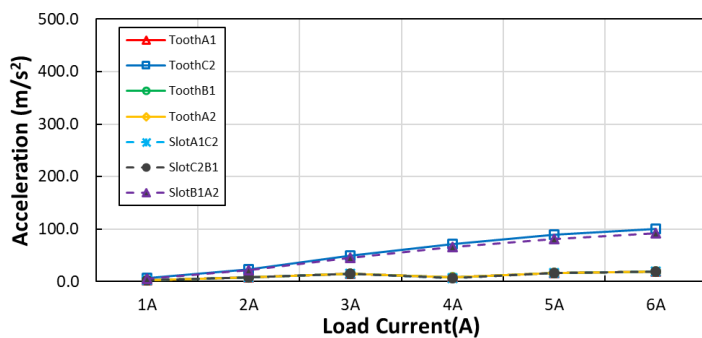
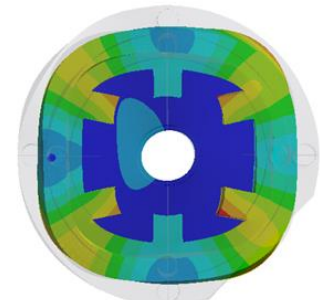
(a) Mode (0, 2a)



(b) Mode (0, 2b)



(c) Mode (0, 4a)



(d) Mode (0, 4b)

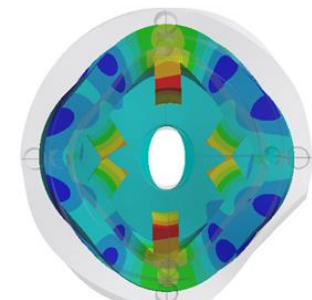
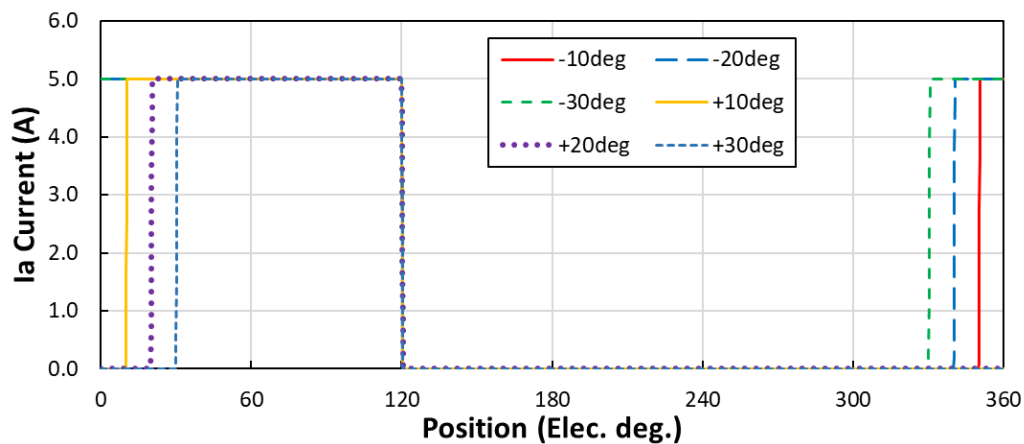


Fig. 3.19 Vibration response to harmonic force loads applied on stator teeth surface, shown for significant mode shapes (a) to (d).

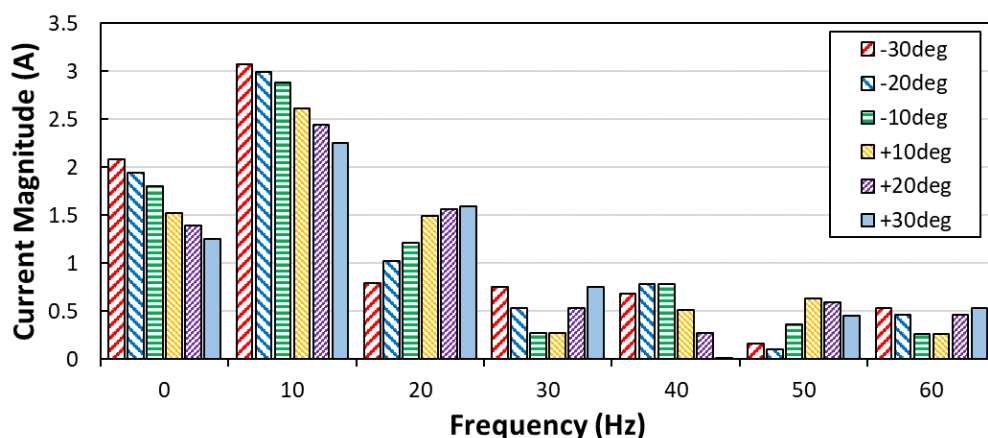
3.4 Influence of conduction angle

3.4.1 Fixed turn-off

To continue the study, a second parameter of the current profile is discussed, focusing on the effect of turn-on of the phase current. This takes the baseline conduction angle established in section 3.3 with 5A excitation, increasing the conduction angle by changing the position at turn-on whilst fixing the turn-off moment with respect to electrical position. The resultant current waveforms exhibit increased conduction angle with overlap between phases. However, overlapping of phase currents occurs in the unaligned region. Factoring this into the hypotheses where radial force is a dominant cause of stator borne vibrations, it is expected that an overlap in the unaligned position has no effect on the vibration response because there is no flux path during periods of extended conduction. As the flux is zero during the extended period, there is expected to be zero additional contribution to the radial force or tangential force production. It is noted that these conditions increase the copper losses in the machine as the same current is applied over an increased time duration.



(a)

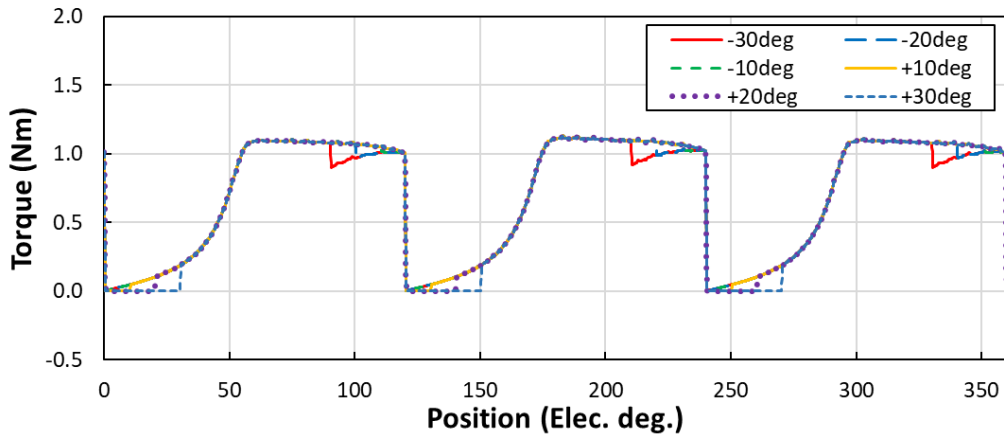


(b)

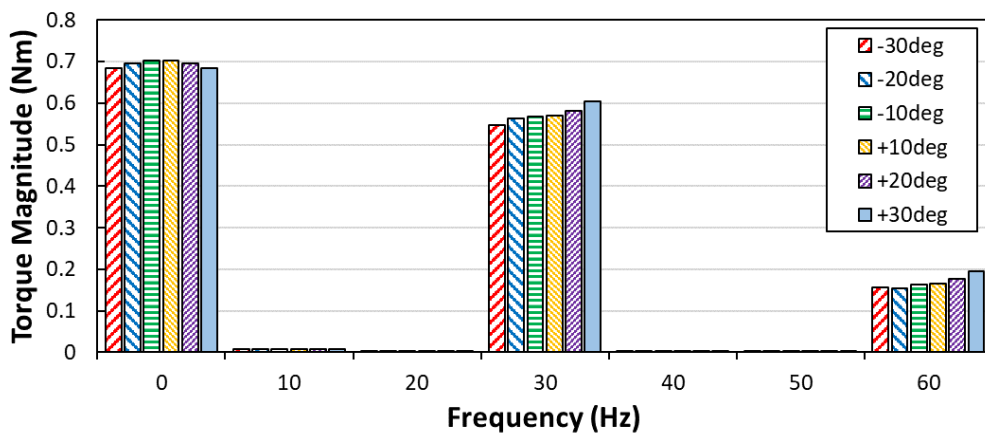
Fig. 3.20 (a) Variation in phase current illustrated for phase A only for varied turn-on position, (b) harmonic components up to 60Hz based on 150rpm operating speed.

3.4.1.1 Electromagnetic results

The influence of torque is caused by the overlapping of phase excitations at severe levels, in this case $\pm 30^\circ$ electrical. A negative variation in turn-on angle can be considered as an extension of the conduction period introducing overlap between adjacent phase currents. This results in the production of a negative torque in phase A whilst concurrently the peak positive torque is being produced in phase B, replicated in other phases for a full electrical cycle. This is not desirable for the machine as it introduces additional variance in the torque profile, whereas many applications desire a steady peak torque for smooth operation. Furthermore, in the cases of delayed turn-on, +10, +20 and +30deg, a dead time of zero torque production in the simulation is introduced. Obviously, this is not desirable as it reduces the average torque production whilst forcing the machine down to zero torque, a situation where current is being fed to the windings for zero gain. This is a reduction in efficiency, an increase in thermal losses, and may cause mechanical issues also. In a real world application under these conditions, the inertia of a machine this size will “carry” the rotor through to the next conduction period provided reasonable coupling of the system. Hence, there will be an increase in torque ripple, reduction in average torque and additional stress on mechanical components such as bearings caused by the jump in torque after dead time and the drop at the point of overlap.



(a)

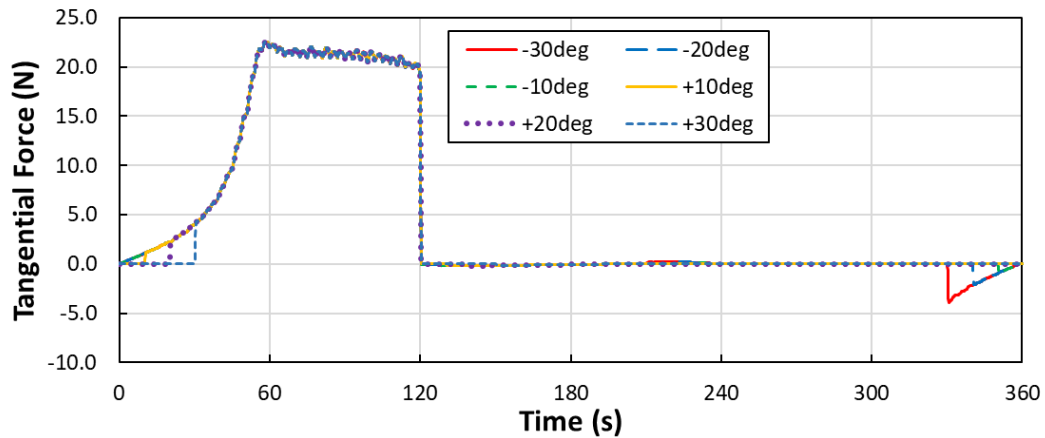


(b)

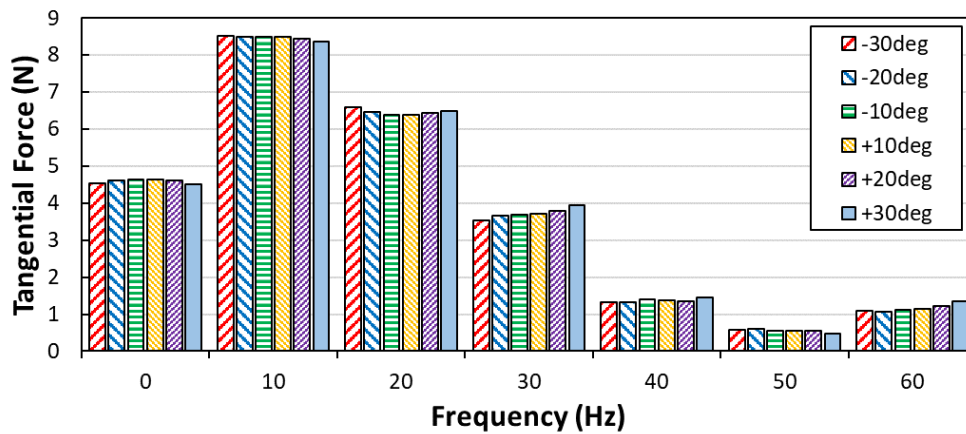
Fig. 3.21 (a) Influence of turn-on angle on torque, (b) harmonic content of torque produced up to 60Hz operating at 150rpm.

The tangential force calculated for flux density in the air gap along an arc covering 1 stator pole pitch further supports the ideas discussed in the torque profile for these variations in turn-on angle. In the case of a negative change in turn-on position, thus lengthening the conduction time, there is a period of overlap with the following phase resulting in a negative tangential force being produced. The single phase torque profile of a doubly salient 3-phase SR machine of 6s/4r configuration is dominated by the fundamental, similar in nature to a sinusoidal waveform. Considering the torque to be sinusoidal in nature at 180° electrical the tangential forces are zero, at the fully aligned position. From the fully aligned position to the fully unaligned position the tangential forces produced in the air gap are negative, effectively pulling the rotor back to the fully aligned position. The overlap introduced with these current profiles results in the following phase conducting in a period of negative tangential forces attracting the rotor back to the previous aligned position. In the case of the negative change in turn-on angle, shortening the conduction period, this results in a jump in tangential force as the stator is excited after the fully unaligned position. The electromagnetic forces are only produced in periods of excitation in

the teeth windings, with tangential forces at a maximum as the machine comes into alignment and there is a crossover between stator and rotor teeth.



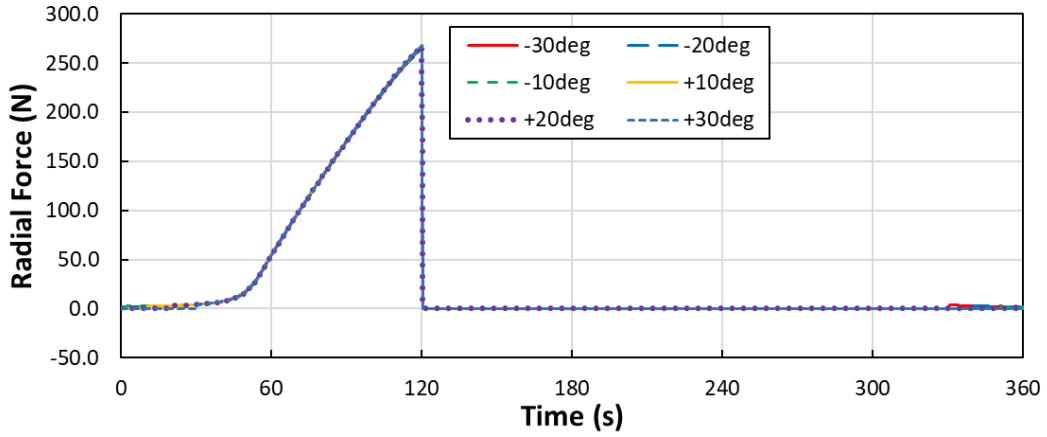
(a)



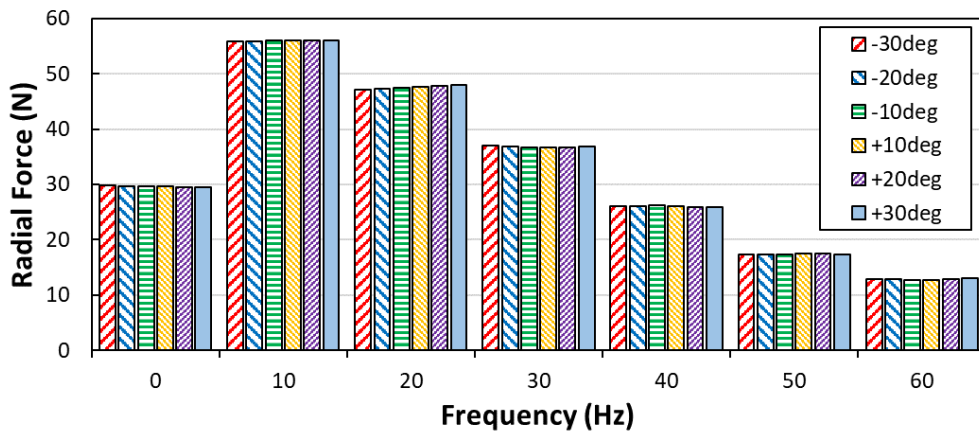
(b)

Fig. 3.22 (a) Air gap tangential forces measured across 1 pole pitch (tooth A1), (b) harmonic content of tangential forces produced up to 60Hz operating at 150rpm.

The impact of turn-on angle evidently has little effect on the resultant radial forces acting on each tooth, as shown for all analyses in this section. In the following, the radial forces calculated across the air gap adjacent to each stator pole pitch are indistinguishable from one another, with a minor radial force from overlapping of phases in extreme circumstances. This is supported by the contribution of low order harmonics in the radial force waveform, variance in these harmonics is negligible with a minor increase in the second harmonic as the conduction period is reduced. Radial force is at a maximum when the stator and rotor are in full alignment, and minimum at fully unaligned. Therefore, as varying the turn-on angle, if only changes phase excitation in the region before alignment there is little to no influence on the radial force produced. As is evident from the peak change in radial force and integral of radial force, the variance in turn-on angle has a negligible effect on radial force per tooth. The fundamental component of force applied to each tooth further supports this phenomenon.



(a)



(b)

Fig. 3.23 (a) Air gap radial forces measured across 1 pole pitch (tooth A1), (b) harmonic content of radial forces produced up to 60Hz operating at 150rpm.

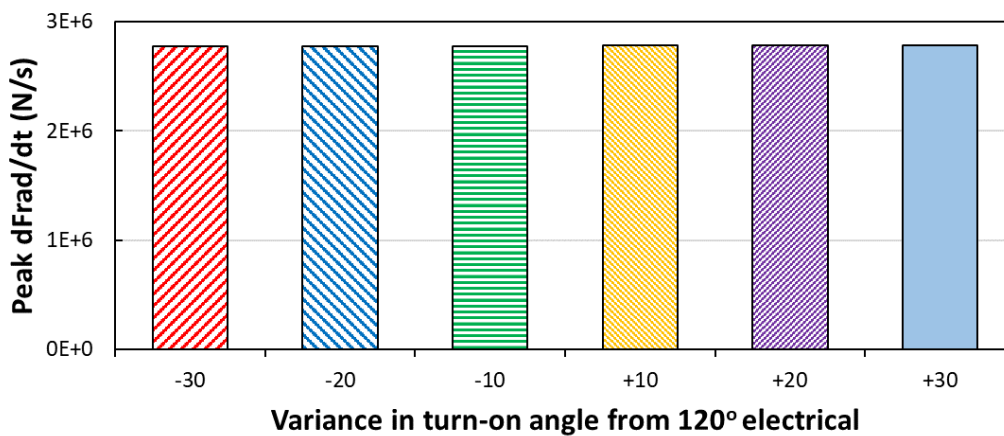


Fig. 3.24 Influence of turn-on angle on peak rate of change of radial force acting on a single stator tooth.

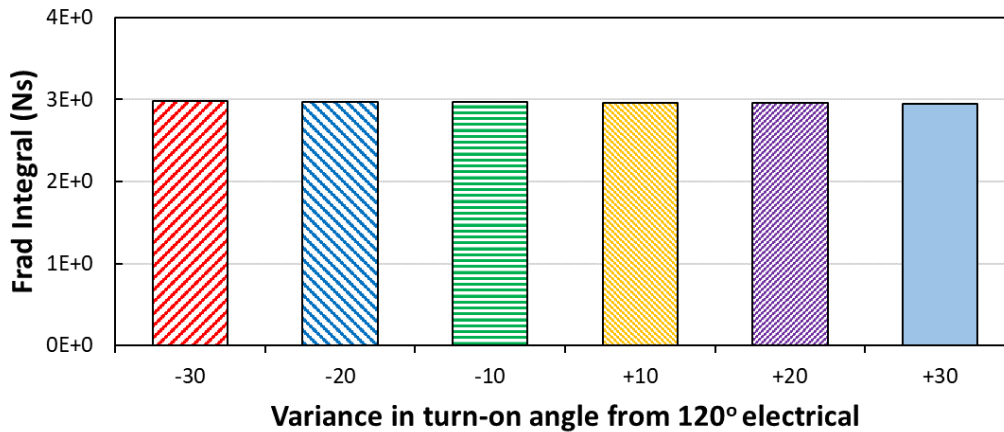


Fig. 3.25 Integral of radial force across one electrical period.

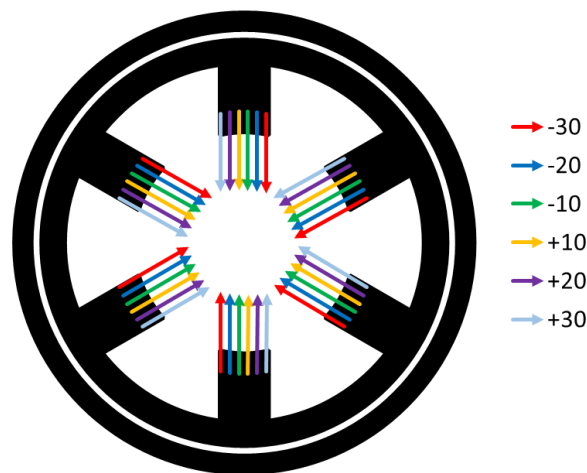
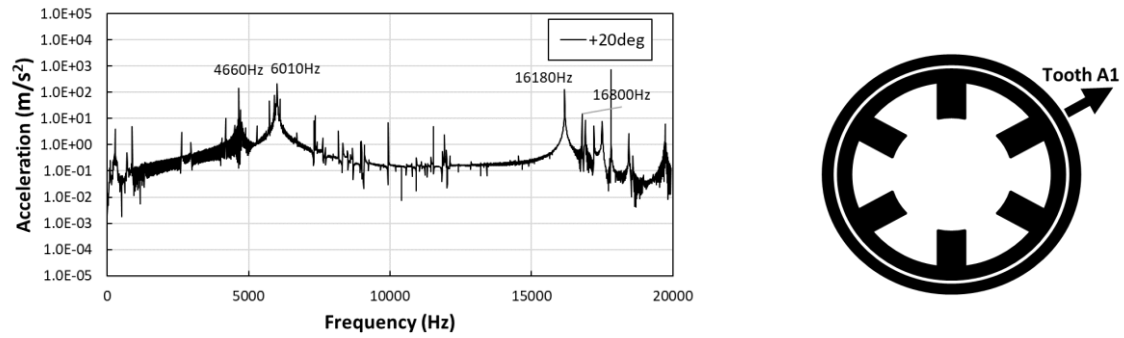


Fig. 3.26 Fundamental components of radial force on each pole shown acting on relative teeth, showing variance in magnitude of harmonic forces.

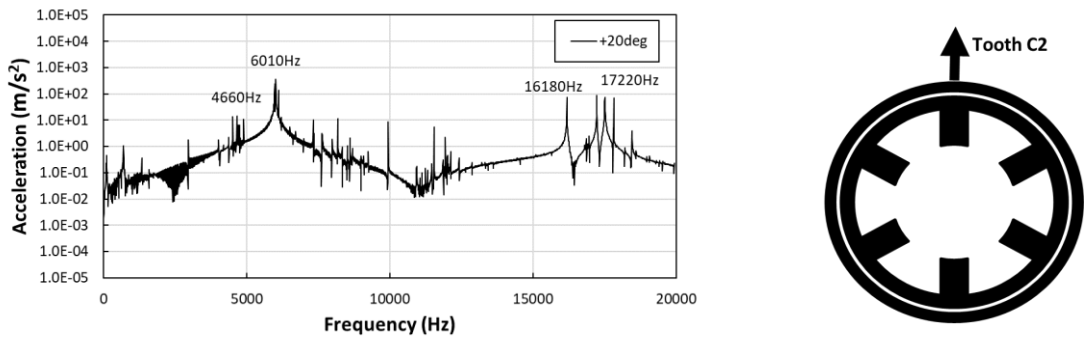
3.4.1.2 Vibration response

The trends in simulated vibration response behind both teeth and slots further support the theory that amplitude of vibration response is unaffected by variance in the turn-on position, provided turn-off occurs at the same electrical position. The amplitude of mode (0, 2a) is significantly lower behind locations aligned with bolted connections, in some cases the peak is no longer visible on the vibration spectra. Therefore, this may be a reasonable consideration in manipulating modal frequencies to avoid excitation if the operating speed of a machine is consistent, although in this case there is only electromagnetic excitation of eigenmodes due to the low speed capabilities of the prototype. Mode (0, 2b) is more consistent at multiple points located axially central on the machine as it is the dominant mode 2, the amplitude of this mode is highest across all measured locations for all variants in this

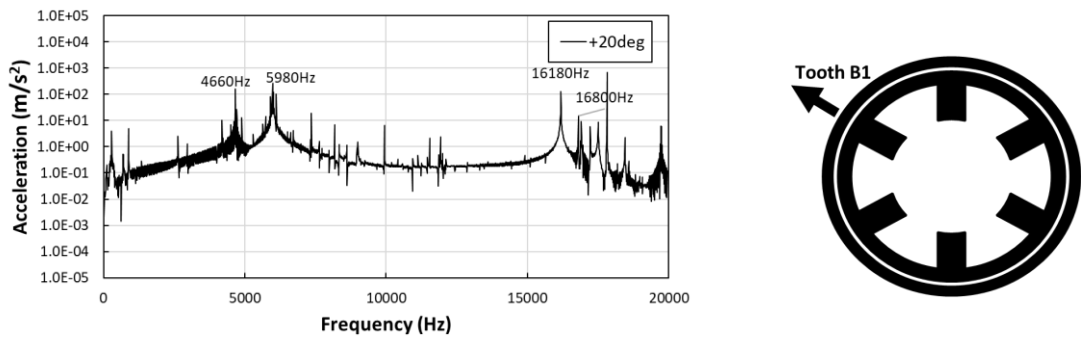
section. The results indicate that both mode (0, 4) eigenmodes have a lower amplitude than mode 2 variants, and so, it is expected that when measuring acoustic noise output from the machine that modes (0, 2a) and (0, 2b) shall be dominant. However, it is worth also noting the trade-off between amplitude and frequency in the audible spectrum, where a low amplitude high frequency noise may be more offensive than a high amplitude low frequency sound. Ultimately, it can be concluded from the vibration response that the turn-on position for a fixed turn-off position has no effect on the stator-borne vibrations. The variance resulted in significant implications for torque and tangential forces without any clear or obvious gain in vibration reduction.



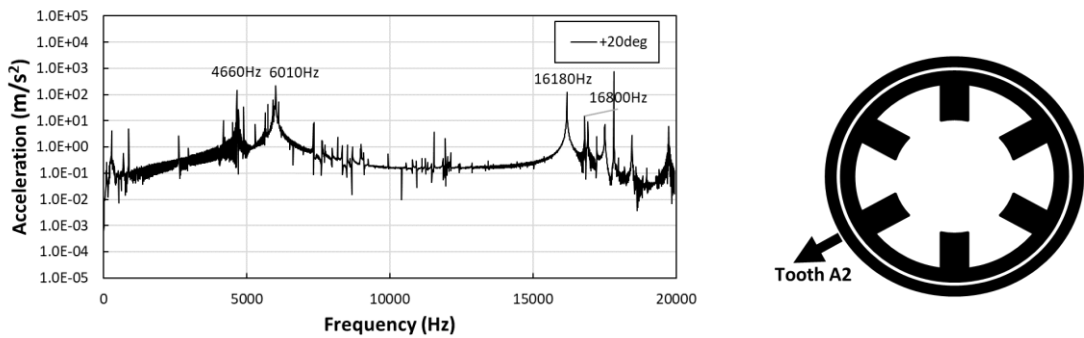
(a)



(b)

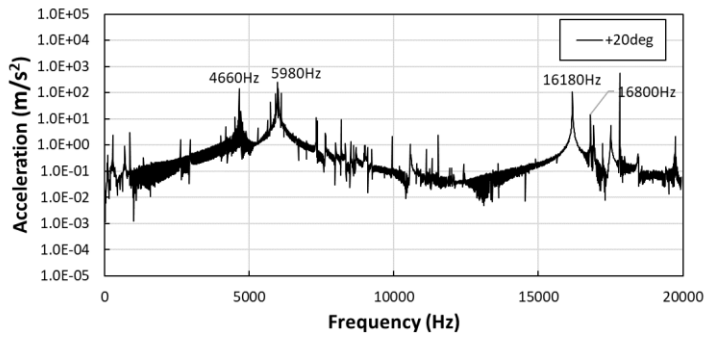


(c)

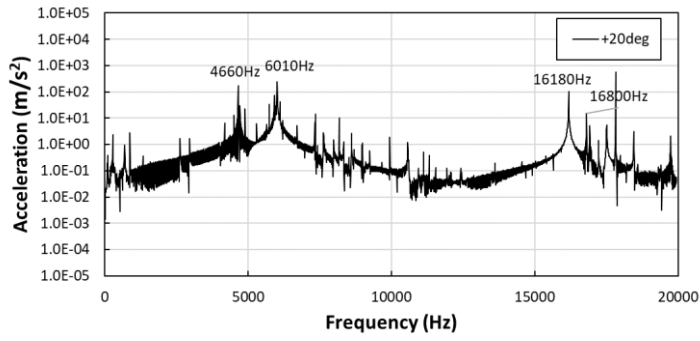
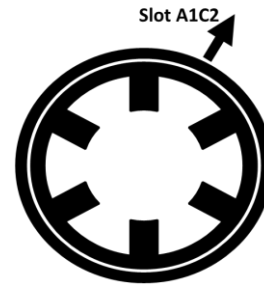


(d)

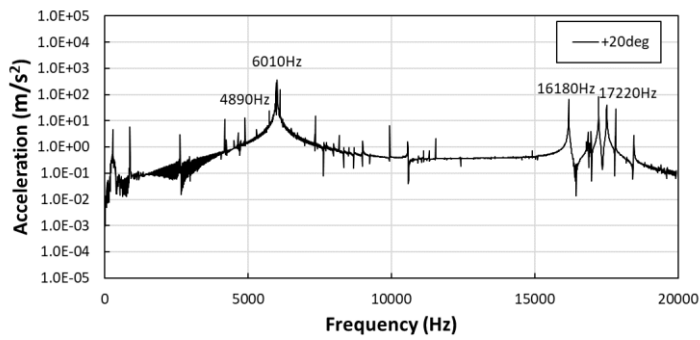
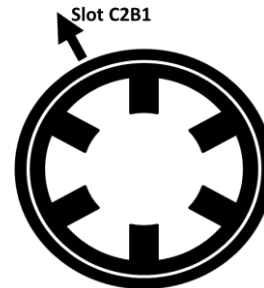
Fig. 3.27 Vibration response of 5A load current with +20° electrical increase from baseline turn-on, simulated output on the casing behind teeth (a) A1, (b) C2, (c) B1, (d) A2.



(a)



(b)



(c)

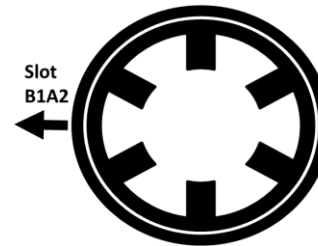
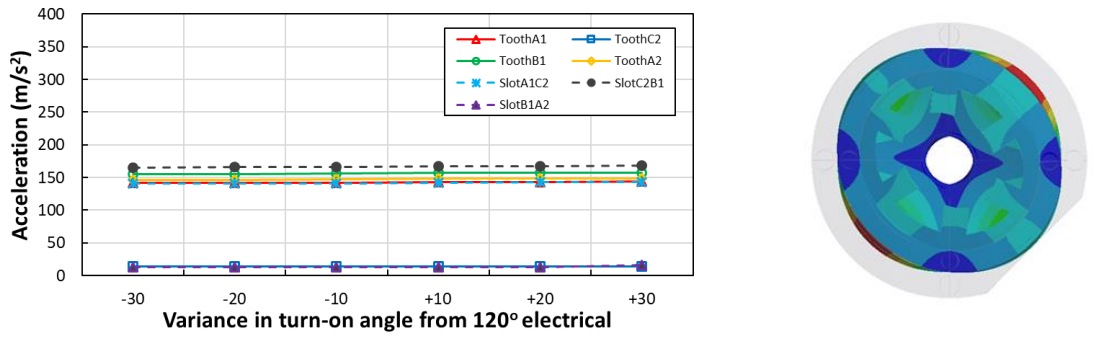
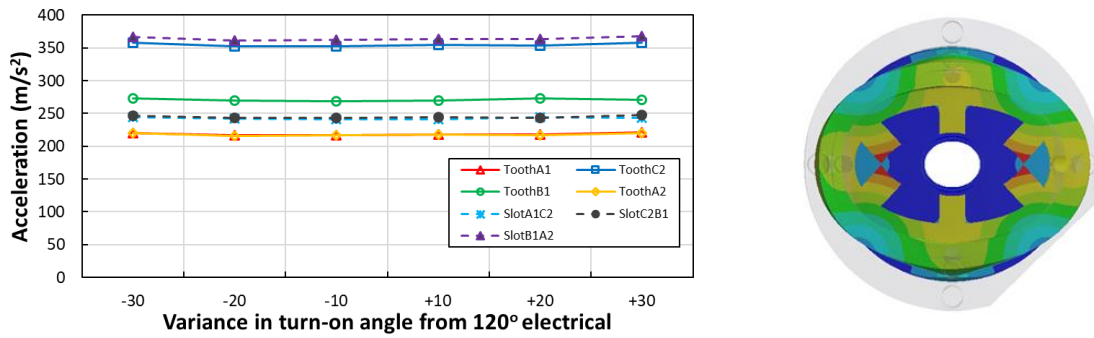


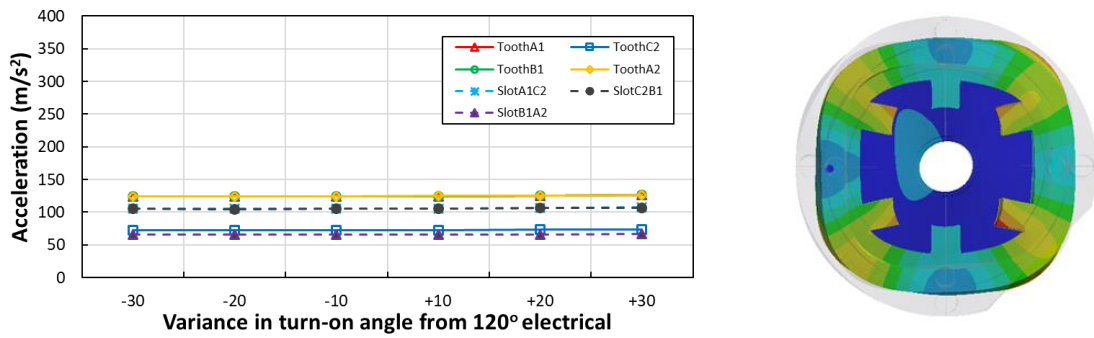
Fig. 3.28 Vibration response of 5A load current with +20° electrical increase from baseline turn-on, simulated output on the casing behind slots (a) A1C2, (b) C2B1, (c) B1A2.



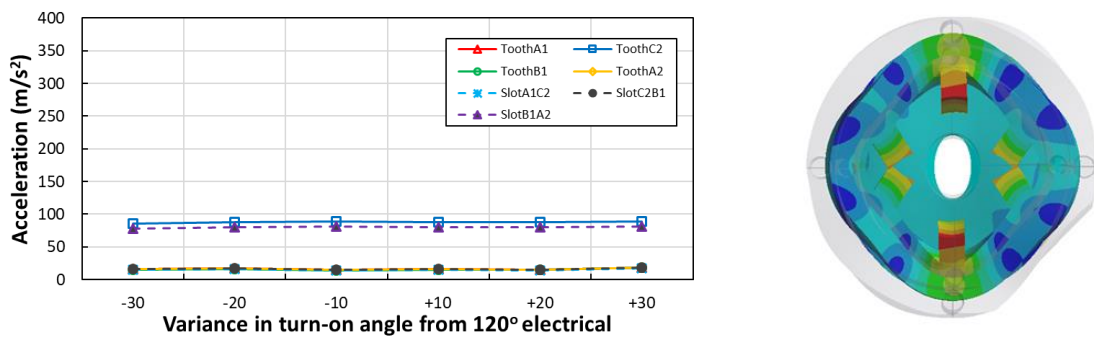
(a) Mode (0, 2a)



(b) Mode (0, 2b)



(c) Mode (0, 4a)

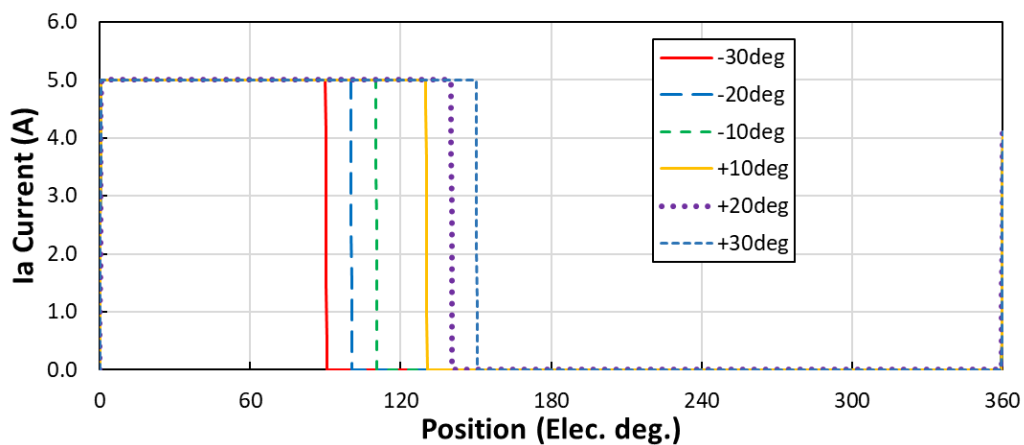


(d) Mode (0, 4b)

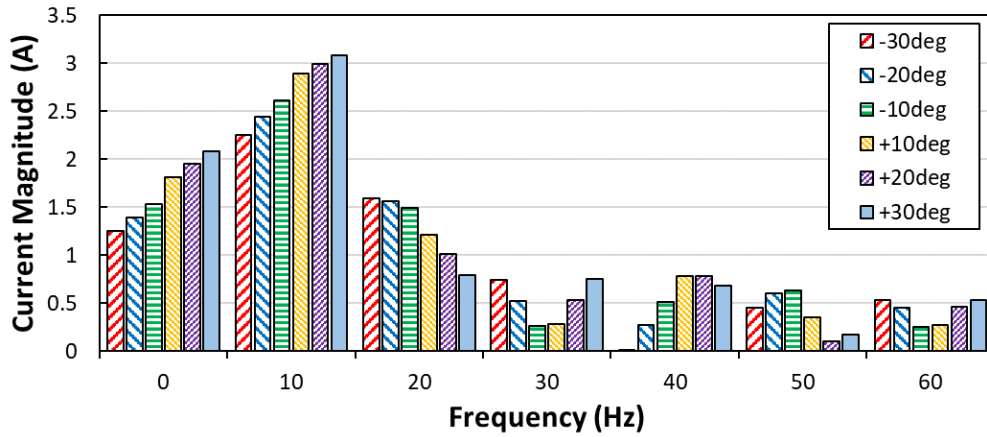
Fig. 3.29 Vibration response for varied turn-on angle, due to harmonic force loads applied on stator teeth surface, shown for significant mode shapes (a) to (d).

3.4.2 Fixed turn-on

Following the conclusion of influence of turn-on for a fixed turn-off, the influence of turn-off must then be analysed and discussed. Previous study in the time domain has indicated a dominant influence of the turn-off shaping and severity, [Wu93], through focus of time domain acceleration results. Due to the time extensive processing and modelling required to generate this solution in the time domain, it is not a practical FE modelling method. Hence, the study continues to focus on the vibration response in the frequency domain alongside supporting electromagnetic results. The turn-on position is kept constant such that the only influence on vibration response is variation in turn-off, manipulating turn-off position from -30° electrical to $+30^\circ$ electrical from the baseline of 120° electrical starting at a fully unaligned position. Furthermore, the variation in turn-off results in a linear rise in DC and fundamental harmonics, with more varied trends in later harmonic components. As the conduction period is increased the copper losses also increase, and hence, for a real world application it is important to consider the conditions of equal copper loss also. In the case studies presented in this section, the peak current is kept constant as this is known to have a significant impact on radial forces and vibration response as shown in 3.3.



(a)

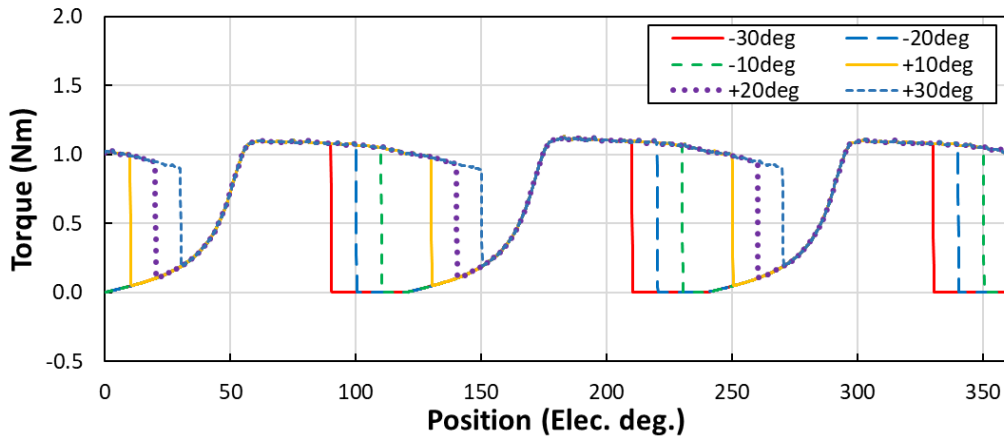


(b)

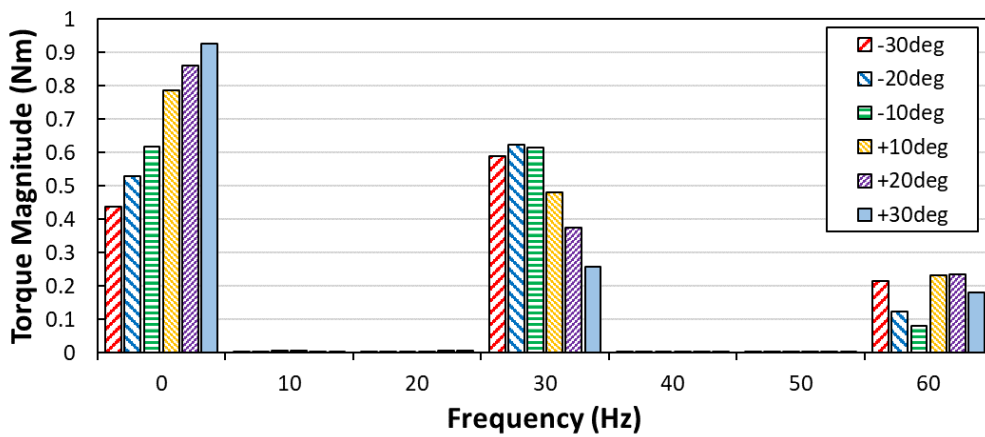
Fig. 3.30 (a) Variation in phase current illustrated for phase A only under varied turn-off conditions, (b) harmonic components up to 60Hz based on 150rpm operating speed.

3.4.2.1 Electromagnetic results

The influence on torque for varied turn-off angle is similar to variance of turn-on. A negative change in turn-off point results in a significant drop in average torque and introduces a dead time period of current. Consequently, there is a drop in torque to zero and a short period of no torque production resulting in a profile that exhibits maximum torque ripple. These characteristics are both significant disadvantages in machine design and control and present themselves as a drop in average torque. However, it is a strong indicator that the conduction angle is a critical parameter for torque production and therefore adjustments to any conduction period to reduce noise should also take note of implications to the average torque and torque ripple. Following this, an increase in turn-off angle can be regarded as an increase in conduction angle, hence causing overlap of phase currents and phase torque. Conversely to the case of overlapping phases in varied turn-on position, in this case the overlap results in increased average torque and reduced torque ripple at the cost of increased copper losses. Torque is still being generated in phase A after 120° electrical, at which time the next phase is turned on resulting in two phases generating simultaneous torque. Furthermore, after turn-off the torque being generated by the sequential phase is apparent, resulting in a reduction of torque ripple also.



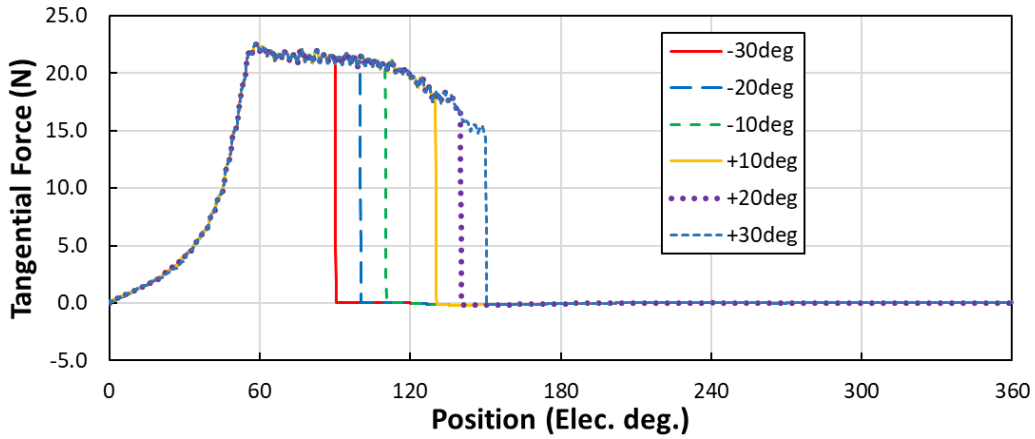
(a)



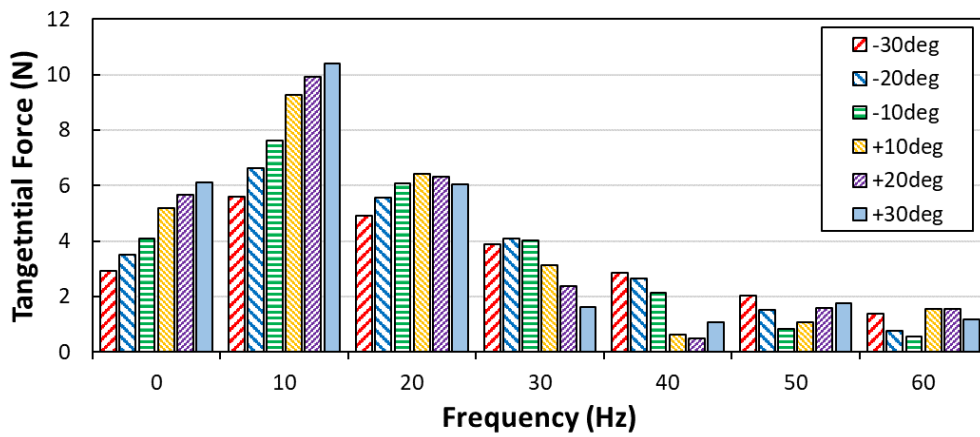
(b)

Fig. 3.31 (a) Influence of turn-off angle on torque, (b) harmonic content of torque produced up to 60Hz operating at 150rpm.

It is generally considered that the radial force is the dominant factor in stator borne vibrations and noise. However, the tangential force and particularly significant drops in tangential force must also be considered. As illustrated, the tangential force is strongly correlated to the torque generated in the machine, but is integrated across one stator pole pitch. The tangential force is at maximum as the stator and rotor teeth are coming into alignment, and zero at the fully aligned and fully unaligned positions. Beyond the baseline 120° electrical turn-off, the tangential forces tend to be zero. This is caused by the ratio of overlap between stator and rotor teeth, as there is more overlapping of poles, tangential force is reduced and radial force increased. As the conduction angle is increased to $+30^\circ$ electrical, the tangential force at turn-off decreases, and hence, the fall in tangential force is also reduced. The harmonic content shows a linear increase for DC and fundamental harmonics. However, there is no logical trend in harmonic content beyond this. This is potentially a result of the meshing in the airgap, across which this result is calculated.



(a)



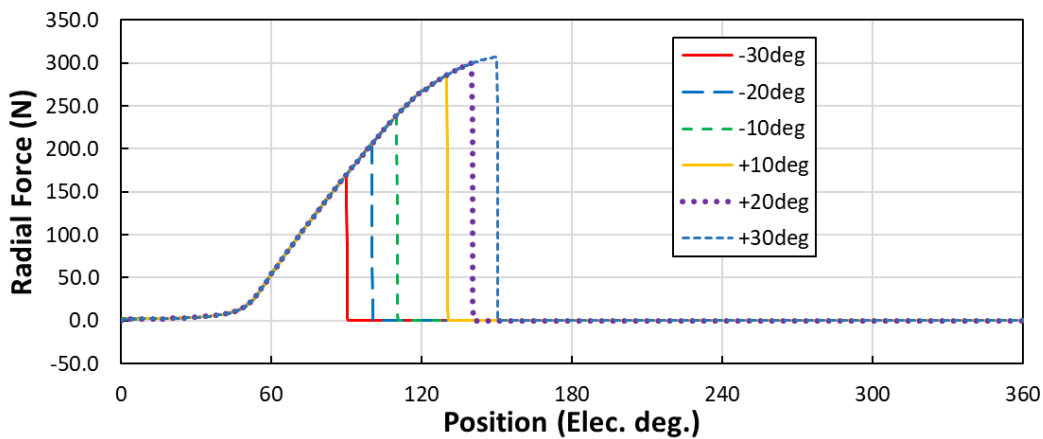
(b)

Fig. 3.32 (a) Air gap tangential forces measured across 1 pole pitch (tooth A1) compared for incremental turn-off angles, (b) harmonic content of tangential forces produced up to 60Hz operating at 150rpm.

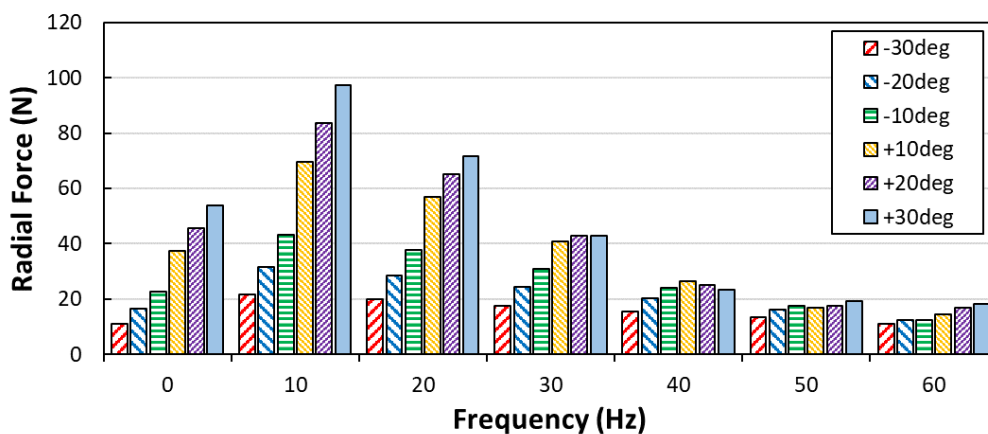
As discussed previously when targeting trends in tangential forces, as the turn-off position is increased the ratio of stator to rotor overlap increases. This is a progression towards the fully aligned position, known to be the position of maximum radial forces. As a result, the radial force increases as turn-off is increased, presenting a significant variance in radial force comparative to the results for a change in turn-on position. However, as the machine nears full alignment the radial force waveform begins to peak and level out. This phenomenon is due to the stator and rotor pole arc. For this machine specifically, pole arc in the rotor and stator are $\beta_r = 33^\circ$ and $\beta_s = 30^\circ$ mechanical, respectively, which can be interpreted as a fully aligned condition 1.5° mechanically ‘early’. Converting this into the electrical domain, the poles are fully aligned at 174° electrical and shall remain in a fully aligned condition until 186° electrical. Assuming the machine is operating under ideal and saturated conditions, the radial force in teeth of phase A is at a maximum from 174° to 186° electrical. Evidence of this is shown in the radial force waveform for extended conduction angle, where the radial force begins to

reach its limit. Thus, the peak radial force no longer falls in the linear region of a radial force profile, but compared to increase in turn-off angle the peak radial force is still increasing.

The magnitude of harmonic components increases for DC, the fundamental and the 2nd harmonic. However, beyond these low order harmonics no obvious trend can be seen particularly for positive changes in turn-off. Therefore, it can be hypothesised that the dominant harmonic components of force beyond the linear region of increasing radial force are the DC component, the fundamental and the 2nd harmonic. An approach to directly reduce these components may be of interest in future studies. From the perspective of rate of change in radial force, the peak change still occurs at turn-off as seen in all studies previous. However, for a significant increase in turn-off position the variance in dF_{rad}/dt reduces, further indicating the trends towards a level of maximum radial force acting on the tooth. The integral of radial force supports this argument, as expected due to the profile of the waveform being extended. The application of forces onto the equivalent teeth indicates that the increase in conduction angle will result in an increase in vibration response also.



(a)



(b)

Fig. 3.33 (a) Air gap radial forces measured across 1 pole pitch (tooth A1) for varied turn-off angles, (b) harmonic content of radial forces produced up to 60Hz operating at 150rpm.

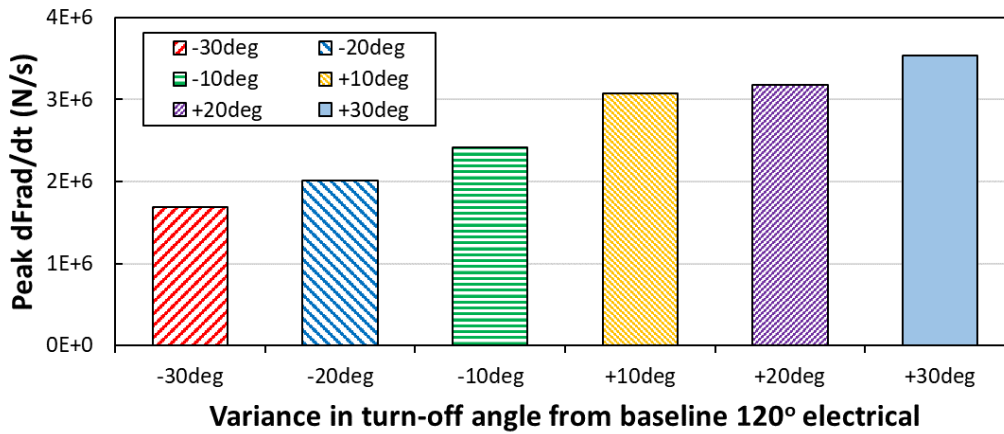


Fig. 3.34 Peak rate of change in radial force compared for variance in turn-off angle from baseline 120° electrical conduction angle.

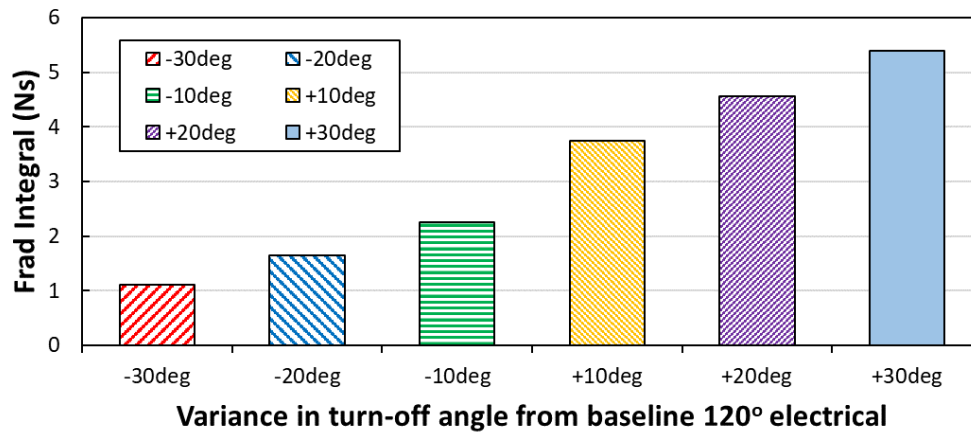


Fig. 3.35 Integral of radial force across 1 electrical period comparing influence of turn-off angle.

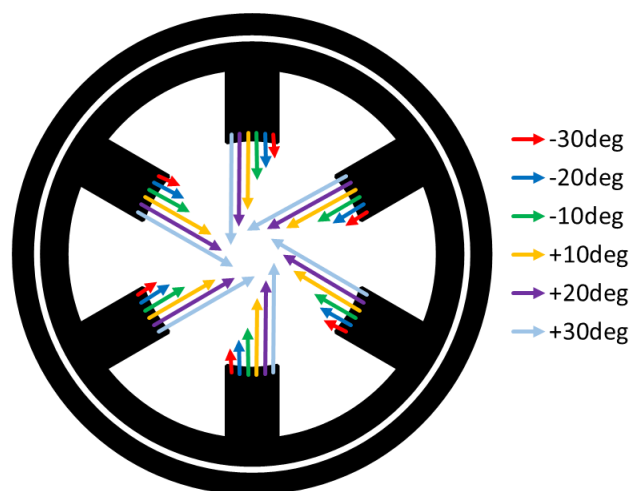


Fig. 3.36 Fundamental components of radial force on each pole shown acting on relative teeth, showing variance in magnitude of harmonic forces due to varied turn-off angle.

3.4.2.2 Vibration response

Based on findings from the electromagnetic results, particularly radial force, it is expected that as the position of turn-off is increased from the baseline 120° electrical, the vibration response will increase. However, the radial force calculations and diagrams are presented for forces acting on a single tooth only, it should not be forgotten that in periods of overlap the forces of adjacent teeth will also influence the vibration response. The vibration response echoes the results shown previously, where the dominant source of stator borne vibrations is of mode shape (0, 2) whilst modes of mode shape (0, 4) are lesser in amplitude. Similarly, under overlapping current phase conditions there is still a comparable difference between results behind tooth C2 and teeth A1 and B1, where the bolted connection of endcaps causes a second mode (0, 2) variant.

Comparing trends in amplitudes of eigenmodes, for mode (0, 2a) there is a linear increase as the turn-off angle is increased. Furthermore, the increase in amplitude settles as the conduction angle reaches the limit specified for this study, a similar trend as seen in the radial force profiles across a single stator pole pitch. Also, the amplitude of mode shape (0, 2a) is unaffected by the increase in conduction angle for locations aligned with bolted connections due to the dominance of the new mode (0, 2b) that is introduced. This also implies that mode (0, 2a) is a result single phase electromagnetic excitation as the trend matches the trend in radial force across a tooth tip. However, the influence on amplitude of mode (0, 2b) tells a different story. For this modal result, the amplitude is significantly higher for the condition of 120° electrical, the baseline for comparisons. It is obvious that a reduction in conduction angle from this point causes a decrease in radial force and a reduction in active radial force, the time over which the force is acting on the tooth. This results in decreased deformation of the stator and hence reduced amplitude of vibrations. Alternatively, an increase in conduction angle causes higher peak radial forces acting on across the pole for a longer period, and hence, the expectation may be that the vibration response is increased. However, this neglects the effect of adjacent phases and poles which experience a radial force in the period of overlapping current between phases. The baseline condition of an 'ideal' waveform operating for 120° electrical conduction angle for 3 phases exhibits the most extreme case. The definition of the baseline causes a 'release' of two diametrically opposed teeth at the exact instance that the next phase is excited, and hence, the radial forces are acting entirely on a single phase. Therefore, the stator experiences a radial force acting in opposite directions only at any one instance. After the conduction angle is increased such that there is overlap between phases at turn-off, this is no longer the case. A second phase pair of forces acting diametrically opposite at an angle away from the original phase is introduced. This reduces the overall deformation experienced as the stator is no longer being mechanically excited in a single plane, now in two radial directions. As can be observed in **Fig. 3.39(b)** this phenomenon is seen across all teeth and slots. Mode (0, 2b) is focussed on phase C as both teeth aligned with bolted connection are of this phase. Observing deformation against time, the stator teeth are attracted inwards for phase C, mode (0, 2b) deformation results in the slots in the x-axis plane being deformed outwards as known for an axial mode 0, radial

mode 2 eigenmode. In this example, phase A is excited after or during phase C operation, depending on conduction angle, and thus produces a radial force acting at 60° to F_{radC} , where F_{radC} is the radial force on phase C excited teeth. Considering the force acting on tooth A1 or A2, F_{radA} , is composed of 2 components F_{XA} and F_{YA} with configuration as depicted throughout the study. F_{XA} shall be larger than F_{YA} and oppose the deformation produced as a result of F_{radC} . Hence, the vibration response caused by a period of overlap between phase excitation will be reduced by influence of other phases.

The influence of turn-off angle on the amplitudes of modes (0, 4a) and (0, 4b) shows similarities with the influence on mode (0, 2b). Shapes of mode (0, 4) are heavily influenced by the stiffness and rigidity introduced with the bolts. The trends indicate the same phenomena as seen for mode (0, 2b), where the baseline waveform of 120° electrical experiences a higher vibration response than other variants. It can also be confirmed that mode (0, 4a) produces a lower vibration response for the bolted locations, indicating that these are not a major influence for this eigenmode.

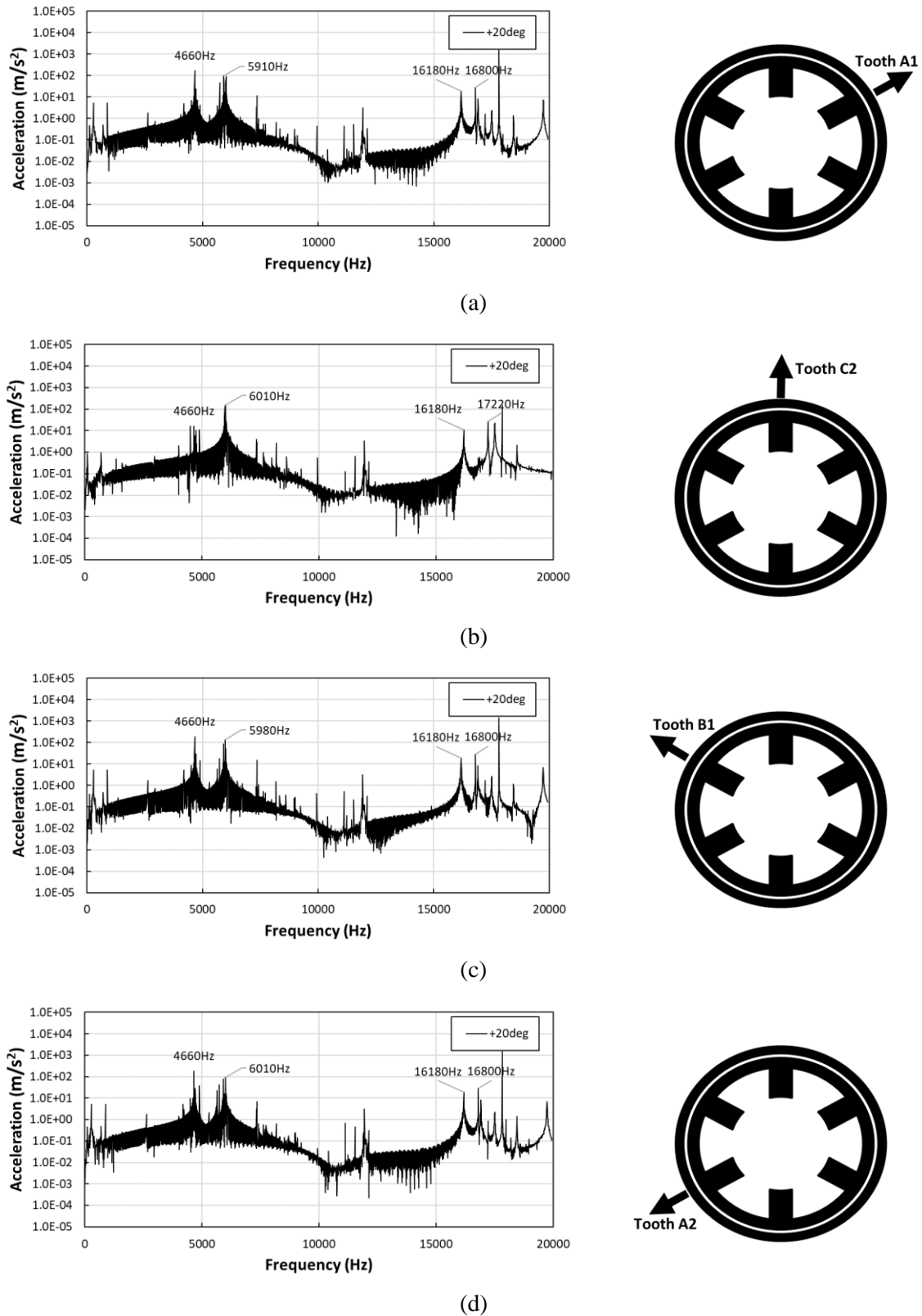
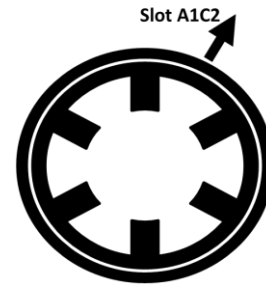
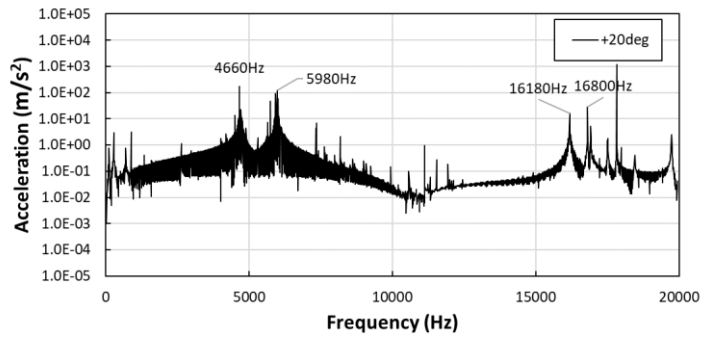
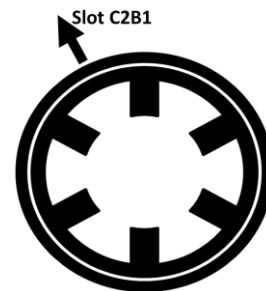
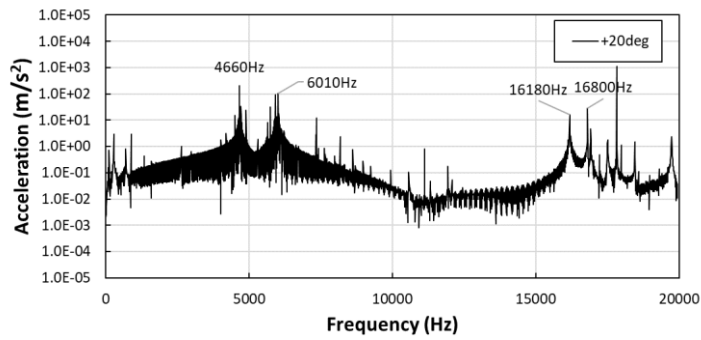


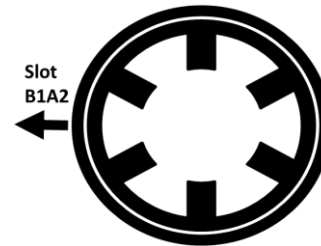
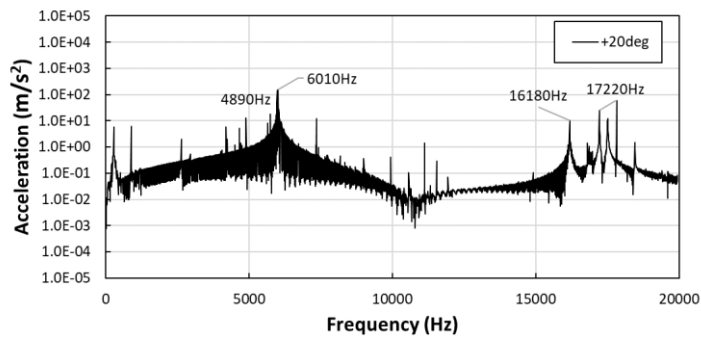
Fig. 3.37 Vibration response of 5A load current with turn-off angle increased by +20° electrical from 120° baseline, simulated output on the casing behind teeth (a) A1, (b) C2, (c) B1, (d) A2.



(a)

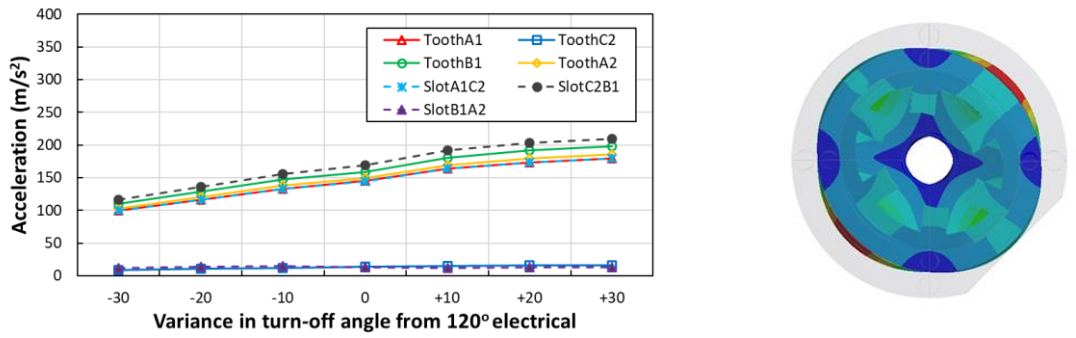


(b)

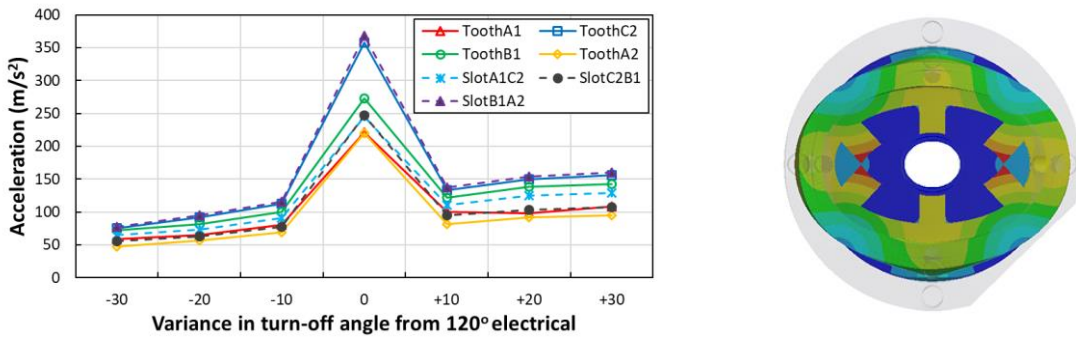


(c)

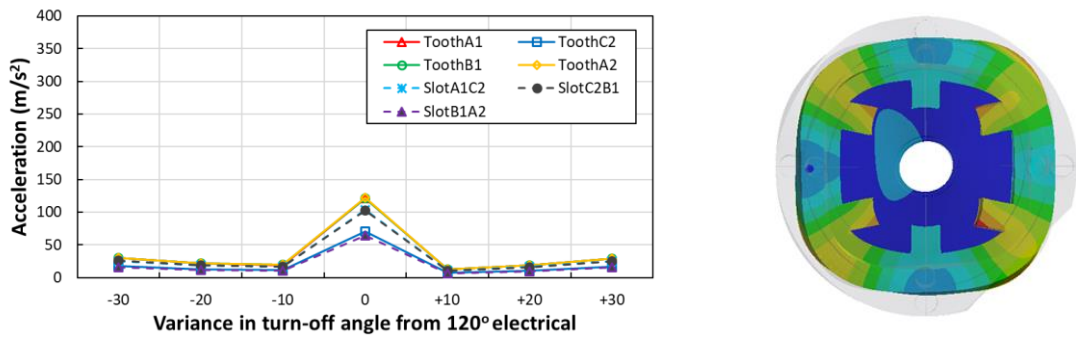
Fig. 3.38 Vibration response of 5A load current with turn-off angle increased by +20° electrical from 120° baseline, simulated output on the casing behind slots (a) A1C2 (b) C2B1 and (c) B1A2.



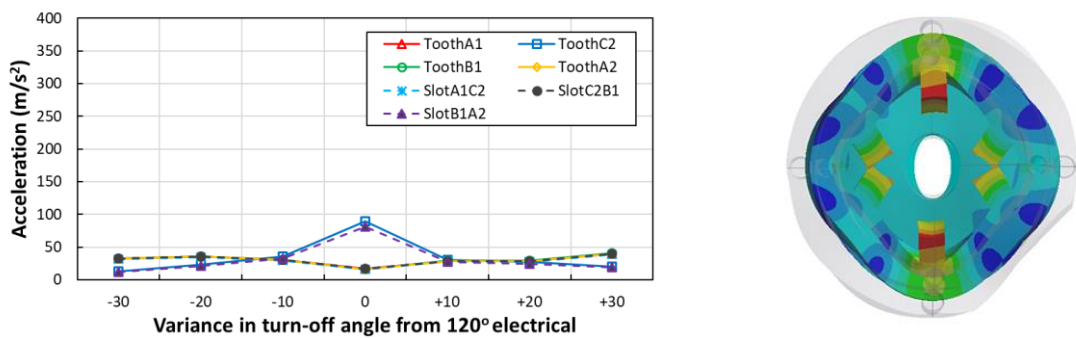
(a) Mode (0, 2a)



(b) Mode (0, 2b)



(c) Mode (0, 4a)



(d) Mode (0, 4b)

Fig. 3.39 Vibration response to harmonic force loads applied on stator teeth surface, shown for significant mode shapes (a) to (d).

3.5 Experimental verification of trends

3.5.1 Experimental setup and testing

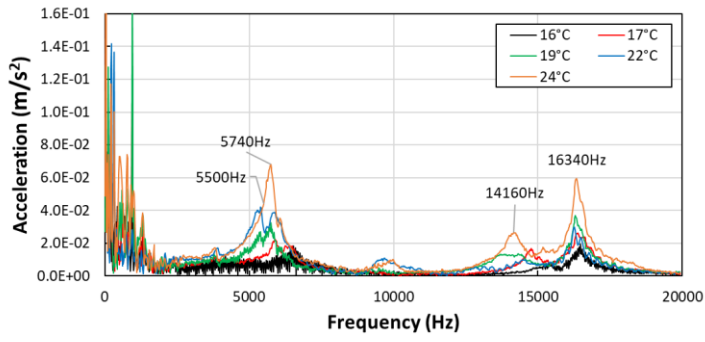
In order to verify the accuracy and suitability of the FE model for predicting trends in vibration response under operating conditions the cases examined thus far are verified experimentally. The prototype machine is limited in respect of its thermal and speed capabilities, with the maximum speed capable at 1000rpm. It is found that the optimum speed to produce clear results for vibration response is 150rpm, which allows for a reasonable current profile and reasonable resolution for vibration spectra. Beyond this there is seen to be considerable overlap between phases in the current profile and an increase in broadband noise in the vibration spectra, making analysis and comparisons more difficult. At this speed of operation, the natural frequencies excited are 10Hz mechanical frequency, followed by 30Hz for 3-phase and 120Hz due to 4 rotor poles. A simple calculation concludes that in order to mechanically resonate the lowest radial mode for axial mode = 0 (mode (0, 2a) = 4500Hz) the speed of the machine must be around 8000rpm which is not feasible for this prototype. Hence, it can be concluded that the experimental results shown are influenced solely by the current profile and electrical excitation, with no mechanical resonance from the prototype. It is worth noting that mechanical resonance from other components within the system may still occur but is unavoidable.

In future work, the current profile is varied such that it utilises a space vector PWM control module with the inverter to include harmonics and operate as a current control machine, not a voltage control machine. This is very useful and of interest due to the simplistic nature of the control and the accessibility for production markets. Utilising a pre-known existing control implementation reduces costs and simplifies the production process, saving space and time for companies. However, this is not a possibility in the case of prototyping for this machine due to the size of the machine and natural frequencies. When operating the machine with a PWM signal, the switching frequency of this is introduced into the system. On a full scale machine this is no issue as mechanical resonance is likely to occur at a level of hundreds of Hertz, with a switching frequency of 10kHz being standard this can be avoided through careful sampling or use of a low pass filter. Unfortunately, this switching frequency falls in the range of vibration spectra being observed for the small prototype, and hence, it is not possible to use a low pass filter to remove the 10kHz signal. Furthermore, the prototype machine exhibits a natural mode 3 around 10kHz, and thus would not be seen if they are swamped by the dominant switching frequency. The reasons discussed result in an experimental verification procedure operating the machine at 150rpm to produce a reasonable square wave current profile, using a voltage control strategy with an on/off DC bus program for each phase winding to remove any switching frequencies.

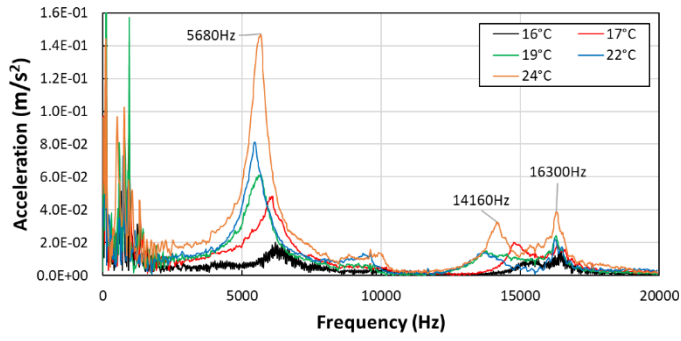
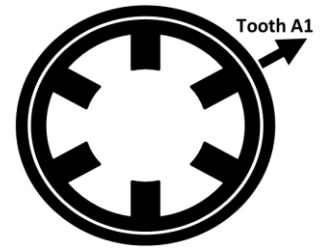
After establishing a suitable set of constraints and operating conditions to allow for clarity of results, the method of calculating vibration spectra was then investigated. The accelerometers utilised for modal analyses are set up behind each tooth, including tooth C2 which is aligned with the bolted connection. The three teeth in the upper half of the machine are selected to improve reliability of results. Under

operation at 5A load the temperature of the prototype machine increases as there is no direct cooling method, this results in a temperature rise in the casing also. This rise in temperature can cause the adhesive wax to soften, and hence, any accelerometers on the underside of the machine are liable to loosen and reduce reliability of results. To minimise this risk, the accelerometers are used to measure the response on the top side of the machine, teeth A1, B1 and C2, such that they are less likely to slip or move. Also, the machine is operated for minimal duration and fan cooled, to reduce overheating which could cause problems for the machine or if more severe could result in damage to the windings.

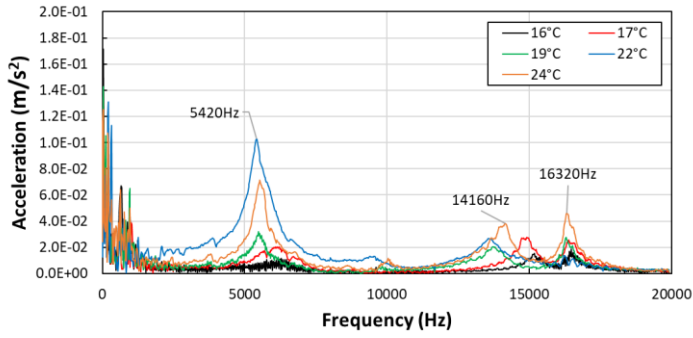
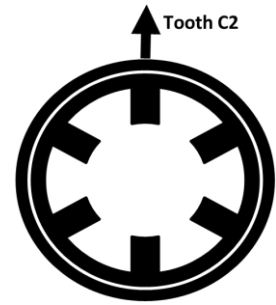
The potential rise in temperature also influences the vibration response of the machine due to variance in material properties with temperature. Literature is relatively thin in this area and the topic is also beyond the scope of this project. However, a brief series of tests were performed to identify potential variance. The prototype machine is operated at 150rpm, 5A voltage fed, and the acceleration measured in 30, 500ms intervals at a sampling rate of 100kS. By operating under these conditions and measuring the temperature of the casing with an infra-red thermal gun, a rough trend can be found in terms of both amplitude and frequency of eigenmodes. It can be seen that as temperature increases, the amplitude of eigenmodes also increases. This is attributed to the variance of material Young's modulus with temperature, as the elasticity increases the deformation for the same excitation is also increased, and hence a rise in acceleration. It is also noted that the rise in temperature of the prototype machine causes a reduction in frequency of eigenmodes as the material softens. In order to produce reliable results, the machine is operated at manageable temperature, approximately 22°C. Under these conditions, mode (0, 2b) is dominant and the peak for mode (0, 2a) is no longer visible on the vibration spectra, and hence, comparisons in trends are focussed mainly on eigenmodes (0, 2b), (0, 4a), and (0, 4b).



(a)



(b)



(c)

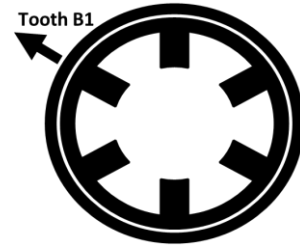
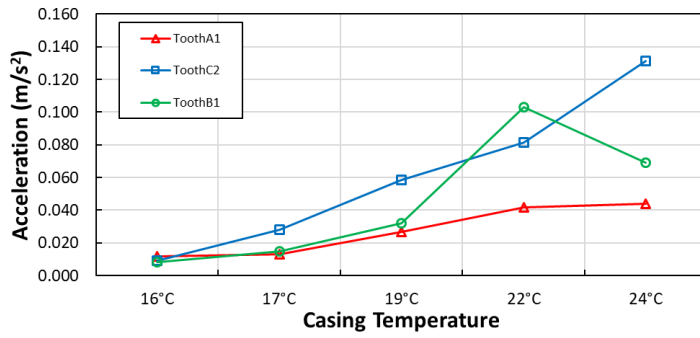
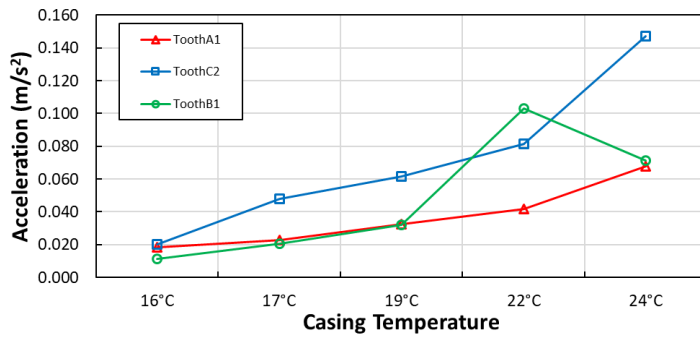
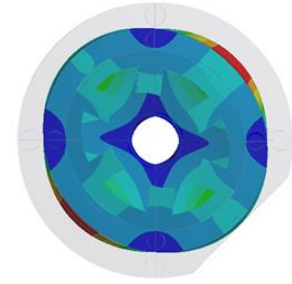


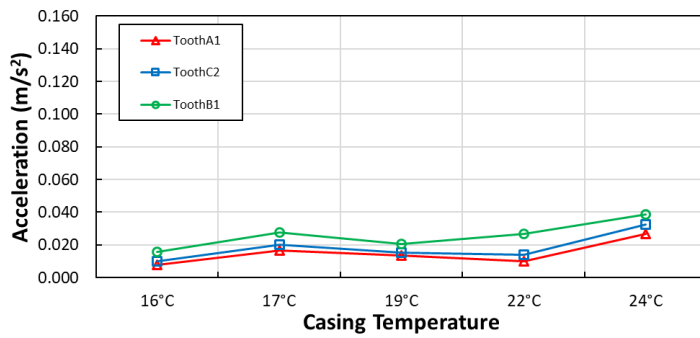
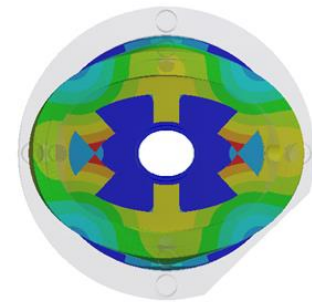
Fig. 3.40 Vibration response of 5A operating at 150rpm for different casing temperatures, measured at teeth (a) A1 (b) C2 and (c) B1.



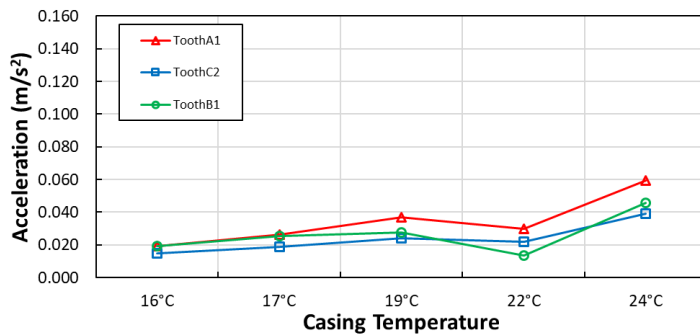
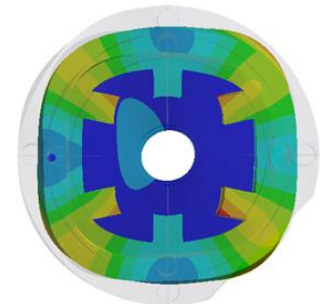
(a) Mode (0, 2a)



(b) Mode (0, 2b)



(c) Mode (0, 4a)



(d) Mode (0, 4b)

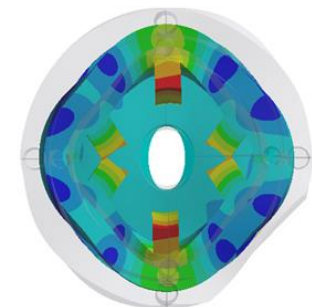
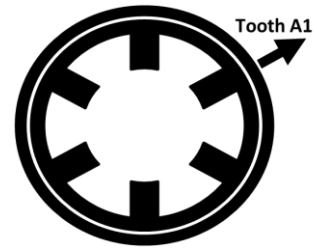
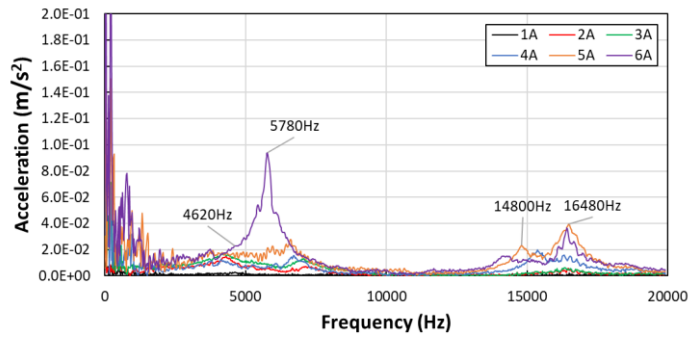


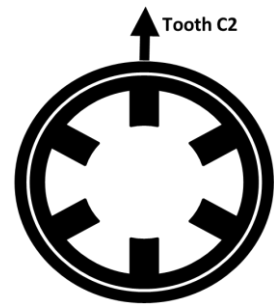
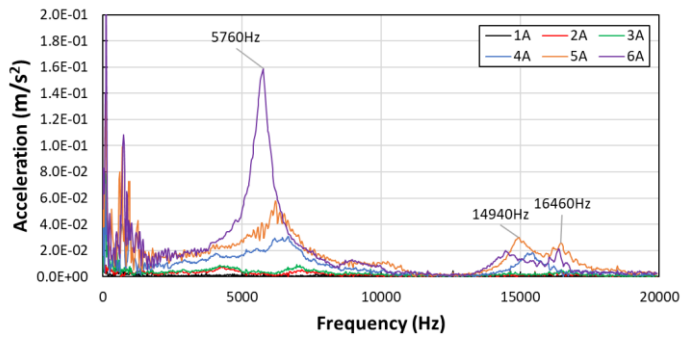
Fig. 3.41 Trend in amplitude of vibration response against temperature, shown for significant mode shapes (a) to (d).

3.5.2 Vibration response under varied load

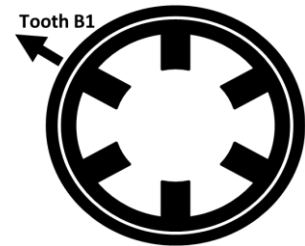
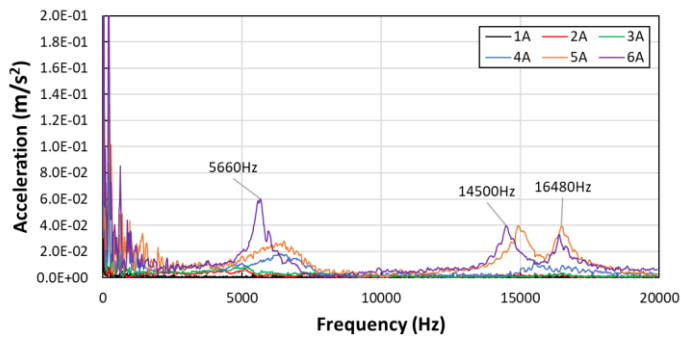
Firstly, the vibration spectra under varied load is verified, thus establishing a reliable load current baseline for analysis and comparison. The prototype machine is operated at 150rpm and the load machine supply is varied such that the speed is constant. The trend from simulated analysis indicated that there is a positive correlation between the phase current and vibration response measured, indicating that as current increases the vibration response will increase across all eigenmodes also. This is verified through experimental analysis for phase currents of 1A to 6A. The experimental data indicates that there is a significant increase in vibration between 5A and 6A particularly for mode (0, 2b). This is attributed to the increase in temperature operating the machine at 6A, even if for a short period only. Further evidence to support this is the lower frequency for the key eigenmodes identified, implying a softening of material from thermal influence, particularly noticeable in toothB1. The experimental results also indicate the dominance of mode (0, 2b) particularly for mode (0, 2b) which correlates well with earlier finite element study. It can be noted that the amplitudes of all identified modes are similar until the more severe case of 6A phase current is included.



(a)

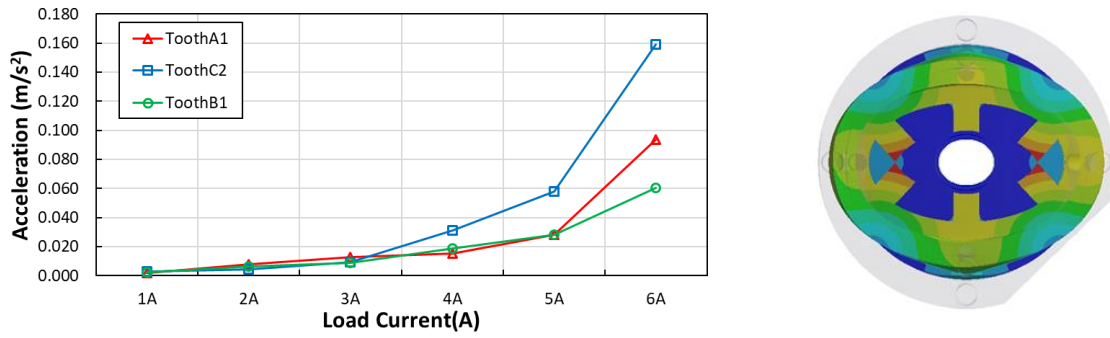


(b)

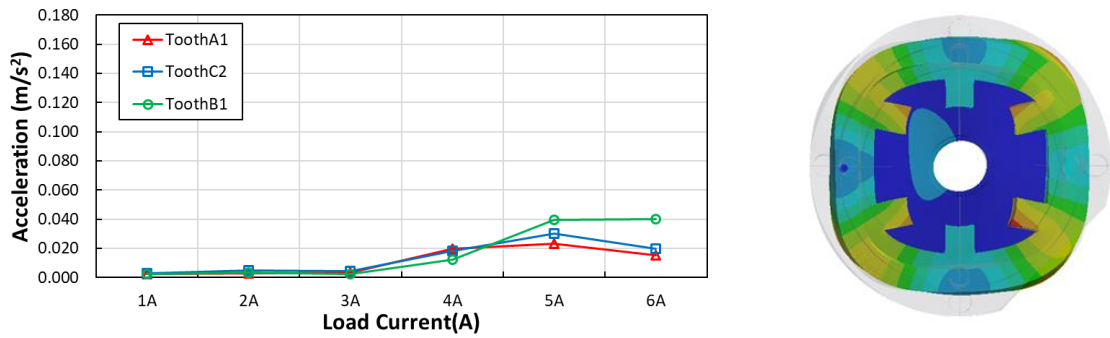


(c)

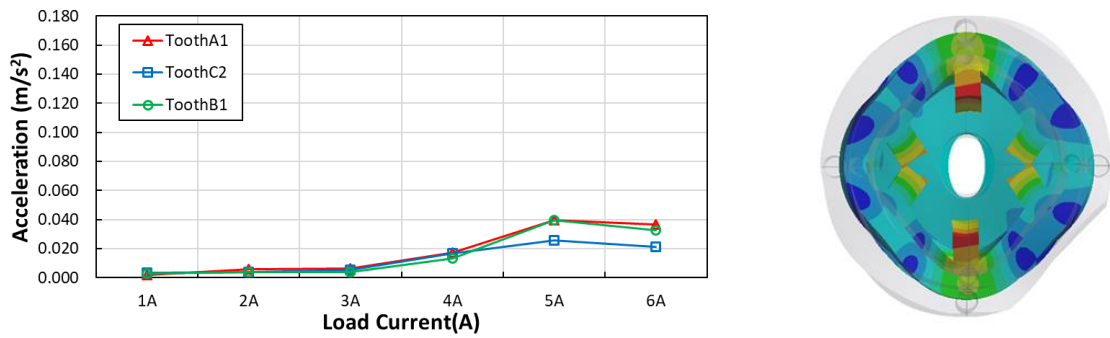
Fig. 3.42 Vibration response operating at 150rpm for load conditions, measured at teeth (a) A1 (b) C2 and (c) B1.



(a) Mode (0, 2a)



(b) Mode (0, 2b)



(c) Mode (0, 4a)

Fig. 3.43 Trend in amplitude of vibration response against load phase current, shown for significant mode shapes (a) to (c).

3.5.3 Vibration response under fixed turn-off conditions

For finite element analysis and simulation, the variance in turn-on angle relative to the baseline current profile was considered to be minimal. It is shown that variance in amplitude of vibration response for all eigenmodes was relatively low although there may be more influence on torque and tangential air gap forces. This is verified experimentally with a small variance on higher order modes of radial mode shape 4 and good correlation for mode (0, 2b). It is clear that behind tooth C1, the bolted connection to both endcaps influences the vibration response, showing a consistently higher amplitude of response. The variance observed in higher order modes is attributed to experimental differences in the baseline test, including temperature and mounting of accelerometers. Accounting for this, the results show good correlation with the ‘ideal’ finite element results and the conclusions drawn are supported.

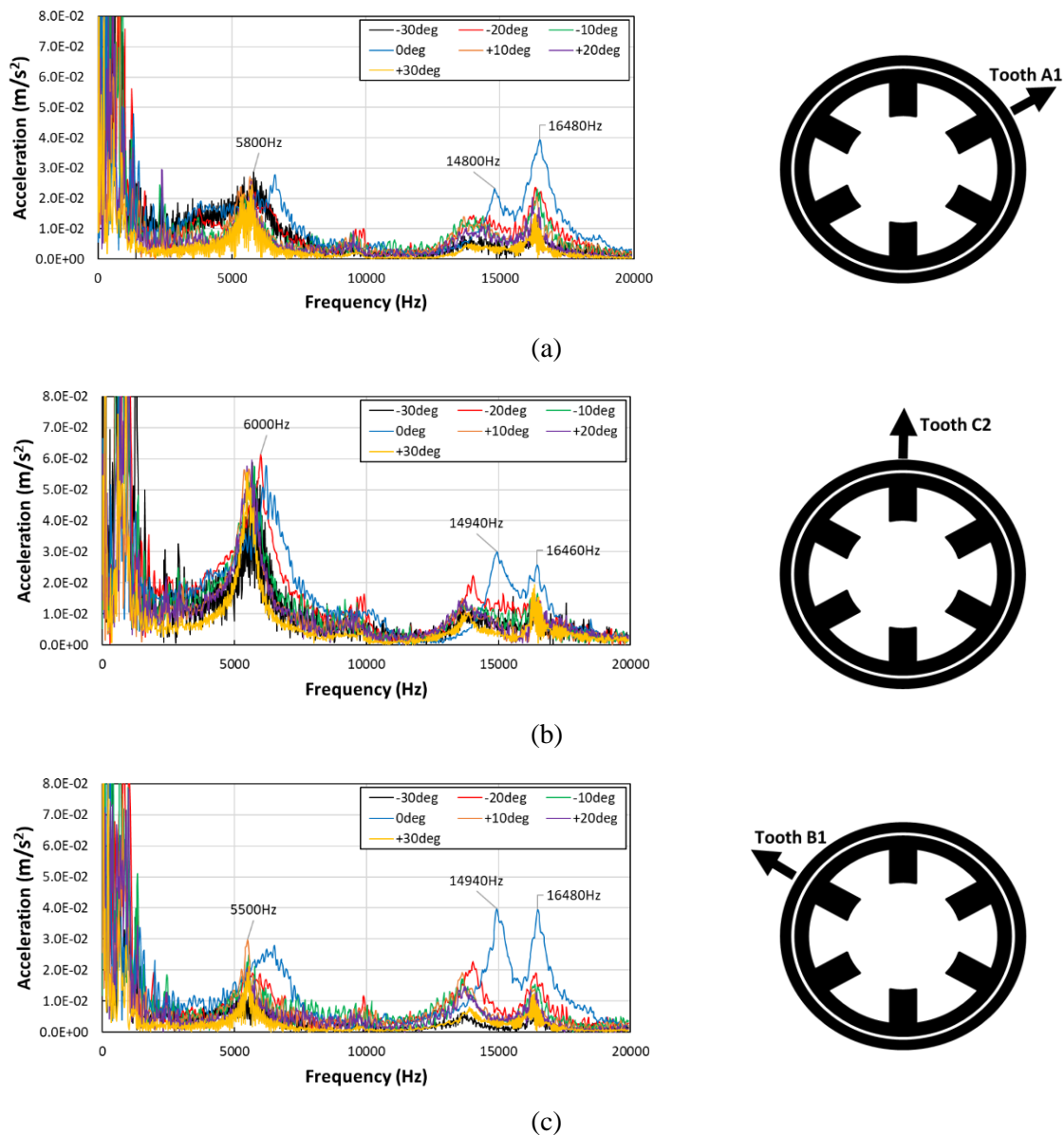
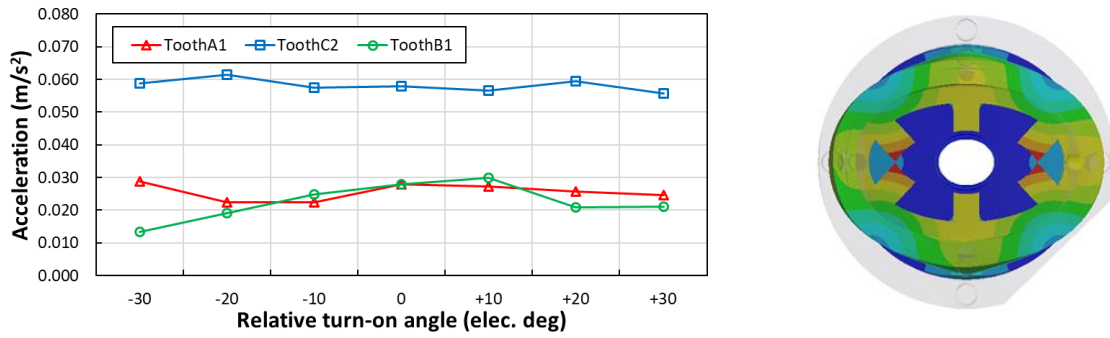
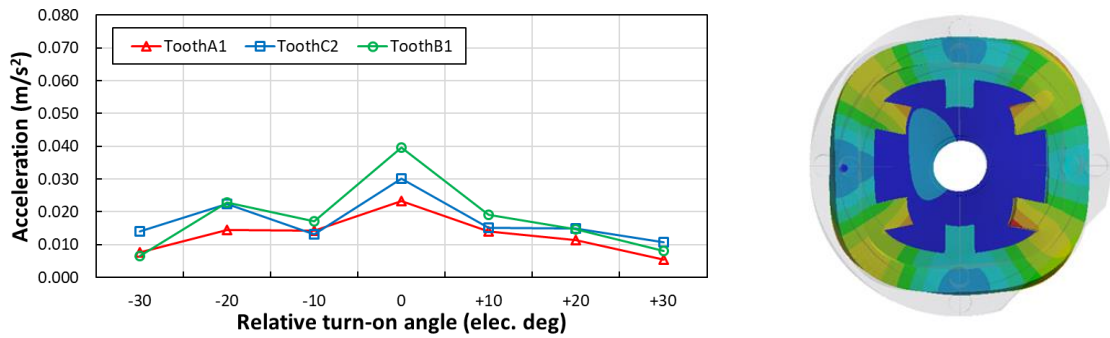


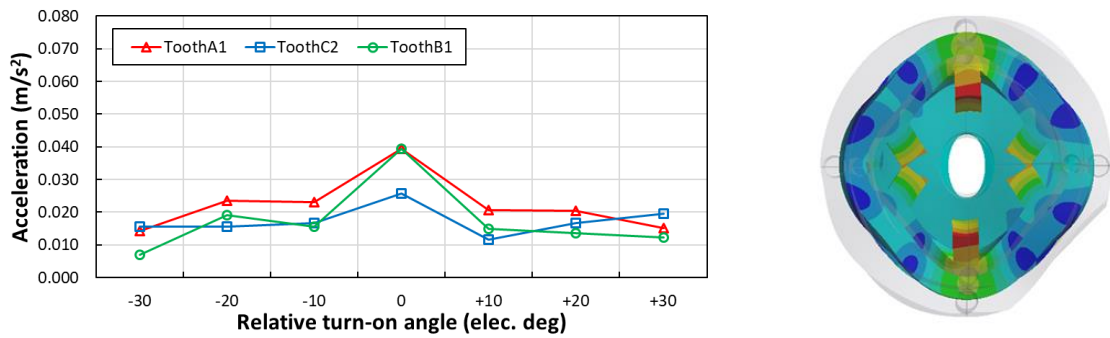
Fig. 3.44 Vibration response of 5A operating at 150rpm for different turn-on angle, measured at teeth (a) A1 (b) C2 and (c) B1.



(a) Mode (0, 2a)



(b) Mode (0, 2b)



(c) Mode (0, 4a)

Fig. 3.45 Trend in amplitude of vibration response against turn-on angle, shown for significant mode shapes (a) to (c).

3.5.4 Vibration response under fixed turn-on conditions

Under fixed turn-on conditions, the influence of turn-off position is analysed for a positive and negative variance from the baseline current profile. The experimental data supports the trends investigated in the simulation study under ‘ideal’ conditions, providing confidence in future investigations. The vibration spectra results show the increase in vibration under baseline 120° electrical conduction angle. It also confirms the rise in vibration with increased turn-off angle in all modes, with the most significant vibration response behind the tooth of phase C which is in alignment with the bolted connection. There is minor deviation compared to the simulated results but this is expected for vibration simulation as it is a notoriously difficult task. The trend in mode (0, 2b) strongly supports suggestions that parameters influencing turn-off are of higher priority than turn-on parameters.

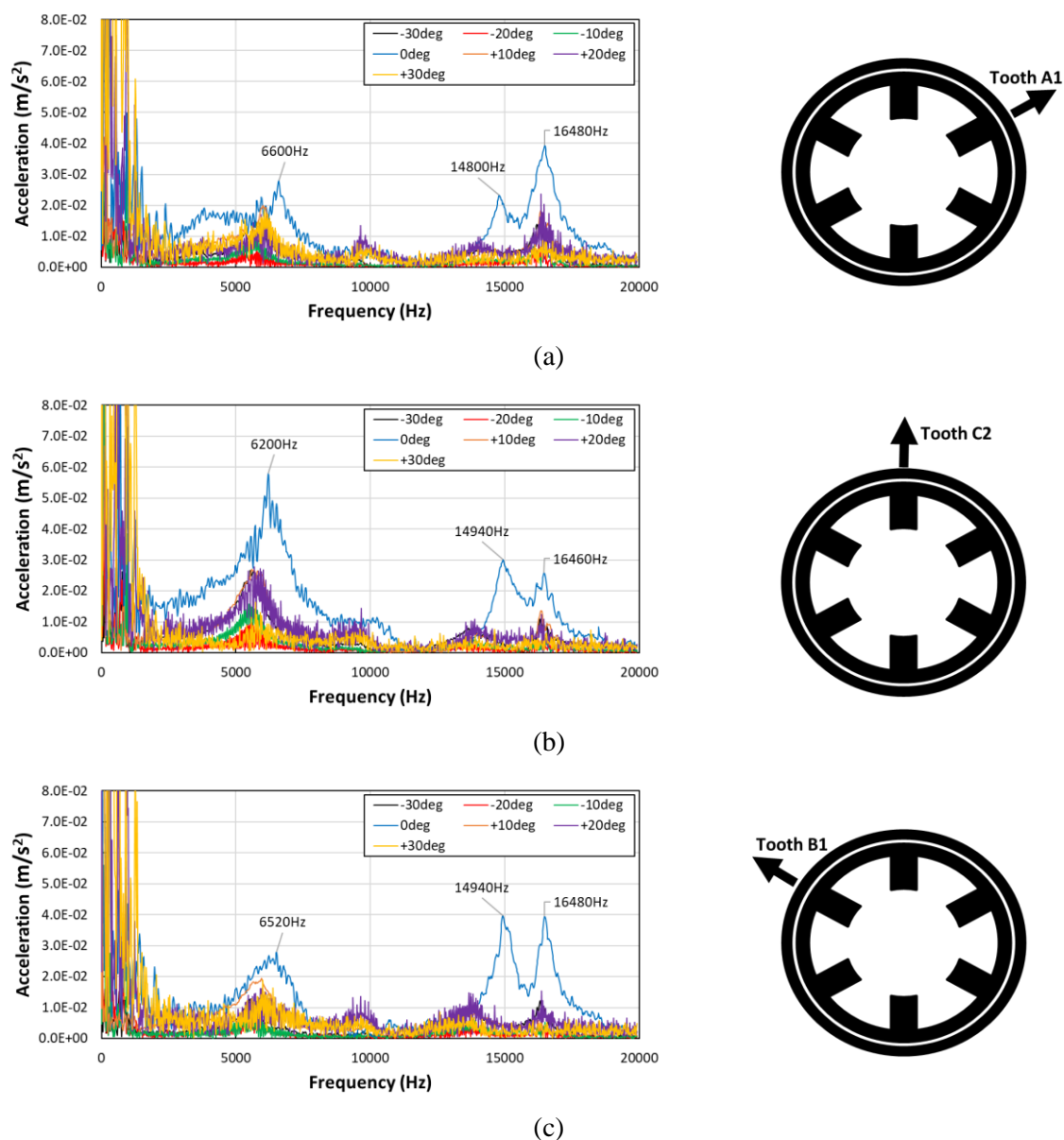
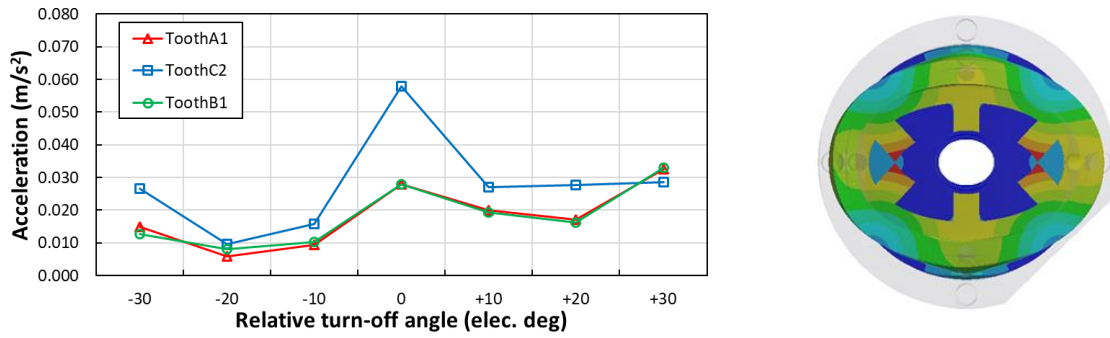
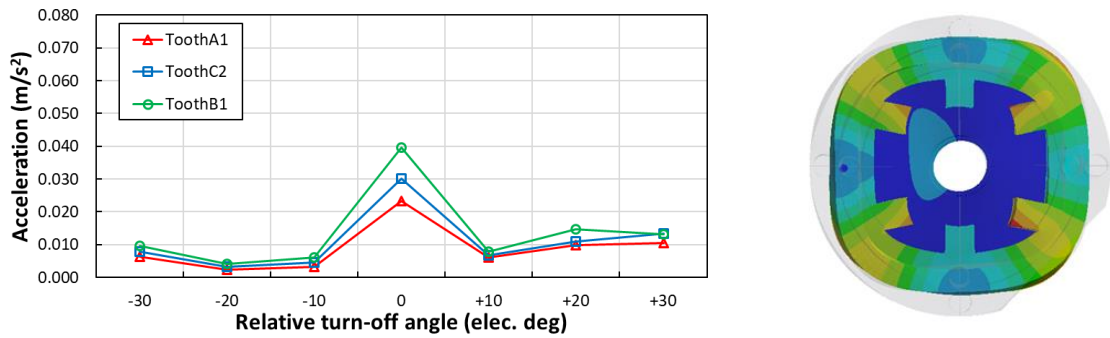


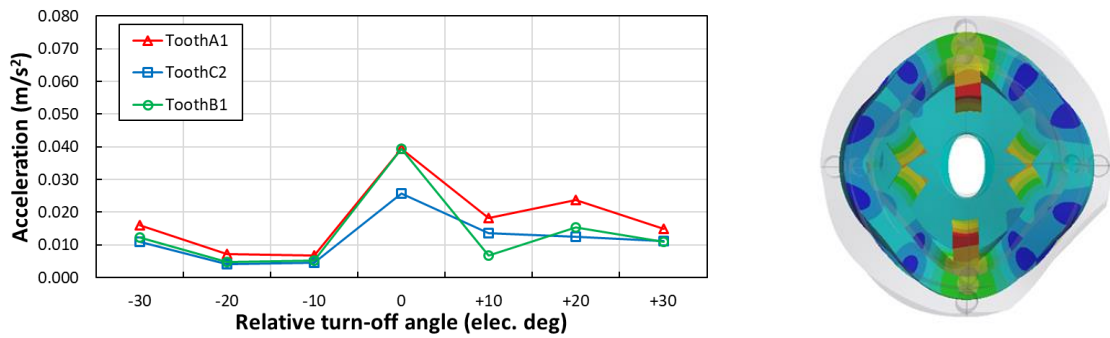
Fig. 3.46 Vibration response of 5A operating at 150rpm for different turn-off angles, measured at teeth (a) A1 (b) C2 and (c) B1.



(a) Mode (0, 2a)



(b) Mode (0, 2b)



(c) Mode 0, 4a

Fig. 3.47 Trend in amplitude of vibration response against turn-off angle, shown for significant mode shapes (a) to (c).

3.6 Summary

This chapter demonstrates the viability and verification of the finite element model introduced in chapter 3 with analysis of multiple current profile parameters both simulated and experimentally. Firstly, the finite element analysis is introduced with calculation of air gap radial force across each stator pole, then applied onto stator teeth in the 3D mechanical model. In order to calculate the vibration response in a time efficient manner the harmonic components of the force up to 20kHz are applied to the stator teeth face in a harmonic response system, from which the acceleration response may be extracted from target nodal locations. From this, a baseline for comparisons is simulated utilising an ‘ideal’ square wave phase excitation neglecting inductance and resistance effects in the windings.

After establishing the baseline current profile, the load condition must be investigated to determine the influence and establish a reasonable amplitude for further testing. It is found that the amplitude of phase current has a significant impact on the vibration response and from experimental results 5A is selected as the load current. Next, the influence of turn-on angle is investigated. The machine is operated such that the baseline current profile consists of a 120° electrical conduction angle with the initial position set to the fully unaligned position. This turn-off point is fixed such that the only variable in the current profile is the turn-on position. It is concluded that this has a minimal effect on the final vibration response of the machine and is verified with experimental results.

Finally, the impact of turn-off angle is analysed and the finite element results are compared to the experimental results under the same conditions. The effect of this parameter is far more significant than turn-on, particularly for mode (0, 2b). It is found that due to the influence of overlapping phase currents and contribution of radial forces from other phases, an increase in turn-off angle from 120° electrical exhibits lower vibration response than an ‘ideal’ waveform. However, this can be considered a special case and it is shown that increasing the turn-off angle increases the vibration response. Hence, the turn-off profile of the machine influences vibration more, and thus, the focus may be applied to this section of the current waveform. All results are shown to match with experimental analysis. Therefore, the use of an ‘ideal’ baseline current profile is a reasonable starting point for future analysis of trends.

Chapter 4 Investigation of Influence of Current Profiling in Time Domain

4.1 Introduction

The verification of the vibration characteristics of the 6s/4r SRM in Chapter 3 proves the influence of switching angles and load currents in SRMs. It is shown that relative to the current profile parameters investigated, the peak load current of a unipolar square wave profile bears the most significance to electromagnetic forces and vibration response of the stator. Furthermore, varying the turn-off angle, and in turn, changing the rotor position at turn-off, is also shown to affect the vibration response, confirming research in [Wu93] and [Wu95]. The equivalent changes to the turn-on angle have little to no effect on the vibration response. Hence, combining these conclusions, the influence of current profiling for the turn-off event is further investigated.

Initially, this is approached through current profiling in the time domain, in order to find the significance and influence of time domain current profiling for vibration reduction. The baseline unipolar square wave current profile is defined in Chapter 3. The definition includes an ‘ideal’ or instantaneous turn-off event, where the current drops from peak current to zero instantly at the change in phase. Hence, this can be considered to be the purest waveform, with a predetermined conduction period of 120° electrical as taken from [Mil93]. Through the introduction of additional components to the current profile from the perspective of time domain additions, the influence of independent current parameters can be identified. In order to achieve this, the current profile is considered to be a series of discrete data points.

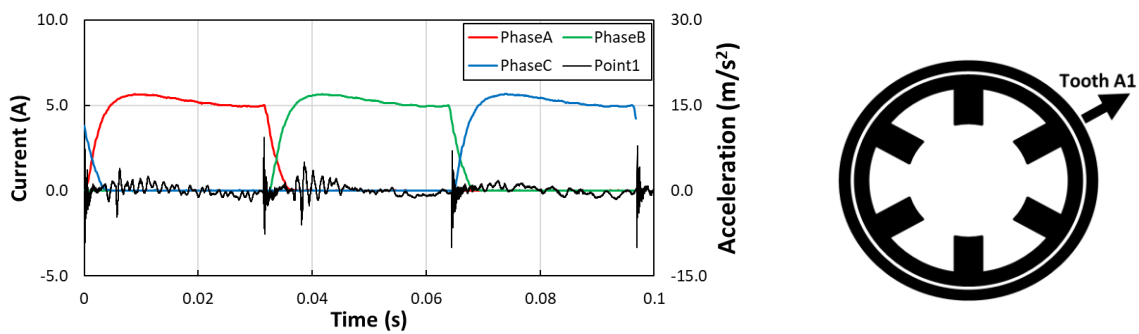
Firstly, the turn-off event is manipulated such that the decay in current excitation for each phase is gradually decreased at a constant rate, as opposed to the instantaneous drop in the baseline current profile. This is referred to as the introduction of a continuous slope differential at turn-off. Secondly, a step down in current at a predefined time before the turn-off event is applied. This results in a reduced peak current at the turn-off event. The investigation considers the impact of the duration of the time step on electromagnetic forces and vibration response.

4.2 Influence of turn-on and turn-off

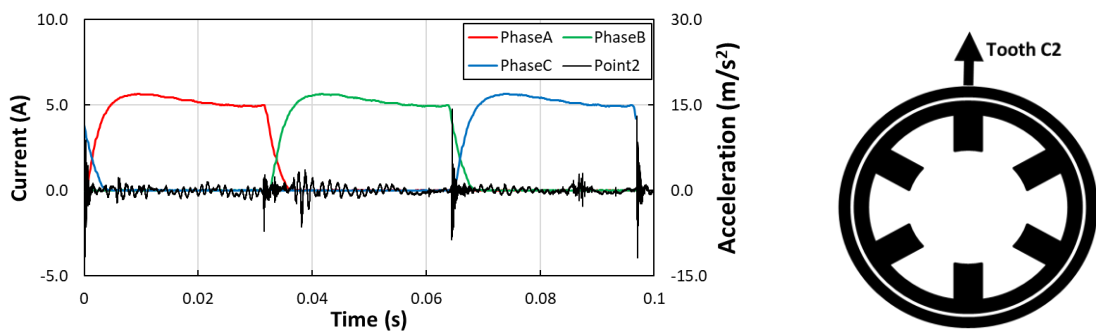
Experimental results in the time domain confirm evidence shown in [Wu93] that it is the change of phase in switched reluctance machines that results in the significant production of stator borne noise and vibration. Comparing results behind tooth C2, **Fig. 4.1**, where dominant vibration response occurs, significant peaks in acceleration are produced in the time domain at the change of phase. Upon closer inspection of these results the acceleration waveform is of a decaying sinusoid in nature. The response is dominated by the eigenmodes investigated thus far in the studies, primarily modes 2 and 4 and

variants of these. The experimental results provided show the significant peaks in acceleration in the time domain at change of phase. It can also be seen that for the excitation shown in **Fig. 4.1** that the vibration response due to a change in phase is observed behind all teeth. This indicates that there is a strong influence of vibrations on adjacent teeth caused by the electromagnetic forces at change of phase. Furthermore, the peak vibration response in the time domain on each tooth occurs at the turn-off of the equivalent phase current, most evident in the response behind tooth B1. Due to the nature of sampling the time domain response of the accelerometers, it can be difficult to achieve consistent results for peak acceleration, and hence, the results shown are considered to be a snapshot in time of the vibration response.

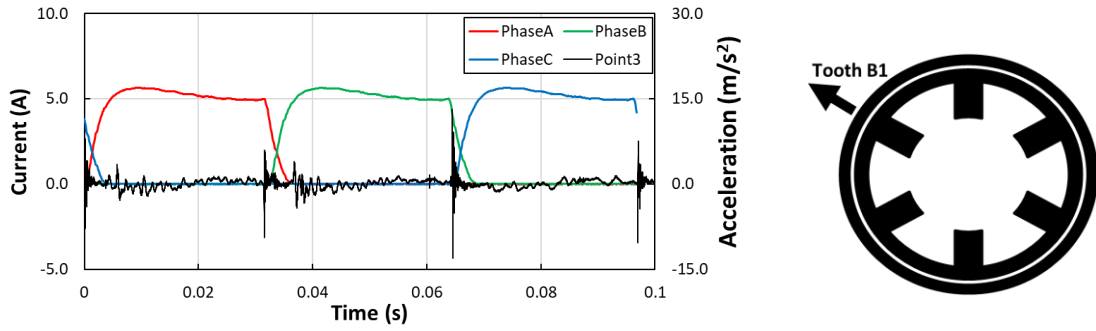
Enhancing the time domain acceleration with a focus on the switching between phases, the acceleration is shown to exhibit similarities with a decaying sinusoidal response such as a second order linear time-varying response. There is significant noise in the acceleration response from the electrical machine, including low frequency mechanical responses. Given the results from simulated studies previously and the known dominance of modes 2 and 4, it is reasonable to consider the acceleration response in the time domain to be composed of multiple decaying sinusoids matching these modal frequencies. Based upon the nature of the time domain acceleration it is clear that the change of phase in switched reluctance machines is leading factor contributing to stator borne noise and vibration production. This has been previously investigated, prompting the development of an active noise cancellation technique [Wu93], [Wu95] and [Lon02].



(a)

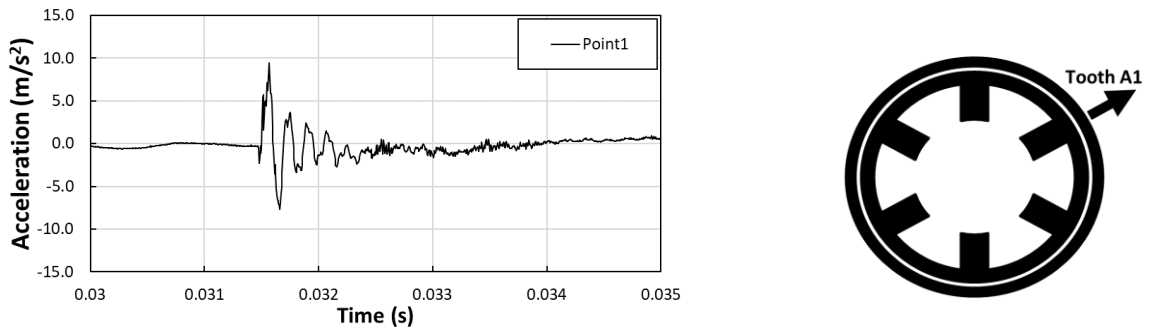


(b)

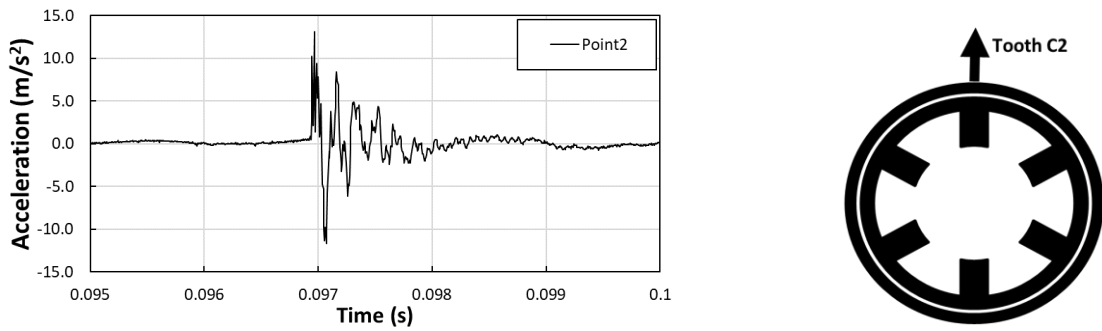


(c)

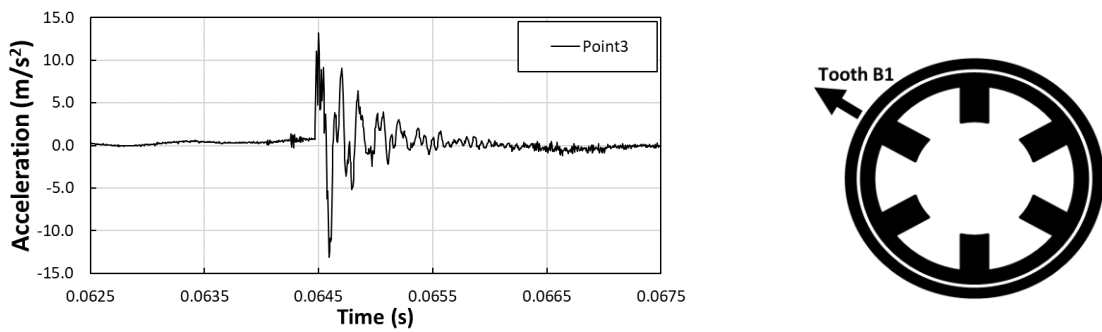
Fig. 4.1 Time-domain current and accelerometer results operating at 150rpm for load conditions, measured at teeth (a) A1 (b) C2 and (c) B1.



(a)



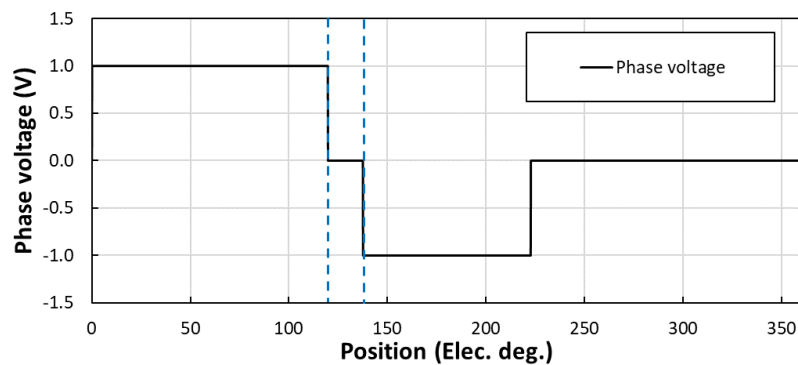
(b)



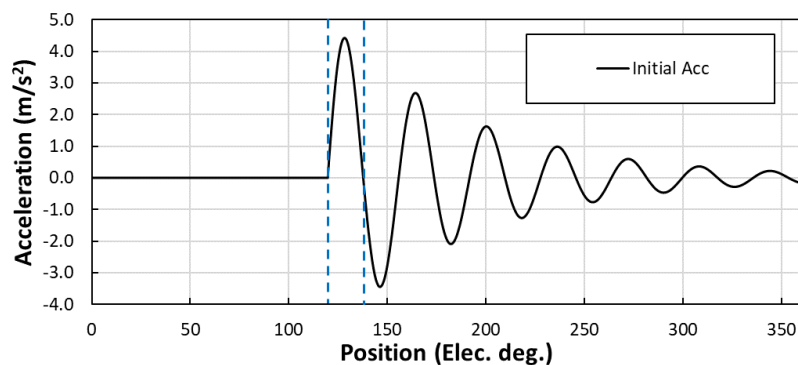
(c)

Fig. 4.2 Enhanced time domain accelerometer results under operation at 150rpm for load conditions, focused on phase turn-off for teeth (a) A1 (b) C2 and (c) B1.

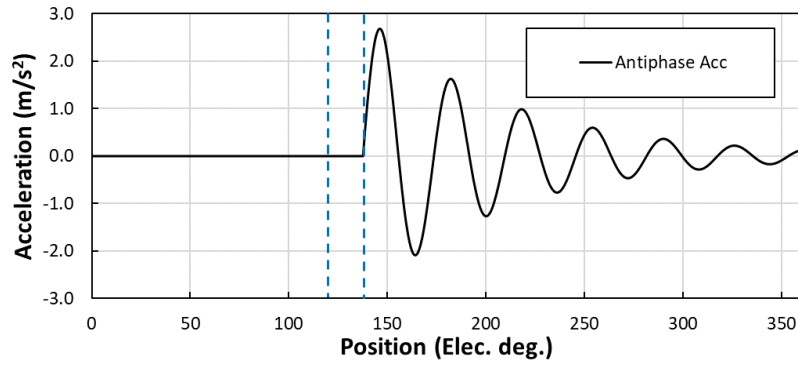
In order to reduce acoustic noise and vibration caused by mechanical resonances in switched reluctance (SR) machines a technique was developed known as active noise cancellation [Wu95]. It was proposed by Wu and Pollock [Wu95] with control operating with voltage PWM, current control and single-pulse mode operation as seen in Chapter 3. The study proposed includes various speeds and no-load and load conditions. The theory behind the active noise cancellation technique stems from work in [Wu93], in which the time domain vibration response of an SR machine is investigated. It is concluded, as confirmed in this thesis, that the dominant cause of acoustic noise and vibrations in SR machines is caused by the turn-off of phase currents. Later, the technique is verified and proven to be very effective for a 4 phase machine [Wu95]. The technique focuses on introducing a second vibration antiphase to the first vibration caused by the turn-off event in the same phase. By controlling the switching of the machine such that the delay between vibration events is $1/2f$, the second antiphase vibration response is aligned such to oppose the initial vibration. In this case $1/2f$ corresponds to a target frequency, typically of mode 2 resonance for SR machines. This is shown to be an effective solution to reduce the acoustic noise and vibration. However, it is limited in application. The limitation is due to the design of the method, where only a single resonant frequency can be targeted. It is also limited by switching times in components, potentially increasing the cost of control.



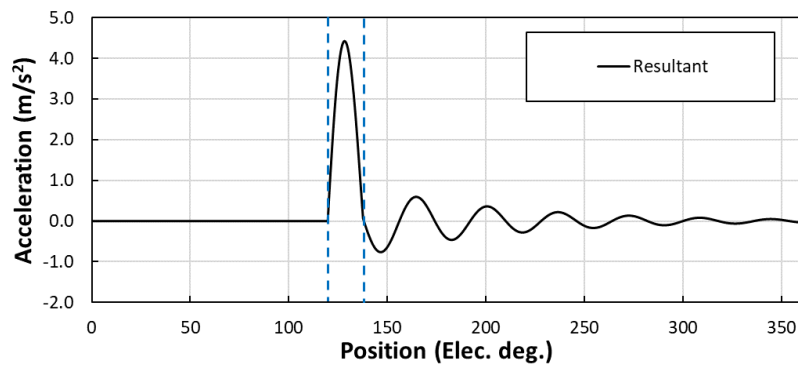
(a)



(b)



(c)



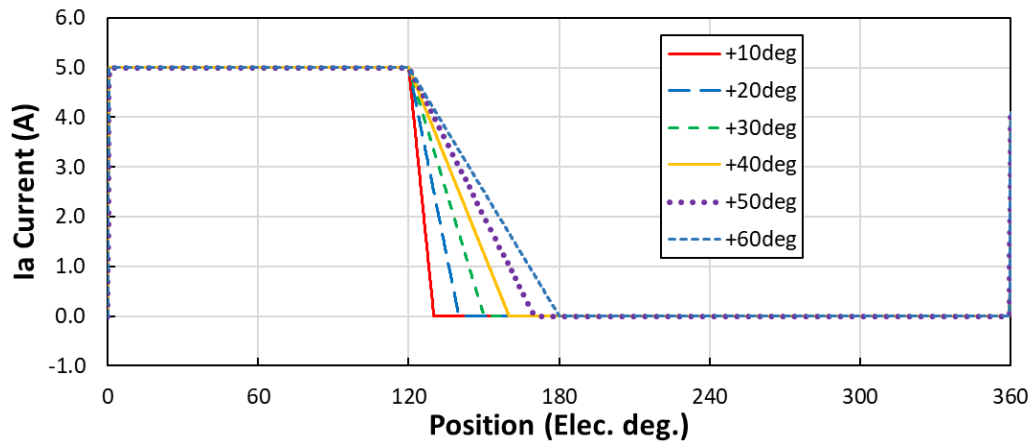
(d)

Fig. 4.3 Example of active noise cancellation technique, introducing antiphase vibration component via negative voltage pulse.

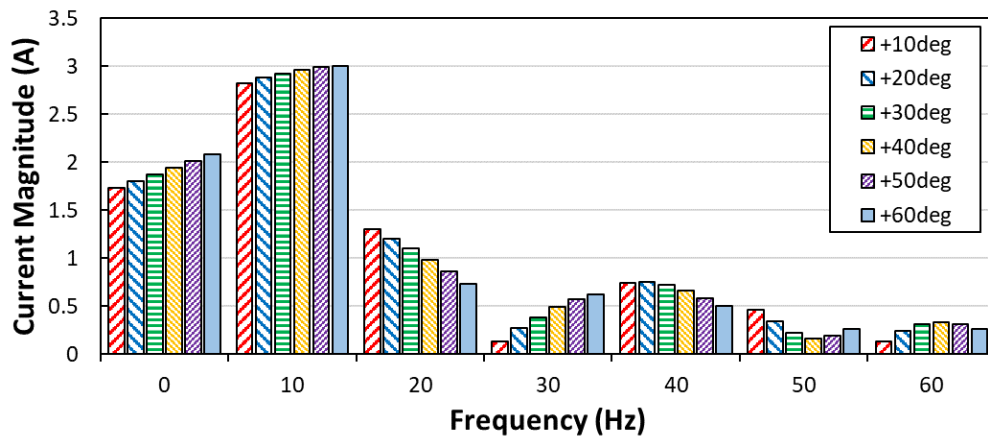
4.3 Continuous slope differential at turn-off

As previously shown based on experimental time domain results and verification of results, the current profile around phase turn-off contributes heavily to the vibration response of the stator and casing. The verified baseline implements an instantaneous turn-off to provide the ‘ideal’ square wave current profile. However, in practice this cannot be achieved due to the intrinsic properties of the machine. Through PWM current control, it is possible to define the desired current profile at any point of operation provided the relative position of the rotor is known. Hence, it is possible to gradually reduce the load of each phase at the position of change of phase, thus reducing the harshness of drop in current. To do this, a continuous slope differential is introduced at turn-off and the gradient of this slope is varied such to analyse the influence on electromagnetic capabilities and vibration response of the machine. Based upon the baseline current profile introduced in Chapter 4 with instantaneous switching, the turn-off of one phase is equivalent in rotor position to the turn-on of the sequential phase. The ‘zero-point’ of the current profile is incrementally increased such that the differential is constant and the gradient decreases. For the real machine the turn-off slop can be considered as an exponential gradient with approximate order 2, dependent on speed and switching capabilities. The impact of copper losses is a priority for much of machine design and optimisation. As shown previously, the peak current and

current at switching has a significant impact on the production of stator borne vibrations. Hence, despite the increased copper loss it is important to keep peak current constant such that it does not contribute to variations in vibration response, allowing for clear conclusions on turn-off slope to be drawn. It is acknowledged that as the duration of turn-off profile is increased, the copper losses increase and thus the current at turn-off shall be reduced under equal copper loss conditions.



(c)



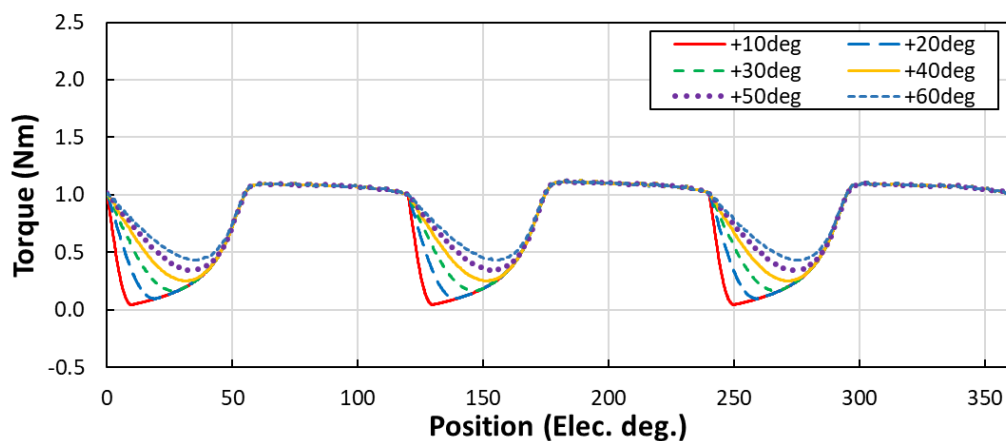
(d)

Fig. 4.4 (a) Variation in phase current illustrated for phase A only with increasing turn-off slope duration, (b) harmonic components up to 60Hz based on 150rpm operating speed.

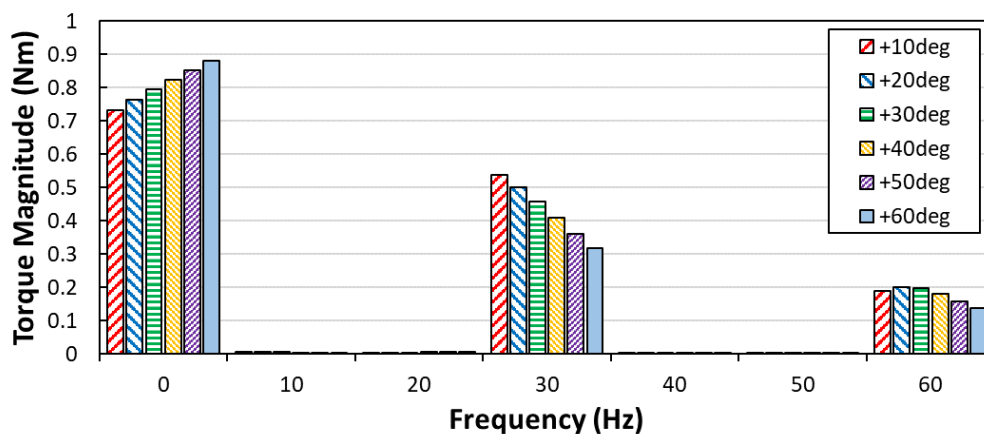
As seen from the harmonic content in the low frequency range, there is an increase in the 1st and 3rd harmonic components as the turn-off duration is increased. However, there is also a reduction in the 2nd order harmonic, in this study equal to 20Hz. Injection of harmonics has been used to influence both the performance of SRMs and acoustic noise and vibration. Although there is focus on time domain current profiling in this chapter, the harmonic content of profiles is important in order to understand the interaction between electrical excitation and mechanical response.

4.3.1 Electromagnetic results

The current turn-off slope affects the torque production significantly, reducing the torque ripple and increasing average torque. A similar effect is observed when increasing the conduction angle at turn-off. As expected due to the nature of switched reluctance machines and the variation introduced the peak torque remains equal. The reduction in torque ripple can be considered to be similar to a damping effect, the torque ripple introduced during switching is softened by the influence of overlap between phases. Previously, links have been made between the torque ripple produced and the acoustic noise and vibration response for example [Ind02], [Lov94], [Tur98], [Meh92], [Hus05] and [Zhu17]. This is not considered in this study as the solely radial forces are applied to the mechanical response system. However, it can be concluded that reduced torque ripple is desirable for the majority of applications hence a small overlap significantly improves the viability of the machine in various applications.

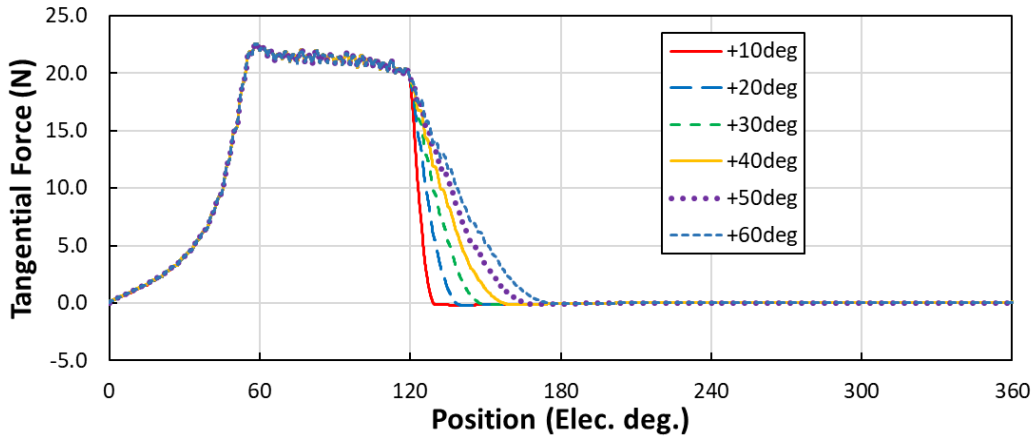


(a)

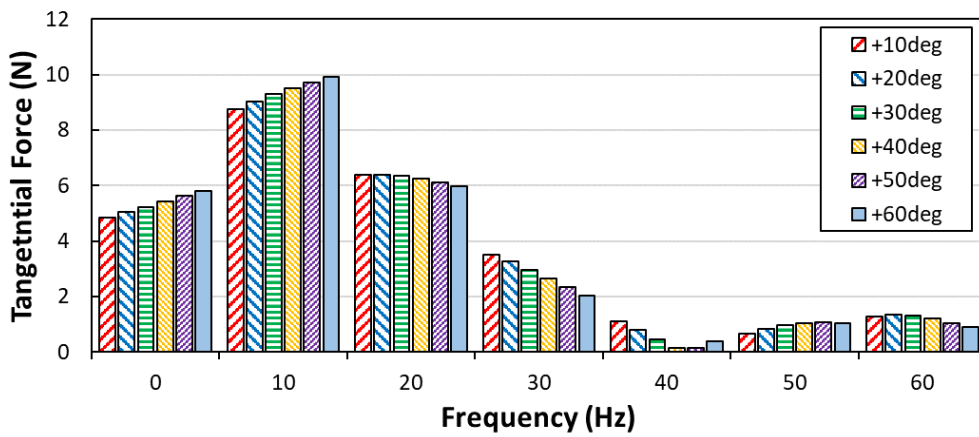


(b)

Fig. 4.5 (a) Variation in 3 phase torque caused by increasing turn-off slope duration, (b) harmonic components up to 60Hz based on 150rpm operating speed.



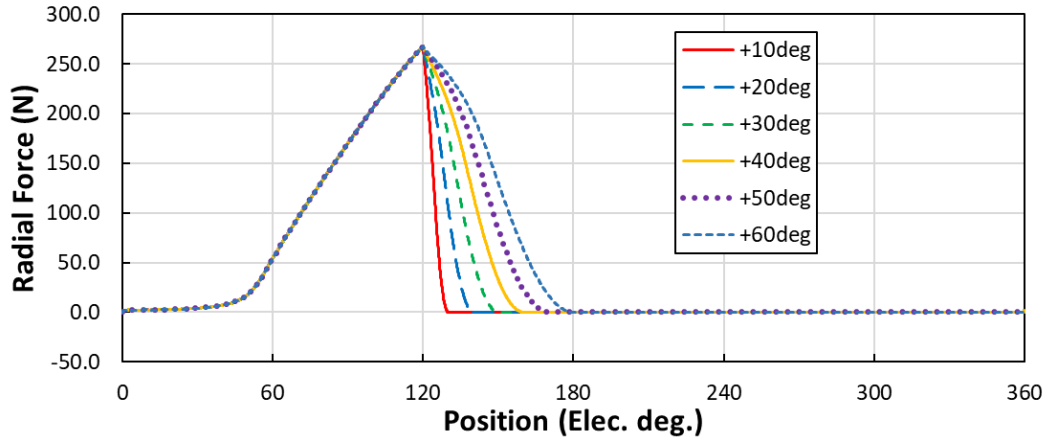
(a)



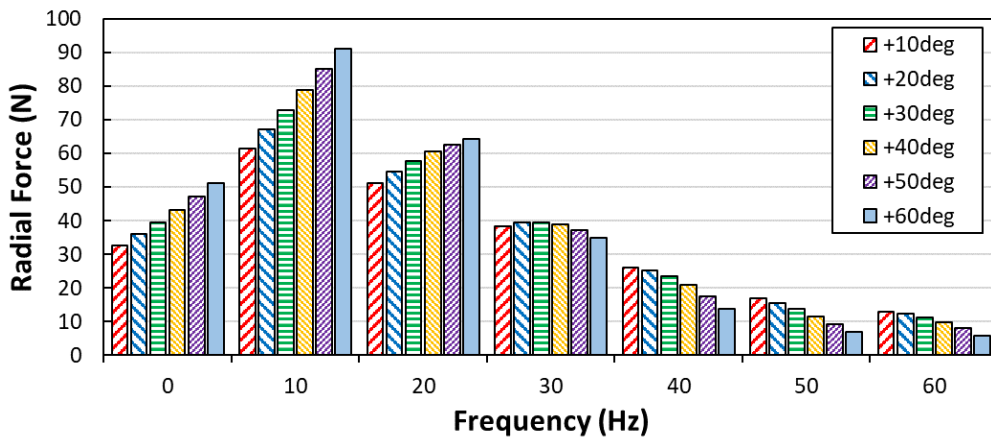
(b)

Fig. 4.6 (a) Variation in tangential forces in the air gap with increasing turn-off slope duration, (b) harmonic components up to 60Hz based on 150rpm operating speed.

The tangential force is considered to be proportional to the torque produced by the machine, yielding similarities in the waveforms. This produces the air gap tangential forces for a single pole, equivalent to the tangential forces for a single phase hence the forces from adjacent phases are not considered. It can be seen that the change in gradient of the turn-off slope is reflected in the tangential force profile, similar to the case of increased conduction angle. This is also a closer representation to a real waveform produced by an SRM. From the perspective of the harmonic content of the tangential force, the fundamental component increases proportionally with the turn-off slope. However, the 2nd harmonic changes are minimal in comparison, these are the two major contributors to the torque production of the machine as identified in chapter 2. There is also a significant reduction in the 3rd harmonic amplitude as the turn-off duration is increased.



(a)



(b)

Fig. 4.7 (a) Variation in air gap radial forces for increasing turn-off slope duration, (b) harmonic components up to 60Hz based on 150rpm operating speed.

The equivalent method as described for tangential forces is employed to calculate the air gap radial forces acting across each stator pole. The turn-off duration in the current profile is echoed in the profile of single tooth radial force, delaying the fall in radial force and controlling the decay. This is expected to significantly reduce the vibration response, as the stator back-iron is not released into a period of free oscillation from maximum radial force. Rather, the radial force steadily decreases to zero with a 2nd order component such that the decay is gradual, the time of decay for the radial force waveform is equivalent to the current profile. The radial force waveform is also heavily influenced by the saturation of the machine: under highly saturated conditions the radial force saturates also. Therefore, extending the excitation duration shall not increase maximum radial force experienced per radial tooth. The harmonic content of the radial force waveform also indicates a proportional increase between the duration of excitation turn-off and radial force profile. It is evident that the fundamental and the 2nd order harmonic increase, whilst the variance of the 3rd order harmonic is indeterminable. Beyond the 3rd order harmonic the amplitude of each harmonic decreases with increased turn-off duration.

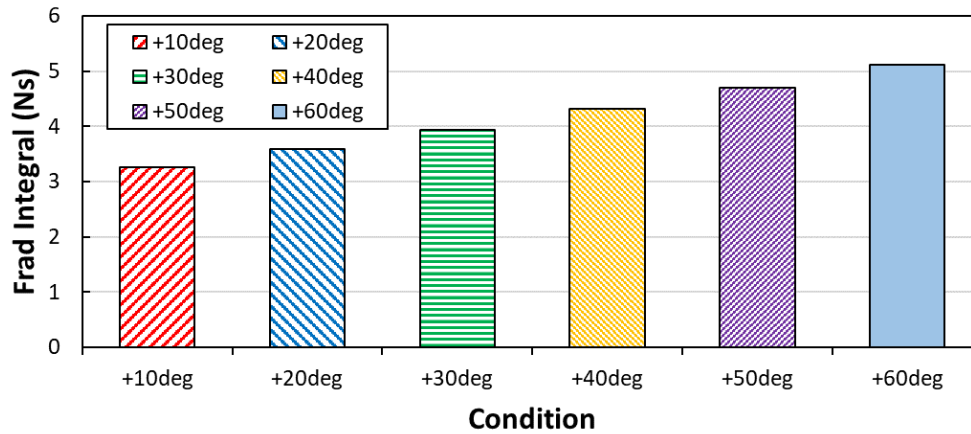


Fig. 4.8 Integral of radial force across 1 electrical period comparing influence of continuous slope duration.

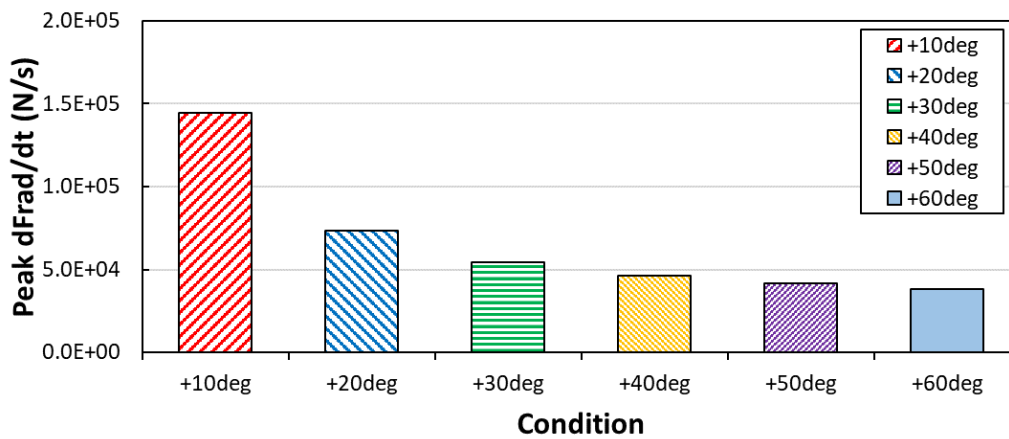


Fig. 4.9 Peak rate of change in radial force across 1 electrical period comparing influence of continuous slope duration.

As discussed, the stator borne vibrations are a product of the deformation of the stator caused primarily by radial forces, followed by a release such that the stator oscillates at various frequencies. The addition of a continuous slope at turn-off influences the moment the radial force is ‘released’ and hence the oscillations of the stator begin. This phenomenon can be quantified by the rate of change in radial force specifically at turn-off, in the baseline control previously covered this is a large increase in dF_{rad}/dt due to the instant decay of radial force. As the turn-off duration is increased, thus reducing the severity of the slope, the rate of change in radial force is significantly reduced. Comparing the peak rate of change in radial force in **Fig. 4.9** shows that increasing the turn-off duration linearly results in an exponential drop in the differential of radial force. In other terms, the advantages gained from increasing the turn-off duration diminish as the duration increases, the highest relative reduction occurs for a minimal increase in duration. When considering conditions of equal copper losses which is important for many applications, this is a useful trend to consider. Increasing the slope duration results in increased

losses, to account for these additional losses the peak current is typically reduced, hence a reduction in torque. Therefore, for minimal reduction in torque under equivalent copper losses, there is no advantage to excessively increasing the slope duration in terms of the rate of change of radial force.

The dc component of radial force per tooth is indicated with a vector on the relevant tooth for each condition investigated in this sub section. The dc component serves as an indicator for the average forces acting per pole. As the duration of slope is increased there is a proportional increase in the average radial forces applied to each tooth. However, it is worth consideration that this was also the case for increased conduction angle as shown and verified under voltage control. In this scenario, the overlapping of currents resulted in reduced vibration response in the frequency domain. Therefore, it is reasonable to hypothesise that the vibration response is reduced due to two factors: the influence of adjacent phases and the reduction in severity of turn-off slope.

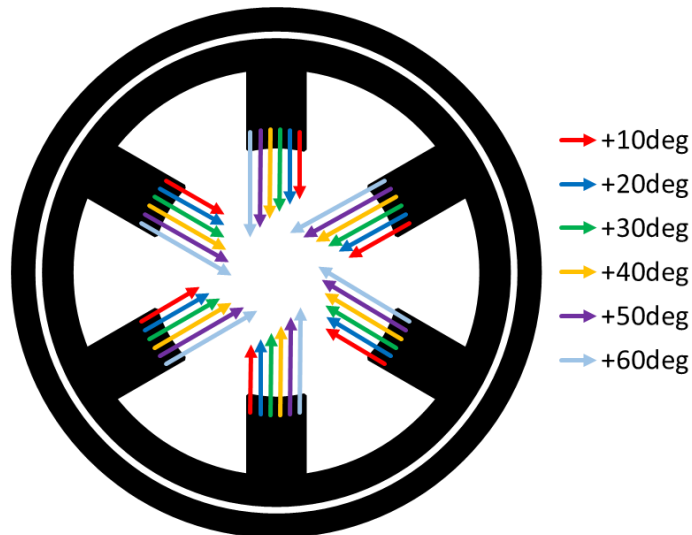
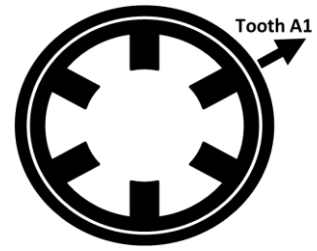
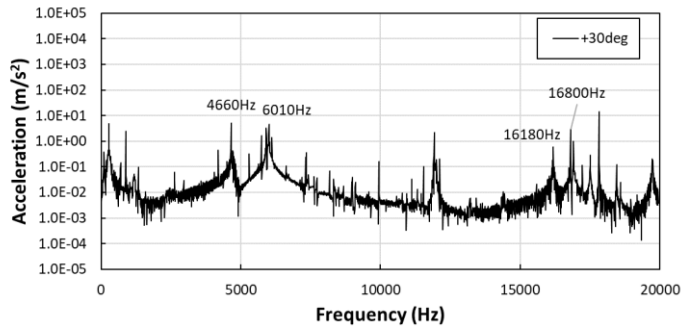


Fig. 4.10 Fundamental components of radial force on each pole shown acting on relative teeth, showing variance in magnitude of harmonic forces due to increased slope duration.

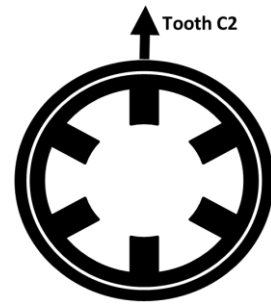
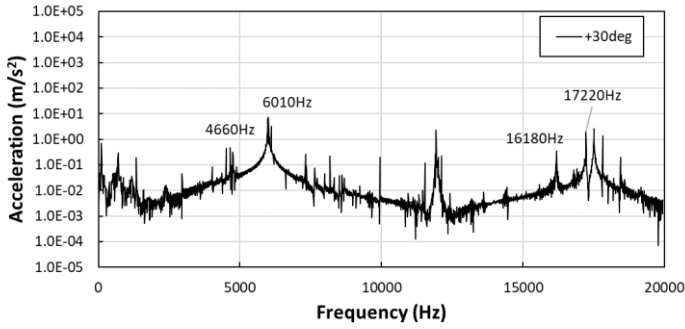
4.3.2 Vibration response

Analysis of the vibration response indicates two significant phenomenon to discuss further: the re-introduction of an eigenmode of order (0, 3) and the reduction in amplitude of vibrations for dominant modes. As discussed during modelling of the machine, the application of equal and opposite forces on teeth balances the machine and eliminates the shapes of mode (0, 3) variant. Under 'ideal' conditions for current profiling, there is no overlap between phases such that they are independent from each other. Hence, at any single point in time only diametrically opposed teeth only are excited, producing a radial force. Introducing the influence from adjacent phases produces a radial force next to the tooth of interest which creates a minor asymmetry in the excitation. Upon reflection this phenomenon may also be seen in the condition of increased overlap and experimental verification. The amplitude of this eigenmode is relatively low compared to mode shapes (0, 2) and (0, 4), these are still dominant modes. A system damping factor is not applied during these simulations, this would further reduce the influence of the eigenmode (0, 3a).

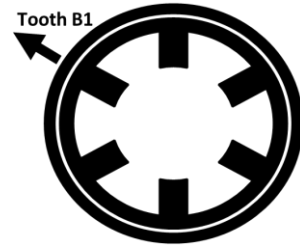
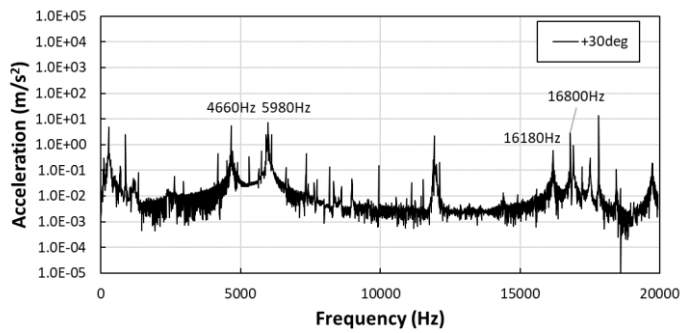
The trend in vibration response as the turn-off slope duration is increased, a reduction in severity of the gradient shows clearly a reduction in amplitude across all modes. The highest amplitude and thus dominant modes for vibration production are the dual modes of shape (0, 2) and mode (0, 4a). The trend in these mode shapes indicate a decaying reduction in amplitude, similar to that seen in the peak rate of change in radial force. This further supports the notion that the not only the turn-off is important, also the nature of radial force at turn-off. By decreasing the gradient of the radial force drop, decreasing the severity of this change, the period of free oscillation is reduced. Furthermore, the oscillation caused by the release of the stator can be considered to be damped, as the radial force decreases. Naturally, the stator tends towards its original shape and orientation, with a reactive force opposing the deformation caused by the electromagnetic radial forces. As the duration of the slope is increased, the duration of decaying radial force is also increased resulting in significant damping of oscillations as the stator returns to a neutral orientation.



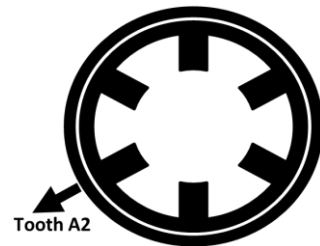
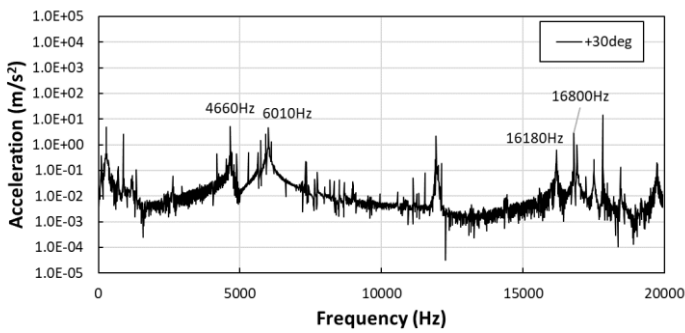
(a)



(b)

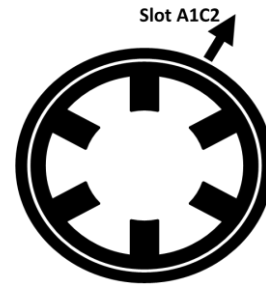
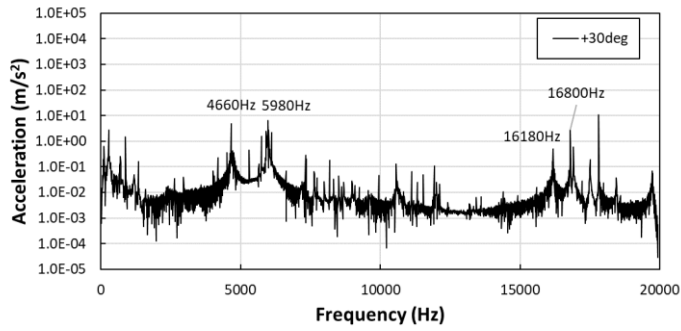


(c)

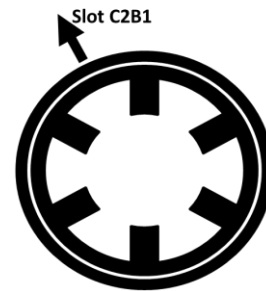
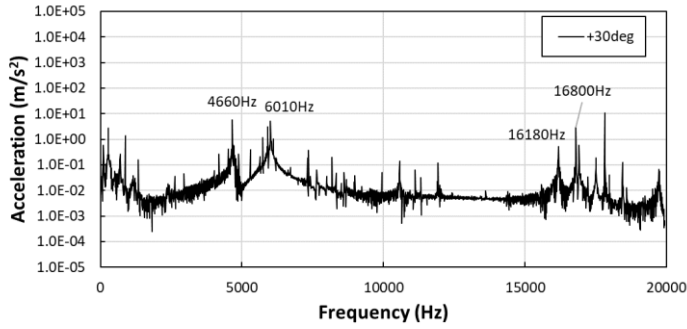


(d)

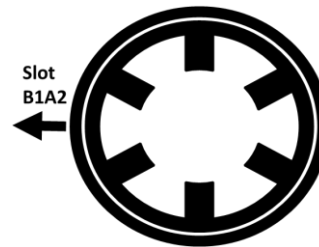
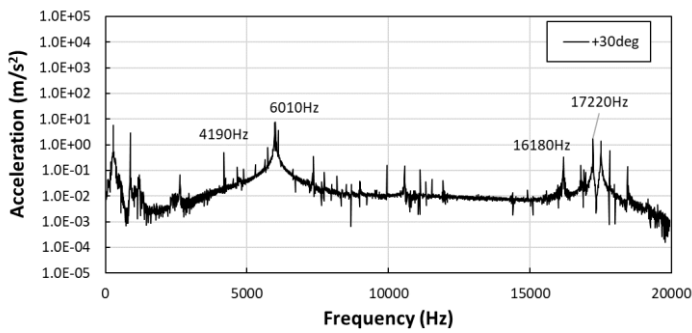
Fig. 4.11 Vibration response of 5A load current with continuous slope duration increased by +30° electrical from 120° baseline, simulated output on the casing behind teeth (a) A1, (b) C2, (c) B1, (d) A2.



(a)

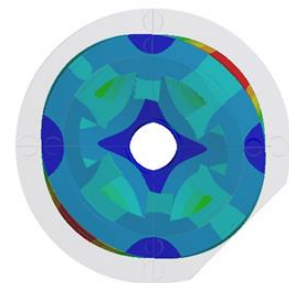
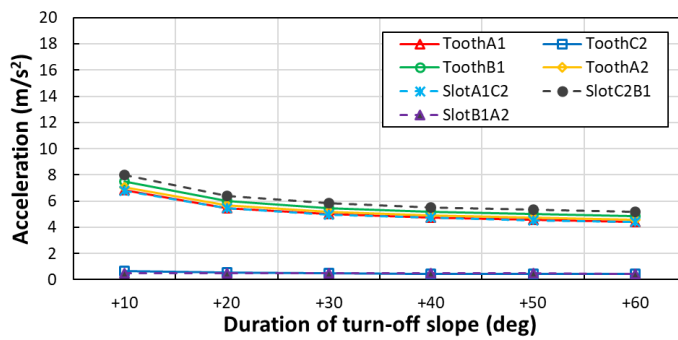


(b)

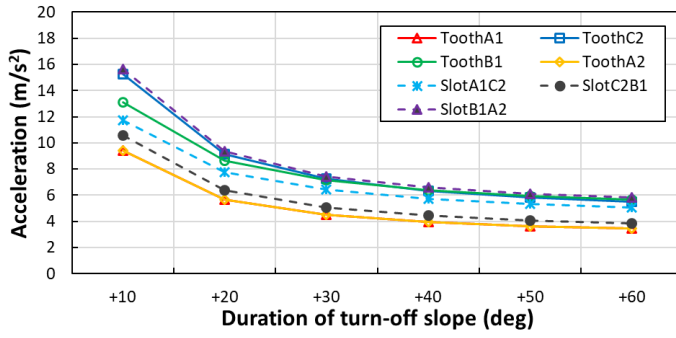


(c)

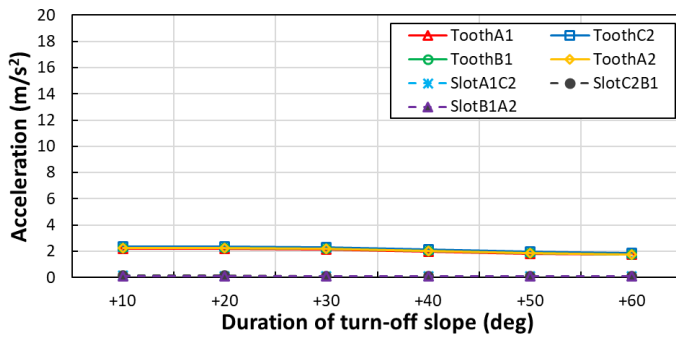
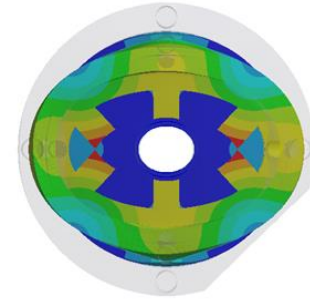
Fig. 4.12 Vibration response of 5A load current with continuous slope duration increased by +30° electrical from 120° baseline, simulated output on the casing behind slots (a) A1C2 (b) C2B1 and (c) B1A2.



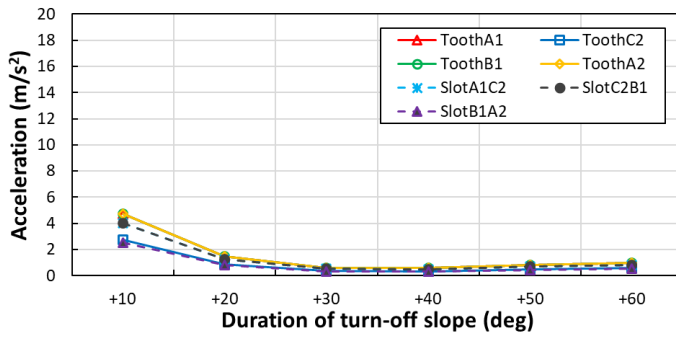
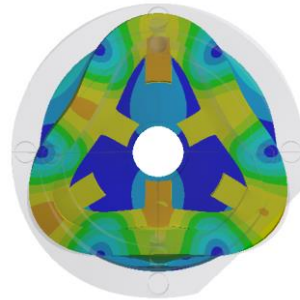
(e) Mode (0, 2a)



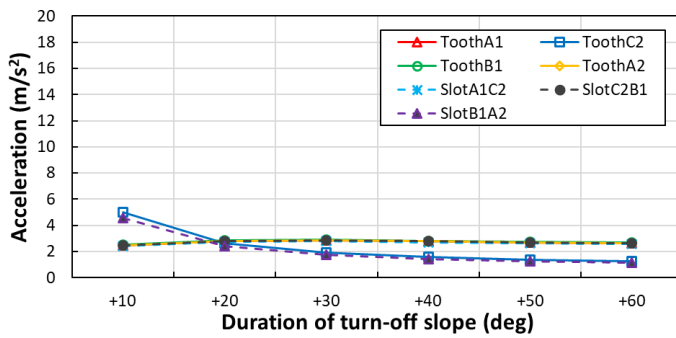
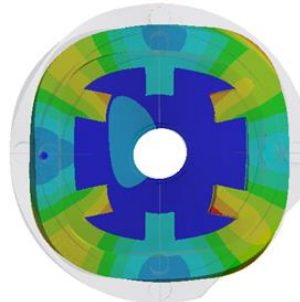
(f) Mode (0, 2b)



(g) Mode (0, 3a)



(h) Mode (0, 4a)



(i) Mode (0, 4b)

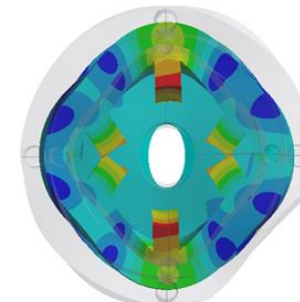
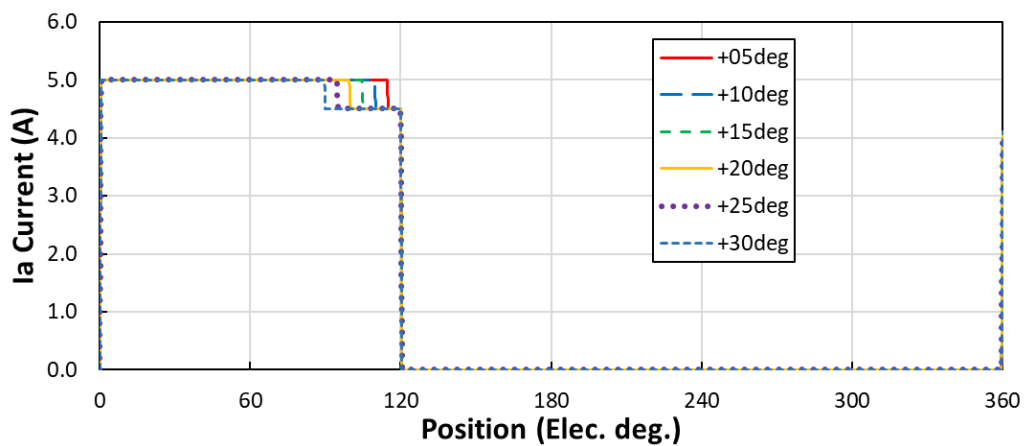


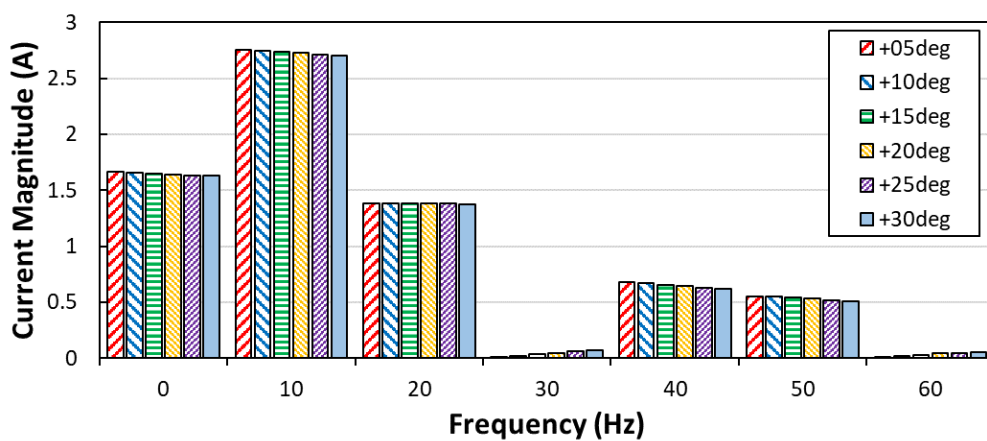
Fig. 4.13 Vibration response to harmonic force loads applied on stator teeth surface, shown for significant mode shapes (a) to (d).

4.4 Two step control

Based on the active noise cancellation technique the time step introduced should be selected such that the time step matches the desired frequency for reduction. An investigation into the general influence of introducing a time step at the end of the current profile produces a generic trend when profiling in this region. It is known from Chapter 4 that the amplitude of phase current at turn-off is a significant factor influencing the amplitude of vibrations, and hence, the step down in current is kept constant. The harmonic content is similar across all conditions with only minor reduction in the fundamental and fourth harmonic components. Furthermore, there is an introduction of low amplitude 3rd harmonic as the time duration of the step function is increased. Introduction of new harmonic components may cause additional mechanical resonance for larger machines or machines operating at significantly higher speed.



(a)



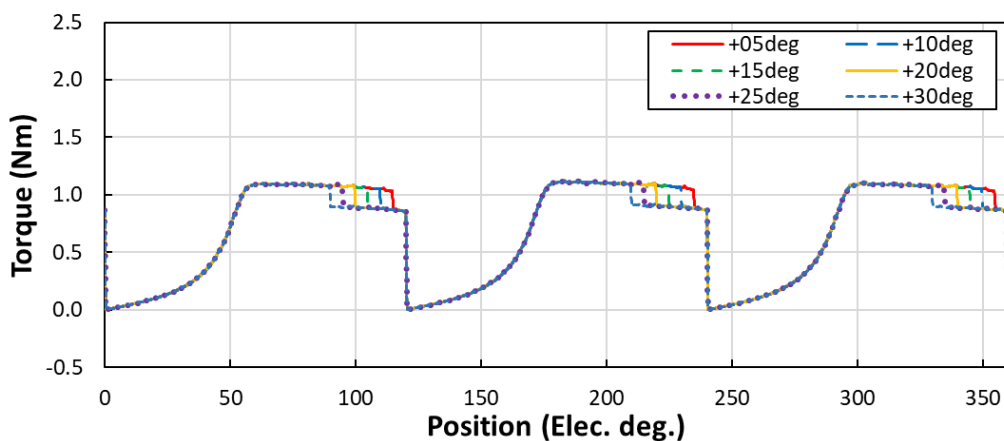
(b)

Fig. 4.14 (a) Variation in phase current illustrated for phase A only with increasing duration in current step, (b) harmonic components up to 60Hz based on 150rpm operating speed.

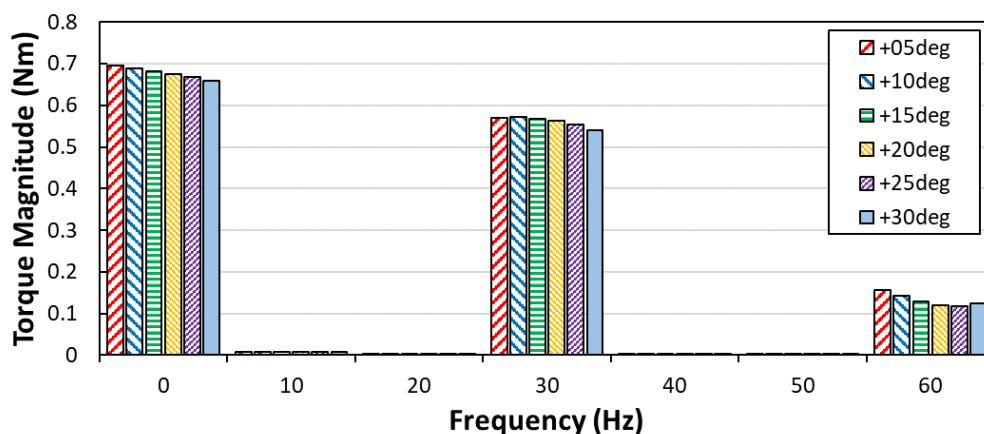
4.4.1 Electromagnetic results

The influence of step time is evident and clear in the torque profile for this machine. The involvement of a stepped square wave at and around the turn-off of each phase causes a momentary drop in torque. The drop in torque correlates to the second amplitude of phase excitation, and hence for a significant time step the average torque is further reduced. From the perspective of torque ripple, this is unchanged within this study although lower than observed in the ‘ideal’ baseline results. For minor changes in step duration, the torque is relatively unaffected therefore the use of a small step can be used without concern over torque production.

As discussed previously, the tangential force presented is calculated across a single stator pole pitch in the air gap. Due to the nature of operations in SRMs, the tangential forces as the rotor pole traverses from the fully unaligned position to an aligned position are relatively steady, particularly in the second half of the conduction region. Therefore, the introduction of a step down in phase current at a specific time produces an equivalent step down in tangential forces also.

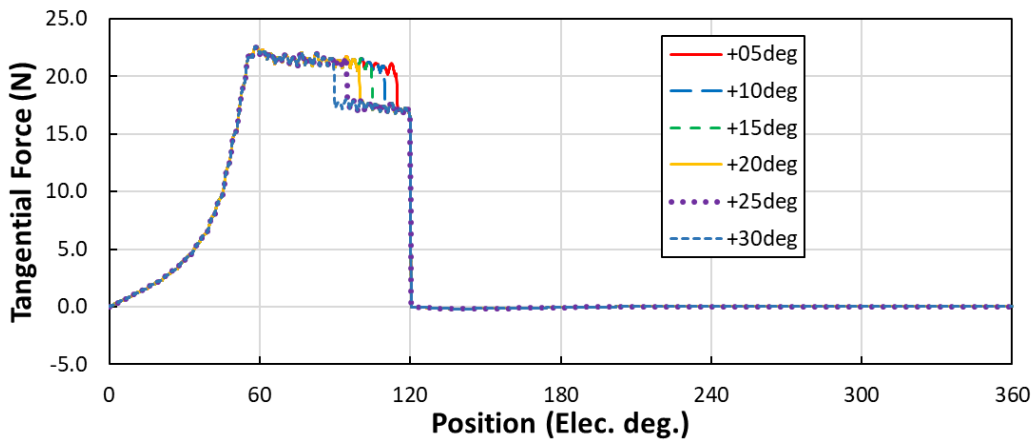


(a)

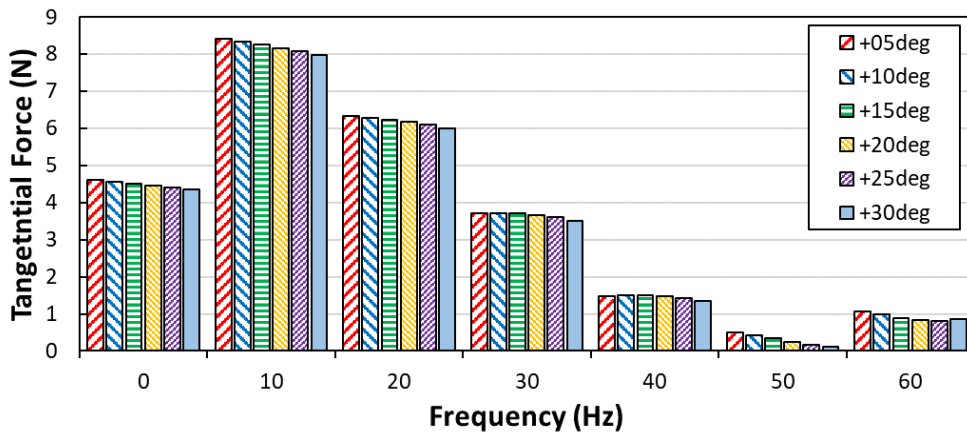


(b)

Fig. 4.15 (a) Variation in 3 phase torque illustrated for increasing current step duration, (b) harmonic components up to 60Hz based on 150rpm operating speed.



(a)



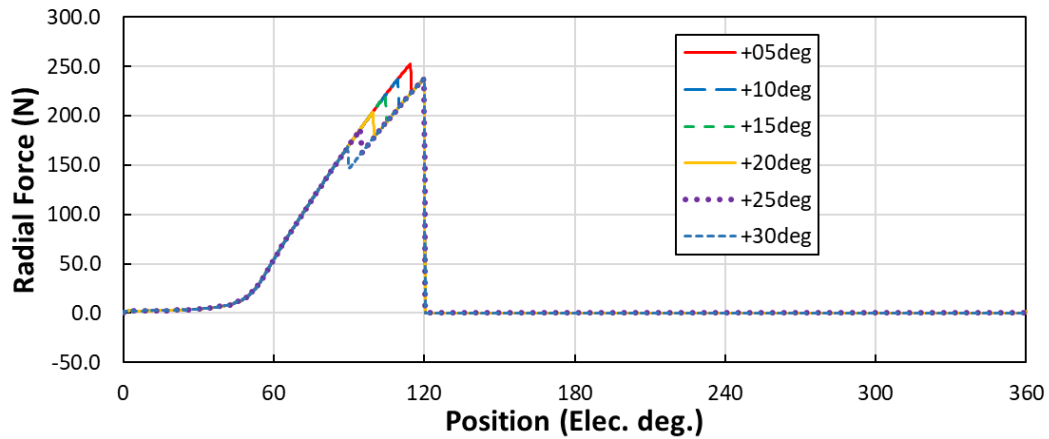
(b)

Fig. 4.16 (a) Variation in air gap tangential forces for increasing duration of current drop, (b) harmonic components up to 60Hz based on 150rpm operating speed.

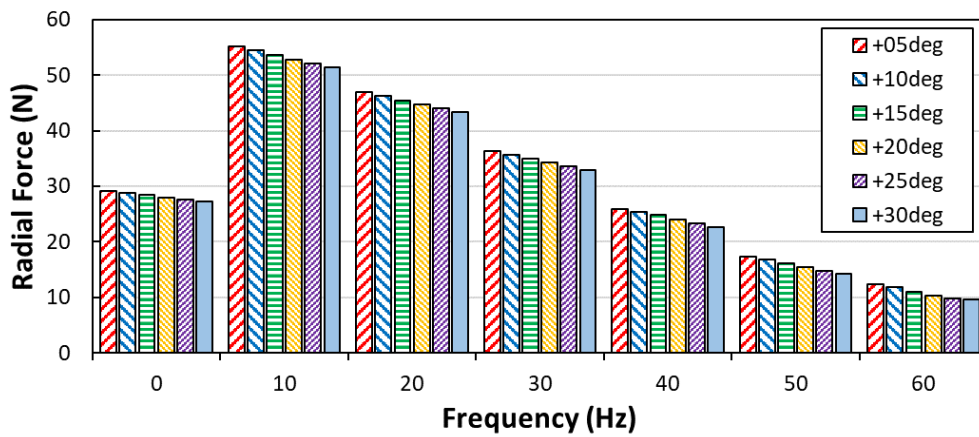
The radial forces acting on the stator are considered to be the major contributor to acoustic noise and vibration production in SR machines. Reducing the amplitude of radial forces as well as the rate of change in radial force is desirable to influence the final vibration response. This study indicates that the amplitude of radial force excitation per tooth is dependent on the amplitude of current at the moment of change of phase. Given that the current excitation across all cases is equal at the switching of phases, it follows that the flux and therefore radial force at this moment shall also be equal in amplitude. The radial force per pole profile can be considered as two radial force profiles mapped on top of each other, one representing the radial force profile under 5A excitation, and a second representing operation at the stepped down current amplitude (4.5A). A variance in duration of step down in current results in a time equivalent drop to the lower radial force profile. Across all low order harmonics analysed, the amplitude decreases with larger duration of current step.

Based on discussion of the radial force profile where the current drop correlates to a drop in flux density, the amplitude at phase switching is equal for each case. Furthermore, equal peak change in

radial force occurs, as the condition at turn-off of phase is the same. However, the integral of the radial force per tooth varies more significantly, decreasing as the duration of step is increased. This correlates to a perceived reduction in ‘impulse’, also considered as a reduced radial force application for the same time period. The fundamental component of radial force is approximately equal across all teeth.



(a)



(b)

Fig. 4.17 (a) Variation in radial force in the air gap, measured across one stator pole pitch, (b) harmonic components up to 60Hz based on 150rpm operating speed.

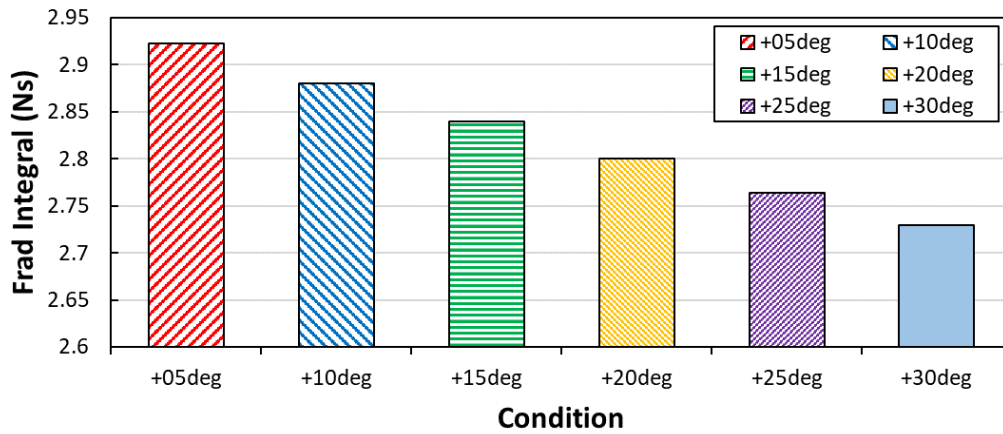


Fig. 4.18 Integral of radial force across 1 electrical period comparing influence of current step duration.

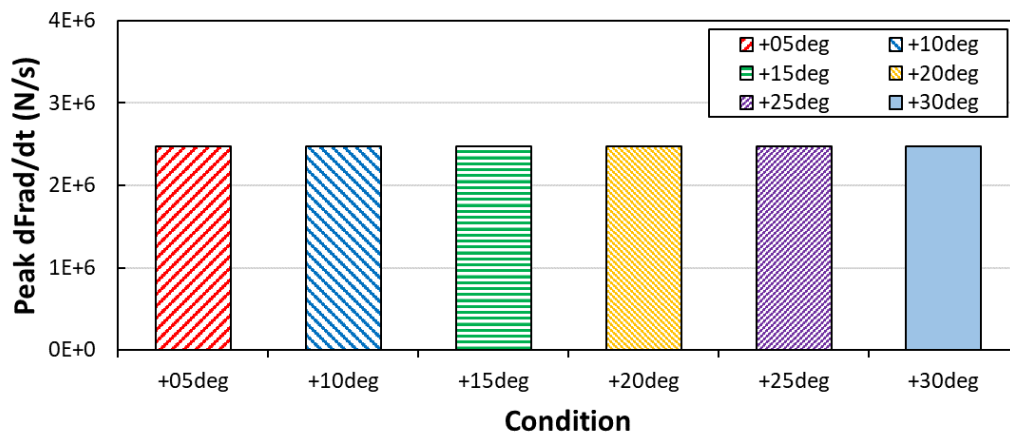


Fig. 4.19 Peak rate of change in radial force across 1 electrical period comparing influence of current step duration.

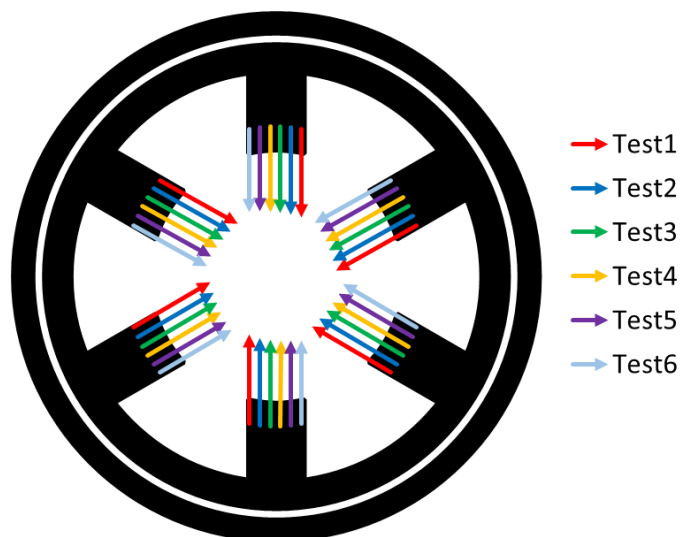


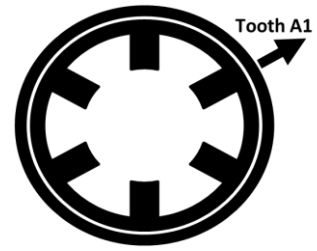
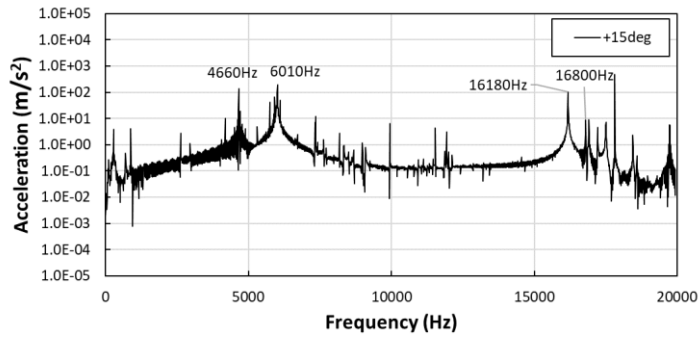
Fig. 4.20 Fundamental components of radial force on each pole shown acting on relative teeth, showing variance in magnitude of harmonic forces due to step down in current.

4.4.2 Vibration response

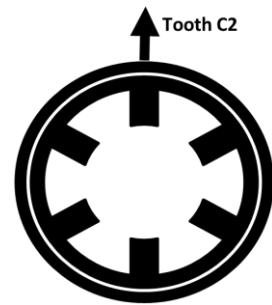
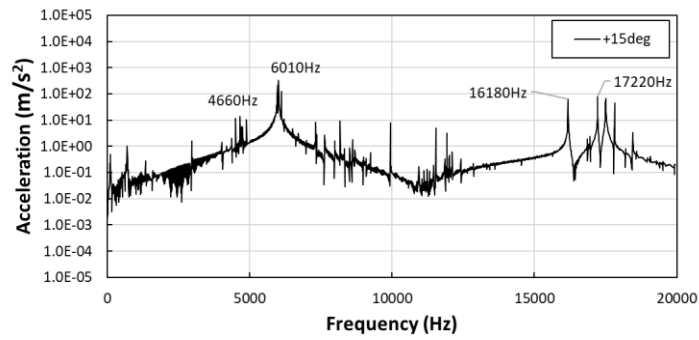
The vibration response at each location included in the simulated analysis exhibits reduced levels of vibration compared to the baseline ‘ideal’ waveform. This is attributed to the reduced phase current at the change in phase, it is previously proven that the amplitude of the phase current square wave is a significant factor in vibration levels. Comparing trends for each mode shape present in the vibration spectrum, the changes in vibration amplitude is negligible given the changes in current stepping. For mode shapes of radial order 2 show a slight ripple in amplitudes but no clear trend, modes of shape 4 nature experience little to no change in amplitude. Thus, the influence of step duration on vibration response is minimal, however the amplitude of the change has a significant impact.

It is observed in the vibration response at locations behind stator poles that there is also a minor increase in mode (0, 3b) at approximately 12500Hz. When considering sources of vibration in SRMs, radial force is often cited as a major contributor. Therefore, it is interesting to note that the total radial force experienced by each tooth during one electrical cycle decreases as the time duration of the step is increased. It would then be expected that as a result of increased total radial force, the total deformation change in the stator may also increase. However, this is not reflected in the vibration response of the simulated model. This indicates that the total radial force acting in the air gap has little to no influence on the vibration response. Rather, it is the peak radial force and rate of change in radial force that carries a larger significance in the reduction of vibrations in the stator.

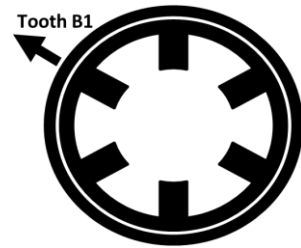
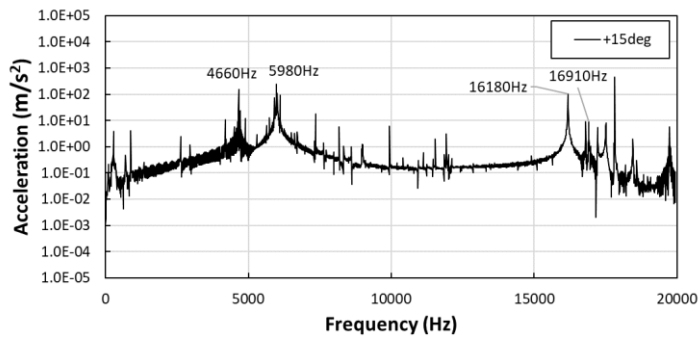
Furthermore, utilising a step down in current close to the turn-off event has similarities to the active vibration cancellation method [Wu95] as presented previously. The time step in the AVC technique is sufficiently short in duration so as to apply an antiphase vibration after the initial oscillation of the stator begins. Therefore, for future work it is worth considering the potential for use of a step down in current applied at the turn-off event, with a significantly lower step duration. Utilising this to target a frequency for reduction of oscillations may exhibit improved results. Furthermore, as the current profile is adjusted in the time domain, the impact on time domain acceleration is also of interest. This is a time consuming process in terms of simulation time and modelling, and hence, is not covered in this study.



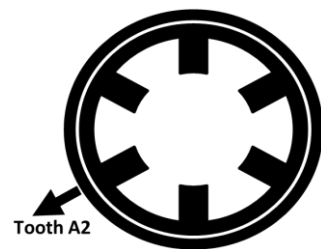
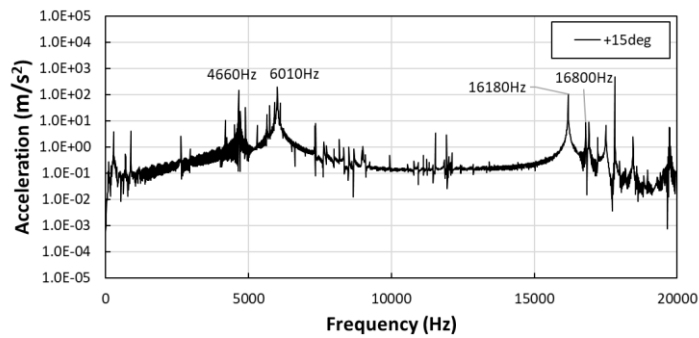
(a)



(b)

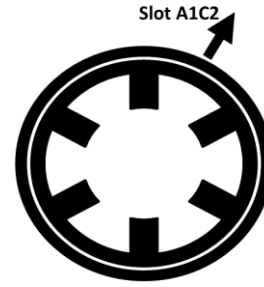
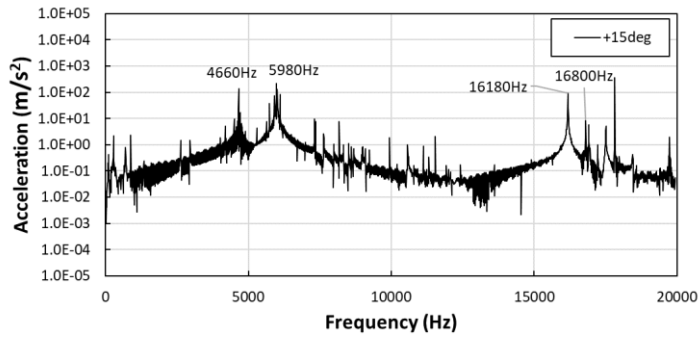


(c)

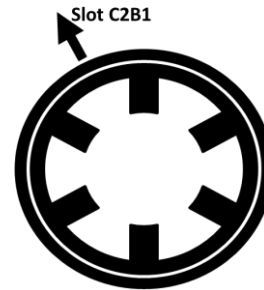
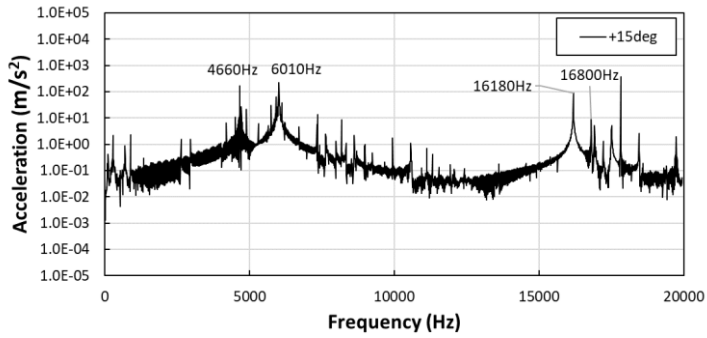


(d)

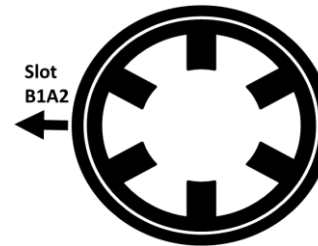
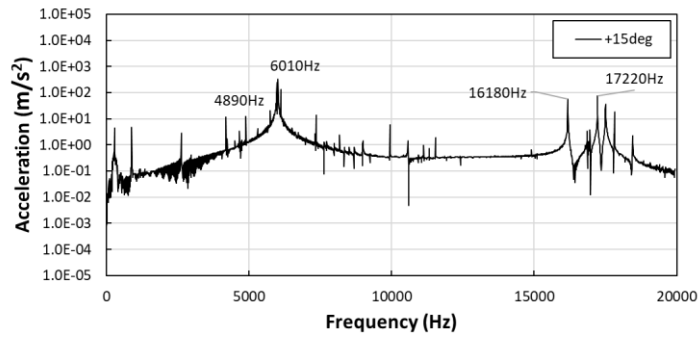
Fig. 4.21 Vibration response of 5A load current with step down duration of 15° electrical from 120° baseline, simulated output on the casing behind teeth (a) A1, (b) C2, (c) B1, (d) A2.



(a)

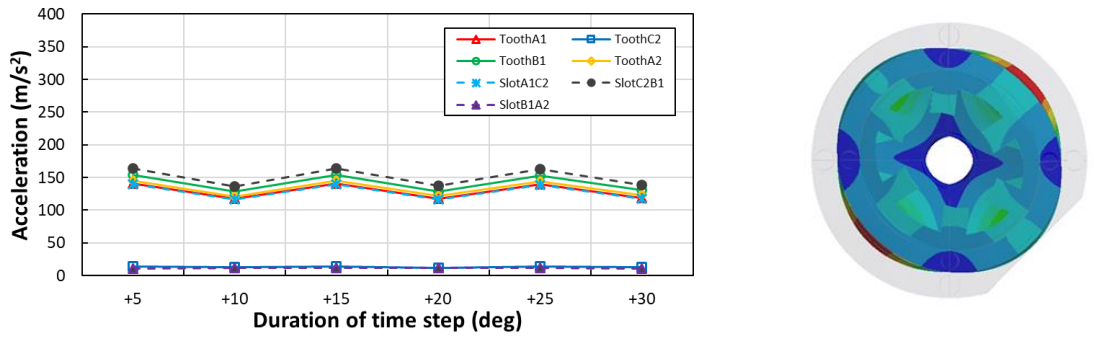


(b)

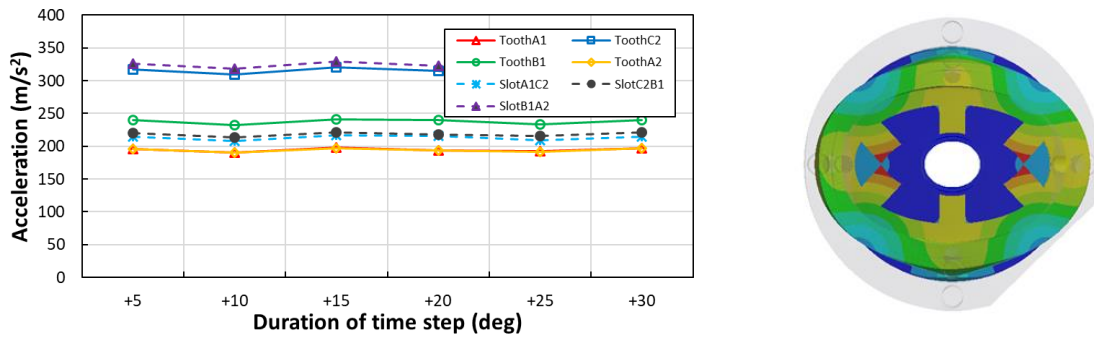


(c)

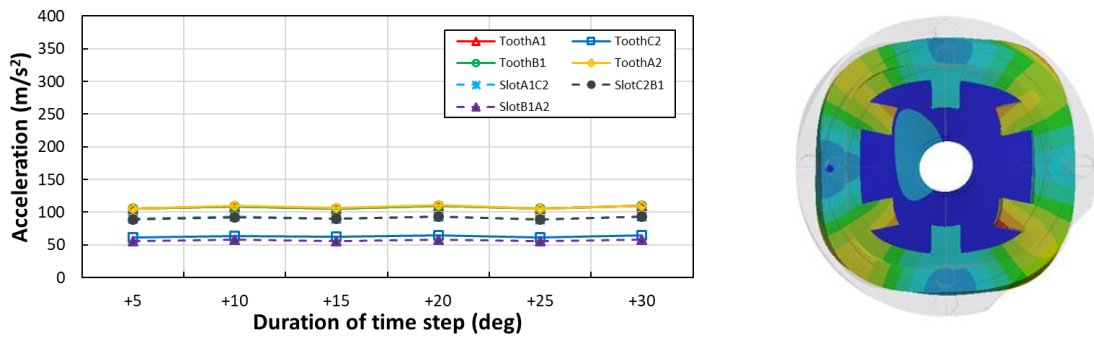
Fig. 4.22 Vibration response of 5A load current with step down duration of 15° electrical from 120° baseline, simulated output on the casing behind slots (a) A1C2 (b) C2B1 and (c) B1A2.



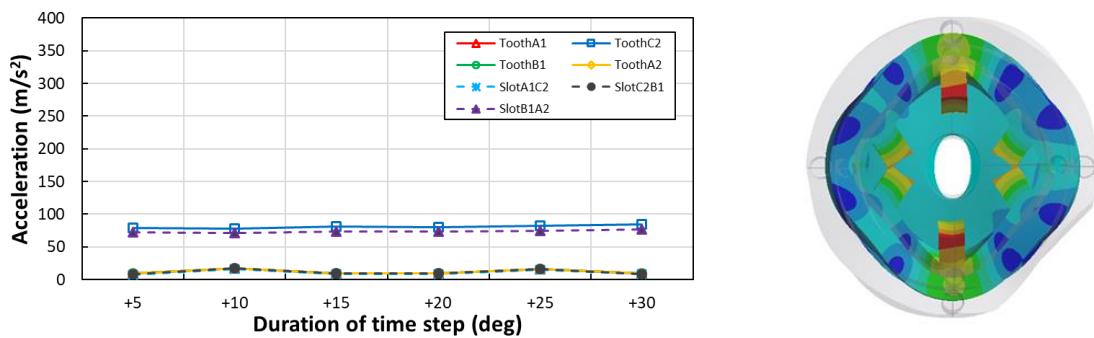
(a) Mode (0, 2a)



(b) Mode (0, 2b)



(c) Mode (0, 4a)



(d) Mode (0, 4b)

Fig. 4.23 Vibration response to harmonic force loads applied on stator teeth surface, shown for significant mode shapes (a) to (d).

4.5 Summary

It is accepted that in conventional SRMs, the turn-off of current in each phase is a dominant source of electromagnetically excited stator borne vibrations [Wu93] and [Wu95]. Hence, the baseline unipolar square wave current profile is manipulated around turn-off. The aim is to investigate the influence of various current profile parameters on the stator vibration response. This is achieved through controlling the current profile from the perspective of the time domain, presenting the current profile as a series of discrete points.

Initially, the influence of a continuous slope differential at turn-off is investigated. In order to find the influence of the severity of gradient, the duration over which the constant decay in current occurs is increased from $+10^\circ$ to $+60^\circ$ electrical. By introducing the slope at turn-off, it is found that the electromagnetic forces are directly affected. The peak radial force is equivalent in all cases, but the fall in radial force varies significantly. The highest reduction in rate of change in radial force occurs for the lower durations of current slope. In other terms, the reduction in severity of radial force decay decreases exponentially as the duration is increased linearly. Therefore, for minimum increase in copper loss due to increased excitation duration, reasonable reduction in electromagnetic excitation can be achieved. In terms of vibration response of the stator, the trends in dominant vibration modes are investigated. It is found that a similar decay in dominant mode amplitudes is observed, thus illustrating the link between the rate of change in radial force and the amplitude of vibration response.

It is shown in [Wu95] that by applying a negative current after the conventional period of excitation, an anti-phase oscillation is produced and the total vibration response is reduced for a target frequency. In this chapter, a current step is applied pre-turn-off so as to reduce the phase current at turn-off. Hence, a corresponding reduction in vibration response is found, relative to the amplitude of the current step. For active vibration cancellation, the time step is varied to target specific frequencies, typically the frequencies of the dominant vibration modes. The investigation of current step considers a more generic scenario, where the duration of the pre-turn-off step down in current is varied from 5° to 30° electrical. The results from simulations indicate that the duration has no influence on the vibration response, although the reduced current causes reduced vibration with reference to the baseline.

For future work on influence of time domain current profiling, the influence of the slope may be investigated further. For an experimental current waveform, the decay in turn-off of current is considered to be exponential and a result of the SRM's inductance. Therefore, by taking the continuous slope at turn-off and converting into a time varying slope, the influence of inductance on vibration response may be investigated. It has been verified in Chapter 3 that the amplitude at turn-off is significant in reducing the vibration response. Hence, as well as considering a two-step control with varied turn-off for the step, the amplitude should also be considered. This may result in a drop in performance due to a reduction in current during the torque producing period. Therefore, there is opportunity here to present an optimisation for two or even multi-step control of turn-off.

Chapter 5 Investigation of Influence of Current Profiling in Frequency Domain

5.1 Introduction

The profile of phase currents for SR machines can be defined by a discrete series of points with respect to time, or sum of consecutive harmonic components. This chapter seeks to examine the influence of current profiling via the use of current harmonics, which are easily implemented into the control via space vector PWM. Simple implementation of control allows the use of more generic and standard components in switching and control, reducing cost and complexity. Similar methods of harmonic decomposition of the current profile have been used in [Hua17], [Hua18], [Lee17], [Hua19a] and [Hua19b] to optimise torque production and minimise torque ripple. Further to these studies, the relationship between SR machines and the more recently introduced variable flux reluctance machine (VFRM) is covered, with optimisation of the VFR machine with the 2nd harmonic introduction. These machine types are also compared for acoustic noise and vibrations in [Liu12].

The use of current harmonics is also investigated in [Tak15] from the perspective of radial forces in the stator, more specifically the influence of harmonics on mutual radial forces across teeth. A novel method is developed to reduce the acoustic noise and vibration response by optimising the driving current as a sum of dc through to the 3rd harmonic component. It seeks to achieve this by focusing on the sum of radial forces acting on a tooth, and minimising the variation in radial force or radial force ripple. In other words, a constant radial force acting on the stator will cause a low vibration response in comparison to a radial force with considerable ripple. This echoes the thoughts and statements previously explored, where the stator is considered to be a mass-spring damper system released at the turn-off moment of each phase. The ideas presented in [Tak15] are then further explored and investigated in [Kur15a] and [Kur15b]. It is worth noting that the investigation focuses on a 36s/24r SR machine, in which the physical separation of teeth is significantly lower compared to the 6s/4r geometry explored in this thesis.

5.2 Decomposition by Fourier series

Utilising the ‘ideal’ baseline current profile introduced in chapters 4 and 5, the harmonic content of the square wave may be derived with the use of Fourier transform. From the perspective of frequency domain, it is possible to interpret the current waveform as a series of consecutive current harmonics (5.1). The Fourier transform produces the series of sinusoidal components of the baseline and their relevant amplitudes and phases. By reintroducing these elements back into the current profile one by one and rebuilding the waveform, the influence of harmonic inclusions can be investigated. The current profile can be defined as follows:

$$I = I_0 + \sum_{k=1,2,3\dots} I_k \cos(k\theta + \alpha_k) \quad (5.1)$$

where I_0 and I_k are the amplitudes of dc and the k -th current harmonics; α_k is the initial angle of the k -th current harmonic. The current profile may then be rebuilt with harmonic components up to and including I_k . The profiles for $k = 1, 2, 4, 10$, and 31 are shown in **Fig. 5.1**. It is noted that the copper losses under these current profiles shall vary. However, in order to analyse the impact of harmonic progression the amplitude and phase are determined by the original unipolar square wave.

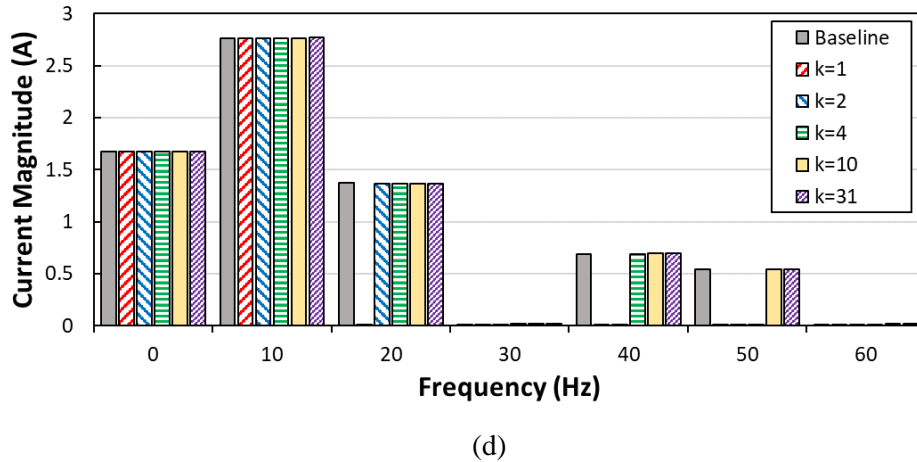
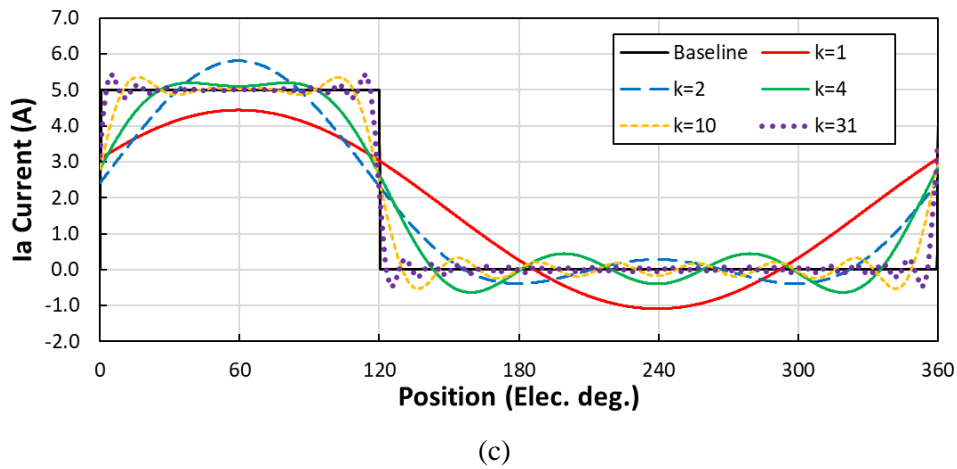
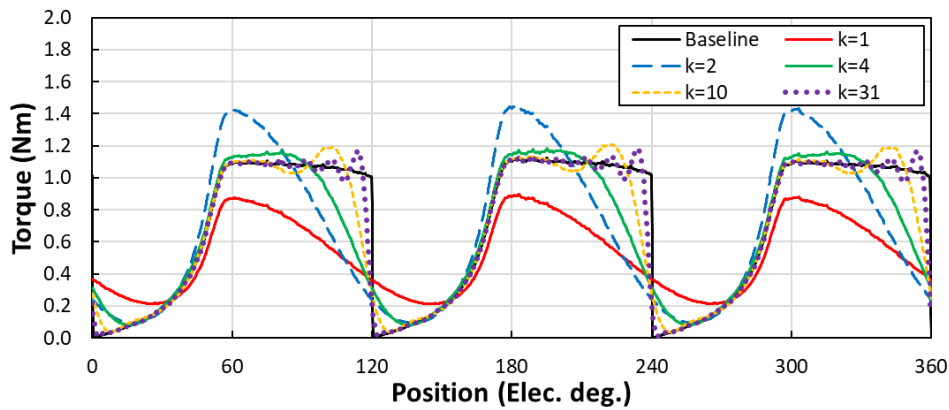


Fig. 5.1 Frequency domain current shaping. (a) current profiles based on values of k , (b) harmonic content of current profiles.

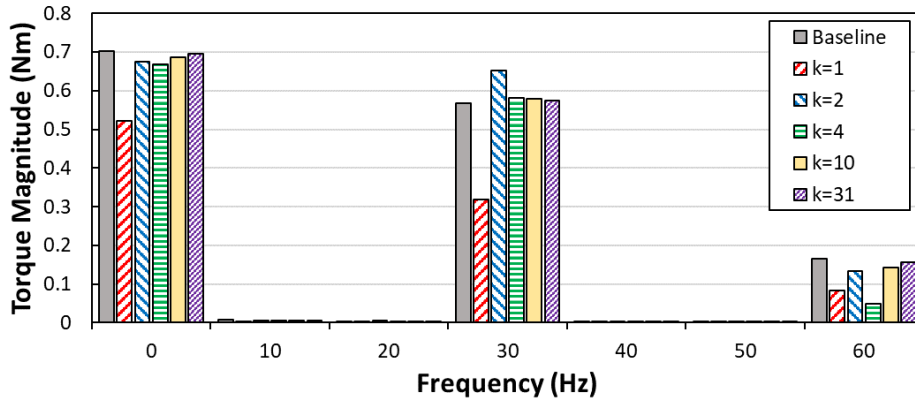
5.2.1 Electromagnetic results

The influence on torque is critical in determining the suitability of utilising current harmonic breakdown in real world applications, without reasonable torque production the machine ultimately serves no purpose. As is evident from **Fig. 5.2**, as the value of k is increased the torque profile moves

closer to the baseline profile. Given the amplitude and phase of each harmonic is calculated by the Fourier transform of the baseline unipolar square wave, the correlation between torque characteristics is not linear with harmonic inclusions. In the case investigated, the torque ripple for inclusion of the second harmonic ($k = 2$) is significantly higher than torque ripple with inclusion up to $k = 4$. As harmonic content k increases the average torque also increases, and the region of near constant torque generation also increases. It is worth noting that the previous work into SR machines with a permanent DC excitation plus a fundamental sinusoidal component exhibit slightly different results [Liu12], [Lee17], [Hua18], [Zhu17] and [Fuk12]. Typically, a ‘fundamental’ component is the current component contributing to the torque production of the motor, and hence, determines the critical performance and is rarely manipulated. However, when considering a VFRM it is both the DC component and sinusoidal component which contribute to torque production. Therefore, it is more appropriate to refer to the sinusoidal component as the 1st harmonic, not fundamental to avoid confusion. In order to optimise torque production in the case of a DC + sinusoid SR machine, the optimal results involve synchronisation between the static magnetic field and the rotating field. This is achieved by aligning the phase back-emf with the 1st current harmonic. In the case of a 6s/4r doubly salient machine this is a variance in initial position of 15° mechanically advanced of the optimum initial position for the unipolar square wave excitation. Further to this, the optimal ratio of DC to 1st current harmonic is found to optimise torque production. Later in this study, the influence of DC and 1st current harmonic is introduced from the perspective of vibration response, rather than optimal torque.

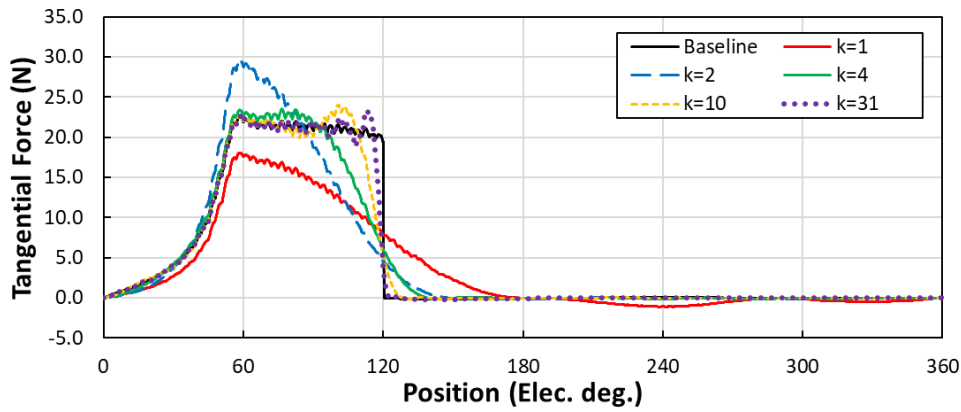


(c)

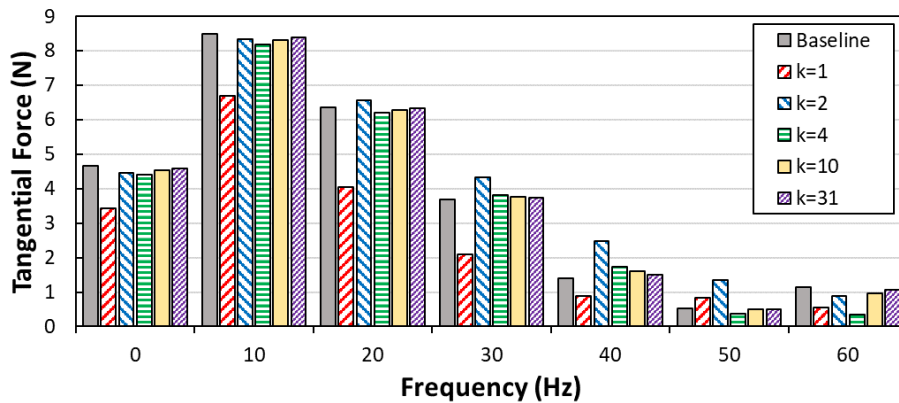


(d)

Fig. 5.2 (a) 3 phase torque profile for one electrical cycle, (b) harmonic components up to 60Hz based on 150rpm operating speed.



(c)



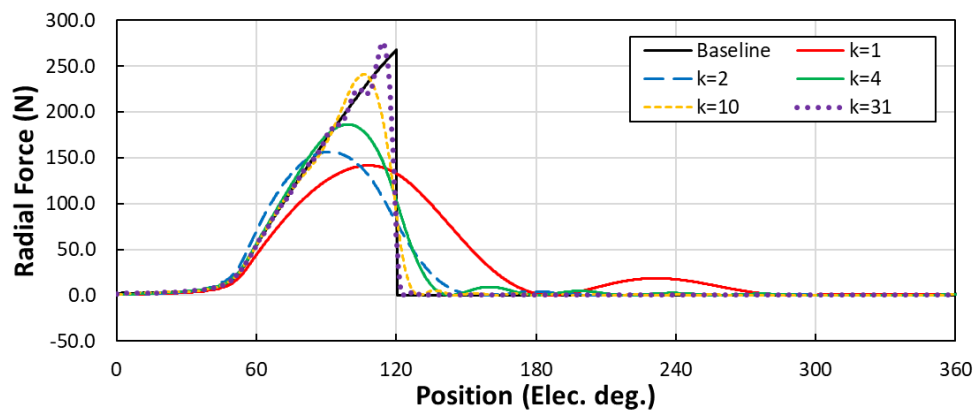
(d)

Fig. 5.3 (a) Tangential forces calculated across an arc in the middle of the air gap, spanning one stator pole arc, (b) harmonic content of tangential force.

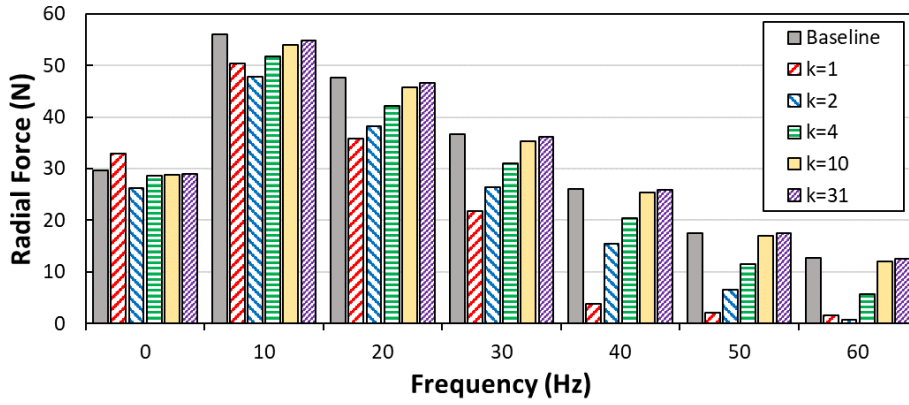
As discussed in previous sections the tangential force directly correlates to the torque produced per phase. From single phase tangential force measured in the middle of the air gap it becomes apparent that as the harmonic content is increased, a number of phenomena occur. It can be shown that the peak tangential force and torque are increased for $k = 2$. However, once the inclusion reaches the 4th harmonic

the tangential force and torque closer resembles the baseline. In [Dex18] the torque production mechanisms of switched reluctance and variable flux reluctance machines are compared and analysed, the low order current harmonics typically dominate and define the torque production of the machine. It can also be seen that the gradient during the period of decaying tangential forces is proportional with harmonic inclusion. In other words, as the harmonic inclusion increases towards that of the baseline unipolar square wave, the rate of change in tangential force per pole increases.

Radial force is regarded as the primary contributor to acoustic noise and vibrations in SR machines, along with derivatives of radial force such as rate of change, peak radial force and radial force ripple. When considering the slope and duration of turn-off current it is determined that the gradient and severity of radial force decay at a change of phase is a critical component of vibration production in the stator. As the harmonic content is increased, it is evident that the peak radial force also increases towards the level of radial force produced by the baseline square wave current. However, as seen in **Fig. 5.4** the position relating to the moment of radial force varies significantly with harmonic force content. That is to say, considering the peak radial force affects the vibration response, by varying harmonic inclusion the peak radial force does not necessarily occur at the same aligned position. Further to this, the rate of change in radial force following the peak radial force (not necessarily ‘turn-off’) increases as harmonic content increases. Hence, the decay of radial force occurs over an increased time period, avoiding the problematic result of instantaneous turn-off and a sudden release of radial forces. It can also be noted that with a high number of harmonic inclusions, $k = 31$, there is also radial force ripple introduced close to the perceived moment of turn-off. There is also ripple introduced in the low order harmonic inclusion. However, this occurs during torque generation of other phases and is not considered to influence the vibration response heavily. The integral of radial force relates to the change in momentum per pole caused by the air gap radial forces. Interestingly, despite reduced peak current and copper losses for low order harmonic inclusion the integral of radial force is the highest for $k = 1$. This is due to the extended duration of major radial force combined with additional radial forces acting across the stator pole during the period of negative current excitation.



(c)



(d)

Fig. 5.4 (a) Radial force profile calculated across an arc in the middle of the air gap for one stator pole pitch, (b) harmonic content of radial force profiles.

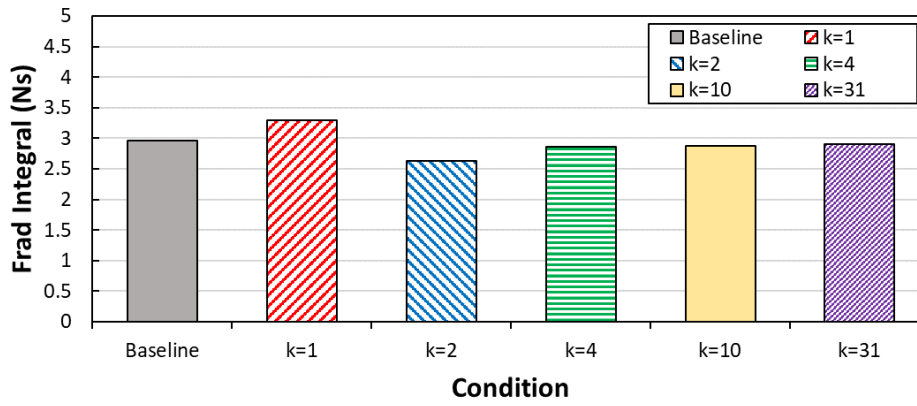


Fig. 5.5 Integral of radial force across 1 electrical period for varied current harmonic inclusion.

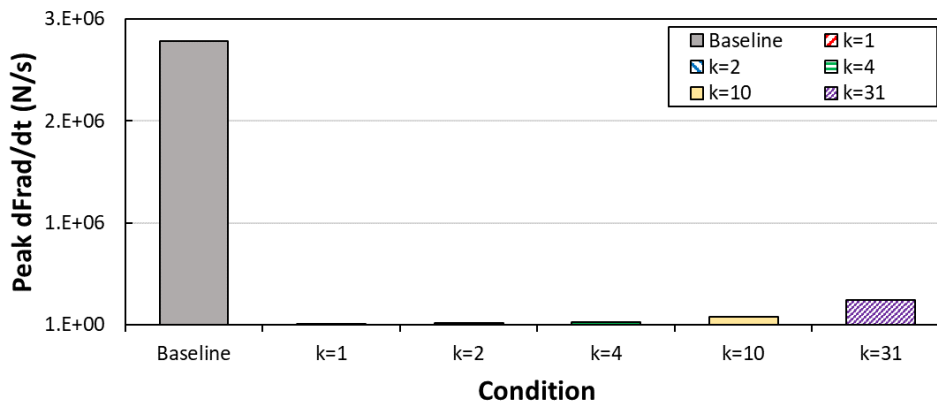


Fig. 5.6 Peak rate of change in radial force for varied current harmonic inclusion.

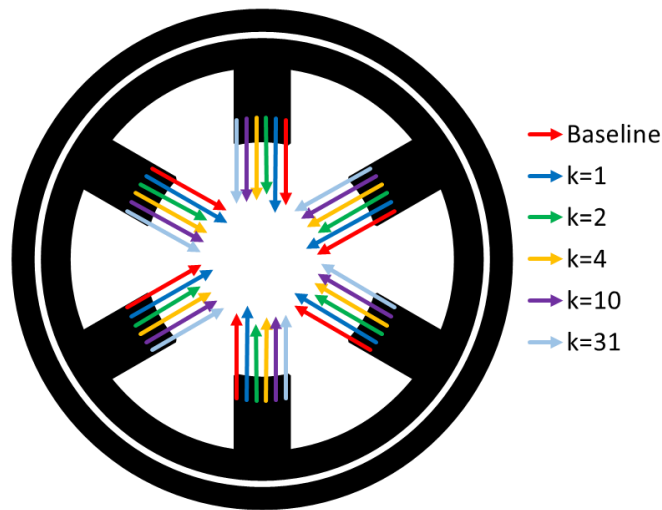


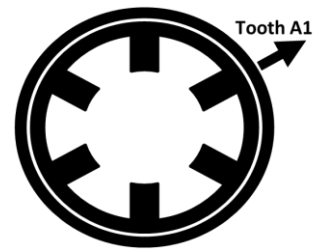
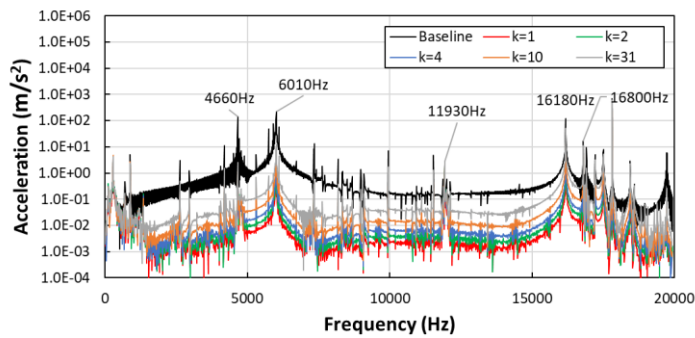
Fig. 5.7 Fundamental components of radial force on each pole, showing variance in current harmonic inclusion up to $k = 31$.

5.2.2 Vibration response

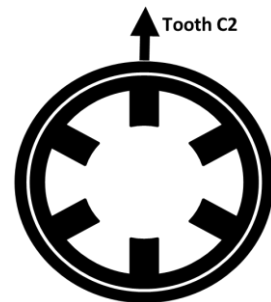
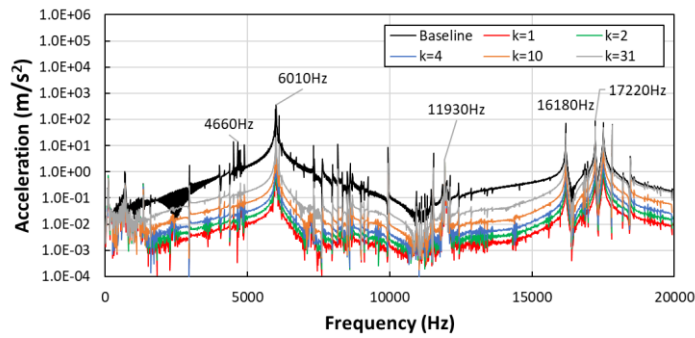
The vibration response is simulated for the full prototype machine including bracket and compared behind 4 of the teeth and 3 slot locations. The results indicate a significant drop in vibration response at all locations dependent on the level of harmonic reconstruction. Furthermore, for harmonic reconstruction up to and including the 31st harmonic, the vibration response is still significantly reduced compared to the baseline unipolar square wave. This is due to the harshness of turn-off in the baseline, and ultimately it would require infinite harmonics to achieve an equivalent result. Typically, the response across all frequencies is reduced and proportional to the harmonic inclusions. It is noted that for response behind teeth, mode 3 is introduced into the vibration spectrum. This is a result of mutual radial force response as observed when introducing a slope at turn-off or any period of overlap. The overlap between phase currents promotes a force acting at multiple teeth, such that the resultant force is no longer acting directly aligned with a stator tooth. Hence, although the forces are equal and opposite there is a force acting between teeth causing asymmetry in the system and resulting in mode 3 excitation.

Comparing results for specific modes indicates a minimal influence for modes (0, 2a) and (0, 3b), where the amplitudes of vibration response are considerably lower than those of the more dominant modes. Under the baseline operation and analysis in the time domain, it is apparent that the dominant mode is (0, 2b), whilst with current profiling in the frequency domain this is no longer the case. It is clear that mode (0, 2b) still exhibits a significant amplitude response, but it is smaller than both mode 4 shape vibration modes. Both eigenmodes of mode 4 consistently show the highest radial vibration response amplitude across all values of k , with mode (0, 4b) being influenced by the bolted connections of the endcap. This is a result of the excitation period being extended under harmonic excitation, where multiple phases are concurrently excited with conditions of overlap. Hence, the radial forces are no

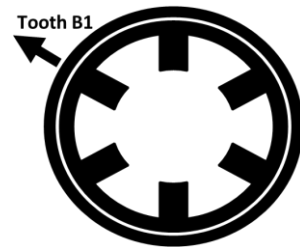
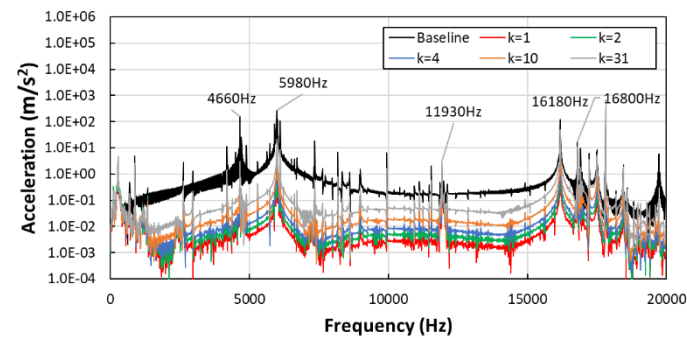
longer being applied solely to two diametrically opposed teeth, rather to four teeth belonging to pairs to two phases. From these results, it is apparent that the vibration response can be significantly reduced by breaking down the harmonic components. Analysing the trends of amplitudes for specific vibration modes, it is estimated that dominant modes are influenced equally for each harmonic inclusion. This could be represented as a proportional increase in vibration response as the harmonic inclusion is increased. This can be advantageous, as the addition of an extra harmonic component may be able to significantly increase the torque production of the machine, whilst retaining a relatively low vibration response in comparison to the baseline unipolar square wave investigated thus far.



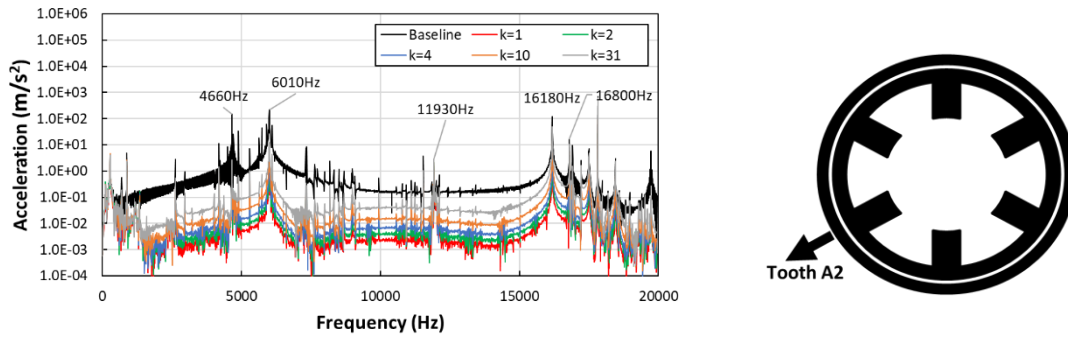
(a)



(b)

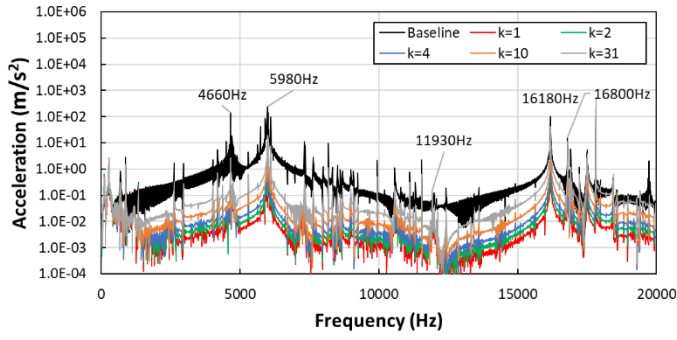


(c)

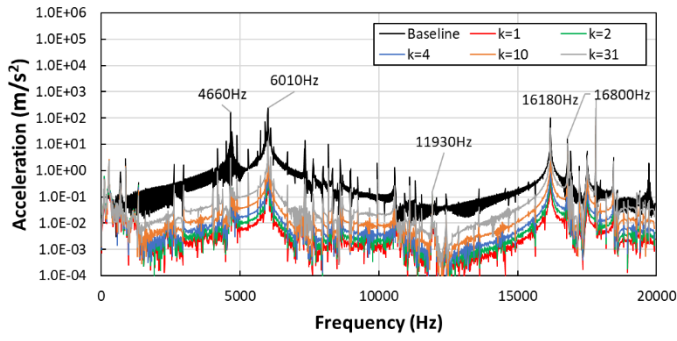


(d)

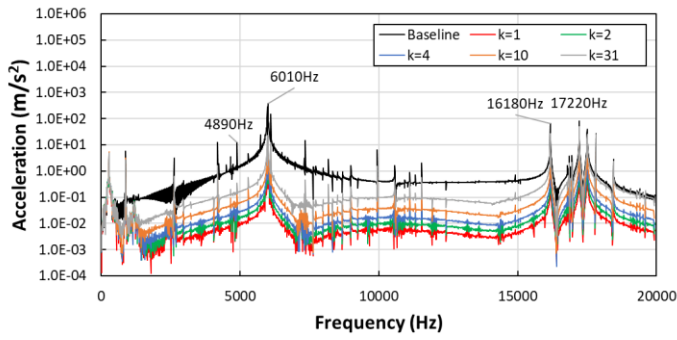
Fig. 5.8 Vibration response of increasing current harmonic inclusion derived from the baseline square wave, simulated output on the casing behind teeth (a) A1, (b) C2, (c) B1, (d) A2.



(a)

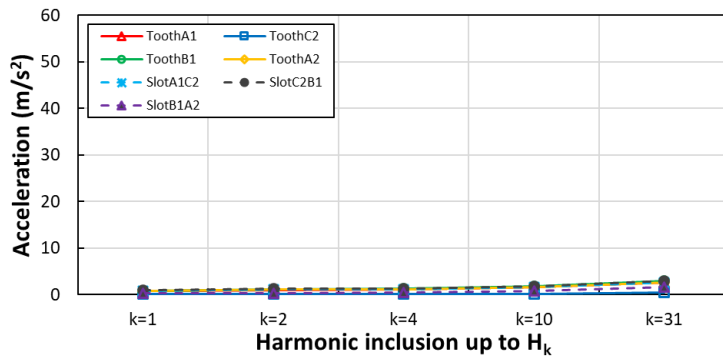


(b)

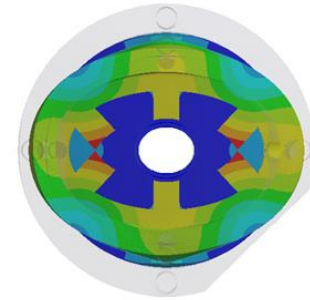
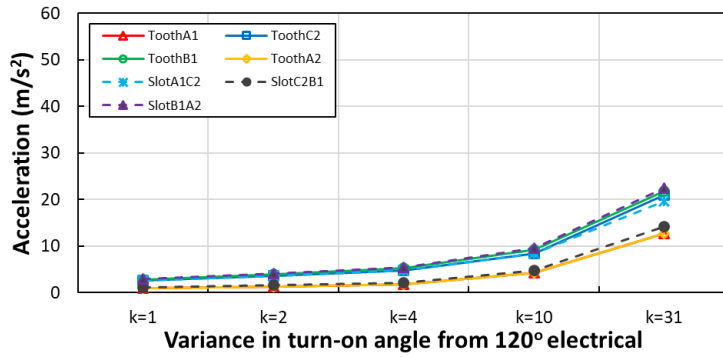


(c)

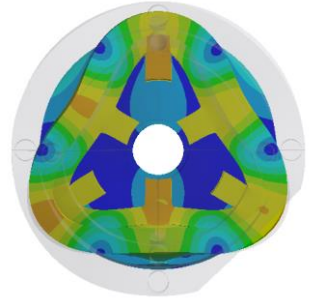
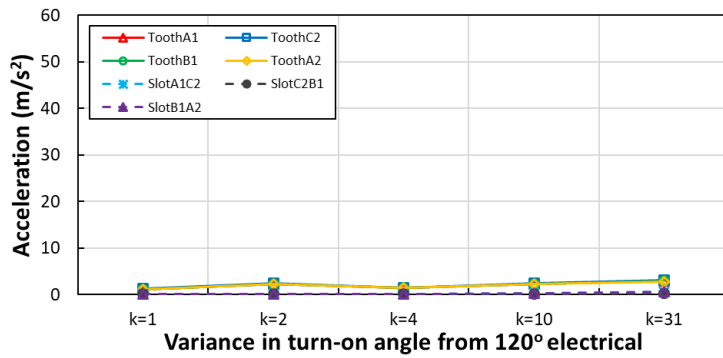
Fig. 5.9 Vibration response of increasing current harmonic inclusion derived from the baseline square wave, simulated output on the casing behind slots (a) A1C2 (b) C2B1 and (c) B1A2.



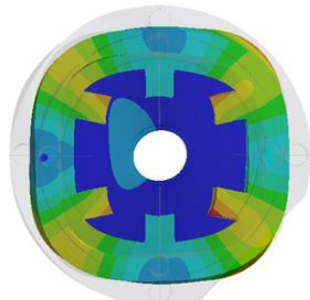
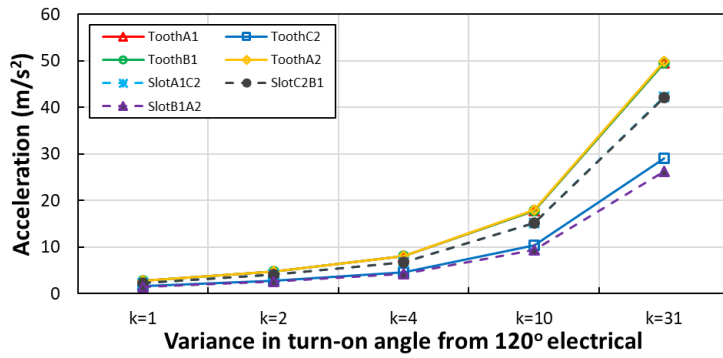
(j) Mode (0, 2a)



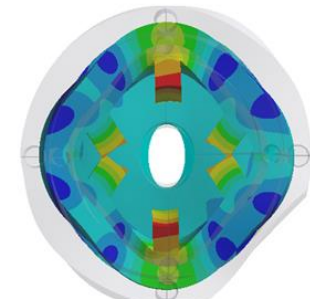
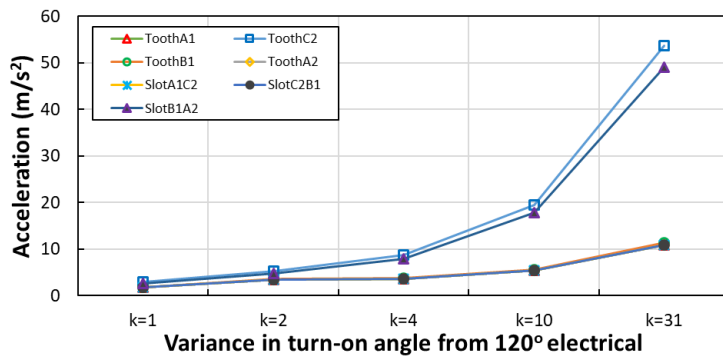
(k) Mode (0, 2b)



(l) Mode (0, 3a)



(m) Mode (0, 4a)

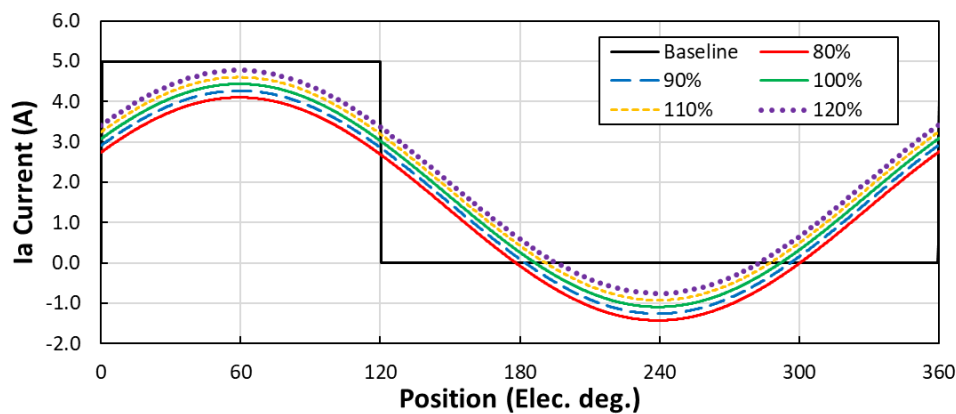


(n) Mode (0, 4b)

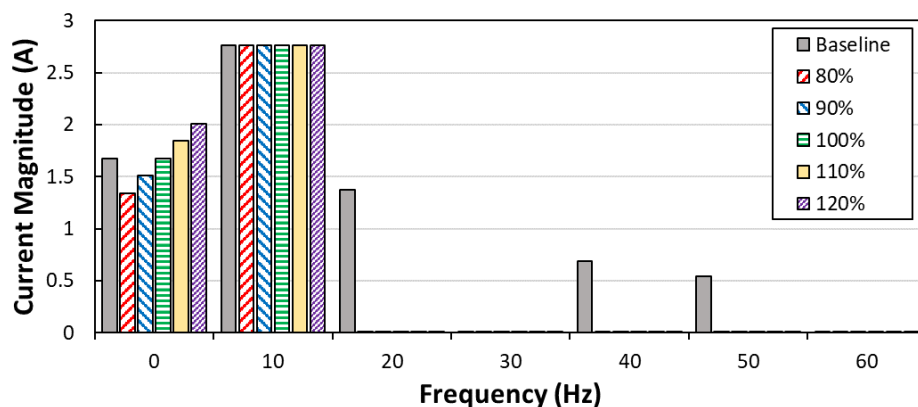
Fig. 5.10 Vibration response to harmonic force loads applied on stator teeth surface, shown for significant mode shapes (a) to (d).

5.3 Amplitude of DC + 1st current harmonic

Considering the significant reduction in vibration response simulated for a harmonic reconstruction of the unipolar square wave with low order harmonics, the influence of these current harmonics is investigated. Firstly, the influence of the DC amplitude is investigated provided the harmonic content of the current profile is limited to the DC + 1st harmonic only. This is the equivalent control to the variable flux machine. However, it is acknowledged that the initial position is varied such to match the decomposition of the unipolar square wave. It is determined in [Hua17] that the optimal AC (1st current harmonic) to DC ratio is 1:1 for torque production. For analysis of vibration response, the DC amplitude is varied between 80% and 120% of the square wave DC component, so as to identify the influence on vibration response. From the Fourier series expansion, it is shown that the $k = 0$ component has a phase also, but this phase has no influence on the harmonic component. The current profiles under the conditions specified also provide a comparison for noise and vibration under approximately equal peak current. In Chapter 3 it is shown that the amplitude of the unipolar square wave current profile significantly impacts vibration response, and hence, the acoustic noise.



(a)



(b)

Fig. 5.11 (a) Variation in phase current illustrated for phase A only with increasing amplitude of DC harmonic, (b) harmonic components up to 60Hz based on 150rpm operating speed.

5.3.1 Electromagnetic results

Initially, the torque produced by these current profiles is analysed across one electrical cycle. It is evident that the torque increases proportionally with the increase in DC excitation. From [Zhu17] and [Liu12a] the torque in VFRMs and SRMs is derived to produce the results seen in (5.2) and (5.3). The torque production in (5.2) is known, and hence, (5.3) may be derived by substituting the Fourier expansion of current, i , and inductance, L . Here, it is proven by Zhu et al and Liu et al [Zhu17] and [Liu12a] that the DC component and 1st harmonic of current are dominant from the perspective of torque production and additionally, the 2nd harmonic has a small influence in SRM torque production. **Table 5.1** also indicates the influence of each current harmonic, it is shown that beyond the 2nd order harmonic the contribution is significantly reduced.

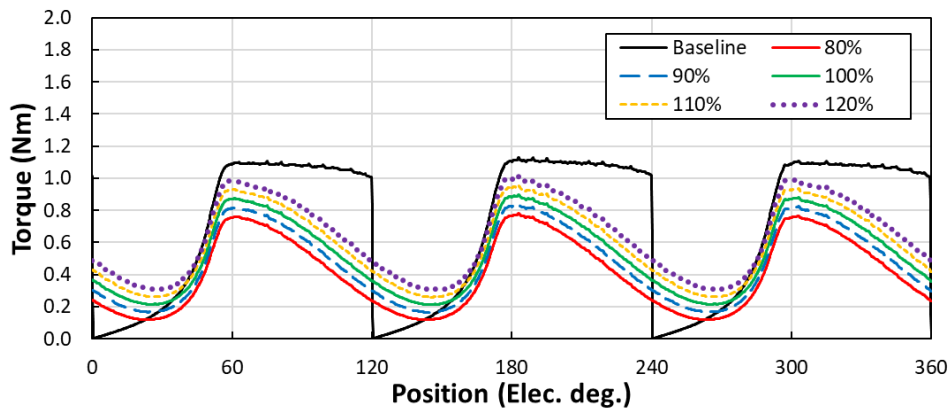
$$T = \frac{1}{2} i^2 \frac{dL(\theta)}{d\theta} \quad (5.2)$$

$$T = \frac{1}{2} \left[I_0 + \sum_{m=1}^{\infty} I_m \sin(m\theta_e + \gamma_m) \right]^2 d \left[L_0 \sum_{n=1}^{\infty} L_n \cos(n\theta_e + \alpha_n) \right] / d\theta \quad (5.3)$$

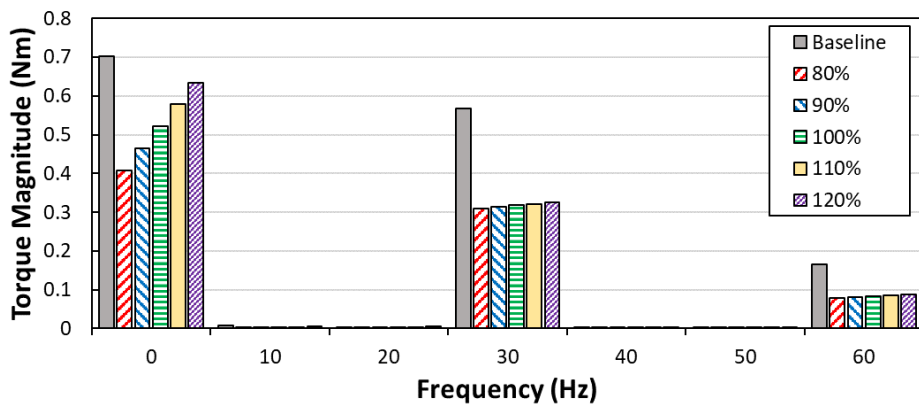
Furthermore, **Fig. 1.1** indicates that the average torque is higher for the baseline profile representing the SRM, even when compared to a 120% DC amplitude. Adjustments to the DC current influences the average torque only, it bears no influence on the torque ripple. Furthermore, as seen from the harmonic content of the torque profiles the variation in DC current predominantly affects the average torque. As mentioned previously, via alignment of the current and inductance profile for the VFRM the average can be increased to provide a comparable control to the SRM. It is noted that in order to achieve comparable average torque I_0 and I_1 must be increased such that the copper losses are significantly higher in the VFRM.

Table 5.1. Harmonic content of SRM baseline unipolar square wave current profile

Current harmonic	Magnitude, A	Phase, ° electrical
I_0	1.67075	-
I_1	2.760943	-60
I_2	1.374886	-120
I_3	0.007333	0
I_4	0.692769	-60
I_5	0.547514768	-120

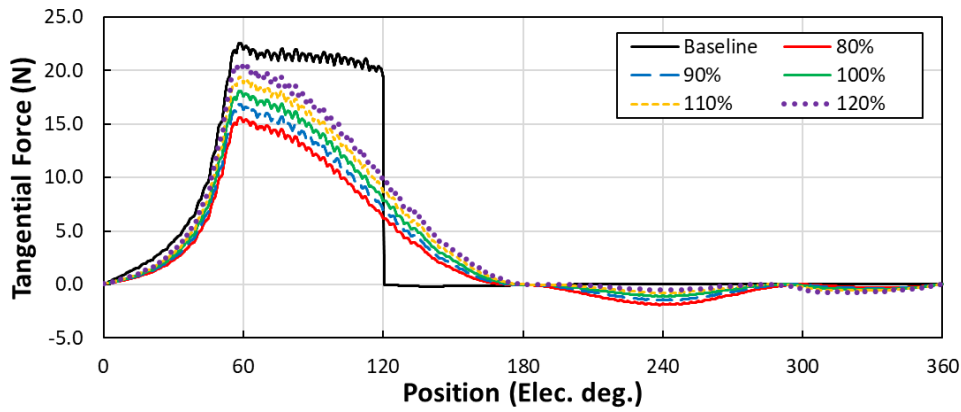


(a)

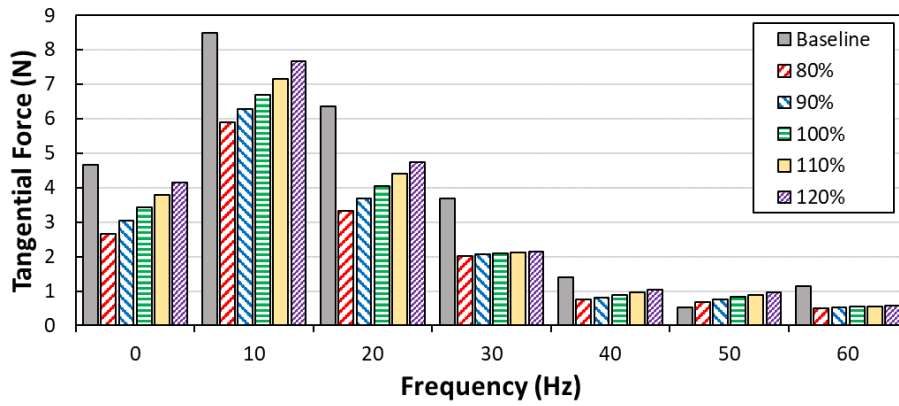


(b)

Fig. 5.12 (a) Torque profile for current profiles of increasing DC component compared with baseline current profile, (b) harmonic components up to 60Hz based on 150rpm operating speed.



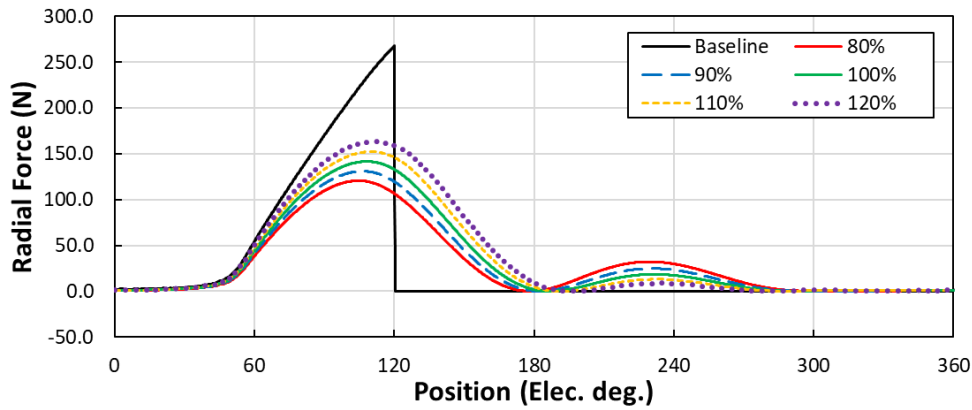
(a)



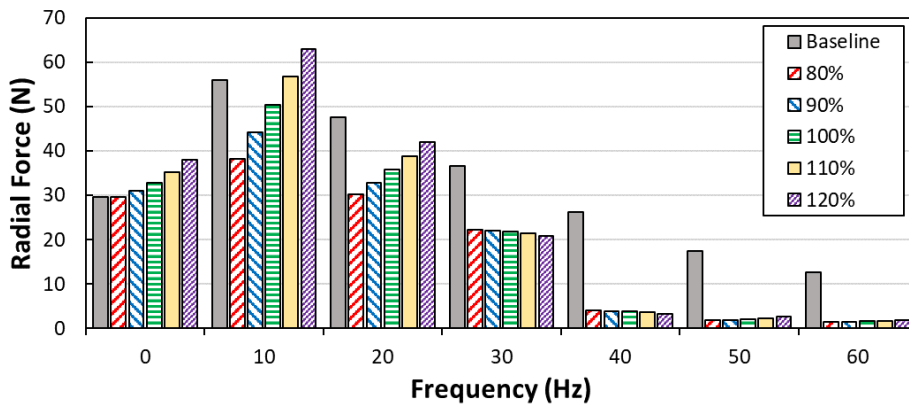
(b)

Fig. 5.13 (a) Tangential forces acting in the air gap across one stator pole pitch, (b) harmonic content up to 60Hz for operation at 150rpm.

The air gap tangential forces are simulated for one stator pole pitch, producing the equivalent single phase torque under the excitation shown in **Fig. 5.11**. As discussed for the torque production, the peak tangential forces are significantly lower than the baseline square wave, particularly for cases below 110% DC current component. The major variations in tangential force harmonics occur in the 1st harmonic and the 2nd harmonic, the 3rd harmonic of tangential force sees little change from DC variation. It can be seen that in comparison to the baseline waveform the harmonic content is typically lower for all variations of DC current analysed. The tangential force profile also shows a low duration period of negative tangential force outside of the typical SR conduction period, when operated as a VFRM. The influence of the DC current is equivalent in the negative and positive force regions of the tangential force per tooth, and hence, no effect is noted in the torque profile.



(a)



(b)

Fig. 5.14 (a) Radial forces acting in air gap across one stator pole pitch for varied DC amplitude, (b) harmonic components up to 60Hz based on 150rpm operating speed.

Similarly, to the tangential forces calculated, the radial forces are calculated across an arc in the middle of the air gap spanning a single stator pole pitch. As seen, when decomposing the baseline square wave current profile and rebuilding it, the peak radial force is significantly reduced for solely DC and 1st current harmonics. Through the use of DC and 1st current harmonic, the duration of acting radial forces per tooth is extended. That is to say that the radial force is applied more consistently, at lower amplitude across a longer time period. Furthermore, it is found that as the amplitude of the DC current is increased, the radial force in the period of alignment is increased, whilst the second period of radial force is decreased. The second period of radial force occurs at approximately 230° electrical in the cycle. This is caused by the negative period of phase current, as the DC component is increased the sinusoidal profile is offset such that the negative period is arbitrarily reduced.

However, despite the reduction in the additional region of radial force, the peak radial force is increased. Additionally, the radial force ripple is increased. As discussed in [Tak15] when mentioning sum of radial force components acting on stator teeth, the ripple may be as important as the peak forces. In the case of reduced DC component, both the peak radial force and the peak to peak radial force, radial

force ripple, are reduced. Hence, it is expected that the vibration response will be approximately proportional in reduction when compared the DC component of the current profile.

The radial force integral, or change in momentum, is the lowest in the case of the baseline waveform. Due to the increased peak radial force for larger DC components the change in momentum is also increased, under reduced condition of 80% DC current the change in momentum is approximately equal to the baseline SR profile. For clearer presentation of the results, the rate of change in radial force for the baseline is removed from **Fig. 5.16**. It is evident from the radial force profiles that the rate of change in radial force is significantly higher in the baseline square wave control. Comparing and analysing the results for increasing DC current component, the maximum decay rate in radial force increases for DC current increase. This is caused by increased current and flux crossing the air gap in a fixed period of time. Hence, as the current reverses, the radial force falls to zero from an increased amplitude of current at the fully unaligned position.

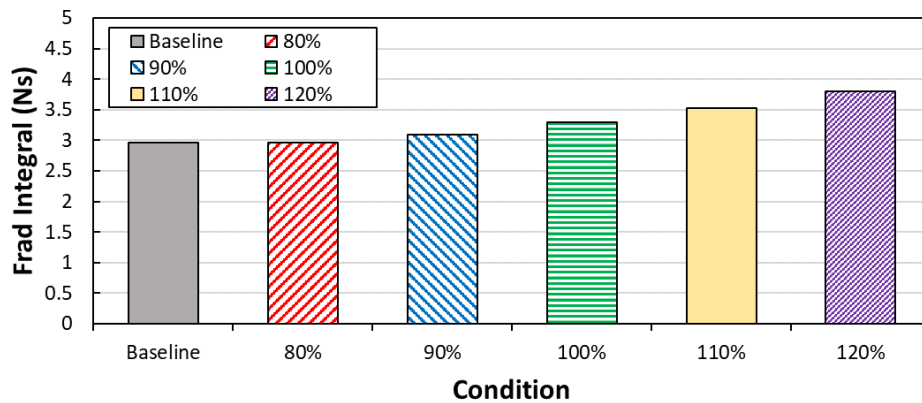


Fig. 5.15 Integral of radial force across 1 electrical period comparing influence of DC amplitude.

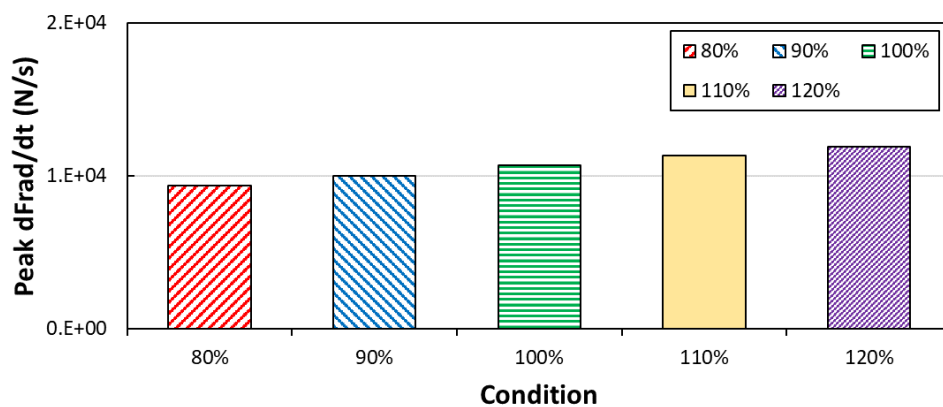


Fig. 5.16 Peak rate of change in radial forces for increasing DC amplitude.

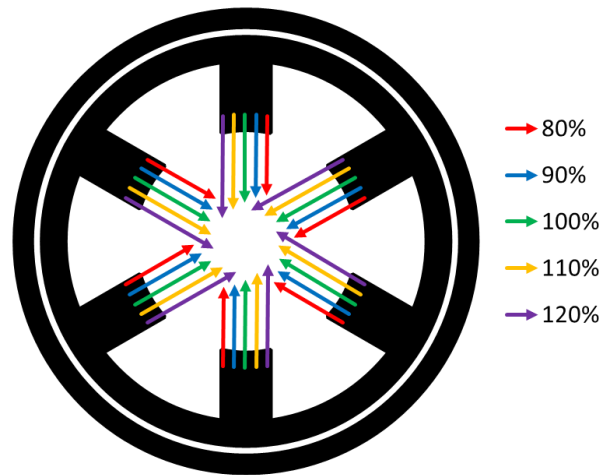


Fig. 5.17 Fundamental components of radial force on each pole shown acting on relative teeth, showing variance in magnitude of harmonic forces due to increasing DC component.

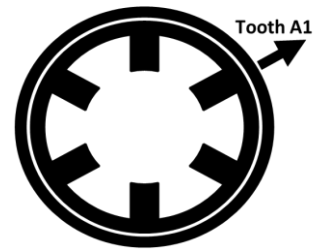
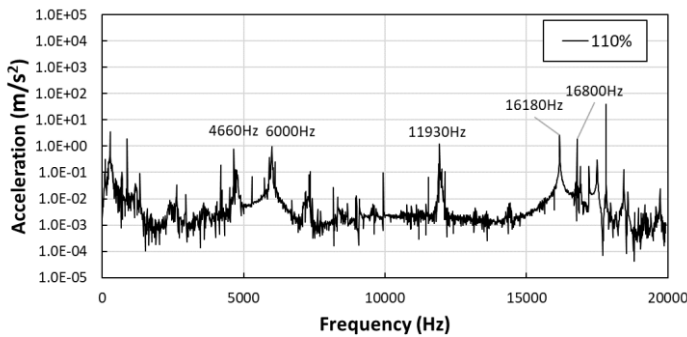
5.3.2 Vibration response

To analyse the vibration response of the varying DC amplitude, the SR machine is simulated under the load conditions specified and the harmonic content of the radial forces applied to the corresponding teeth. Following this simulation, the frequency response of acceleration is measured at a node behind teeth A1, C2, B1 and A2, and slots A1C2, C2B1 and B1A2. The results are presented for each location, under the condition of 110% of the baseline DC current harmonic. This illustrates the vibration spectra in all cases, where the variance in amplitude of mode excitations is illustrated in **Fig. 5.20**. The vibration spectrum behind tooth A1 indicates major excitations for eigenmodes (0, 2a), (0, 2b), (0, 3b), (0, 4a) and (0, 4b). The dual modes of radial order 2 and 4 are caused by the influence of the bolted connections from frame to endcap, located behind the teeth of phase C and the slot between phases A and B. As seen in other analyses of the 6s/4r machine, the dominant mode (0, 2b) occurs behind tooth C2 and slot B1A2.

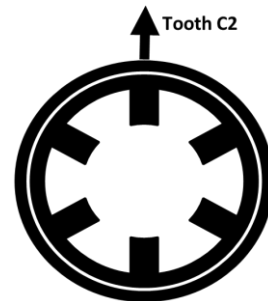
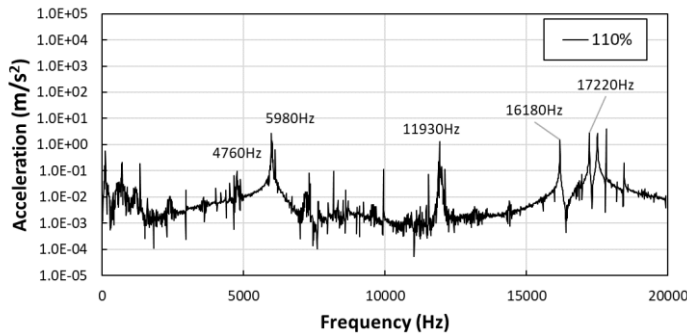
Contrary to simulations of the baseline, under current excitation of the DC + 1st mode (0, 3b) is also excited. Under the baseline unipolar ‘ideal’ square wave, this mode is cancelled due to geometry and independent excitation of phases. When excited under DC + 1st conditions, the phases are no longer independently excited, and hence, the radial forces are no longer diametrically opposite and acting solely on the teeth. Rather, mutual forces are introduced and thus modes of radial order 3 are also excited. Furthermore, the results of the simulation indicate that the amplitude of mode (0, 3b) excitation is similar to those of modes in order 2 and 4. The vibration spectrum is significantly less than the baseline square wave excitation. This phenomenon applies to all frequencies, not limited just to the excitation of natural modes.

Comparing the trend across key natural frequencies, it is evident that an increase in DC current component correlates to an increase in vibration response amplitude also. The resultant increase in amplitudes is more apparent in particular modes, mode (0, 4a) being relatively unaffected by the

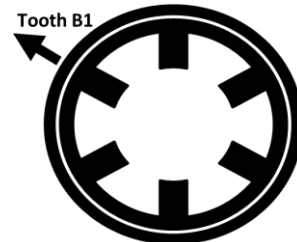
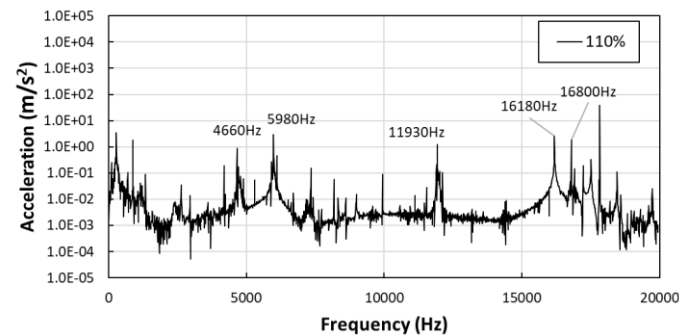
increase in DC current. However, the influence of other mode shapes is more apparent. Mode (0, 2b) experiences the largest increase in amplitude and is also noted to be the natural mode with the highest vibration response. Interestingly, the largest response for mode (0, 2b) is no longer restrained to locations aligned with bolted locations, rather it can be found that it is the dominant mode shape for results behind tooth B2 and slot A1C2 also. These simulation results indicate that the vibration response is significantly lower than that of the baseline square wave excitation across the entire frequency range simulated. Furthermore, although an increase in DC current harmonic increases the vibration response, this is negligible in comparison to the baseline. Therefore, it is a viable option to increase DC current component to improve performance without fear of significantly worsening the vibration response of the machine.



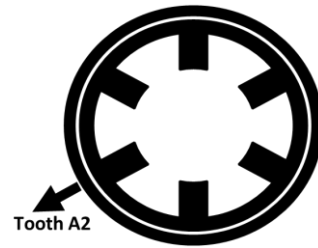
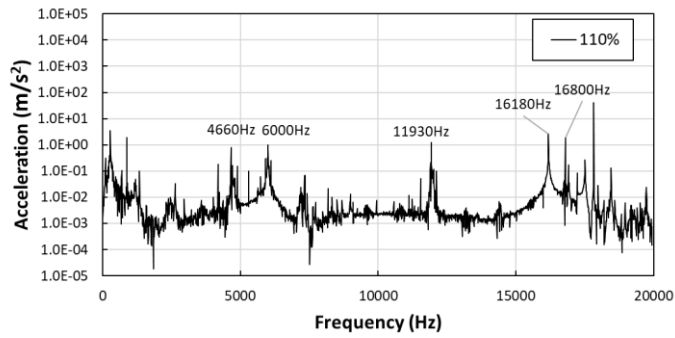
(a)



(b)

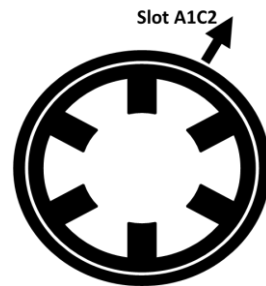
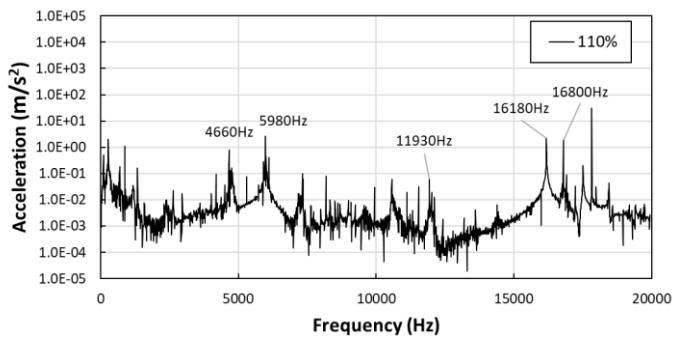


(c)

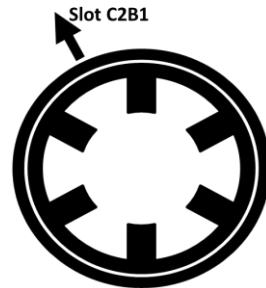
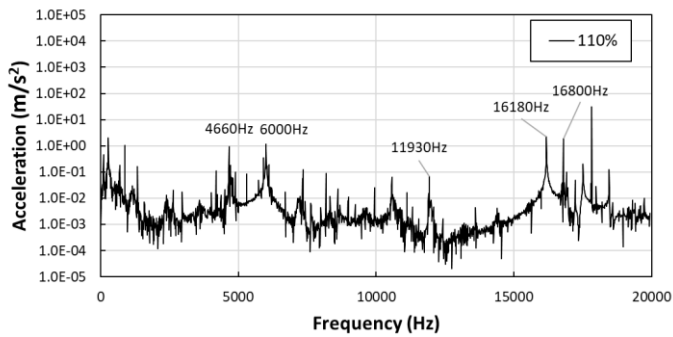


(d)

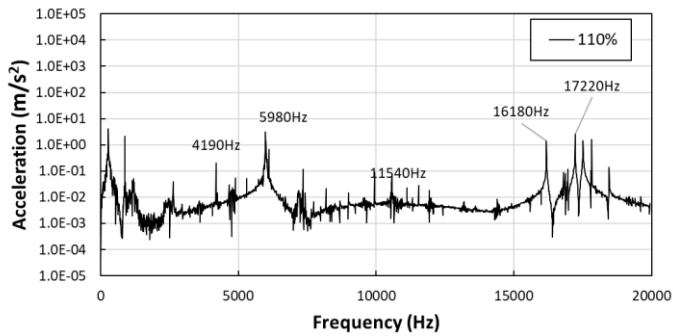
Fig. 5.18 Vibration response for simulated model with 110% DC amplitude, referenced to the baseline current profile, simulated output on the casing behind teeth (a) A1, (b) C2, (c) B1, (d) A2.



(a)

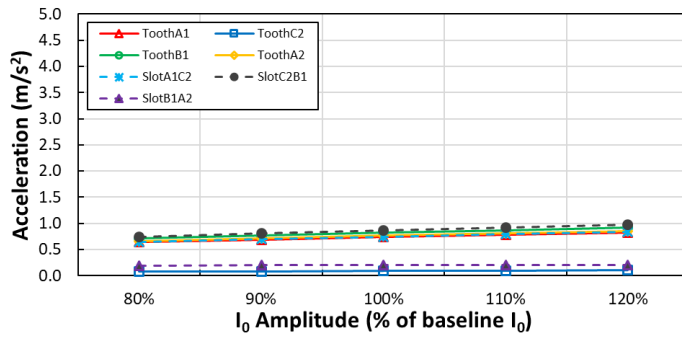


(b)

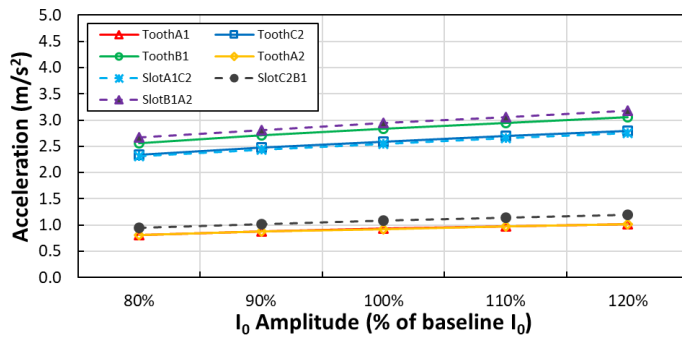
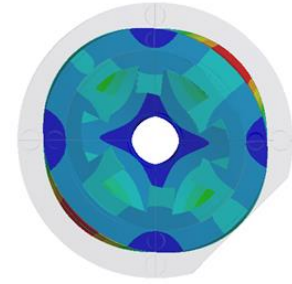


(c)

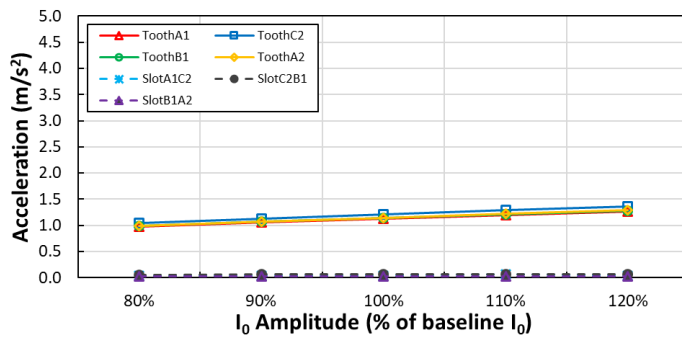
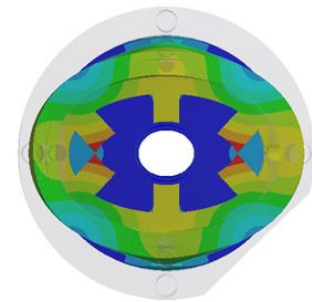
Fig. 5.19 Vibration response for simulated model with 110% DC amplitude, referenced to the baseline profile, simulated output on the casing behind slots (a) A1C2 (b) C2B1 and (c) B1A2.



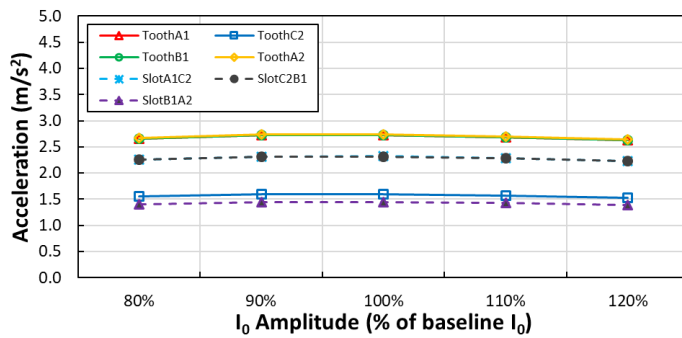
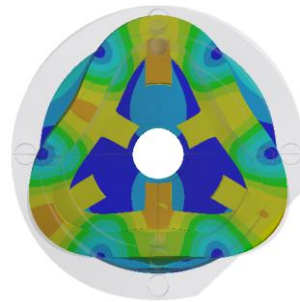
(a) Mode (0, 2a)



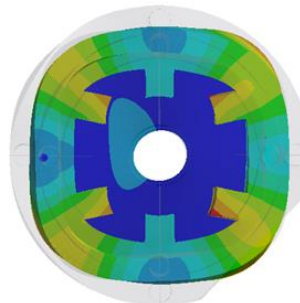
(b) Mode (0, 2b)

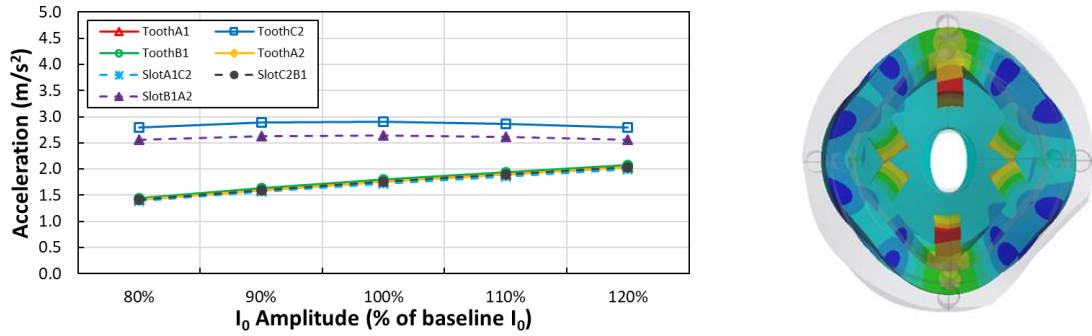


(c) Mode (0, 3b)



(d) Mode (0, 4a)



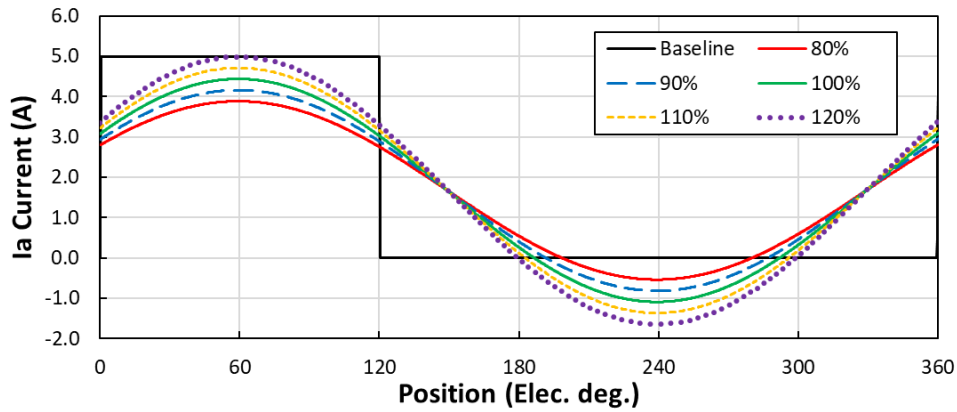


(e) Mode (0, 4b)

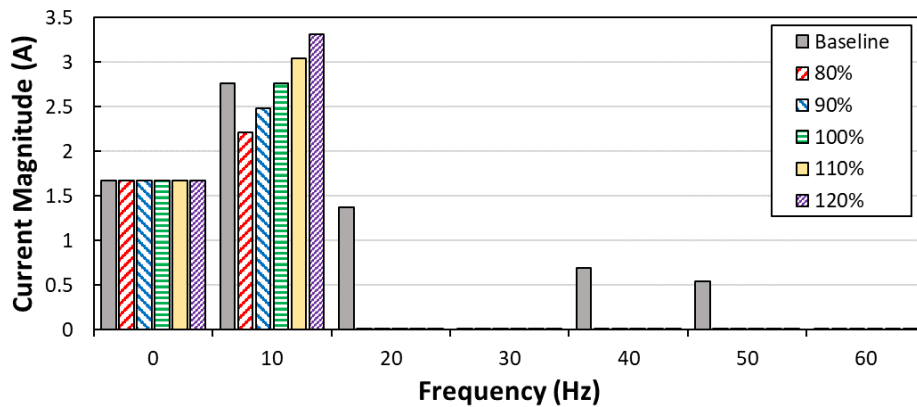
Fig. 5.20 Vibration response to harmonic force loads applied on stator teeth surface, shown for significant mode shapes (a) to (e).

5.4 Influence of 1st current harmonic amplitude

Having considered the influence of the DC current under the condition of DC + 1st current harmonic, equivalent to the variable flux machine (VFRM), the influence of 1st harmonic amplitude must next be investigated. Through finding the influence of these two factors it is possible to consider a current profile for the VFRM with capabilities to optimise torque with minimal vibration characteristics. The DC current harmonic is defined by the Fourier transform of the baseline unipolar square wave. The 1st current harmonic, or AC current, is also defined by the Fourier transform, then varied between 80% and 120% of this value in order to analyse the influence. The phase of each harmonic is kept constant and defined by the unipolar square wave decomposition. Hence, by keeping the phase shift of each harmonic equal to that of the baseline current profile, it is solely the influence of the 1st harmonic that is analysed. As can be seen from **Fig. 5.21** the region of negative current increases with increased 1st harmonic component, and additionally, the peak current is equal for 120% 1st current harmonic amplitude.



(a)

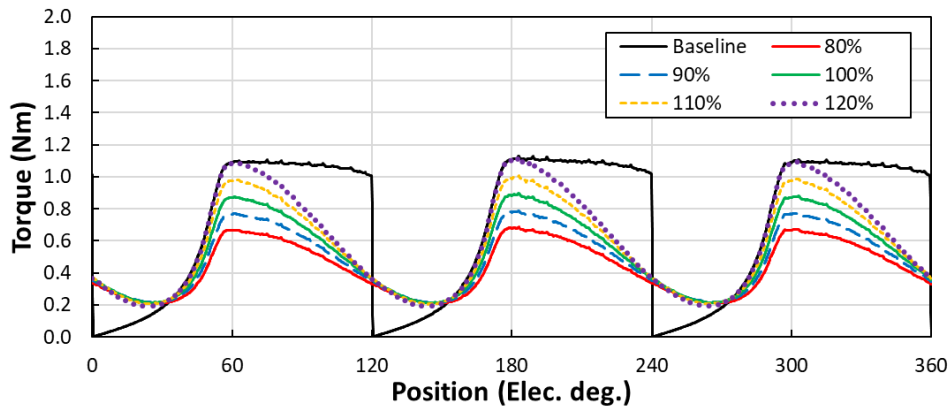


(b)

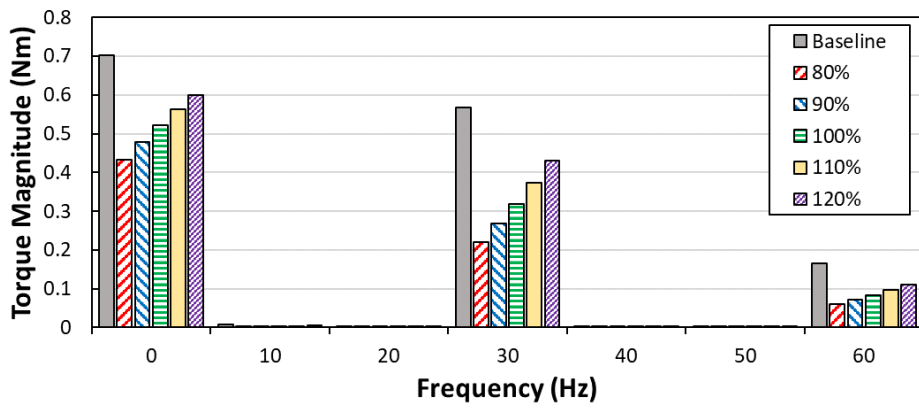
Fig. 5.21 (a) Variation in phase current illustrated for phase A only with increasing 1st current harmonic, (b) harmonic components up to 60Hz based on 150rpm operating speed.

5.4.1 Electromagnetic results

The torque profile produced across one electrical period is simulated under 3 phase excitations for the varied current profiles introduced in **Fig. 5.21**. It can be seen that for the case of 120% 1st current harmonic amplitude, the torque profile from 0° to 60° electrical follows the baseline torque profile. This is the period in which the rotor and stator poles are transitioning from the fully unaligned position and coming into a period of alignment. In other words, the two poles begin to overlap resulting in increased flux crossing the air gap. As the poles are unaligned and overlap is still low, the tooth tips are saturated under both excitation conditions, the baseline square wave and increased 120% of the 1st harmonic component. Due to the nature of the current profile of DC + 1st harmonic, the VFRM current excitation, the torque is reduced in the period of overlap between stator and rotor poles, this is the period of maximum torque in baseline simulation. As the 1st current harmonic component is increased, the average torque increases proportionally. Despite the increased 1st current harmonic, the average torque is still higher under unipolar square wave control as a conventional SR machine.

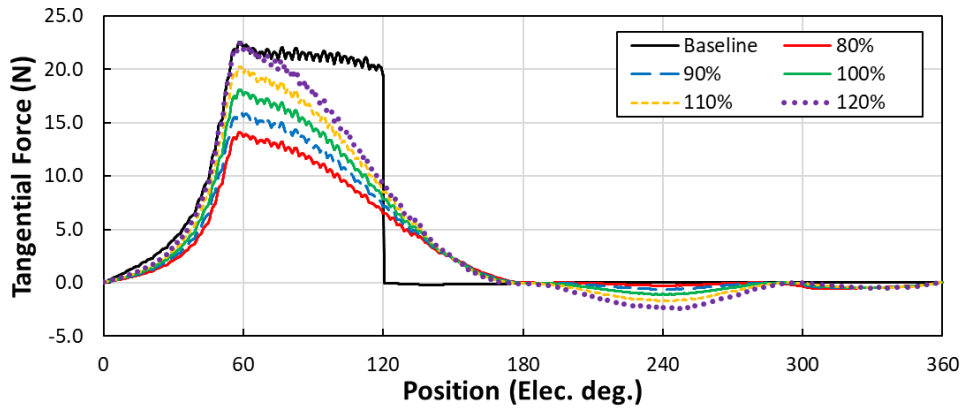


(a)

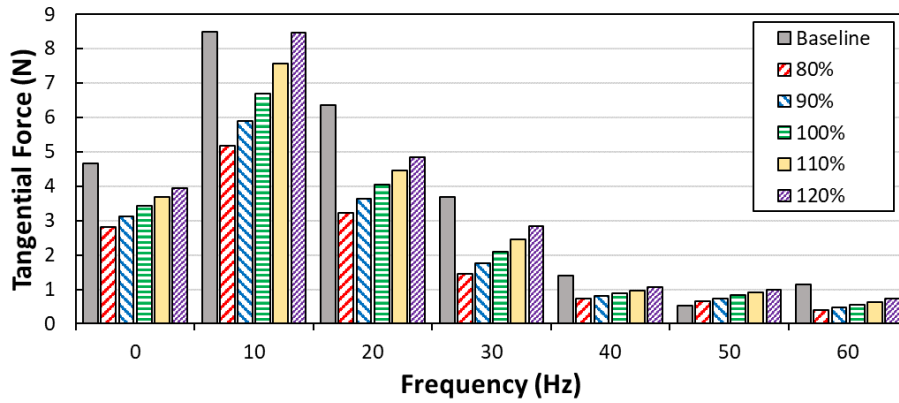


(b)

Fig. 5.22 (a) Torque profile variation for increasing 1st current harmonic, (b) harmonic components up to 60Hz based on 150rpm operating speed.



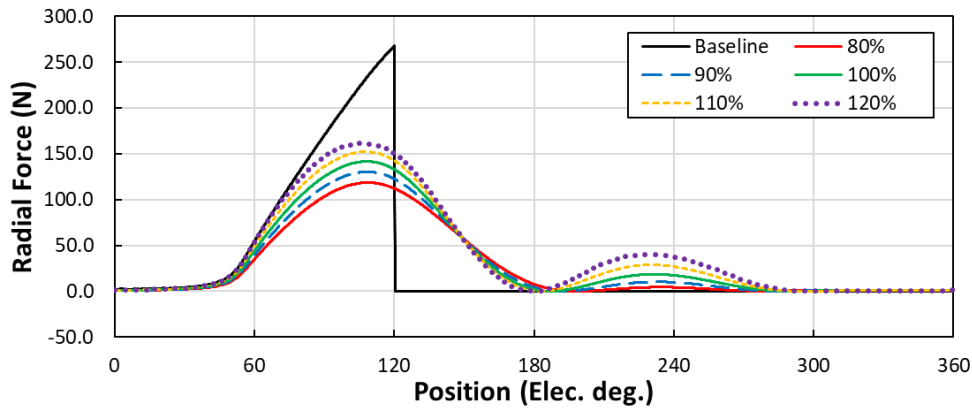
(a)



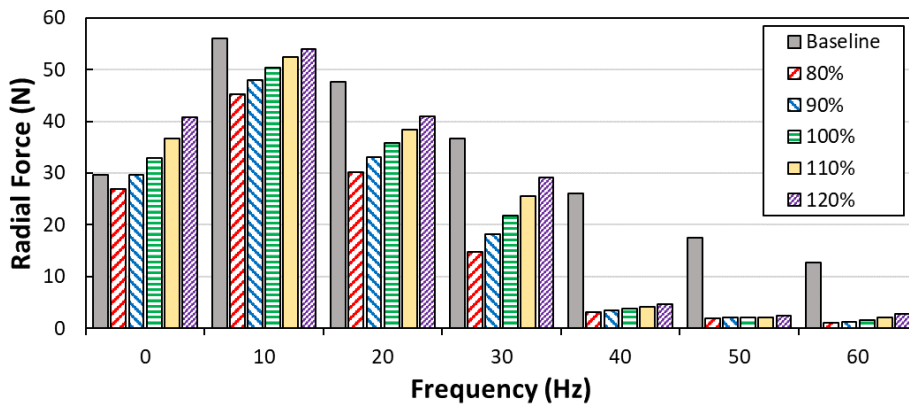
(b)

Fig. 5.23 (a) Tangential force calculated across one stator pole pitch, (b) harmonic content of tangential forces.

The turn-on period of tangential force matches the 3 phase torque profile, the tangential force is closely related to single phase torque. As evident from **Fig. 5.23** the bipolar current introduces a negative tangential force acting in the second half of the electrical cycle. The negative tangential force occurs in a region of torque generation for other phases, and this will detract from the overall torque production. As is observed in the torque production of VFRMs, the 1st current harmonic is proportional to the average torque. Therefore, this can also be applied to the tangential forces, and the tangential force is also proportional to the 1st current harmonic. The decay in tangential force increases as the 1st harmonic component is increased. It is noted that the increase in 1st current harmonic or AC current correlates to a rise in copper losses also. Furthermore, the increase in copper loss produced from the boosted DC and 1st harmonics may cause thermal management issues. Particularly for the DC component, considering the excitation as a permanent flow of current the temperature rise will be significant without suitable cooling techniques.



(a)



(b)

Fig. 5.24 (a) Radial forces simulated in the air gap across one stator pole pitch, (b) harmonic components up to 60Hz based on 150rpm operating speed.

The trend for increased 1st current harmonic amplitude is similar to that of increased DC amplitude. The peak radial force increases, although this trend is not linear. As the 1st current harmonic amplitude is gradually increased, the increase in peak radial force becomes smaller. This is attributed to the increased saturation in the stator as the phase current is increased, and hence, a saturation in the radial force also. From the perspective of radial force harmonics, there is significant variance in the average radial force and the radial force harmonics up to the 3rd harmonic. Beyond the 3rd harmonic component at 30Hz there is little to no change in low order radial force harmonics. Each of these harmonics has the potential to excite mechanical resonances of the machine, particularly if operated at significantly higher speeds. Therefore, minimal excitation of these harmonics or minimising these harmonics is desirable to reduce the mechanical resonance influencing vibration response. It is also seen from **Fig. 5.24** that the radial force profile, for all variations in I_1 amplitude, decays to zero before a minor rise outside of the excitation period of the relevant phase. Due to the decay to zero, as the peak radial force increases, the radial force ripple is also seen to increase at the same rate. The differential of the radial force profile provides an indication into the rate of change in radial force. The peak rate of change in F_{rad} is significantly lower than the baseline due to the ‘ideal’ nature of current excitation in the baseline current

profile. As the percentage of baseline 1st current harmonic is increased, the rate of change in radial force also increases. However, due to the sinusoidal nature of excitation forces under this control, the changes in radial forces are gradual. This significantly reduces the harshness of the vibration response based on the linear mass spring damper system, acting as a damping effect on the stator.

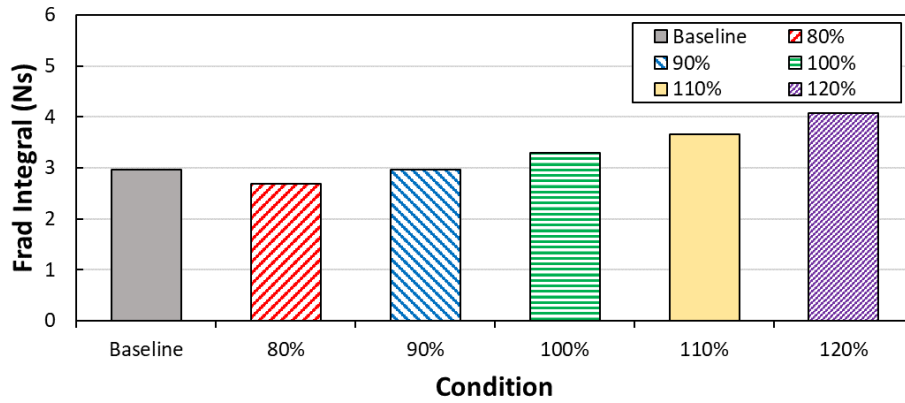


Fig. 5.25 Integral of radial force across 1 electrical period comparing influence of 1st current component.

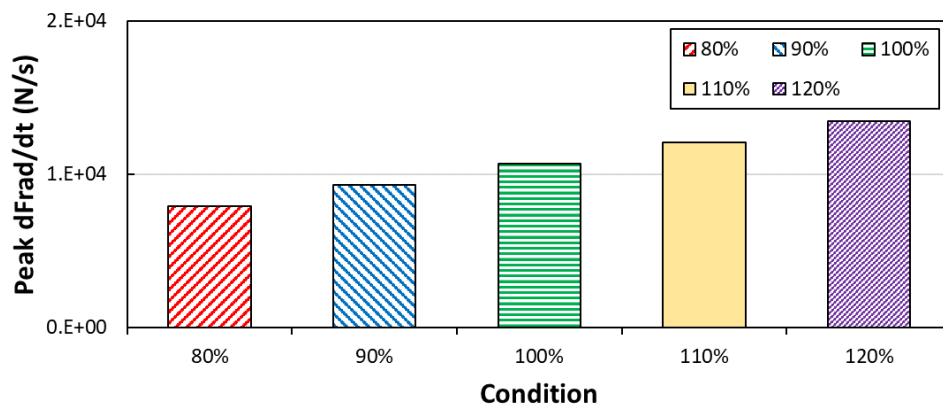


Fig. 5.26 Peak rate of change in radial force profile for increasing 1st current harmonic.

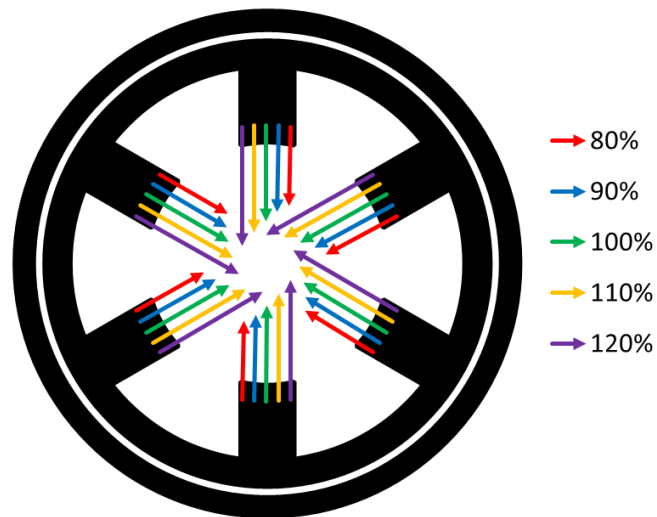


Fig. 5.27 Fundamental components of radial force on each pole, showing variance in magnitude of harmonic forces due to increased 1st current harmonic.

5.4.2 Vibration response

Firstly, the vibration spectra at each location is compared for a selected load condition, providing an indication of which modes are excited and an approximation of their dominance in the spectra. As with variance in DC current component, the reintroduction of mode (0, 3b) behind teeth is observed. This is a feature of the mutual excitation of phases, in comparison to the independent excitation for the conventional control of the SRM. It can also be observed to a lesser degree that the asymmetric mode (0, 3a) is also found for response measured behind the slots. This mode is less commonly found in these analyses and is of lower amplitude than dominant modes such as (0, 2b), and hence, may be neglected in further analysis. However, it is noted that for a larger machine with lower natural frequencies, it is advisable to avoid resonance with this mode shape also.

The trends in vibration response for each mode, against variation in 1st current harmonic amplitude, indicate a larger increase in acceleration than observed for the increase in DC component. The maximum vibration response for increased DC current amplitude is approximately 3.05mm/s² for mode (0, 2b). Under increased 1st current harmonic, this level of response occurs in mode (0, 4b) and is exceeded in mode (0, 2b). It is also noted that the amplitude of vibration response increases across all eigenmodes selected. However, this increase can be considered as minor in comparison to the level of vibration response found under unipolar square wave operation.

It can be concluded in this section that the influence of amplitude of the DC and 1st current components on vibration response is similar, and significantly reduced in comparison to the baseline 'ideal' SR operation. For an equivalent percentage increase in 1st current harmonic the vibration response is higher than that compared to DC component increase, although not significantly. It is worth considering the impact of DC:AC ratio for this configuration, operating as a VFRM. Further to this, the values of DC and 1st current harmonic may also be varied to operate for maximum torque production.

The influence of harmonic phase shift is not analysed in this study, for DC + 1st current harmonic only this is expected to have a significant impact as it is equivalent to variance in initial position.

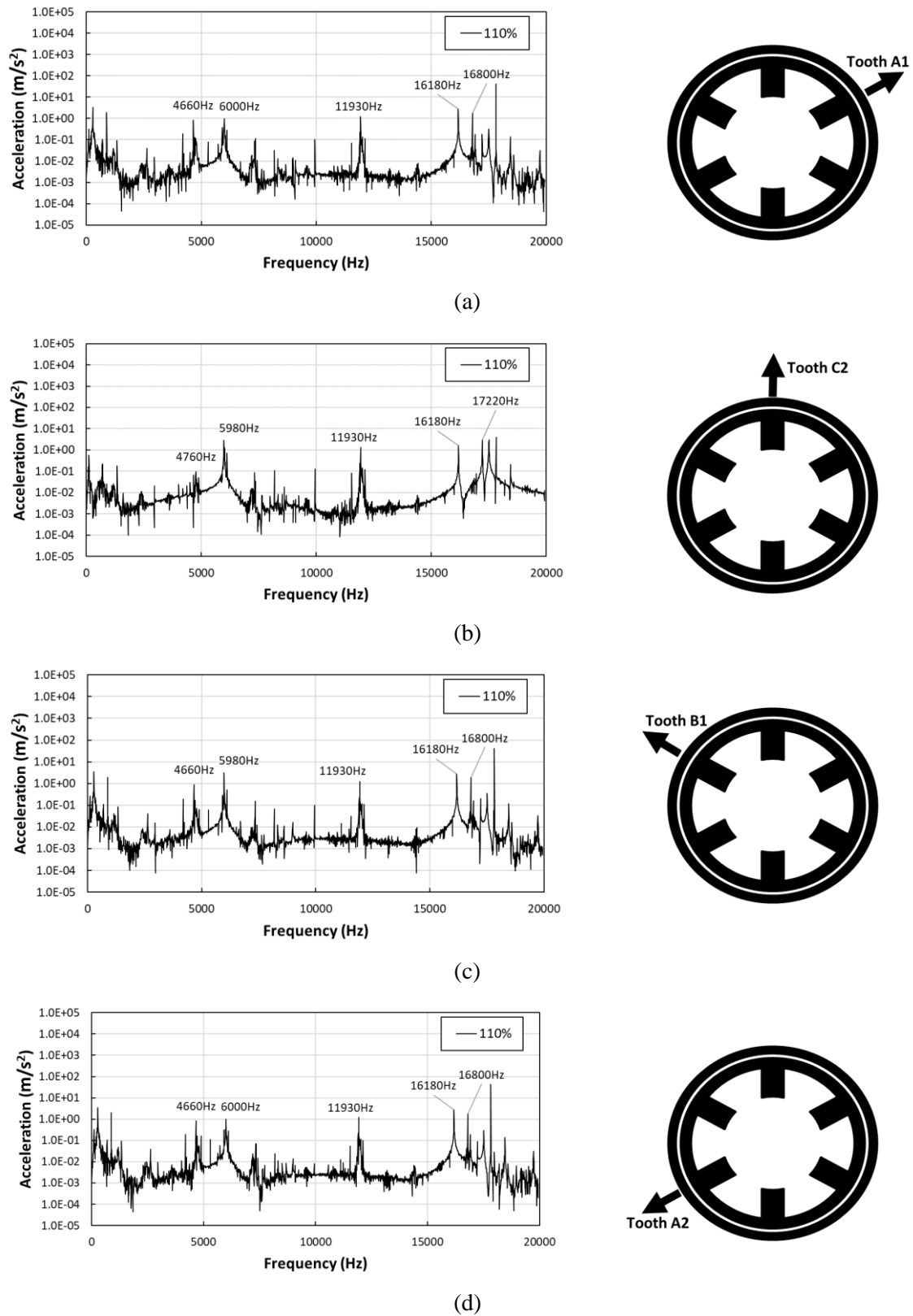
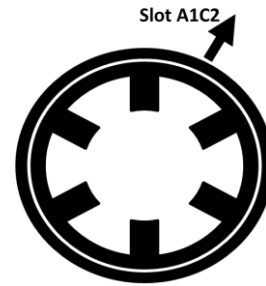
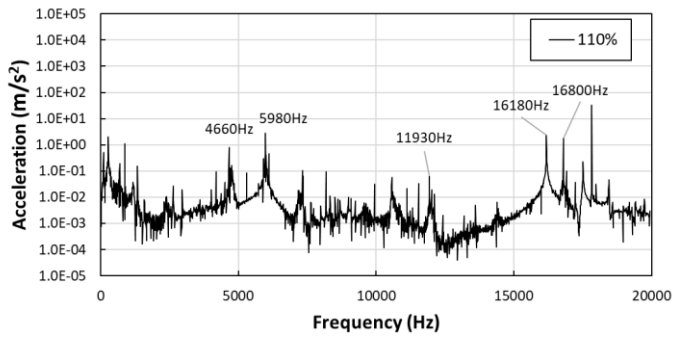
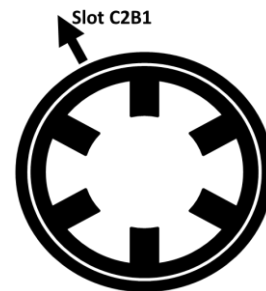
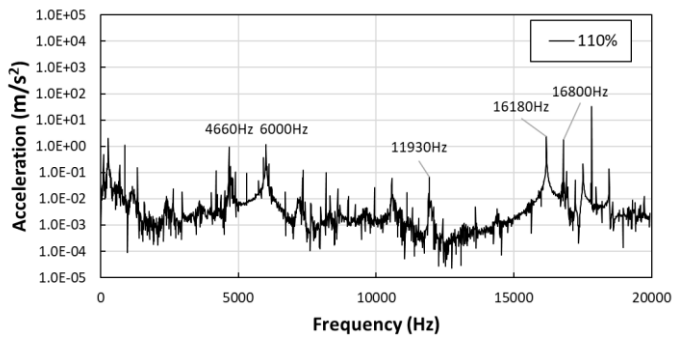


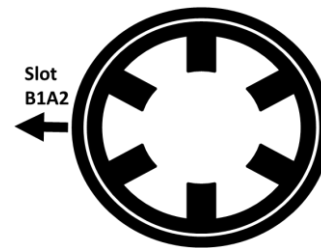
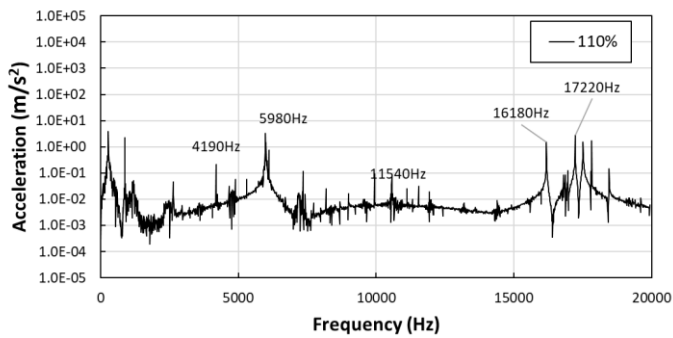
Fig. 5.28 Vibration response for 1st current harmonic equal to 110% amplitude of the baseline 1st harmonic, simulated output on the casing behind teeth (a) A1, (b) C2, (c) B1, (d) A2.



(a)

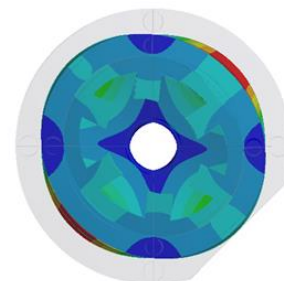
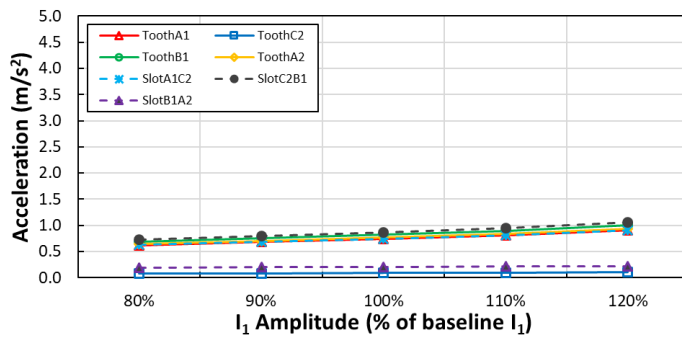


(b)

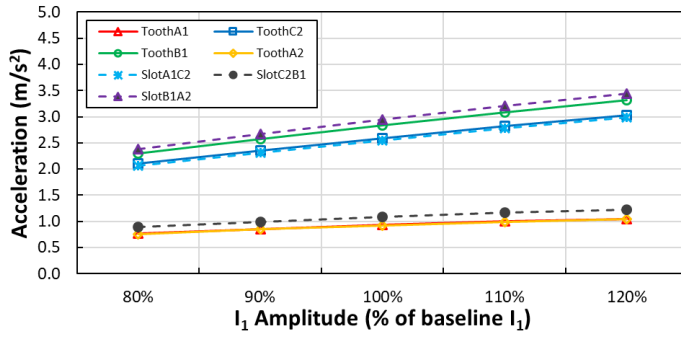


(c)

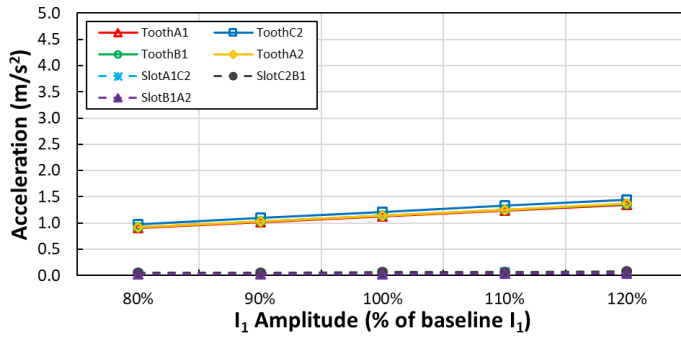
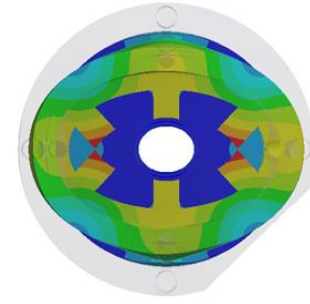
Fig. 5.29 Vibration for 1st current harmonic equal to 110% amplitude of the baseline 1st harmonic, simulated output on the casing behind slots (a) A1C2 (b) C2B1 and (c) B1A2.



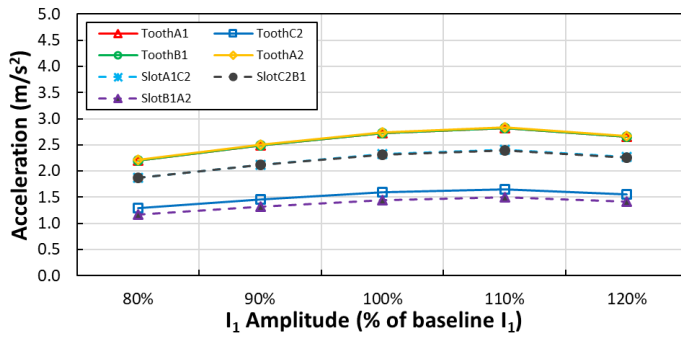
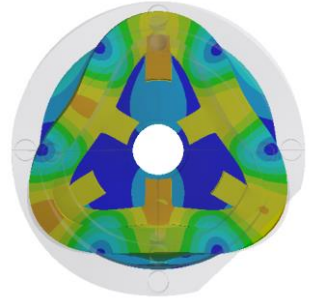
(a) Mode (0, 2a)



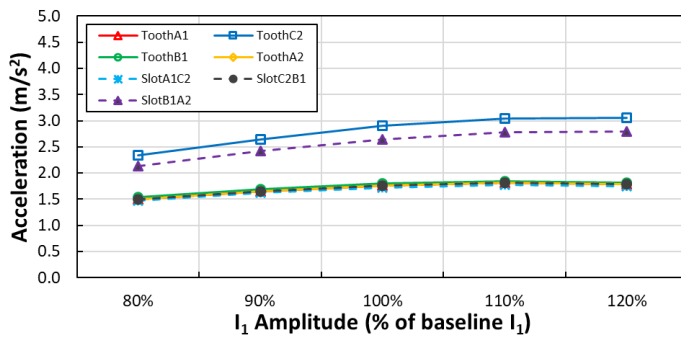
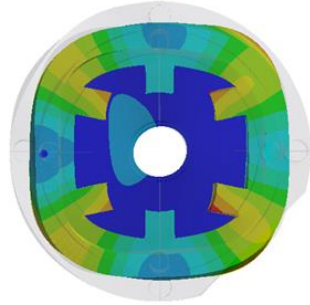
(b) Mode (0, 2b)



(c) Mode (0, 3a)



(d) Mode (0, 4a)



(e) Mode (0, 4b)

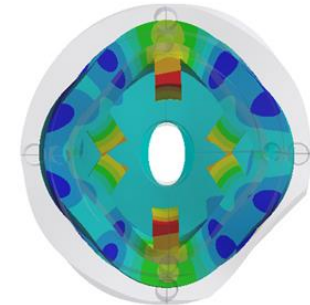
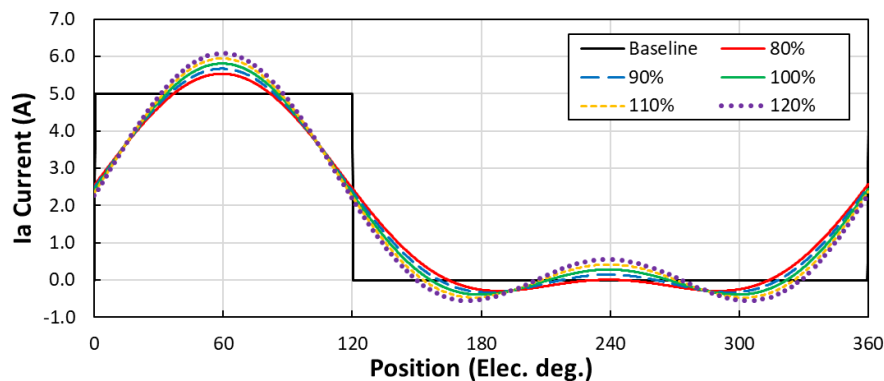


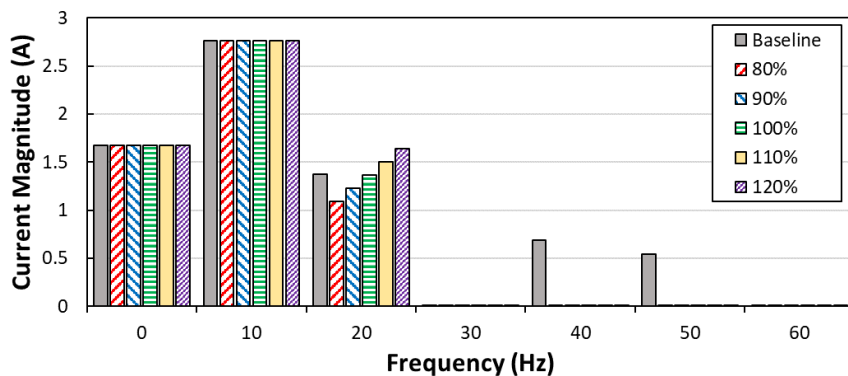
Fig. 5.30 Vibration response to harmonic force loads applied on stator teeth surface, shown for significant mode shapes (a) to (e).

5.5 Influence of second harmonic amplitude

Previous work on minimisation of acoustic noise and vibration in SRMs has involved the use of the second harmonic and third harmonic in order to influence the relevant harmonics of the radial force sum [Tak15], [Bay15], [Kur15a] and [Kur15b]. It is also shown by Lee et al [Lee17] that the torque production in SRMs is dominated by the DC, 1st and 2nd current harmonics. Furthermore, work on the inclusion of the 2nd harmonic for enhancing the variable flux reluctance machine is investigated in depth by Feng [Fen19]. Hence, it is important to analyse and investigate any influence the 2nd current harmonic may have on the performance and vibration response of SR machines. In order to achieve this, the same methodology as implemented with the DC and 1st current harmonic is employed. The phase shift of the 2nd harmonic is kept constant so as to match that of the baseline current profile. Then, the amplitude of the 2nd harmonic component is varied between 80% and 120% of the baseline 2nd harmonic current amplitude. As is evident in **Fig. 5.31**, the amplitude of the 2nd harmonic significantly affects the current during the typical SR conduction period. Furthermore, the 2nd harmonic inclusion reduces the negative amplitude of the current profile in the second half of the electrical cycle. The amplitudes of the DC and 1st current harmonic are set to be equal to the harmonic contents of the baseline.



(a)

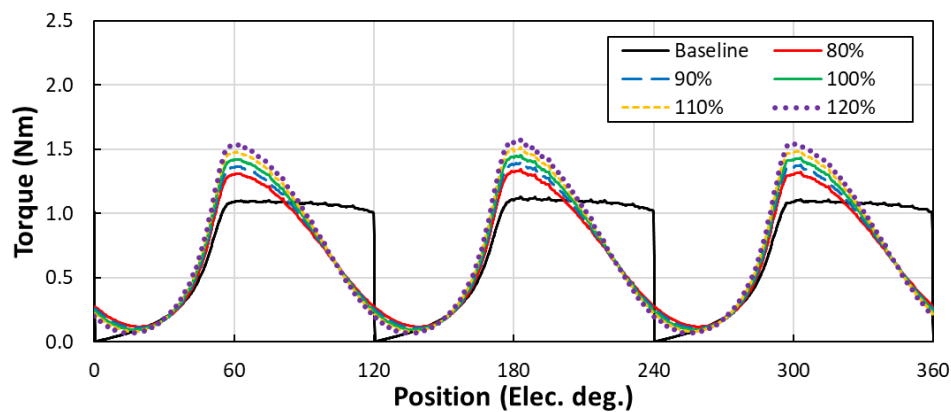


(b)

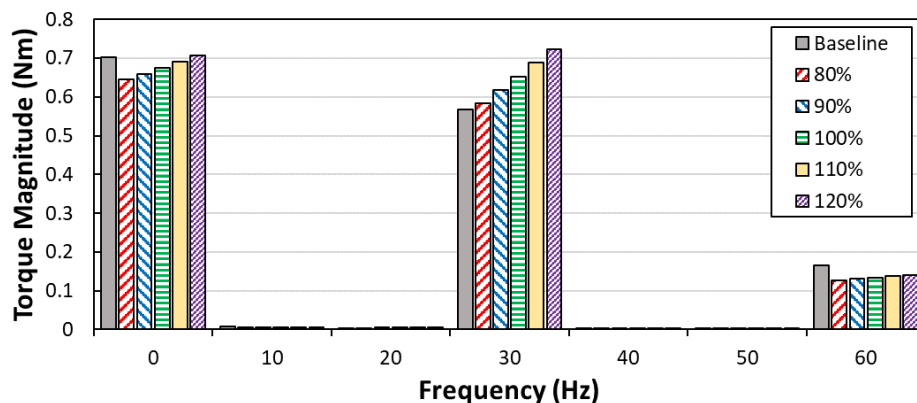
Fig. 5.31 (a) Variation in phase current illustrated for phase A only for increasing 2nd harmonic amplitude, (b) harmonic components up to 60Hz based on 150rpm operating speed.

5.5.1 Electromagnetic results

The peak torque is increased with the inclusion of the second harmonic. However, the resultant 3 phase torque also exhibits increased torque ripple in comparison to the VFRM control, where only the DC and 1st current harmonic are utilised. Although the inclusion of a 2nd current harmonic increases the peak torque, the period of this maximum torque is momentary. The harmonic content of the 3 phase torque indicates that the average torque for the baseline SR profile is higher, with approximately equal average torque for 120% I_2 amplitude. Increasing the amplitude of the 2nd current harmonic influences the peak torque. However, the rest of the 3 phase torque profile is relatively unaffected. This is a result of the reduced negative period which occurs in the torque production period of the other phases, in this example the period around 240° electrical. Due to the reduced negative period, the resultant negative torque is reduced also and hence the impact on the final 3 phase torque is also minimal in this period. Introducing the additional 2nd order harmonic component into the current profile increases the maximum torque produced by the SR machine whilst also reducing the negative torque production interfering with adjacent phases.

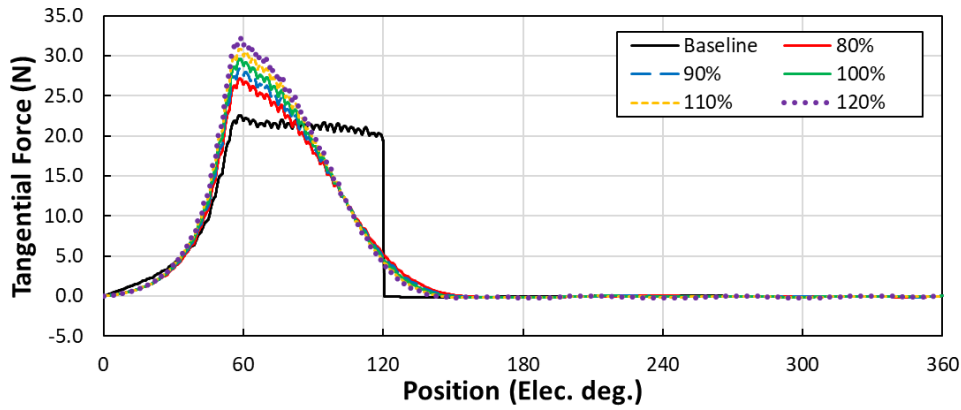


(a)

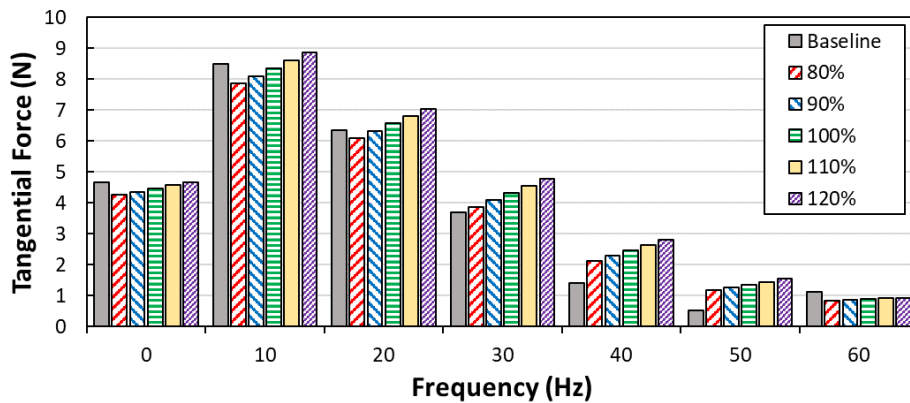


(b)

Fig. 5.32 (a) Torque profile under 3 phase operation for one electrical period, (b) harmonic components up to 60Hz based on 150rpm operating speed.



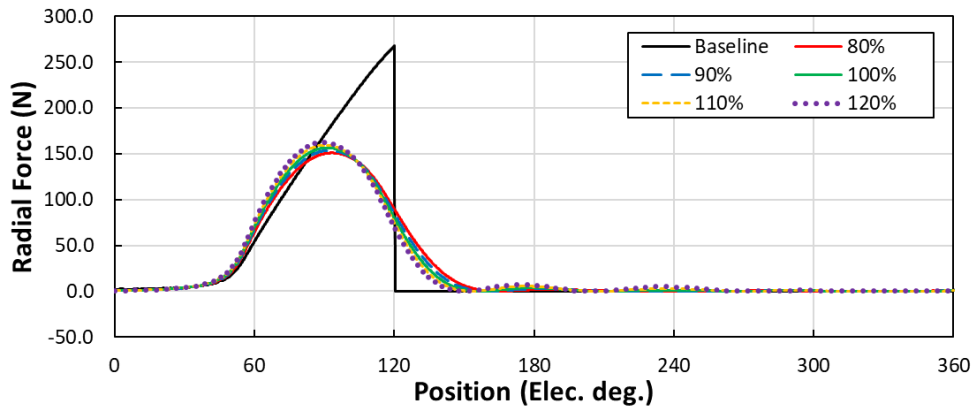
(a)



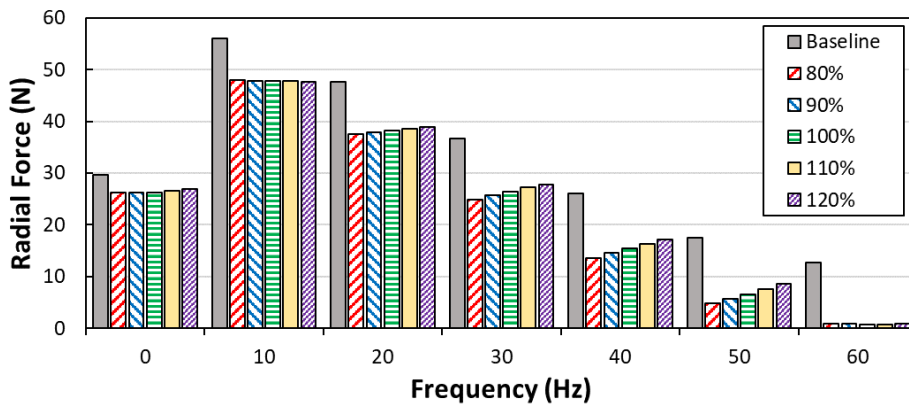
(b)

Fig. 5.33 (a) Tangential force profile calculated in the air gap across one stator pole pitch, (b) harmonic components up to 60Hz based on 150rpm operating speed.

As seen in the 3 phase torque profile, the 2nd order current harmonic is capable of significantly increasing the maximum tangential force. Analysing the tangential force for a single phase indicates that outside of the conventional 120° conduction period as used in the baseline waveform, the tangential forces and thus torque is negligible. This is an indication that the majority of the torque production is achieved with this harmonic composition. The increase in amplitude of I_2 produces an increase in all low order harmonics for the tangential force per stator tooth. The harmonic content of the baseline ‘ideal’ square wave used for replicating the SR performance is spread across a wider array of harmonics. It is possible to achieve a similar average tangential force, and thus torque also, by increasing the second harmonic but it should be noted that this will also result in increased copper losses. For future work, it is worth considering the impact of the phase of the 2nd harmonic of the current, this is touched upon in work by [Tak15]. For the 1st current harmonic, the phase can be equated to the initial position of the machine, and hence, will have a significant impact on all performance aspects of the SR machine. Conversely, the 2nd harmonic has a lesser impact and hence may be used to optimise torque and minimise the air gap forces also.



(a)



(b)

Fig. 5.34 (a) Radial force profile calculating on an arc in the air gap spanning one stator pole, (b) harmonic components up to 60Hz based on 150rpm operating speed.

The air gap radial force profile appears to be relatively unaffected by changes in amplitude of the 2nd current harmonic. Comparing the influence of the amplitude of 2nd harmonic of current against the equivalent variations in DC and 1st harmonic components, the resultant profile experiences less change. Considering the current profile for the 2nd harmonic inclusion, the peak radial force occurs at a point of considerable saturation as the stator and rotor poles come into alignment. Hence, the radial forces are already close to saturation for this period of rotation. Therefore, a slight increase in the amplitude of excitation in this period has a diminished effect on the radial forces experienced by the stator. This result is echoed in the harmonic content of the radial force profile. The fundamental and 2nd harmonic of the radial force are relatively unchanged, and these are the components that will have the most significant influence on the radial forces. It is noted that for some harmonics in the low order spectrum of radial force, there is an increase in amplitude as the amplitude of the 2nd current is also increased. However, these are considered to be negligible in comparison to the fundamental and 2nd order radial force harmonics.

The change in momentum, or integral of radial force, across 1 electrical period is considerably lower under excitation including the 2nd order current harmonic, compared to the baseline SR waveform. As the level of 2nd harmonic current is increased, the change in momentum increases also. However, this is negligible for low amplitudes of I_2 , and more significant once the amplitude is increased. The peak change in radial force varies slightly when increasing the amplitude of I_2 . The change is noticeable due to the slight increase in peak radial force and shorter decay time, resulting in a sharper drop. Furthermore, the peak gradient of slope is significantly lower than the baseline, and hence, it is expected that the vibration response will also be significantly reduced.

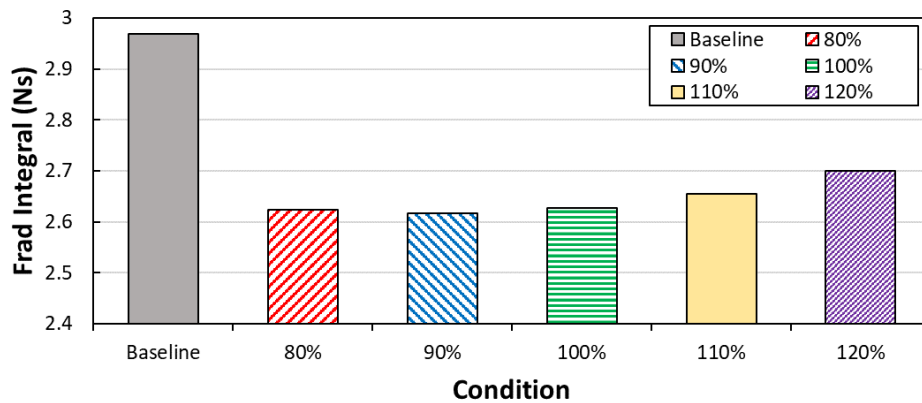


Fig. 5.35 Integral of radial force across 1 electrical period comparing influence of 2nd current harmonic.

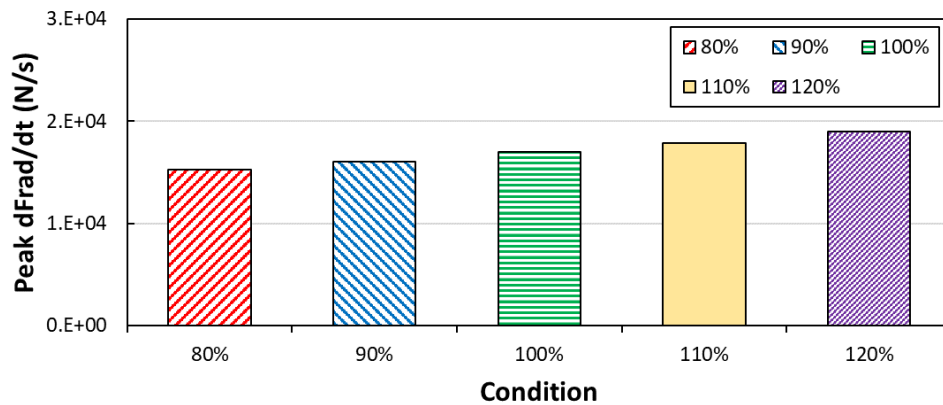


Fig. 5.36 Peak rate of change in radial force across one electrical period.

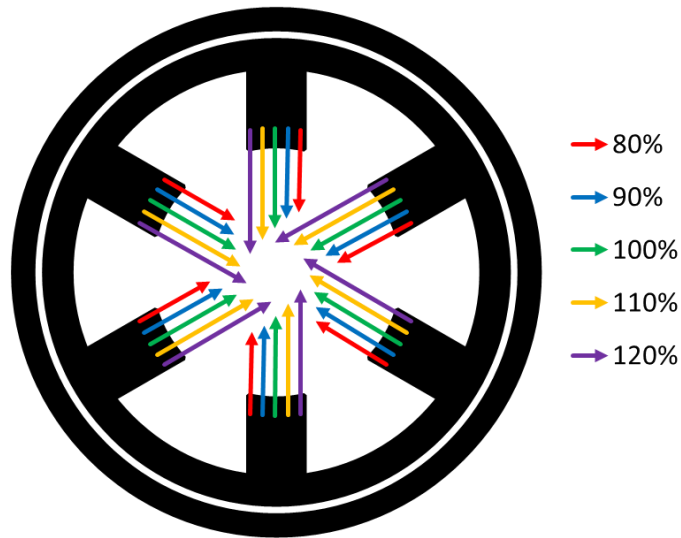
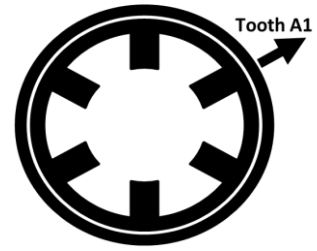
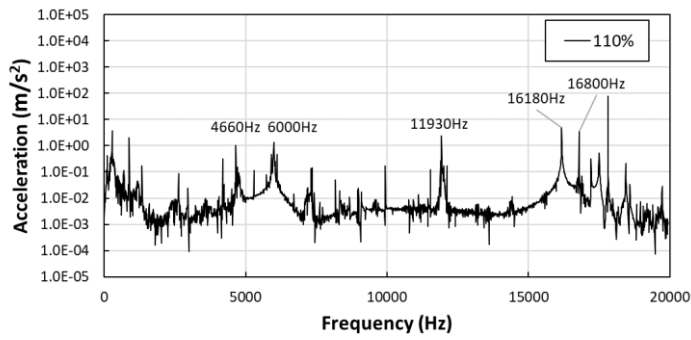


Fig. 5.37 Fundamental components of radial force on each pole, showing variance in magnitude of harmonic forces due to varied 2nd current harmonic amplitude.

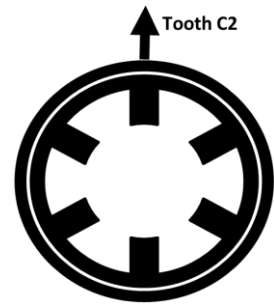
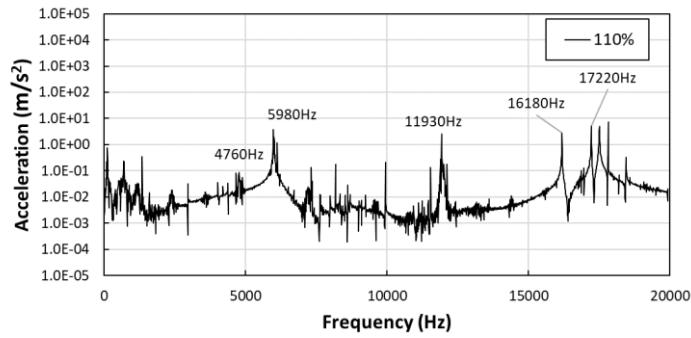
5.5.2 Vibration response

The introduction of the 2nd current harmonic significantly influences the peak current and the rate of change in current and radial force, in comparison to the operation of DC + 1st current harmonic only. Therefore, it follows that the level of vibration response shall be higher, although significantly lower than the baseline unipolar square wave excitation. The vibration response behind each tooth indicates that the mode (0, 3b) excitation is clearly excited at all locations under the excitation conditions presented, whilst mode (0, 3a) is apparent behind slots only. The vibration response as a whole is higher than the vibration response under DC + 1st current harmonic, due to the additional current injection into the windings. Thus, the flux crossing the air gap is increased and the radial forces are increased, resulting in higher deformation of the stator and increased vibration response. Similar vibration response at bolted locations is observed, where the dominant mode shape (0, 2b) is enhanced and mode shape (0, 2a) is no longer apparent.

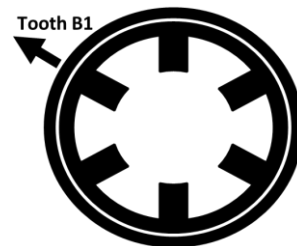
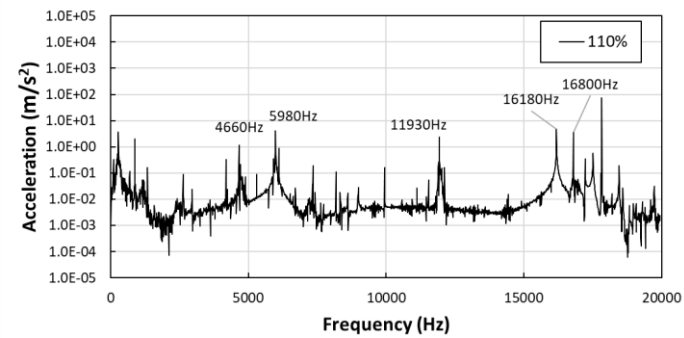
From the analysis of trends in modes, it is clear that the amplitude of vibration response is higher across all variants of 2nd harmonic current injection, compared to DC + 1st harmonic. The influence of 2nd harmonic amplitude on higher order mode shapes, (0, 4a) and (0, 4b), is most significant. These mode shapes experience the largest increase in amplitude for the percentage increase in I_2 amplitude. However, comparatively to the changes observed for increases in DC or 1st harmonic, the influence is minor. It can be considered that for mode (0, 2a) there is no influence. Given the work on influence of the 2nd harmonic on radial sum by [Tak15], the amplitude must be varied in conjunction with the phase of the harmonic component also. It can also be said that increasing the 2nd harmonic has minimal effect on noise and vibration. Hence, maximising the torque production with 2nd harmonic injection is achievable for minimal impact on the acoustic noise and vibration performance.



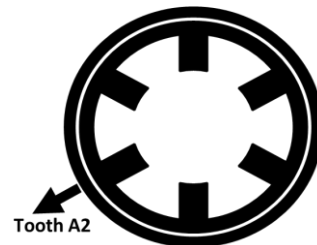
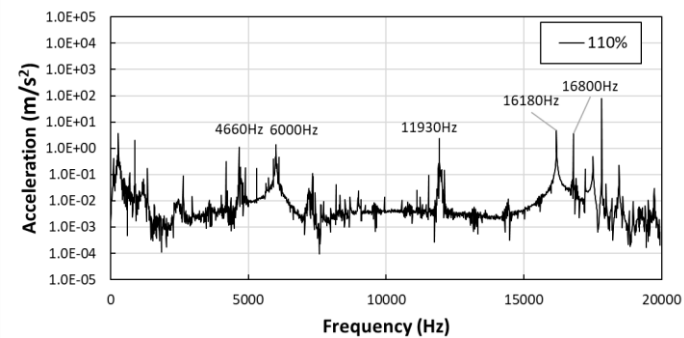
(a)



(b)

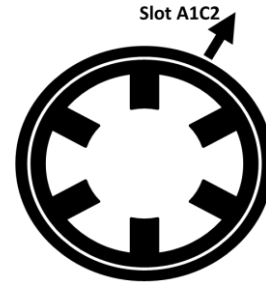
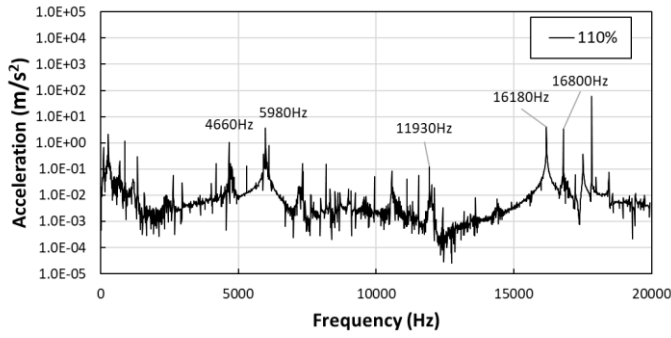


(c)

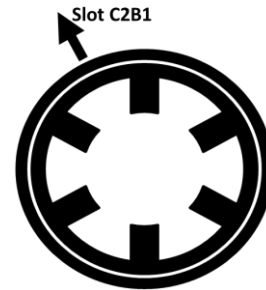
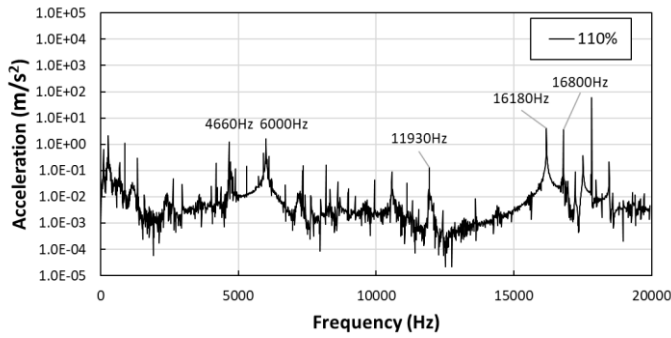


(d)

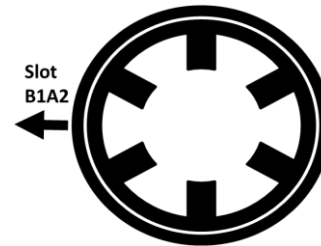
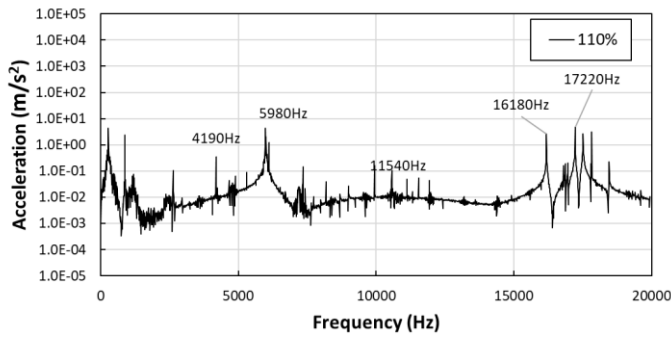
Fig. 5.38 Vibration response for 2nd current harmonic component equal to 110% of the baseline 2nd harmonic, simulated output on the casing behind teeth (a) A1, (b) C2, (c) B1, (d) A2.



(a)

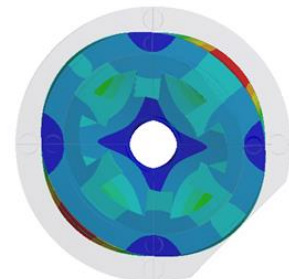
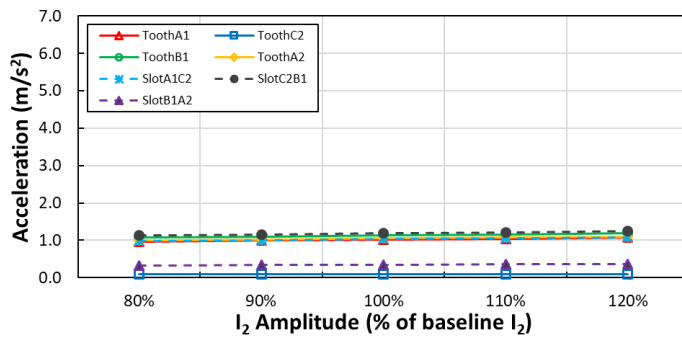


(b)

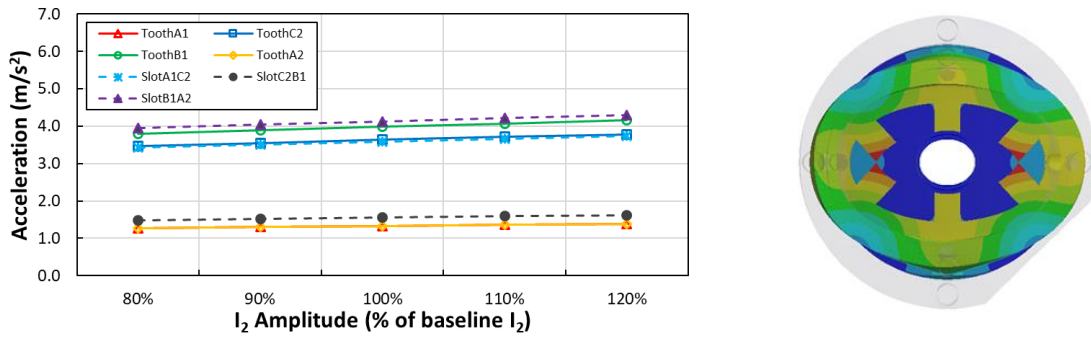


(c)

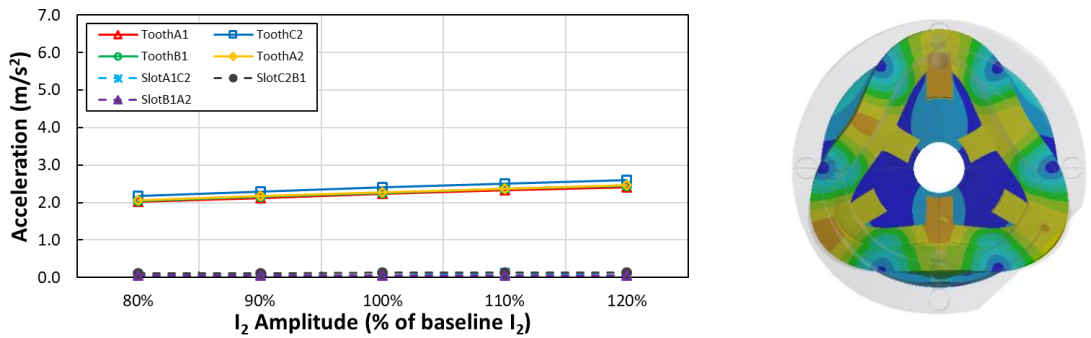
Fig. 5.39 Vibration response for 2nd current harmonic component equal to 110% of the baseline 2nd harmonic, simulated output on the casing behind slots (a) A1C2 (b) C2B1 and (c) B1A2.



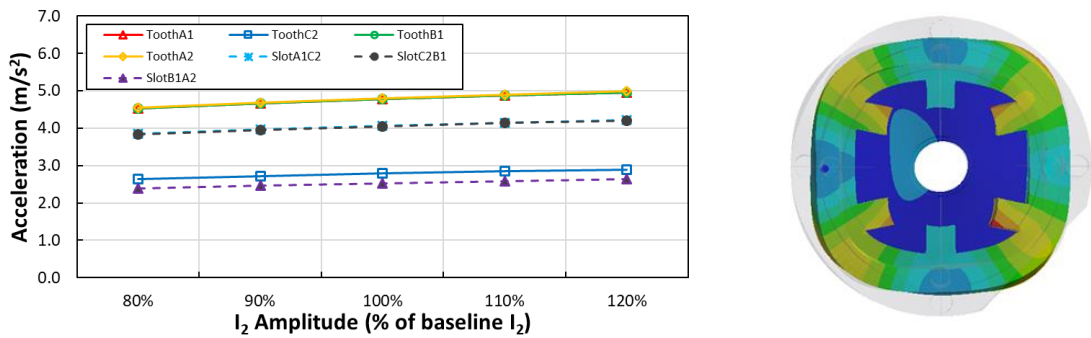
(a) Mode (0, 2a)



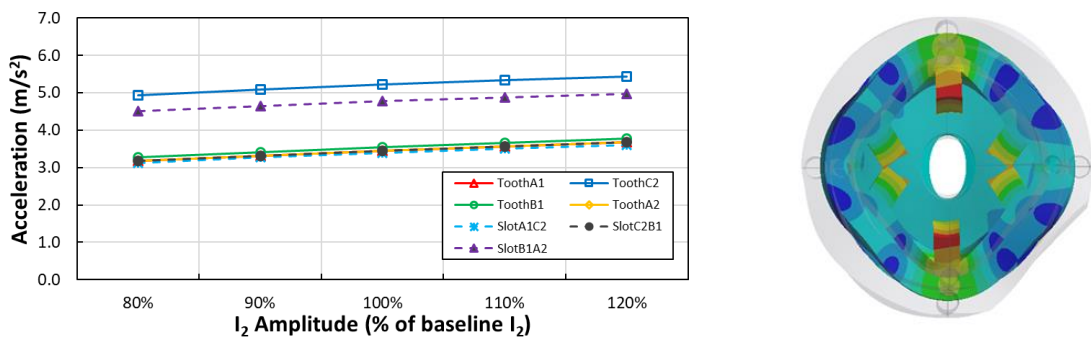
(b) Mode (0, 2b)



(c) Mode (0, 3a)



(d) Mode (0, 4a)



(e) Mode (0, 4b)

Fig. 5.40 Vibration response to harmonic force loads applied on stator teeth surface, shown for significant mode shapes (a) to (e).

5.6 Summary

This chapter seeks to analyse and investigate the influence of current profiling from the perspective of frequency domain. The baseline for all comparisons and analysis is established previously as the ‘ideal’ unipolar square wave with a conduction angle of 120° electrical. The harmonic composition of the baseline current excitation is found via the Fourier series expansion, providing a series of consecutive current harmonics that sum to produce the baseline waveform. In order to investigate the significance of each harmonic component, the baseline current profile is rebuilt from the harmonic components. The amplitude and phase of each harmonic component is determined by the content of the baseline, so as to form a fair comparison. After the current profiles are defined, the electromagnetic performance is analysed for each. It is determined that the average torque and torque ripple are both reduced for lower order harmonic inclusion, as the number of harmonic components is increased the electromagnetic performance nears that of the baseline. It is noted that the copper losses are not equal under these conditions. The vibration response is significantly improved in comparison to the baseline, this is attributed to the reduction in gradient of radial force decay. Considering a current profile including all harmonics up to the 31st harmonic still results in a vibration response that is significantly reduced. Under low order harmonic inclusions, mode (0, 3b) is reintroduced into the vibration spectra, as a result of the mutual excitation of phases.

The use of a DC current component and 1st current harmonic has previously been developed into a variable flux machine, with a focus on improving torque production. The control strategy also significantly reduces the acoustic noise and vibration when compared to an SR machine under unipolar square wave control. The influence on vibration response of both DC current amplitude and the 1st current harmonic amplitude are analysed individually. The harmonic components are varied between 80% and 120% of the baseline harmonic content. It is found that the increasing the amplitude of each harmonic corresponds to an increase in vibration response also. Increasing the 1st current harmonic causes a larger increase in vibration comparatively, although still a minor change compared to the baseline established.

Conversely, the amplitude of 2nd harmonic has minimal effect on noise and vibration. It is shown that the dominant current harmonics in torque production are the DC, the 1st and the 2nd, and hence, it is important to consider any influence the 2nd harmonic may have on vibration response. Concluding that the 2nd current harmonic amplitude has minimal to no effect on the vibration response, it must be investigated further. Specifically, the phase of the harmonic components, as this has been shown to be a suitable method to manipulate the radial force sum and thus reduce acoustic noise and vibration. Furthermore, it is concluded from the results and analyses presented that the inclusion and amplitude of low order harmonics can be optimised for torque production, whilst causing minimal increase in the vibration response of the SR machine.

Chapter 6 General Conclusions

In this thesis, an extensive FE modelling process is systematically performed in order to develop a complex 3D mechanical model which matches the structural behaviours of the experimental SR prototype. The SR machine is modelled at multiple stages of construction, from a laminated annular ring, to unwound stator, all the way through to the final mounted prototype. Modal analysis is carried out to identify the natural modes of the stator and the frequencies which produce the highest levels of acoustic noise and vibration in SR machines due to resonance. Furthermore, the influence of endcaps is investigated, with particular attention to suitable modelling techniques in order to find a time efficient and accurate method for simulating the mechanical connection.

The mechanical modelling is initially performed and validated with static tests, in particular hammer impact testing. In order to justify the use of the FE model for trend analysis, it is verified under operating conditions. The experimental prototype is operated at 150rpm, with single pulse voltage control, and a number of parameters are varied to provide trends in amplitude of key modes. The parameters may be outlined as:

- Varied load current (peak);
- Fixed turn-off angle, varied turn-on angle;
- Fixed turn-on angle, varied turn-off angle.

It is shown that the FE simulations exhibit the same trends as found experimentally, and hence, the FE models are suitable for further current profiling analysis.

Given that one of the most notable and effective methods of noise reduction in SRMs is the use of active vibration cancellation (AVC) [Wu95], the influence of current profiling in the time domain is investigated. Utilising the 'ideal' unipolar square wave current profile established in Chapter 3, 2 key parameters are investigated by manipulating the current profile as a series of discrete points. Firstly, a continuous linear slope is introduced at turn-off, and the duration of this slope is increased. It is found that this significantly reduces vibration response compared to the baseline current waveform. Secondly, a step down in current is introduced before turn-off, in which the amplitude of the current drop is constant. The trend in amplitudes of dominant vibration modes indicates minimal change in vibration response as the step duration is increased.

The baseline unipolar square wave current profile is then manipulated in the frequency domain, by converting the current profile into a Fourier series of harmonic components. It is then possible to rebuild the baseline current profile by summing the current harmonics up to various harmonic orders. The vibration response is significantly reduced for low order harmonic inclusion. Given that the inclusion of the DC component and 1st current harmonic has been implemented successfully as a novel machine type, variable flux reluctance machines (VFRMs), the influence of these current components is

analysed. The amplitude of current harmonics is varied between 80% and 120% of the original baseline current profile. It is found that the vibration response is more susceptible to changes in the 1st current harmonic. Furthermore, the inclusion of the 2nd current harmonic in VFRMs is shown to improve torque production [Fen19], and hence, its influence on vibration response is investigated. The amplitude of the 2nd current harmonic component is found to have minimal effect on the radial force and vibration response, although it is noted that in the case investigated the phase is kept constant.

6.1 Modelling of SR machine

Through systematic assembly of the electrical machine, the natural frequencies of the SRM are found and verified experimentally with multiple hammer tests. The assembly of the machine is approached in the following steps:

- Laminated annular ring;
- Laminated unwound stator;
- Stator and housing frame;
- Addition of endcaps;
- Mounted prototype.

It has been shown that at each stage of the modelling and assembly process, the natural frequencies and damping ratio of the system are heavily influenced. Particularly, the addition of teeth onto the annular ring introduce geometric asymmetries, and thus, introducing dual natural frequencies for some mode shapes. In the case of a 6-pole-stator investigated, a dual mode of order 3 is introduced. However, it is then shown that for equal and opposite forces acting on teeth, the influence of mode 3 shapes is negated by the geometry. Furthermore, this replicates the operation of the machine in which opposite stator poles are of the same phase, and hence, mode 3 is not observed in the vibration spectra during conventional operation.

The addition of the stator housing is shown to increase the natural frequencies in all modes, such that only modes of radial order 2, 3a, 3b and 4 exist within the audible frequency range. Next, the influence of endcaps on the natural frequencies of the SRM is investigated. To successfully model the connection of endcaps to housing, a variety of boundary conditions and connection types are investigated. It is shown that the optimal method comprises of a ‘perfect’ bonding condition applied to an area equivalent to the active area of the bolt. Furthermore, for the 6s/4r SR machine investigated the influence of the bolts is significant. The bolted locations are equally spaced around the housing separated by 90°, located behind two teeth and two slots in the 6s/4r SR prototype. Consequently, the locations of these bolts significantly amplifies the mode of order 2, providing additional mass at the locations and stiffening the structure. Furthermore, the amplification of mode shapes 2 and 4 behind bolted locations introduces asymmetry into the electrical machine, and hence, dual modes of mode

shape of orders 2 and 4 are seen. This phenomenon is confirmed and verified by experimental modal analysis.

6.2 Time domain investigation

In order to verify the FE model for vibration analysis, the 6s/4r SR prototype is simulated for various load conditions and switching angles. Firstly, the influence of peak load current is investigated with a conduction angle of 120° electrical. Utilising a unipolar square wave current profile with instantaneous turn-on and turn-off, the peak load current significantly increases the vibration response. The vibration response under operation shows that the dominant mode shape is mode (0, 2b). The increase in amplitude of the dominant mode due to increase in load current is proportional. Following this, the case of 5A load current is selected as a baseline, and the influence of switching angles is investigated allowing for focused current profiling to be implemented. Initially the turn-off angle is fixed, and the turn-on angle is varied by $\pm 30^\circ$ electrical. Subsequently, the inverse is investigated, the turn-on angle is fixed and the influence of turn-off angle is varied. It is shown from these analyses that variance in turn-on angle has minimal impact on the amplitude of dominant vibration modes, although influence at turn-off is more apparent. Verification of these results and trends is presented with experimental results, and thus, the baseline unipolar square wave current profile is confirmed as a reasonable reference.

Further analysis of time domain current profiling is investigated with reference to the baseline current profile established in Chapter 3. Considering the current profile as a series of discrete points, the profile at turn-off is varied and trends in vibrational behaviour compared. A continuous slope differential is introduced at turn-off, and the duration of the current decay is varied. The vibration response is shown to be reduced, with reduction proportional to the duration of the continuous slope. This is due to the gradual decay in the resultant radial force, and thus, a reduction in amplitude of oscillations in the stator back iron. Concluding the current profiling in the time domain, a step in current is introduced at a predetermined time before turn-off instance in the baseline unipolar square wave current profile. The duration of the time step is varied whilst the amplitude is kept constant. Analysis under these conditions shows that the duration of time step has little to no influence on the resulting vibration response. However, the vibration response is reduced with reference to the baseline. Therefore, it is shown that the amplitude at turn-off is more important when considering a drop in current before turn-off. In conclusion for time domain current profiling, it is shown that the moment of turn-off in each phase is the main contributor to stator borne vibrations. Moreover, the amplitude of current profile at the instance of turn-off is shown to be most significant, whilst the graduating of the current decay may reduce the vibration response further.

6.3 Frequency domain investigation

With the aim of current profiling from the perspective of frequency domain, the baseline unipolar square wave current profile can be derived as a sum of sinusoidal harmonic components via a Fourier series transform. In order to find out the contribution of each harmonic component to the electromagnetic forces and vibration response, the current waveform is systematically rebuilt with progressive harmonic inclusion. It is found that inclusion of only low order current harmonics produces a significantly lower vibration response across all mode shapes. As the number of harmonic components reintroduced into the current profile is increased, the resultant vibration response is closer to the baseline reference. It has been shown that a current profile with the inclusion of DC component and 1st current harmonic is capable of producing reasonable torque with reduced torque ripple. Hence, the influence of these current components on vibration response is analysed. It is concluded that the amplitude of 1st current harmonic has more influence on the vibration response. However, an increase in the DC component also results in increased vibration response, and therefore, both shall be considered when optimising the current profile. Finally, the influence of the 2nd current harmonic amplitude is investigated. It is evident from the simulated results that variance in amplitude of the 2nd current harmonic results in minimal variance in vibration response.

6.4 Future work

The investigation into the influence of various current parameters is verified and simulated on a small scale 6s/4r SRM. The relatively small size of the prototype SRM results in high natural frequencies, and thus, the excitation of the dominant modes is caused purely by electromagnetic excitation. It is known that the contribution of resonant components of forces is a major factor in the high acoustic noise and vibrations in SRMs. By increasing the size of the electrical machine, the natural frequencies of eigenmodes shall be lowered, and therefore, the machine may be operated at a lower speed so as to excite these resonances. This would lead to an investigation of current parameters on the vibration response, caused by both electromagnetic excitation and mechanical, i.e. rotational resonance.

The focus of this research is to single out current parameters and approach the influence of each parameter individually. Based on investigation in Chapter 3, the peak load current of the unipolar current square wave is determined to be a critical factor in the amplitude of vibration response. Hence, additions to this profile, such as the slope at turn-off, increase the resultant copper loss of the SRM. In many applications in industry, copper loss is a key parameter in the design process, and therefore, this must be taken into account. Future investigations into the trends shown throughout this research can be further analysed under conditions of equal copper loss, particularly the current profiling in the frequency domain.

Furthermore, this thesis compares current profiling on a single machine with 6s/4r pole combination at a single speed determined by experimental verification and limitations. In order to expand

conclusions and the potential improvements in acoustic noise and vibration performance, both slot/pole number combination and operating speed should be investigated. An increase in slot/pole number combination or operating speed results in a shorter electrical cycle, or increased operating frequency. This increases the opportunity for resonance to occur between radial force harmonic components and natural mode shapes of the motor, due to the higher frequency of fundamental radial forces per tooth. The influence of this phenomenon may be investigated for multiple speeds and slot/pole number combinations, in conjunction with current profiling strategies outlined in this thesis. Further to this, an increase in slot/pole number combination brings the stator teeth closer together, relative to the size of the machine. This increases the influence of radial forces from adjacent teeth, and hence, current profiling can be considered from the perspective of minimum sum of radial forces acting per tooth [Tak15], [Bay16]. By increasing the slot/pole number combination from that seen in this thesis, the sum of radial forces per tooth may be investigated to find the influence of various current profile parameters.

The frequency domain current profiling investigated covers the influence of the amplitudes of the DC, 1st harmonic and 2nd harmonic components. Previously, the introduction of 2nd current harmonic has been shown to enhance torque density [Fen19]. The work achieved in this research shows that the amplitude of 2nd current harmonic has minimal influence on vibration response. To fully understand and verify the influence of the current harmonic components, the phase of current harmonics must also be considered, as well as the influence of harmonic contributions to maximum torque. The use of generic “off the shelf” controllers and inverters supports the further advancement of this work. If it is possible to design a machine as robust and simple as an SRM with a simple controller arrangement that is easily attainable and relatively cheap; whilst minimising acoustic noise and vibration for a small drop in performance, then it becomes a promising prospect in terms of future machines.

The work in this thesis also supports further research on the design and manufacture of electric motors with regards to dominant mode shapes as a result of assembly practice. It is a simple change for the machine to be designed and constructed such that bolted connections are no longer aligned with stator poles. This provides an opportunity to consider the mechanical implications of the design, but from an electromagnetic perspective. By adjusting the position of these connections it may be possible to minimise specific mode shapes and derivatives, for example, modes 2, 4, 6 etc. Furthermore, it is not fixed that the construction bolts shall be spaced equally about the yoke of the casing. Although this may be a constraint from a mechanical perspective, it may be of interest to investigate the vibrations of natural modes when these are located asymmetrically for example. This work can be investigated in FE first before being verified in experimental testing. The use of FE for this is relatively simple, and therefore, the investigation can lead to the optimisation of construction design in order to minimise acoustic noise and vibration, with no effect on machine performance.

References

- [And97] G.K. Andersen, H. Christiansen, R. Gurholt, L. Helle, T.G. Hovet, C.H. Jensen, and E. Ritchie, "Dynamic model of a switched reluctance motor for vibration analysis", Proc. University Power Engineering Conference, (UPEC), 1997, pp. 53-56.
- [ANS12] ANSYS Inc. Release 14.0 Documentation for ANSYS. HTML help-file. 2012.
- [Anw00] M. N. Anwar and I. Husain, "Radial force calculation and acoustic noise prediction in switched reluctance machines," *IEEE Trans. Ind. Appl.*, 2000.
- [Aya99] S. Ayari, M. Besbes, M. Lecrivain, and M. Gabsi, "Effects of the airgap eccentricity on the SRM vibrations", Proc. IEEE International Electrical Machines and Drives Conference, (IEMDC), 1999, pp. 138-140.
- [Bar99] F.J. Bartos, "Forward to the past with SR technology", Control Engineering, Nov/Dec. 1999, <http://www.controleng.com>.
- [Bay16] J. Bayless, N. Kurihara, H. Sugimoto, and A. Chiba, "Acoustic noise reduction of switched reluctance motor with reduced RMS current and enhanced efficiency," *IEEE Transactions on Energy Conversion*, vol. 31, no. 2, pp. 627-636, June 2016.
- [Bes08] J. Le Besnerais, "Reduction of magnetic noise in PWM-supplied induction machines – low-noise design rules and multi-objective optimisation." PhD thesis. Laboratoire d'Electricité et d'Electronique de Puissance de Lille; Ecole Centrale de Lille, Nov. 2008.
- [Bes94] M. Besbes, Z. Ren, A. Razeq, and S. Allano, S., "Vibration diagnostic for doubly salient variable reluctance motors", Proc. International Conference on Electrical Machines, (ICEM), 1994, pp. 415-418.
- [Bes98] M. Besbes, C. Picod, F. Camus, and M. Gabsi, "Influence of stator geometry upon vibratory behaviour and electromagnetic performances of switched reluctance motors", Proc. IEE Electric Power Applications, vol. 145, no. 5, September, 1998, pp. 462-468.
- [Bin01] Fachinformationsdienst Karlsruhe: Projektinfo 12/01 BINE Informationsdienst
- [Bla94] F. Blaabjerg, J.K. Pederson, P. Nielsen, L. Anderson, and P.C. Kjaer, "Investigation and reduction of acoustical noise from switched reluctance drives in current and voltage control", Proc. International Conference on Electrical Machines, (ICEM), 1994, pp. 589-594.
- [Boe13] M. Boesing, M. Niessen, T. Lange, and R. De Doncker, R. "Modeling spatial harmonics and switching frequencies in PM synchronous machines and their electromagnetic forces." 2012 XXth International Conference on Electrical Machines (ICEM), Sept. 2012, pp. 3001–3007
- [Bru84] Bruel & Kjaer, "Measuring sound", booklet, English DK BR0047-13, 1984, pp. 8.

- [Cai01] W. Cai and P. Pillay, "Resonant frequencies and mode shapes of switched reluctance motors," *IEEE Trans. Energy Convers.*, vol.6, no.1, pp.43-48, 2001.
- [Cai99] W. Cai and P. Pillay, "Resonance frequencies and mode shapes of switched reluctance motors", *Proc. IEEE International Electrical Machines and Drives Conference*, 1999, pp. 44-47.
- [Cam92] D.H. Cameron, J.H. Lang, and S.D. Umans, "The origin and reduction of acoustic noise in doubly salient variable-reluctance motors," *IEEE Transactions on Industry Applications*, vol. 26, no. 6, pp. 1250-1255, 1992.
- [Cha06] J. Chai, Y. Lin, and C. Liaw, "Comparative study of switching controls in vibration and acoustic noise reductions for switched reluctance motor", *IEE Proceedings - Electric Power Applications*, vol. 153, no. 3, p. 348-360, 2006.
- [Cha89] L. Chang, A. R. Eastham, and G. E. Dawson, "Permanent magnet synchronous motor: Finite element torque calculations," in *Conference Record - IAS Annual Meeting (IEEE Industry Applications Society)*, 1989, pp. 69–72.
- [Cho07] Y. Choi, H. Yoon, and C. Koh, "Pole-shape optimization of a switched-reluctance motor for torque ripple reduction", *IEEE Transactions on Magnetics*, vol. 43, no. 4, pp. 1797-1800, 2007.
- [Col96] R.S. Colby, F. Mottier, and T.J.E. Miller, "Vibration modes and acoustic noise in a four-phase switched reluctance motor", *IEEE Transactions on Industry Applications*, vol. 32, no. 6, pp. 1357-1364, 1996.
- [Dev17] E. Devillers, M. Hecquet, J. Le Besnerais and M. Régniez, "Tangential effects on magnetic vibrations and acoustic noise of induction machines using subdomain method and electromagnetic vibration synthesis", *2017 IEEE International Electric Machines and Drives Conference (IEMDC)*, Miami, FL, 2017, pp. 1-8.
- [Dex18] J. Dexter, L. Huang, Z. Q. Zhu, and X. Vinamata, "Comparison of torque production and design of switched reluctance and variable flux reluctance machines," *2018 21st International Conference on Electrical Machines and Systems (ICEMS)*, Jeju, South Korea, 2018, pp. 1924-1929.
- [Don11] R. De Doncker, D.W. Pulte, and A. Veltman, *Advanced Electrical Drives Analysis, Modeling, Control*. 1st ed. Springer Science+Business Media B.V., 2011.
- [Edr05] C. S. Edrington, D. C. Kaluvagunta, J. Joddar, and B. Fahimi, "Investigation of electromagnetic force components in SRM under single and multiphase excitation", *IEEE Transactions on Industry Applications*, vol. 41, no. 4, pp. 978-988, July-Aug. 2005.

- [Ela18] M. Elamin et al., "Acoustic noise mitigation of switched reluctance machines with windows in both stator and rotor poles," 2018 IEEE Applied Power Electronics Conference and Exposition (APEC), San Antonio, TX, 2018, pp. 1205-1210.
- [Erd57] E. Erdelyi, and G. Horvay, G., "Vibration modes of stators of induction motors," ASME Trans., [E], vol. 24, 1957, pp. 39-45.
- [Fen19] J. Feng, L. Huang, Z. Q. Zhu, S. Guo, and J. Shi, "Torque density enhancement of 6/4 variable flux reluctance machine with second-harmonic current injection," IEEE Trans. Energy Convers., vol. 34, no. 2, pp. 1135–1145, 2019.
- [Fie04] J.O. Fiedler, N.H. Fuengwarodsakul, and R.W. De Doncker, "Calculation of switching frequency in current-hysteresis controlled switched reluctance drives," IEEE Power Electronics Specialists Conference PESC04, Aachen Germany, 2004
- [Fie06] J. Fiedler, "Design of low-noise switched reluctance drives." PhD thesis. RWTH Aachen University, Faculty of Electrical Engineering, Information Technology, Institute for Power Electronics, and Electrical Drives, 2006.
- [Fue07] N. Fuengwarodsakul, "Predictive PWM-based direct instantaneous torque control for switched reluctance machines." PhD thesis. RWTH Aachen University, Faculty of Electrical Engineering, Information Technology, Institute for Power Electronics, and Electrical Drives, 2007.
- [Fuk12] T. Fukami, Y. Matsuura, K. Shima, M. Momiyama, and M. Kawamura, "A multipole synchronous machine with nonoverlapping concentrated armature and field windings on the stator," IEEE Trans. Ind. Electron., vol. 59, no. 6, pp. 2583–2591, 2012.
- [Gab97] M. Gabsi, F. Camus, B. Humeau, and M. Besbes, "Vibrations in the switched reluctance motor. Influence of the feeder mode", Proc. European Power Electronics Conference, (EPE), 1997 pp. 2.495-2.499.
- [Gab99] M. Gabsi, F. Camus, T. Loyau, and J.L. Barby, "Noise reduction of switched reluctance machine," Proc. IEEE Int. Electric Machine and Drives Conference IEMDC 1999.
- [Gan15] C. Gan, J. Wu, M. Shen, S. Yang, Y. Hu, and W. Cao, "Investigation of skewing effects on the vibration reduction of three-phase switched reluctance motors," IEEE Transactions on Magnetics, vol. 51, no. 9, pp. 1-9, Sept. 2015.
- [Gar97] S. Garvey, J. Penny, M. Friswell, and C. Glew, "Modelling the vibrational behaviour of stator cores of electrical machines with a view to successfully predicting machine noise." IEE Colloquium on Modeling the Performance of Electrical Machines (Digest No: 1997/166), Apr. 1997, pp. 3/1–3/13.
- [Gie01] J.T. Gierer, K.D. Cox, and G.E. Hendrix, Emerson Electric Co.: Switched reluctance motor having stator inserts for noise reduction, magnet positioning, and coil retention, US Patent No 6232693B1, 15.05.2001.

- [Gie06] J.F. Gieras, C. Wang, and J.C. Lai, *Noise of Polyphase Electric Motors*. Taylor and Francis Group, 2006.
- [Gie09] V. d. Giet, M., Rothe, R., and Hameyer, K. "Asymptotic Fourier decomposition of tooth forces in terms of convolved air gap field harmonics for noise diagnosis of electrical machines." *COMPEL* 28.4 (2009), pp. 804–818. issn: 0332-1649. doi: 10.1108/03321640910958937.
- [Gie11] M. V. d. Giet, "Analysis of electromagnetic acoustic noise excitations: A contribution to low-noise design and to the auralization of electrical machines." PhD thesis. RWTH Aachen University, Faculty of Electrical Engineering and Information Technology, Institute for Electrical Machines, Jan. 2011.
- [Gir79] R. S. Girgis, and S.P. Verma, "Resonant frequencies and vibration behaviour of stators of electrical machines as affected by teeth, windings, frame and laminations," *IEEE Transactions on Power Apparatus and Systems*, vol.98, no.4, pp. 1446-1455, 1979.
- [Ham04] www.hamiltonsundstrandcorp.com
- [Hua17] L. R. Huang, J. H. Feng, S. Y. Guo, J. X. Shi, W. Q. Chu, and Z. Q. Zhu, "Analysis of torque production in variable flux reluctance machines," *IEEE Transactions on Energy Conversion*, vol. 32, no. 4, pp. 1297-1308, Dec. 2017.
- [Hua18] L. R. Huang, J. H. Feng, S. Y. Guo, Y. F. Li, J. X. Shi, and Z. Q. Zhu, "Rotor shaping method for torque ripple mitigation in variable flux reluctance machines," *IEEE Transactions on Energy Conversion*, vol. 33, no. 3, pp. 1579-1589, Sept. 2018.
- [Hua19a] L. R. Huang, Z. Q. Zhu, J. H. Feng, S. Y. Guo, and J. X. Shi, "Stator/rotor pole combinations of variable flux reluctance machines with 2nd harmonic current injection method," 2019 IEEE International Electric Machines & Drives Conference (IEMDC), San Diego, CA, USA, 2019, pp. 1493-1500.
- [Hua19b] L. Huang, Z. Q. Zhu, J. Feng, S. Guo, J. X. Shi, and W. Chu, "Analysis of stator/rotor pole combinations in variable flux reluctance machines using magnetic gearing effect," *IEEE Transactions on Industry Applications*, vol. 55, no. 2, pp. 1495-1504, March-April 2019.
- [Hus00] I. Husain, A. Radun, and J. Nairus, "Unbalanced force calculation in switched reluctance machines", *IEEE Transactions on Magnetics*, vol. 36, no. 1, pp. 330-338, January 2000.
- [Hus02] I. Husain, "Minimization of torque ripple in SRM drives", *IEEE Transactions on Industry Electronics*, vol. 49, no. 1, pp. 28-39, 2002.
- [Hus05] I. Husain and S. Hossain, "Modeling, simulation, and control of switched reluctance motor drives", *IEEE Transactions on Industry Electronics*, vol. 52, no. 6, pp. 1625-1634, 2005.

- [Ind02] R.B. Inderka: Direkte Drehmomentregelung Geschalteter Reluktanzantriebe, Dissertation RWTH Aachen 2002, Shaker Verlag
- [Ind03] R.B. Inderka, and R. W. De Doncker, "DITC-direct instantaneous torque control of switched reluctance drives." IEEE Transactions on Industry Applications, vol. 39, no.4, pp. 1046–1051, July 2003.
- [Jor50] H. Jordan, Gerauscharme Elektromotoren - Larmbildung und Larmbeseitigung bei Elektromotoren. Verlag W. Giradet, Essen., 1950.
- [Kas10] K. A. Kasper, "Analysis and control of the acoustic behavior of switched reluctance drives." PhD thesis. RWTH Aachen University, Faculty of Electrical Engineering, Information Technology, Institute for Power Electronics, and Electrical Drives, 2010.
- [Kri01] R. Krishnan: Switched Reluctance Motor Drives, CRC Press, ISBN 0-8493-0838-0.
- [Kri88] R. Krishnan, R. Arumugan, and J. Lindsay, "Design procedure for switched reluctance motors", IEEE Transactions on Industry Applications, vol. 24, no. 3, pp. 456-461, 1988.
- [Kur15a] N. Kurihara, A. Chiba, K. Yamada, and A. Souda, "A relationship of radial force sum and current waveforms in switched reluctance motor for noise reduction," 2015 IEEE Energy Convers. Congr. Expo. ECCE 2015, pp. 5560–5566, 2015.
- [Kur15b] N. Kurihara J. Bayless, and A. Chiba, "Noise and vibration reduction of switched reluctance motor with novel simplified current waveform to reduce force sum variation," IEEE International Electric Machines & Drives Conference (IEMDC), 2015, pp.1794-1800.
- [Law80] P. Lawrenson, J. Stephenson, N. Fulton, P. Blenkinsop, and J. Corda, "Variable-speed switched reluctance motors", IEE Proc. B, Electr. Power Appl. UK, vol. 127, no. 4, p. 253, 1980.
- [Lee17a] B. Lee, Z. Q. Zhu, and L. R. Huang, "Torque ripple reduction for 6-stator / 4-rotor-pole variable flux reluctance machines by using harmonic field current injection," IEEE Transactions on Industry Applications, vol. 53, no. 4, pp. 3730–3737, 2017.
- [Leo12] J. Leong and Z. Q. Zhu, "Acoustic noise and vibration of direct-torque-controlled permanent magnet brushless DC drives", 6th IET International Conference on Power Electronics, Machines and Drives (PEMD 2012), 2012.
- [Liu12a] X. Liu, Z. Q. Zhu, and Z. P. Pan, "Analysis of electromagnetic torque in sinusoidal excited switched reluctance machines having DC bias in excitation," Proc. 20th Int. Conf. Electr. Mach. ICEM 2012, pp. 2882–2888, 2012.
- [Liu12b] X. Liu, Z. Q. Zhu, M. Hasegawa, A. Pride, and R. Deodhar, "Vibration and noise in novel variable flux reluctance machine with DC-field coil in stator," Proc. Int. Conf. Power Electron. Motion Control, Jun. 2012, pp.1100-1107.

- [Liu12c] X. Liu, Z. Q. Zhu, M. Hasegawa, A. Pride, and R. Deodhar, "Investigation of PWMs on vibration and noise in SRM with sinusoidal bipolar excitation", IEEE International Symposium on Industrial Electronics, 2012, pp.674-679.
- [Liu13] X. Liu and Z. Q. Zhu, "Comparative study of novel variable flux reluctance machines with doubly fed doubly salient machines", IEEE Trans. Magn., vol. 49, no. 7, pp. 3838-3841, 2013.
- [Lon00] S.A. Long, Z.Q. Zhu, and D. Howe, "Influence of windings on the natural frequency of switched reluctance motors," Int. Seminar on Vibrations and Acoustic Noise of Electric Machinery, VANEM 2000.
- [Lon01] S.A. Long, Z.Q. Zhu, and D. Howe, "Vibration behavior of stators of switched reluctance motors" IEE Proc. Electric Power Applications, vol. 148, no. 3, pp 257-264, May 2001.
- [Lon02] S. A. Long, "Acoustic noise and vibration of switched reluctance machines." PhD thesis. University of Sheffield, 2002.
- [Lov94] H. C. Lovatt and J. M. Stephenson, "Computer-optimised current waveforms for switched-reluctance motors", IEE Proc. Electric Power Applications, vol. 141, no. 2, pp. 45-51, March 1994.
- [Mah96] J. Mahn, D. Williams, P. Wung, G. Horst, J. Lloyd, and S. Randall, "A systematic approach toward studying noise and vibration in switched reluctance machines: Preliminary results", Proceedings on IEEE Industry Applications Conference, vol. 2, pp. 779-785, 1996.
- [Meh92] M. Moallem, C. Ong, and L. E. Unnewehr, "Effect of rotor profiles on the torque of a switched reluctance motor", IEEE Transactions on Industry Applications, vol. 28, no. 2, pp. 364-369, March/April, 1992.
- [Mil01] T.J.E. Miller, Electronic Control of Switched Reluctance Machines, Newnespress 2001.
- [Mil93] T.J.E. Miller, Switched Reluctance Motors and Their Control, Magna Physics, Oxford, 1993.
- [Mil95] T.J.E. Miller, "Faults and unbalanced forces in the switched reluctance machine," IEEE Transactions on Industry Applications, vol. 31, no. 2, pp. 319-328, 1995.
- [Nak02] K. Nakata, K. Hiramoto, M. Sanada, S. Morimoto, and Y. Takeda, "Noise reduction for switched reluctance motor with a hole," *Proceedings of the Power Conversion Conference-Osaka 2002 (Cat. No.02TH8579)*, Osaka, Japan, 2002, pp. 971-976.
- [Nev01] C.G.C. Neves, R. Carlson, N. Sadowski, J.P.A. Bastos, N.S. Soeiro, and S.N.Y. Gerges: "Calculation of electromagnetic-mechanic-acoustic behavior of a switched reluctance motor", IEEE Transactions on Magnetism, vol. 36, no.4, July 2000.

- [Nev97] C.G.C., Neves, R. Carlson, N. Sadowski, J.P.A. Bastos, S.L. Nau, "The influence prediction of the current waveforms on the vibrational behavior of switched reluctance motors", IEEE International Electric Machines and Drives Conference Record, 1997, pp. TB1-7.1-TB1-7.3.
- [Nod87] S. Noda, S. Mori, F. Ishibashi, and K. Itomi, "Effect of coils on natural frequencies of stator cores in small induction motors," IEEE Transactions on Energy Conversion, vol. 2, no. 1, pp. 93-99, March, 1987.
- [Pil99] P. Pillay and W. Cai, "An investigation into vibration in switched reluctance motors", IEEE Transactions on Industry Applications, vol. 35, no. 3, pp. 589-596, May/June 1999.
- [Pol03] C. Pollock and M. Brackley, "Comparison of the acoustic noise of a flux-switching and a switched reluctance drive," IEEE Trans. Ind. Appl., vol. 39, no. 3, pp. 826–834, 2003, doi: 10.1109/TIA.2003.810626.
- [Pul93] D.W.J. Pulle, J.C.S. Lai, J.F. Milthorpe, and N. Huynh, "Quantification and analysis of acoustic noise in switched reluctance motors", Proc. European Conference on Power Electronics and Applications, (EPE), 1993, pp. 65-70.
- [Pul98] D. Pulle, and I. Petersen, "A unified approach to switched reluctance drive modeling: application to an axial flux (SRAF) motor." Record. 29th Annual IEEE Power Electronics Specialists Conference, 1998. PESC 98. May 1998, pp. 1681–1686.
- [Ras01] P.O. Rasmussen, J. Andreasen, and J.M. Pijanowski, "Structural slot tension spacers: The key to silent electrical machines," Proc. of Industry Applications Conference IAS 2001, pp. 33-39.
- [Ras99] P.O. Rasmussen, F. Blaabjerg, J.K. Pedersen, P.C. Kjaer, and T.J.E. Miller, "Acoustic noise simulation for switched reluctance motors with audible output", Proc. CD-ROM EPE'99, Lausanne, Switzerland, 1999.
- [Ray49] Lord Rayleigh, Theory of Sound, Macmillan, 2nd Edition, London, 1849.
- [Rus98] K. Russa, I. Husain, and M. Elbuluk, "Torque-ripple minimization in switched reluctance machines over a wide speed range", IEEE Transactions on Industry Applications, vol. 34, no. 5, pp. 1105-1112, 1998.
- [Sad96] N. Sadowski, Y. Lefevre, C.G.C. Neves, and R. Carlson, "Finite elements coupled to electrical circuit equations in the simulation of switched reluctance drives: attention to mechanical behaviour", IEEE Transactions on Magnetics, vol. 32, no. 3, pp. 1086-1089, 1996.
- [Sah00] F. Sahin, H. Ertan, and K. Leblebicioglu, "Optimum geometry for torque ripple minimization of switched reluctance motors", IEEE Transactions on Energy Conversion, vol. 15, no. 1, pp. 30-39, 2000.

- [Sch97] N. Schofield, "Brushless permanent magnet traction machines with extended speed capability", Ph.D. Thesis, University of Sheffield, 1997.
- [Sei92] H.O. Seinsch, *Oberfelderscheinungen in Drehfeldmaschinen*. Ed. by Hannover, U. B. G. Teubner, Stuttgart, 1992.
- [SRDrives] www.srdrives.com
- [Sta95] D. Staton, W. Soong, and T.J.E. Miller, "Unified theory of torque production in switched reluctance and synchronous reluctance motors." *IEEE Transactions on Industry Applications*, vol.31, no.2, pp. 329–337, March 1995.
- [Sta96] D. Staton, R. Deodhar, W. Soong, and T.J.E. Miller, "Torque prediction using the flux-MMF diagram in AC, DC, and reluctance motors." *IEEE Transactions on Industry Applications*, vol.32, no.1, pp. 180–188, Jan. 1996.
- [Sri03] K. N. Srinivas and R. Arumugam, "Analysis and characterization of switched reluctance motors," 29th Annual Conference of the IEEE Industrial Electronics Society (IECON), Roanoke, VA, USA, vol.3, pp. 2690-2698, 2003.
- [Sri04] K. N. Srinivas and R. Arumugam, "Static and dynamic vibration analyses of switched reluctance motors including bearings, housing, rotor dynamics, and applied loads.", *IEEE Transactions on Magnetics*, vol. 40, no. 4, pp. 1911-1919, July 2004.
- [Tak15] M. Takiguchi, H. Sugimoto, N. Kurihara, and A. Chiba, "Acoustic noise and vibration reduction of SRM by elimination of third harmonic component in sum of radial forces," *IEEE Transactions on Energy Conversion*, vol. 30, no. 3, pp. 883-891, Sept. 2015.
- [Tan97] Y. Tang, "Characterization, numerical analysis, and design of switched reluctance motors", *IEEE Transactions on Industry Applications*, vol. 33, no. 6, pp. 1544-1552, 1997.
- [Tur98] J.M. Turner, "Output smoothing in a switched reluctance machine", Patent, GB2313498, 1998.
- [Wu93] C.Y. Wu and C. Pollock, "Time domain analysis of vibration and acoustic noise in the switched reluctance drive", *Proc. International Conference on Electrical Machines and Drives, (EMD)*, 1993, pp. 558-563.
- [Wu95] C.Y. Wu, and C. Pollock, "Analysis and reduction of acoustic noise in the switched reluctance drive", *IEEE Transactions on Industry Applications*, vol. 31, no.6, pp. 91-98, 1995.
- [Wu96] X. Wu, S. Haramura, and J. Ueda, "Development of switched reluctance motor for electric vehicle – acoustic noise reduction", *Proc. Drives and Controls Conference*, 1996, pp. 1-5.

- [Xue09] X. Xue, K. Cheng, and S. Ho, "Optimization and evaluation of torque-sharing functions for torque ripple minimization in switched reluctance motor drives", IEEE Transactions on Power Electronics, vol. 24, no. 9, pp. 2076-2090, 2009.
- [Yan13] H. Yang, Y. Lim, and H. Kim, "Acoustic noise/vibration reduction of a single-phase srm using skewed stator and rotor," IEEE Transactions on Industrial Electronics, vol. 60, no. 10, pp. 4292-4300, Oct. 2013.
- [Yon97] Y. X. Chen, W. Jianhua, H. Jun, "Analytical calculation of natural frequencies of stator switched reluctance motor", Proc. Electric Machines and Drives conference, (EMD), 1997, pp. 81-85.
- [Zhu06] Z. Q. Zhu, Y. Liu, and D. Howe, "Minimizing the influence of cogging torque on vibration of PM brushless machines by direct torque control," IEEE Trans. Magn., vol. 42, no. 10, pp. 3512-3514, 2006.
- [Zhu07] Z. Q. Zhu, D. Ishak, D. Howe, and J. T. Chen, "Unbalanced magnetic forces in permanent-magnet brushless machines with diametrically asymmetric phase windings," IEEE Trans. Ind. Appl., vol.43, no.6, pp.1544-1553, 2007.
- [Zhu11] Z. Q. Zhu, "Switched flux permanent magnet machines - innovation continuous," International Conf. on Electrical Machines and Systems (ICEMS) 2011, pp.1-10.
- [Zhu17] Z. Q. Zhu, B. Lee, L. Huang, and W. Chu, "Contribution of current harmonics to average torque and torque ripple in switched reluctance machines," IEEE Transactions on Magnetics, vol. 53, no. 3, pp. 1-9, March 2017.
- [Zhu91] Z. Q. Zhu, "The electromagnetic performance of brushless permanent magnet DC motors – with particular reference to noise and vibration", PhD thesis, University of Sheffield, 1991.
- [Zhu94] Z.Q. Zhu, and D. Howe, "Improved methods for prediction of electromagnetic noise radiated by electrical machines," Proc. IEE-B, vol.141, no.2, pp.109-120, 1994.